Distribution Agreement

In presenting this thesis or dissertation as a partial fulfillment of the requirements for an advanced degree from Emory University, I hereby grant to Emory University and its agents the non-exclusive license to archive, make accessible, and display my thesis or dissertation in whole or in part in all forms of media, now or hereafter known, including display on the world wide web. I understand that I may select some access restrictions as part of the online submission of this thesis or dissertation. I retain all ownership rights to the copyright of the thesis or dissertation. I also retain the right to use in future works (such as articles or books) all or part of this thesis or dissertation.

Signature:

_____ _____

John Christopher Rounds Date

The Disease-Associated Proteins *Drosophila* Nab2 and Ataxin-2 Interact with Shared RNAs and Coregulate Neuronal Morphology

By

J. Christopher Rounds
Doctor of Philosophy

Graduate Division of Biological and Biomedical Science
Genetics and Molecular Biology

Kenneth H. Moberg, Ph.D. Advisor	Anita H. Corbett, Ph.D. Advisor
Gary Bassell, Ph.D. Committee Member	Roger Deal, Ph.D. Committee Member
Yue Feng, Ph.D. Committee Member	James Zheng, Ph.D. Committee Member

Accepted:

Lisa A. Tedesco, Ph.D.
Dean of the James T. Laney School of Graduate Studies

Date

The Disease-Associated Proteins *Drosophila* Nab2 and Ataxin-2 Interact with Shared RNAs and Coregulate Neuronal Morphology

By

J. Christopher Rounds
B.S., The University of North Carolina at Chapel Hill, 2013

Advisor: Kenneth H. Moberg, Ph.D.

Advisor: Anita H. Corbett, Ph.D.

An abstract of
a dissertation submitted to the Faculty of the
James T. Laney School of Graduate Studies of Emory University
in partial fulfillment of the requirements for the degree of
Doctor of Philosophy
in Genetics and Molecular Biology
2021

Abstract

The Disease-Associated Proteins *Drosophila* Nab2 and Ataxin-2 Interact with Shared RNAs and Coregulate Neuronal Morphology

By J. Christopher Rounds

Nab2 encodes a conserved polyadenosine RNA-binding protein (RBP) with broad roles in post-transcriptional regulation, including in poly(A) RNA export, poly(A) tail length control, transcription termination, and mRNA splicing. Mutation of the *Nab2* human ortholog *ZC3H14* gives rise to an autosomal recessive intellectual disability, but understanding of Nab2/ZC3H14 function in metazoan nervous systems is limited. No comprehensive identification of metazoan Nab2/ZC3H14-associated RNA transcripts has yet been conducted, and many Nab2/ZC3H14 functional protein partnerships likely remain unidentified. Moreover, the global effects of Nab2/ZC3H14 loss on RNAs and proteins are either incompletely understood or, more often, unknown. Here we present an RNA-sequencing experiment defining the effects of *Drosophila melanogaster* Nab2 loss on RNA abundance and structure in neuron-enriched head tissue at high resolution. We then present evidence that *Drosophila* Nab2 interacts with the RBP Ataxin-2 (Atx2), a neuronal translational regulator, and implicate these proteins in coordinate regulation of neuronal morphology and adult viability. We next detail the first high-throughput identifications of Nab2- and Atx2-associated RNAs in *Drosophila* brain neurons using an RNA immunoprecipitation-sequencing (RIP-Seq) approach. Critically, the RNA interactomes of each RBP overlap, and Nab2 exhibits high specificity in its RNA associations in neurons *in vivo*, associating with a small fraction of all polyadenylated RNAs. The identities of shared associated transcripts (e.g. *drk*, *me31B*, *stai*) and of transcripts specific to Nab2 or Atx2 (e.g. *Arpc2*, *tea*, respectively) promise insight into neuronal functions of and interactions between each RBP. Significantly, Nab2-associated RNAs are overrepresented for internal A-rich motifs, suggesting these sequences may partially mediate Nab2 target selection. Taken together, these data demonstrate that Nab2 opposingly regulates neuronal morphology and shares associated neuronal RNAs with Atx2, and that *Drosophila* Nab2 associates with a more specific subset of polyadenylated mRNAs than its polyadenosine affinity alone may suggest. By identifying RNAs associated with neuronal Nab2, our results supply clear direction for the ongoing study of *Drosophila* Nab2, enabling future definition of the precise molecular function of this RBP on its neuronal target RNAs. Beyond these insights, our results provide an essential foundation for expanding understanding of human ZC3H14 and ZC3H14-linked intellectual disability and neuronal development.

The Disease-Associated Proteins *Drosophila* Nab2 and Ataxin-2 Interact with Shared RNAs and Coregulate Neuronal Morphology

By

J. Christopher Rounds
B.S., The University of North Carolina at Chapel Hill, 2013

Advisor: Kenneth H. Moberg, Ph.D.

Advisor: Anita H. Corbett, Ph.D.

A dissertation submitted to the Faculty of the
James T. Laney School of Graduate Studies of Emory University
in partial fulfillment of the requirements for the degree of
Doctor of Philosophy
in Genetics and Molecular Biology
2021

ACKNOWLEDGEMENTS

I am honestly grateful and thankful for more people than I can list here, and I'd like to acknowledge you all. Thank you to everyone who has helped me reach this point and has supported me throughout pursuit of my Ph.D. With that in mind, I would like to express my gratitude to all members of the Moberg and Corbett labs, past and present, for enlightening discussion, experimental assistance, emotional support, and our positive lab environment throughout our time working together. I am especially grateful to fellow members of the *Drosophila* Nab2 Crew, past and present—ChangHui Pak, Seth Kelly, Rick Bienkowski, Binta Jalloh, and Edwin Corgiat. I would like to thank the members of my dissertation committee, Gary Bassell, Roger Deal, Yue Feng, and James Zheng, for their continued insights, direction, and assistance. I would also like to thank my co-mentors Anita H. Corbett and Kenneth H. Moberg for their sustained guidance, financial support, and mentorship throughout my graduate career.

Personally, I am so grateful for my Genetics and Molecular Biology program cohort— Kameryn Butler, Sara Fielder, PamelaSara Head, Stephanie Jones, Alex Kotlar, Mike Nichols, Brittany Phillips, and Cristina Trevino—for our friendship and comradery, which started as soon as we entered our program in 2013 and continues today. I am also so grateful to the friends I met in college and with whom I am still close to this day—James Brown, Kyle Bryant, Michael Conlin, Matt Danzi, Ryan Hurd, Justin Hurd, Sam Stinson, and Sam Otterbourg. You all are like family and have been essential to helping me through all of this. I am so thankful to my whole family, to my wonderful parents, grandparents, and in-laws, and especially to my siblings Zachary and Elizabeth Rounds—we've always been there for each other, and you have always been there to support me during my time in graduate school. Though she does not know it yet, I am also so thankful to my newborn daughter, Maeve Elizabeth Ramsdell Rounds—you're already the best kid a dad could ask for, and you have given me enormous clarity as I've wrapped up my graduate work these past few months.

Finally, I am thankful beyond description to my best friend, my wonderful wife, my one and only, and my partner for life, Lauren Ramsdell. The past few years have been so tough, and your unflappable support has meant the world to me, every time. You have always been there for me, whatever I need, no matter how tough it got, through thick and thin, and I cannot thank you enough for that, and I cannot thank you enough for always loving me. I couldn't have done this or made it through this struggle without you, darling, and I couldn't dream of doing what's next unless we did it together.

TABLE OF CONTENTS

LIST OF FIGURES

CHAPTER 2

CHAPTER 3

List of Tables

CHAPTER 1: GENERAL INTRODUCTION

This chapter has been written by J. Christopher Rounds specifically for inclusion in this dissertation.

INTRODUCTION

The intellectual-disability-linked gene family Nab2/ZC3H14

Intellectual disability refers to a broad group of neurodevelopmental disorders defined by significant limitations in intellectual functioning and adaptive behavior (Vissers *et al.* 2016). These criteria are met diagnostically by an IQ score below 70 and by limitations in independent functioning into adulthood, respectively (Boat *et al.* 2015; Tassé *et al.* 2016; WHO Europe 2020). Intellectual disability is common, affecting approximately 1% of the world population (Maulik *et al.* 2011), and etiologically heterogeneous, caused by a wide range of genetic and environmental factors (Ropers 2010). These causes may be monogenic as in Fragile X Syndrome, under environmental influence as in Fetal Alcohol Syndrome, or genetically more complex. Underscoring this complexity, over 700 genes have already been linked to intellectual disability, and this list is ultimately expected to number in the thousands (Ropers 2010; Vissers *et al.* 2016). To wit, while the links already established between these over 700 genes and intellectual disability represent an enormous achievement, etiology is still unresolved in 60% of individuals diagnosed with intellectual disability (Srivastava and Schwartz 2014).

Importantly though, efforts to understand the complexity of intellectual disability have yielded a key insight—many genes linked to intellectual disability encode proteins that converge on a comparatively limited set molecular pathways, suggesting disparate intellectual disabilities are unified by underlying molecular dysfunctions (Chelly *et al.* 2006; Najmabadi *et al.* 2011; van Bokhoven 2011; Agha *et al.* 2014; Verma *et al.* 2019). Thus, monogenic forms of intellectual disability represent experimentally tractable systems to potentially expand our understanding of many disorders at once, promising to reveal potential dysfunctions underlying other monogenic and more genetically complex forms of intellectual disability in addition to the form under study. A set of such informative monogenic intellectual disabilities is caused by mutations affecting genes

encoding RNA-binding proteins (RBPs) (reviewed in Bardoni *et al.* 2012). For example, one recessive, monogenic form of intellectual disability is caused by loss-of-function mutations in *ZC3H14*, a gene encoding a ubiquitously expressed polyadenosine-RNA-binding protein whose molecular functions in humans are largely unknown (Pak *et al.* 2011; Al-Nabhani *et al.* 2018). We turn to genetic model systems to address this gap in knowledge, dissect ZC3H14 function, and gain insight into the neurodevelopmental and molecular etiology of ZC3H14-linked intellectual disability.

Drosophila melanogaster has already proven a powerful model system to understand intellectual disability in general, and in systematic reviews approximately 75% of human intellectual disability genes are found to have orthologs in *Drosophila*, underscoring the potential of this approach for human disorder insight (Inlow and Restifo 2004; Oortveld *et al.* 2013). By exploiting this evolutionary conservation, research in *Drosophila* has already provided crucial insights into intellectual disabilities linked to specific RBPs, such as Fragile X Syndrome (Pan *et al.* 2008), the most common inherited form of intellectual disability (Hunter *et al.* 2014). We have similarly employed the *Drosophila* model system to begin to dissect ZC3H14 function through study of its *Drosophila* ortholog Nab2 (Pak *et al.* 2011; Kelly *et al.* 2014, 2016; Bienkowski *et al.* 2017). Like ZC3H14, Nab2 is a polyadenosine RBP with functional importance in neurons— loss of Nab2 substantially limits adult viability, which pan-neuronal expression of Nab2 or ZC3H14 isoform 1 on an otherwise null background significantly and almost fully rescues (Pak *et al.* 2011; Kelly *et al.* 2014). Based on mutant analyses, Nab2 contributes to both appropriate neuronal morphology and proper neuronal functioning. Genomic loss of Nab2 in $Nab2^{ex3}$ homozygous nulls induces structural defects in the axonal projections of the mushroom bodies (Kelly *et al.* 2016), a principal olfactory learning and memory center of the insect brain (Heisenberg 2003; Kahsai and

Zars 2011; Yagi *et al.* 2016; Takemura *et al.* 2017). Pan-neuronal RNAi-mediated knockdown of *Nab2* in males induces short-term memory defects in a courtship conditioning assay (Kelly *et al.* 2016), raising the possibility the neuronal morphological defects observed upon Nab2 dysfunction may correspond with functional consequences or neuronal functioning deficits. Other organismal phenotypes of Nab2 loss show the range of functions to which Nab2 contributes—$Nab2^{ex3}$ homozygous nulls exhibit severe locomotor deficits, a penetrant wings-held-out defect, and humeral or scutal bristle kinking (Pak *et al.* 2011; Lee *et al.* 2020; and data not shown).

However, understanding how Nab2 molecularly functions to contribute to the processes underlying these neuronal and organismal phenotypes remains very limited. Prior to the work described in this dissertation, only a few molecular phenotypes of *Drosophila* Nab2 knockdown or loss were known. Loss of Nab2 moderately increases bulk poly(A) tail length in *Drosophila* adult heads (Pak *et al.* 2011; Kelly *et al.* 2014; Bienkowski *et al.* 2017). Knockdown of *Drosophila* Nab2 increases fluorescence from a transgenic *CaMKII* 3'UTR reporter construct, pointing to possible roles for Nab2 in translational regulation (Bienkowski *et al.* 2017). Moreover, Nab2 physically and functionally associates with Fmr1, the *Drosophila* homolog of the Fragile X Syndrome RBP FMRP (Verkerk *et al.* 1991; Ashley *et al.* 1993; Wan *et al.* 2000), to support axonal morphology and olfactory memory (Bienkowski *et al.* 2017). Beyond these links to poly(A) tail length control and protein translation, however, few other molecular phenotypes of Nab2 loss were established prior to the work by our group described herein (Jalloh *et al.* 2020; Rounds *et al.* 2021) and performed in parallel (Lee *et al.* 2020; Corgiat *et al.* 2020). Moreover, neither of these molecular links established the direct function of Nab2 on its associated RNA transcripts.

A much broader set of possible functional roles of Nab2 are suggested by synthesizing research on murine ZC3H14, human ZC3H14, and the most well-studied Nab2/ZC3H14 ortholog,

S. cerevisiae Nab2 (reviewed in Fasken *et al.* 2019). Nab2 is proposed to be the central nuclear poly(A) binding protein in *S. cerevisiae* (Moore 2005; Chen and Shyu 2014; Schmid *et al.* 2015). In this organism, Nab2 is essential for viability (Anderson *et al.* 1993) and plays key roles in nuclear RNA processing, regulating bulk poly(A) tail length (Kelly *et al.* 2010), poly(A) RNA export from the nucleus (Green *et al.* 2002; Hector *et al.* 2002), transcription termination (Alpert *et al.* 2020), and transcript stability pervasively across many transcripts (Schmid *et al.* 2015). *S. cerevisiae* Nab2 associates pervasively with much of the transcriptome—the exact fraction bound by Nab2 differs between studies and remains an active research question (Guisbert *et al.* 2005; Batisse *et al.* 2009; Tuck and Tollervey 2013). Importantly, this polyadenosine RBP binds not only with high frequency to 3'UTRs and, presumably, poly(A) tails, but it also binds with lower frequency throughout genetically encoded transcript sequences (Tuck and Tollervey 2013; Baejen *et al.* 2014).

Murine and human ZC3H14 also contribute to nuclear RNA processing, but not as pervasively as *S. cerevisiae* Nab2. Murine ZC3H14 may be linked in a more nuanced way to poly(A) tail length control, as loss or RNAi-mediated knockdown of full-length ZC3H14 moderately increases bulk poly(A) tail length in some but not all murine tissues and cells (Pak *et al.* 2011; Kelly *et al.* 2014; Bienkowski *et al.* 2017; Rha *et al.* 2017), exerting less dramatic effects than observed for bulk poly(A) tails following Nab2 dysfunction in *S. cerevisiae* (Kelly *et al.* 2010). ZC3H14 functions in some way in RNA quality control as well, as ZC3H14 knockdown in a mouse neuroblastoma N2A or a human breast cancer MCF-7 cell line induces increases in steady-state levels of select intron-retaining pre-mRNAs in the cytoplasm (Wigington *et al.* 2016; Morris and Corbett 2018), possibly due to faulty splicing, nuclear export, or transcript degradation. Metazoan Nab2/ZC3H14 does not detectably alter bulk poly(A) export from the nucleus in the

contexts examined so far (Farny *et al.* 2008; Pak *et al.* 2011), though based on homology to *S. cerevisiae* Nab2 these proteins may still influence nuclear export for select associated transcripts. Unlike in *S. cerevisiae*, the effects of Nab2 loss on transcription termination or transcript stability have not been comprehensively tested or conclusively established. Finally, unlike in *S. cerevisiae*, metazoan Nab2/full-length ZC3H14 is dispensable for cellular viability in *Drosophila* (Bienkowski *et al.* 2017), mice (Rha *et al.* 2017), and, seemingly, humans (Pak *et al.* 2011; Al-Nabhani *et al.* 2018). The diminished requirement for Nab2/ZC3H14 in metazoans as compared to *S. cerevisiae* strongly argues for a more specific role for the former in nuclear RNA processing on a more select set of transcripts.

The deeper molecular and functional understanding of *S. cerevisiae* Nab2 as compared to metazoan Nab2/ZC3H14 reflected by these data manifests in the level of detail to which the function of each can be modeled thus far. One current model for how *S. cerevisiae* Nab2 functionally guides nuclear RNA processing proposes that Nab2: 1) binds to A-rich stretches of nascent RNAs and to poly(A) tails during transcription and polyadenylation; 2) ultimately dimerizes once tails reach about 60 nucleotides in length, physically altering and limiting the orientation of the tail to disrupt poly(A) polymerase processivity and thus limit tail length; 3) compacts RNA in preparation for nuclear export; 4) associates with nuclear export machinery to aid in transcript export from the nucleus (proposed and reviewed in Fasken *et al.* 2019; and Stewart 2019). Moreover, the association of Nab2 with poly(A) tails is predicted to protect many transcripts from degradation, explaining the link between Nab2 and transcript stability (Schmid *et al.* 2015). On the other hand, no such detailed, overarching model has yet to be established for the molecular function of metazoan Nab2/ZC3H14. Attempts to define the potential precise molecular functions of these proteins have been more limited and focused on a few different possible

functions across only a very small set of transcripts, preventing the establishment of detailed, cohesive, overarching models of metazoan Nab2/ZC3H14 molecular function. Establishing the precise molecular function of metazoan Nab2/ZC3H14 is therefore essential for understanding human ZC3H14 and ZC3H14-linked intellectual disability and neurodevelopment.

Major gaps in knowledge impede understanding of Nab2/ZC3H14 function and its contributions to intellectual disability and neurodevelopment

The critical task of defining the exact molecular function of metazoan Nab2/ZC3H14 has been thoroughly impeded by three fundamental gaps in knowledge. The first gap arises from the findings detailed above that metazoan Nab2/ZC3H14, unlike *S. cerevisiae* Nab2, does not exert effects when mutated that are consistent with a role as the central nuclear poly(A) binding protein pervasively regulating nuclear RNA stability and poly(A) tail length while contributing to poly(A) RNA export from the nucleus. Fundamentally, as noted above and unlike *S. cerevisiae* Nab2 (Anderson *et al.* 1993), metazoan Nab2/ZC3H14 is not essential for cellular viability in *Drosophila* (Bienkowski *et al.* 2017), mice (Rha *et al.* 2017), or, seemingly, humans (Pak *et al.* 2011; Al-Nabhani *et al.* 2018). Compared to effects of *S. cerevisiae* Nab2 dysfunction on bulk poly(A) tail lengths (Kelly *et al.* 2010), effects of metazoan Nab2/ZC3H14 loss or knockdown on bulk poly(A) tail lengths are more moderate or do not occur in tested *Drosophila* head samples, mouse cells, and mouse tissues (Pak *et al.* 2011; Kelly *et al.* 2014; Bienkowski *et al.* 2017; Rha *et al.* 2017). Loss of knockdown of *Drosophila* Nab2 does not detectably alter bulk poly(A) RNA export from the nucleus (Farny *et al.* 2008; Pak *et al.* 2011), though effects on nuclear export of individual transcripts remain to be tested. Finally, only about 1% of the tested human transcriptome exhibited statistically significant, greater than 1.5-fold differences in steady-state levels compared to controls upon ZC3H14 knockdown in MCF-7 cells (Wigington *et al.* 2016). These data suggest an

intriguing possibility—that metazoan Nab2/ZC3H14 may exhibit much greater **specificity** in RNA association patterns, and thus in functional consequences, than its *S. cerevisiae* counterpart.

The second gap in knowledge impeding definition of metazoan Nab2/ZC3H14 molecular function arises from the indirect functional links (e.g. to protein translation) established for this protein family. Such links, if ultimately proven to represent direct molecular function, would represent roles for metazoan Nab2/ZC3H14 that are evolutionarily novel compared to its *S. cerevisiae* ortholog. Conversely, metazoan Nab2/ZC3H14 has not been thoroughly tested for functional roles in all nuclear RNA processing events to which *S. cerevisiae* Nab2 has already been linked. For example, prior to the research presented in this dissertation, possible links between *Drosophila* Nab2 and mRNA splicing had not yet been explored. The acquisition or loss of major molecular functions for homologous proteins over evolutionary time is thoroughly possible and likely somewhat common; but, if such changes have occurred, determining which functional links for metazoan Nab2/ZC3H14 reflect **directness** (i.e. reflective of activities performed on target transcripts) and which are indirect (i.e. reflective of downstream, knock-on effects of Nab2/ZC3H14 dysfunction on other transcripts) carries additional challenge in concert with additional importance.

The third gap in knowledge impeding definition of metazoan Nab2/ZC3H14 molecular function is the question of **associated RNA identity**—that is, what are the identities of the RNAs metazoan Nab2/ZC3H14 targets and binds? No comprehensive identification of metazoan-Nab2/ZC3H14-associated transcripts has yet been conducted, and only very few RNAs associating with this protein family have been identified at all (Wigington *et al.* 2016; Bienkowski *et al.* 2017; Morris and Corbett 2018). In contrast, *S. cerevisiae* Nab2-associated transcripts have been identified via multiple high-throughput approaches (Guisbert *et al.* 2005; Batisse *et al.* 2009; Tuck

and Tollervey 2013; Baejen *et al.* 2014). Answering all other questions of metazoan Nab2/ZC3H14 function relies on robustly answering the question of associated RNA identity. Without identifying metazoan Nab2/ZC3H14-associated RNAs, and without identifying a large set of them, establishing the precise molecular function of metazoan Nab2/ZC3H14 on its endogenous target transcripts cannot be done, and thus the biological function of metazoan Nab2/ZC3H14 in general, in neurons, and in intellectual disability and neurodevelopment cannot be well understood.

Research detailed in this dissertation and its substantial contributions to addressing gaps in understanding Nab2/ZC3H14

In this dissertation, we address these three fundamental impediments to understanding metazoan Nab2/ZC3H14 molecular function in general and *Drosophila* Nab2 function in particular. We provide insight into the questions of **specificity**, **directness**, and **associated RNA identity**, focusing particularly on the first and third topics. In Chapter 2, we describe among other results an RNA-sequencing (RNA-Seq) experiment which defines the effect of Nab2 loss on steady-state RNA abundance and structure in neuron-enriched adult head tissues. In addition to specific transcript changes of interest, we find critical evidence for specificity in *Drosophila* Nab2 function, supporting the assertion that *Drosophila* Nab2 indeed functions on and affects a more specific subset of transcripts than its *S. cerevisiae* counterpart, which is thought to pervasively regulate the transcriptome (Moore 2005; Tuck and Tollervey 2013; Chen and Shyu 2014; Baejen *et al.* 2014; Schmid *et al.* 2015; Fasken *et al.* 2019; Stewart 2019; Alpert *et al.* 2020).

In Chapter 3, we find further, more direct evidence for Nab2 specificity, while also presenting the first high-throughput identification of Nab2-associated RNAs in any metazoan, focusing in this case on neuronal cells. We show epitope-tagged Nab2 associates with a specific subset of 141 transcripts in *Drosophila* neurons, approximately 2.2% of the detectable and

statistically testable transcript set. We demonstrate that neuronal Nab2-associated transcripts encode proteins of various neuronal and neurodevelopmental functions with links to phenotypes of Nab2 loss or dysfunction. We find that neuronal Nab2-associated transcripts are overrepresented for A-rich sequence motifs within genetically encoded transcript sequences (i.e. outside of the poly(A) tail), representing possible sites of Nab2-transcript association and a factor which may contribute to Nab2-transcript association specificity for only certain polyadenylated transcripts despite their universal poly(A) tails.

In addition, in Chapter 3 we identify a new functional interacting partner of Nab2, the neuronal translational regulator and human-disease-linked RBP Ataxin-2 (Atx2) (Atx2 reviewed in Ostrowski *et al.* 2017; and Lee *et al.* 2018). Atx2 functions to suppress the translation of some mRNA transcripts (McCann *et al.* 2011; Sudhakaran *et al.* 2014; Bakthavachalu *et al.* 2018) and active the translation of others (Lim and Allada 2013; Zhang *et al.* 2013; Lee *et al.* 2017) in *Drosophila* neurons. Atx2 is a protein of particular interest to human health, as Atx2 mutations are linked to multiple neurodegenerative and neurological diseases. Expansion of a polyglutamine tract within ATXN2, the human Atx2 ortholog, from its most frequent length of 22-23 to a length greater than 34 gives rise to the autosomal dominant neurodegenerative disease spinocerebellar ataxia type 2 (SCA2) (Imbert *et al.* 1996; Pulst *et al.* 1996; Sanpei *et al.* 1996). Additionally, moderate expansions of the same polyglutamine tract to lengths 32-43 and 27-33 are associated with parkinsonism and the neurodegenerative disease amyotrophic lateral sclerosis (ALS), respectively (Gwinn-Hardy *et al.* 2000; Elden *et al.* 2010; Park *et al.* 2015). We present the first high-throughput identification of Atx2-associated RNAs in *Drosophila* neurons and find overlap between the Nab2- and Atx2-associated transcript sets. This overlap may explain genetic interactions we present between the genes encoding each RBP. Intriguingly, localization and co-

immunoprecipitation experiments we present suggest Nab2 and Atx2 may function on these shared transcripts in a sequential handoff system, rather than by co-occupying the same RNP complexes for extended periods of time. This model represents a promising insight and evidence for the importance of testing the **directness** of Nab2 functional links going forward, with the establishment of Nab2 **specificity** and **associated RNA identity** in the research presented here.

Finally, in Chapter 4 we present additional data that expands on the themes of the preceding chapters and provides further valuable methodological insights. We describe additional tests of *Nab2-Atx2* genetic interactions, explore limitations of our RIP-Seq approach caused by unsuccessful rRNA depletion, and present results of a $Nab2^{ex3}$ outcross along with techniques to improve $Nab2^{ex3}$ adult viability for use by future experimentalists. To close, in Chapter 5 we discuss the presented data as a whole and conclude, summarizing and reiterating the contributions to Nab2/ZC3H14 research and understanding represented by and provided in this dissertation.

REFERENCES

Abraham K. J., J. N. Y. Chan, J. S. Salvi, B. Ho, A. Hall, *et al.*, 2016 Intersection of calorie restriction and magnesium in the suppression of genome-destabilizing RNA-DNA hybrids. Nucleic Acids Res. 44: 8870–8884. https://doi.org/10.1093/nar/gkw752

Agha Z., Z. Iqbal, M. Azam, H. Ayub, L. E. L. M. Vissers, *et al.*, 2014 Exome Sequencing Identifies Three Novel Candidate Genes Implicated in Intellectual Disability, (O. R. Bandapalli, Ed.). PLoS One 9: e112687. https://doi.org/10.1371/journal.pone.0112687

Al-Nabhani M., S. Al-Rashdi, F. Al-Murshedi, A. Al-Kindi, K. Al-Thihli, *et al.*, 2018 Reanalysis of exome sequencing data of intellectual disability samples: Yields and benefits. Clin. Genet. https://doi.org/10.1111/cge.13438

Alpert T., K. Straube, F. Carrillo Oesterreich, and K. M. Neugebauer, 2020 Widespread Transcriptional Readthrough Caused by Nab2 Depletion Leads to Chimeric Transcripts with Retained Introns. Cell Rep. 33: 108324. https://doi.org/10.1016/j.celrep.2020.108324

Anderson J. T., S. M. Wilson, K. V Datar, and M. S. Swanson, 1993 NAB2: a yeast nuclear polyadenylated RNA-binding protein essential for cell viability. Mol. Cell. Biol. 13: 2730–2741. https://doi.org/10.1128/mcb.13.5.2730

Ashley C. T., K. D. Wilkinson, D. Reines, and S. T. Warren, 1993 FMR1 protein: Conserved RNP family domains and selective RNA binding. Science (80-.). 262: 563–566. https://doi.org/10.1126/science.7692601

Baejen C., P. Torkler, S. Gressel, K. Essig, J. Söding, *et al.*, 2014 Transcriptome Maps of mRNP Biogenesis Factors Define Pre-mRNA Recognition. Mol. Cell 55: 745–757. https://doi.org/10.1016/j.molcel.2014.08.005

Bakthavachalu B., J. Huelsmeier, I. P. Sudhakaran, J. Hillebrand, A. Singh, *et al.*, 2018 RNP-Granule Assembly via Ataxin-2 Disordered Domains Is Required for Long-Term Memory and Neurodegeneration Article RNP-Granule Assembly via Ataxin-2 Disordered Domains Is Required for Long-Term Memory and Neurodegeneration. Neuron 98: 754-766.e4. https://doi.org/10.1016/j.neuron.2018.04.032

Bardoni B., S. Abekhoukh, S. Zongaro, and M. Melko, 2012 Intellectual disabilities, neuronal posttranscriptional RNA metabolism, and RNA-binding proteins: Three actors for a complex scenario, pp. 29–51 in *Progress in Brain Research*, Elsevier B.V.

Batisse J., C. Batisse, A. Budd, B. Bö ttcher, and E. Hurt, 2009 Purification of Nuclear Poly(A)-binding Protein Nab2 Reveals Association with the Yeast Transcriptome and a Messenger Ribonucleoprotein Core Structure. J. Biol. Chem. 284: 34911–34917. https://doi.org/10.1074/jbc.M109.062034

Bienkowski R. S., A. Banerjee, J. C. Rounds, J. Rha, O. F. Omotade, *et al.*, 2017 The Conserved, Disease-Associated RNA Binding Protein dNab2 Interacts with the Fragile X Protein Ortholog in Drosophila Neurons. Cell Rep. 20: 1372–1384. https://doi.org/10.1016/j.celrep.2017.07.038

Boat T., J. Wu, Committee to Evaluate the Supplemental Security Income Disability Program for

Children with Mental Disorders, Board on the Health of Select Populations, Board on Children Youth and Families, *et al.*, 2015 *Mental Disorders and Disabilities Among Low-Income Children.*(T. Boat, and J. Wu, Eds.). National Academies Press (US), Washington (DC).

Bokhoven H. van, 2011 Genetic and epigenetic networks in intellectual disabilities. Annu. Rev. Genet. 45: 81–104. https://doi.org/10.1146/annurev-genet-110410-132512

Chelly J., M. Khelfaoui, F. Francis, B. Chérif, and T. Bienvenu, 2006 Genetics and pathophysiology of mental retardation. Eur. J. Hum. Genet. 14: 701–713.

Chen C. Y. A., and A. Bin Shyu, 2014 Emerging mechanisms of mRNP remodeling regulation. Wiley Interdiscip. Rev. RNA 5: 713–722. https://doi.org/10.1002/wrna.1241

Corgiat E. B., S. M. List, J. C. Rounds, A. H. Corbett, and K. H. Moberg, 2020 The RNA binding protein Nab2 regulates the proteome of the developing Drosophila brain. bioRxiv 2020.12.10.419846. https://doi.org/10.1101/2020.12.10.419846

Duncan K., J. G. Umen, and C. Guthrie, 2000 A putative ubiquitin ligase required for efficient mRNA export differentially affects hnRNP transport. Curr. Biol. 10: 687–696. https://doi.org/10.1016/S0960-9822(00)00527-3

Elden A. C., H.-J. Kim, M. P. Hart, A. S. Chen-Plotkin, B. S. Johnson, *et al.*, 2010 Ataxin-2 intermediate-length polyglutamine expansions are associated with increased risk for ALS. Nature 466: 1069–1075. https://doi.org/10.1038/nature09320

Farny N. G., J. A. Hurt, and P. A. Silver, 2008 Definition of global and transcript-specific mRNA export pathways in metazoans. Genes Dev. 22: 66–78. https://doi.org/10.1101/gad.1616008

Fasken M. B., A. H. Corbett, and M. Stewart, 2019 Structure-function relationships in the Nab2 polyadenosine-RNA binding Zn finger protein family. Protein Sci. 28: 513–523. https://doi.org/10.1002/pro.3565

Green D. M., K. A. Marfatia, E. B. Crafton, X. Zhang, X. Cheng, *et al.*, 2002 Nab2p is required for poly(A) RNA export in Saccharomyces cerevisiae and is regulated by arginine methylation via Hmt1p. J. Biol. Chem. 277: 7752–7760. https://doi.org/10.1074/jbc.M110053200

Guisbert K. K., K. Duncan, H. Li, and C. Guthrie, 2005 Functional specificity of shuttling hnRNPs revealed by genome-wide analysis of their RNA binding profiles. RNA 11: 383–393. https://doi.org/10.1261/rna.7234205

Gwinn-Hardy K., J. Y. Chen, H. C. Liu, T. Y. Liu, M. Boss, *et al.*, 2000 Spinocerebellar ataxia type 2 with parkinsonism in ethnic Chinese. Neurology 55: 800–805. https://doi.org/10.1212/WNL.55.6.800

Hector R. E., K. R. Nykamp, S. Dheur, J. T. Anderson, P. J. Non, *et al.*, 2002 Dual requirement for yeast hnRNP Nab2p in mRNA poly(A) tail length control and nuclear export. EMBO J. 21: 1800–10. https://doi.org/10.1093/emboj/21.7.1800

Heisenberg M., 2003 Mushroom body memoir: From maps to models. Nat. Rev. Neurosci. 4: 266–275. https://doi.org/10.1038/nrn1074

Hunter J., O. Rivero-Arias, A. Angelov, E. Kim, I. Fotheringham, *et al.*, 2014 Epidemiology of fragile X syndrome: A systematic review and meta-analysis. Am. J. Med. Genet. Part A 164: 1648–1658. https://doi.org/10.1002/ajmg.a.36511

Imbert G., F. Saudou, G. Yvert, D. Devys, Y. Trottier, *et al.*, 1996 Cloning of the gene for spinooerebellar ataxia 2 reveals a locus with high sensitivity to expanded CAG/glutamine repeats. Nat. Genet. 14: 285–291. https://doi.org/10.1038/ng1196-285

Inlow J. K., and L. L. Restifo, 2004 Molecular and Comparative Genetics of Mental Retardation. Genetics 166: 835–881. https://doi.org/10.1534/genetics.166.2.835

Jalloh B., J. C. Rounds, B. E. Brown, I. J. Kremsky, A. Banerjee, *et al.*, 2020 The Nab2 RNA binding protein promotes sex-specific splicing of Sex lethal in Drosophila neuronal tissue. bioRxiv 2020.11.13.382168. https://doi.org/10.1101/2020.11.13.382168

Kahsai L., and T. Zars, 2011 Learning and memory in drosophila: Behavior, genetics, and neural systems, pp. 139–167 in *International Review of Neurobiology*, Academic Press Inc.

Kelly S. M., S. W. Leung, L. H. Apponi, A. M. Bramley, E. J. Tran, *et al.*, 2010 Recognition of polyadenosine RNA by the zinc finger domain of nuclear poly(A) RNA-binding protein 2 (Nab2) is required for correct mRNA 3'-end formation. J. Biol. Chem. 285: 26022–32. https://doi.org/10.1074/jbc.M110.141127

Kelly S. M., S. W. Leung, C. Pak, A. Banerjee, K. H. Moberg, *et al.*, 2014 A conserved role for the zinc finger polyadenosine RNA binding protein, ZC3H14, in control of poly(A) tail length. RNA 20: 681–8. https://doi.org/10.1261/rna.043984.113

Kelly S. M., R. Bienkowski, A. Banerjee, D. J. Melicharek, Z. A. Brewer, *et al.*, 2016 The Drosophila ortholog of the Zc3h14 RNA binding protein acts within neurons to pattern axon projection in the developing brain. Dev. Neurobiol. 76: 93–106. https://doi.org/10.1002/dneu.22301

Lee J., E. Yoo, H. Lee, K. Park, J.-H. Hur, *et al.*, 2017 LSM12 and ME31B/DDX6 Define Distinct Modes of Posttranscriptional Regulation by ATAXIN-2 Protein Complex in Drosophila Circadian Pacemaker Neurons. Mol. Cell 66: 129-140.e7. https://doi.org/10.1016/j.molcel.2017.03.004

Lee J., M. Kim, T. Q. Itoh, and C. Lim, 2018 Ataxin-2: A versatile posttranscriptional regulator and its implication in neural function. Wiley Interdiscip. Rev. RNA 9: e1488. https://doi.org/10.1002/wrna.1488

Lee W.-H., E. B. Corgiat, J. C. Rounds, Z. Shepherd, A. H. Corbett, *et al.*, 2020 A Genetic Screen Links the Disease-Associated Nab2 RNA-Binding Protein to the Planar Cell Polarity Pathway in Drosophila melanogaster. G3 GENES, GENOMES, Genet. https://doi.org/10.1534/g3.120.401637

Lim C., and R. Allada, 2013 ATAXIN-2 Activates PERIOD Translation to Sustain Circadian Rhythms in Drosophila. Science (80-.). 340. https://doi.org/10.1126/science.1234785

Maulik P. K., M. N. Mascarenhas, C. D. Mathers, T. Dua, and S. Saxena, 2011 Prevalence of intellectual disability: A meta-analysis of population-based studies. Res. Dev. Disabil. 32: 419–436.

McCann C., E. E. Holohan, S. Das, A. Dervan, A. Larkin, *et al.*, 2011 The Ataxin-2 protein is required for microRNA function and synapse-specific long-term olfactory habituation. Proc. Natl. Acad. Sci. U. S. A. 108: E655-62. https://doi.org/10.1073/pnas.1107198108

Moore M. J., 2005 From birth to death: The complex lives of eukaryotic mRNAs. Science (80-.). 309: 1514–1518. https://doi.org/10.1126/science.1111443

Morris K. J., and A. H. Corbett, 2018 The polyadenosine RNA-binding protein ZC3H14 interacts with the THO complex and coordinately regulates the processing of neuronal transcripts. Nucleic Acids Res. 46: 6561–6575. https://doi.org/10.1093/nar/gky446

Najmabadi H., H. Hu, M. Garshasbi, T. Zemojtel, S. S. Abedini, *et al.*, 2011 Deep sequencing reveals 50 novel genes for recessive cognitive disorders. Nature 478: 57–63. https://doi.org/10.1038/nature10423

Oortveld M. A. W., S. Keerthikumar, M. Oti, B. Nijhof, A. C. Fernandes, *et al.*, 2013 Human Intellectual Disability Genes Form Conserved Functional Modules in Drosophila, (J. Flint, Ed.). PLoS Genet. 9: e1003911. https://doi.org/10.1371/journal.pgen.1003911

Ostrowski L. A., A. C. Hall, and K. Mekhail, 2017 Ataxin-2: From RNA control to human health and disease. Genes (Basel). 8: 2–21.

Pak C., M. Garshasbi, K. Kahrizi, C. Gross, L. H. Apponi, *et al.*, 2011 Mutation of the conserved polyadenosine RNA binding protein, ZC3H14/dNab2, impairs neural function in Drosophila and humans. Proc. Natl. Acad. Sci. U. S. A. 108: 12390–5. https://doi.org/10.1073/pnas.1107103108

Pan L., E. Woodruff, P. Liang, and K. Broadie, 2008 Mechanistic relationships between Drosophila fragile X mental retardation protein and metabotropic glutamate receptor A signaling. Mol. Cell. Neurosci. 37: 747–760. https://doi.org/10.1016/j.mcn.2008.01.003

Park H., H. J. Kim, and B. S. Jeon, 2015 Parkinsonism in spinocerebellar ataxia. Biomed Res. Int. 2015.

Pieretti M., F. Zhang, Y. H. Fu, S. T. Warren, B. A. Oostra, *et al.*, 1991 Absence of expression of the FMR-1 gene in fragile X syndrome. Cell 66: 817–822. https://doi.org/10.1016/0092-8674(91)90125-I

Pulst S. M., A. Nechiporuk, T. Nechiporuk, S. Gispert, X. N. Chen, *et al.*, 1996 Moderate expansion of a normally biallelic trinucleotide repeat in spinooerebellar ataxia type. Nat. Genet. 14: 269–276. https://doi.org/10.1038/ng1196-269

Rha J., S. K. Jones, J. Fidler, A. Banerjee, S. W. Leung, *et al.*, 2017 The RNA-binding protein, ZC3H14, is required for proper poly(A) tail length control, expression of synaptic proteins, and brain function in mice. Hum. Mol. Genet. 26: 3663–3681. https://doi.org/10.1093/hmg/ddx248

Ropers H. H., 2010 Genetics of early onset cognitive impairment. Annu. Rev. Genomics Hum. Genet. 11: 161–187.

Rounds J. C., E. B. Corgiat, C. Ye, J. A. Behnke, S. M. Kelly, *et al.*, 2021 The Disease-Associated Proteins Drosophila Nab2 and Ataxin-2 Interact with Shared RNAs and Coregulate Neuronal

Morphology. bioRxiv 2021.03.01.433469. https://doi.org/10.1101/2021.03.01.433469

Salvi J. S., J. N. Y. Chan, K. Szafranski, T. T. Liu, J. D. Wu, *et al.*, 2014 Roles for Pbp1 and Caloric Restriction in Genome and Lifespan Maintenance via Suppression of RNA-DNA Hybrids. Dev. Cell 30: 177–191. https://doi.org/10.1016/j.devcel.2014.05.013

Sanpei K., H. Takano, S. Igarashi, T. Sato, M. Oyake, *et al.*, 1996 Identification of the spinocerebellar ataxia type 2 gene using a direct identification of repeat expansion and cloning technique, DIRECT. Nat. Genet. 14: 277–284. https://doi.org/10.1038/ng1196-277

Schmid M., P. Olszewski, V. Pelechano, I. Gupta, L. M. Steinmetz, *et al.*, 2015 The Nuclear PolyA-Binding Protein Nab2p Is Essential for mRNA Production. Cell Rep. 12: 128–139. https://doi.org/10.1016/j.celrep.2015.06.008

Srivastava A. K., and C. E. Schwartz, 2014 Intellectual disability and autism spectrum disorders: Causal genes and molecular mechanisms. Neurosci. Biobehav. Rev. 46: 161–174.

Stewart M., 2019 Polyadenylation and nuclear export of mRNAs. J. Biol. Chem. 294: 2977–2987. https://doi.org/10.1074/jbc.REV118.005594

Sudhakaran I. P., J. Hillebrand, A. Dervan, S. Das, E. E. Holohan, *et al.*, 2014 FMRP and Ataxin-2 function together in long-term olfactory habituation and neuronal translational control. Proc Natl Acad Sci U S A 111: E99–E108. https://doi.org/10.1073/pnas.1309543111

Takemura S. ya, Y. Aso, T. Hige, A. Wong, Z. Lu, *et al.*, 2017 A connectome of a learning and memory center in the adult Drosophila brain. Elife 6. https://doi.org/10.7554/eLife.26975

Tassé M. J., R. Luckasson, and R. L. Schalock, 2016 The relation between intellectual functioning and adaptive behavior in the diagnosis of intellectual disability. Intellect. Dev. Disabil. 54: 381–390. https://doi.org/10.1352/1934-9556-54.6.381

Tuck A. C., and D. Tollervey, 2013 A transcriptome-wide atlas of RNP composition reveals diverse classes of mRNAs and lncRNAs. Cell 154: 996–1009. https://doi.org/10.1016/j.cell.2013.07.047

Verkerk A. J. M. H., M. Pieretti, J. S. Sutcliffe, Y. H. Fu, D. P. A. Kuhl, *et al.*, 1991 Identification of a gene (FMR-1) containing a CGG repeat coincident with a breakpoint cluster region exhibiting length variation in fragile X syndrome. Cell 65: 905–914. https://doi.org/10.1016/0092-8674(91)90397-H

Verma V., A. Paul, A. A. Vishwanath, B. Vaidya, and J. P. Clement, 2019 Understanding intellectual disability and utism spectrum disorders from common mouse models: Synapses to behaviour. Open Biol. 9. https://doi.org/10.1098/rsob.180265

Vissers L. E. L. M., C. Gilissen, and J. A. Veltman, 2016 Genetic studies in intellectual disability and related disorders. Nat. Rev. Genet. 17: 9–18.

Wan L., T. C. Dockendorff, T. A. Jongens, and G. Dreyfuss, 2000 Characterization of dFMR1, a Drosophila melanogaster Homolog of the Fragile X Mental Retardation Protein. Mol. Cell. Biol. 20: 8536–8547. https://doi.org/10.1128/mcb.20.22.8536-8547.2000

WHO Europe, 2020 Definition: intellectual disability. World Heal. Organ.

Wigington C. P., K. J. Morris, L. E. Newman, and A. H. Corbett, 2016 The Polyadenosine RNA-binding Protein, Zinc Finger Cys 3 His Protein 14 (ZC3H14), Regulates the Pre-mRNA Processing of a Key ATP Synthase Subunit mRNA * □ S. Publ. JBC Pap. Press. https://doi.org/10.1074/jbc.M116.754069

Yagi R., Y. Mabuchi, M. Mizunami, and N. K. Tanaka, 2016 Convergence of multimodal sensory pathways to the mushroom body calyx in Drosophila melanogaster. Sci. Rep. 6. https://doi.org/10.1038/srep29481

Zhang Y., J. Ling, C. Yuan, R. Dubruille, and P. Emery, 2013 A Role for Drosophila ATX2 in Activation of PER Translation and Circadian Behavior. Science (80-.). 340.

CHAPTER 2: THE NAB2 RNA BINDING PROTEIN PROMOTES SEX-SPECIFIC SPLICING OF *SEX LETHAL* IN *DROSOPHILA* NEURONAL TISSUE

This chapter has been excerpted from a manuscript under revision in preparation for publication in *eLife*. This manuscript, on which J. Christopher Rounds is co-second author, was submitted as:

The Nab2 RNA binding protein promotes sex-specific splicing of *Sex lethal* in *Drosophila* neuronal tissue

Binta Jalloh[1,2,3], J. Christopher Rounds[1,2,3†], Brianna E. Brown [1,2†], Isaac J. Kremsky[1], Ayan Banerjee[1], Derrick J. Morton[1,4], Rick S. Bienkowski[1,2,3], Milo B. Fasken[1], Anita H. Corbett[1]*, and Kenneth H. Moberg[2]*

[1] Department of Biology, Emory University, Atlanta, Georgia, USA
[2] Department of Cell Biology Emory University School of Medicine
[3] Graduate Program in Genetics and Molecular Biology, Emory University
[4] Emory Institutional Research and Academic Career Development Award (IRACDA), Fellowships in Research and Science Teaching (FIRST) Postdoctoral Fellowship

[†]These authors contributed equally to this study.

*Co-corresponding authors

J. Christopher Rounds performed as the bioinformatics lead on the RNA-Sequencing experiment and analyses described in this chapter. He authored Figures 2-1A, 2-1C, 2-1D and 2-2A; Table 2-1; Figure 2-S2; and Table 2-S1. He contributed to analyses underlying Figures 2-1B, 2-1E, 2-2B, 2-3A, and 2-3G; Figures 2-S1, 2-S3, and 2-S4; and Tables 2-S2 and 2-S3. He administratively coordinated the RNA-Seq with the sequencing core. He also wrote the RNA-Sequencing Methods Table and multiple RNA-Sequencing Methods subsections and edited the RNA-Sequencing Results text.

For the RNA-Sequencing experiment, Binta Jalloh collected samples and performed RNA extractions; the Georgia Genomics and Bioninformatics core prepared cDNA libraries and performed sequencing; Isaac J. Kremsky performed MISO, RBM, and other bioinformatic analyses; and Kenneth H. Moberg contributed to IGV analyses and DEX-Seq.

All other experiments were performed and associated text was written and edited by authors other than J. Christopher Rounds, especially Binta Jalloh, Brianna E. Brown, Anita H. Corbett, and Kenneth H. Moberg.

ABSTRACT

The *Drosophila* polyadenosine RNA binding protein Nab2, which is orthologous to a human protein lost in a form of inherited intellectual disability, controls axon projection, locomotion, and memory. Here we define an unexpectedly specific role for Nab2 in regulating splicing of ~150 exons/introns in the head transcriptome and link the most prominent of these, female retention of a male-specific exon in the sex determination factor *Sex-lethal* (*Sxl*), to a role in m^6A-dependent mRNA splicing. Genetic evidence indicates that aberrant *Sxl* splicing underlies multiple phenotypes in *Nab2* mutant females. At a molecular level, Nab2 associates with *Sxl* pre-mRNA and ensures proper female-specific splicing by preventing m^6A hypermethylation by Mettl3 methyltransferase. Consistent with these results, reducing Mettl3 expression rescues developmental, behavioral and neuroanatomical phenotypes in *Nab2* mutants. Overall these data identify Nab2 as a required regulator of m^6A-regulated *Sxl* splicing and imply a broad link between Nab2 and Mettl3-regulated brain RNAs.

INTRODUCTION

RNA binding proteins (RBPs) play important roles in guiding spatiotemporal patterns of gene expression that distinguish different cell types and tissues within organisms. There are an estimated ~1500 RBPs that distribute between the nucleus and cytoplasm (Gerstberger et al., 2014), and each has the potential to interact with RNAs to modulate post-transcriptional gene expression. Such regulation is particularly critical in highly specialized cells such as neurons (Conlon and Manley, 2017) where highly regulated alternative splicing of coding regions and 3'UTRs, cleavage/polyadenylation, trafficking and local translation are contribute to precise regulation of gene expression (Brinegar and Cooper, 2016). The critical roles of RBPs in neurons is highlighted by many functional studies that reveal the importance of this class of proteins in brain development and function (Darnell and Richter, 2012) and by the prevalence of human neurological diseases linked to mutations in genes encoding RBPs (Brinegar and Cooper, 2016). Many of these RBPs are ubiquitously expressed and play multiple roles in post-transcriptional regulation. Thus, defining the key neuronal functions of these proteins is critical to understanding both their fundamental roles and the links to disease.

Among the RBPs linked to human diseases are a group of proteins that bind with high affinity to polyadenosine RNAs, which are termed poly(A) RNA binding proteins or Pabs (Kelly et al., 2010). Functional studies of classical nuclear and cytoplasmic Pabs, which utilize RNA recognition motifs (RRMs) to recognize RNA, have uncovered diverse roles for these proteins in modulating mRNA stability, alternative cleavage and polyadenylation and translation (Smith et al., 2014). A second, less well-studied, group of Pabs uses zinc-finger (ZnF) domains to bind target RNAs. Among these is the Zinc Finger Cys-Cys-Cys-His-Type Containing 14 (ZC3H14) protein, which binds with high affinity to poly(A) RNAs via a set of C-terminal tandem Cys-Cys-Cys-His type zinc-finger domains (Leung et al., 2009). ZC3H14 is broadly expressed in many tissues and

cell types but mutations in the human *ZC3H14* gene are associated with a heritable form of intellectual disability (Pak et al., 2011), implying an important requirement for this protein in the central nervous system. ZC3H14 has well-conserved homologs in eukaryotes, including *S. cerevisiae* Nuclear poly(A)-binding protein 2 (Nab2), *Drosophila melanogaster* Nab2, *C. elegans* SUT-2 and murine ZC3H14 (Fasken et al., 2019). Zygotic loss of *ZC3H14* in mice and *Drosophila* impairs neuronal function (Pak et al., 2011; Rha et al., 2017), while neuron-specific depletion of *Drosophila* Nab2 is sufficient to replicate these effects (Pak et al., 2011). Reciprocally, expression of human ZC3H14 in Nab2-deficient neurons rescues this defect, demonstrating a high degree of functional conservation between human ZC3H14 and *Drosophila* Nab2 (Kelly et al., 2014). Collectively, these data focus attention on what are critical, but poorly understood, molecular roles for ZC3H14/Nab2 proteins in neurons.

Neuronal ZC3H14/Nab2 can be divided into two pools, a nuclear pool that accounts for the majority of ZC3H14/Nab2 in the cell, and a small cytoplasmic pool of protein detected in mRNA ribonucleoprotein particles (mRNPs) of axons and dendrites (Bienkowski et al., 2017; Leung et al., 2009; Rha et al., 2017). Depletion of both pools in *Drosophila* neurons cause defects in axon genesis within the brain mushroom bodies (Kelly et al., 2016), a pair of twin neuropil structures involved in learning and memory (Armstrong et al., 1998; Heisenberg, 2003). This requirement has been linked to a physical association between cytoplasmic Nab2 and the *Drosophila* Fragile-X mental retardation protein homolog, Fmr1 (Wan et al., 2000), and translational repression of shared Nab2-Fmr1 target RNAs in the cytoplasm (Bienkowski et al., 2017). Despite this insight into a cytoplasmic function of Nab2, molecular roles of the abundant population of Nab2 in neuronal nuclei remain undefined.

Here, we employed a broad and an unbiased RNA sequencing approach to identify transcriptome-wide changes in the heads of *Nab2* loss-of-function mutant flies. While the steady-state levels of most transcripts were not significantly changed, we uncovered a striking effect on splicing of a subset of neuronal RNA transcripts. We focused our analysis on a well-characterized sex-specific alternative splicing event in the *Sex-lethal* (*Sxl*) transcript. Results reveal that *Nab2* plays a novel role in regulating the alternative splicing of *Sxl* in a sex-specific manner. Recent works has revealed a role for m^6A RNA methylation by the enzyme Mettl3 in modulating this splicing event (Kan et al., 2017; Lence et al., 2016). Similar to *Mettl3*, the requirement for *Nab2* in alternative splicing of *Sxl* is only essential for neuronally-enriched tissues. Genetic and biochemical experiments support a functional link between m^6A methylation and Nab2 function. These results demonstrate the role for *Drosophila Nab2* in RNA alternative splicing as well as RNA methylation and sex determination in the neurons.

RESULTS

Nab2 loss affects levels and processing of a subset of RNAs in the head transcriptome

To assess the role of Nab2 in regulating the central nervous system transcriptome, a high-throughput RNA Sequencing (RNA-Seq) analysis was carried out in triplicate on *Nab2* null mutant heads ($Nab2^{ex3}$ imprecise excision of *EP3716*) (Pak et al., 2011) and isogenic control heads ($Nab2^{pex41}$ precise excision of *EP3716*). To capture sex-specific differences, heads were collected from both male and female flies of each genotype. Briefly, total RNA from 1-day old adults was rRNA-depleted and used to generate stranded cDNA libraries that were sequenced (150 cycles) on a NextSeq 500 High Output Flow Cell. This generated a total of approximately 1.1 billion 75 base-pair (bp) paired-end reads (91 million/sample) that were mapped onto the Dmel6.17 release of the *Drosophila* genome using RNA STAR (Dobin et al., 2013). Read annotation and per-gene tabulation was conducted with featureCounts (Liao et al., 2014) and differential expression analysis was performed with DESeq2 (Love et al., 2014).

RNA sequencing reads across the *Nab2* gene are almost completely eliminated in $Nab2^{ex3}$ mutants, confirming the genetic background and integrity of the analysis pipeline (**Figure 2-S1**). Principal component analysis (PCA) performed with DESeq2 output data confirms that the 12 RNA-seq datasets distribute into four clusters that diverge significantly from one another based on genotype ($Nab2^{ex3}$ vs. $Nab2^{pex41}$ control; PC1 58% variance) and sex (male vs. female; PC2 26% variance) (**Figure 2-1A**). The DESeq2 analysis detects 3,799 and 1,545 genes in females and males, respectively, that exhibit statistically significant differences in RNA abundance between $Nab2^{ex3}$ and control (Benjamini-Hochberg [BH] adjusted *p*-value/false discovery rate (FDR)<0.05) (**Table 2-S1**). Comparison of fold-changes ($Nab2^{ex3}$ vs. control) among these significantly different RNAs reveals a high degree of correlation in female vs. male samples (R=0.79), particularly among RNAs whose levels are most elevated upon Nab2 loss (**Figure 2-**

1B). Applying a 2-fold change cutoff ($|\log_2[\text{fold-change}]| \geq 1$) trims these sets to 453 significantly changed RNAs in females (294 'up', 159 'down'), and 305 significantly changed RNAs in males (150 'up', 155 'down') (**Figure 2-1C**), which merge into a combined set of 570 significantly affected RNAs that trend similarly in heatmap analysis of mutant vs. control samples (**Figure 2-1D**). A majority of the 453 affected 'female' RNAs are mRNAs (439) and the remaining are snoRNAs (8), snRNAs (1), pre-rRNAs (1), and tRNAs (4) (**Figure 2-1E**). A similar distribution occurs in male heads: a majority of the affected RNAs are mRNAs (297) and the remainder are snoRNAs (4), snRNAs (1), pre-rRNAs (1), and tRNAs (2) (**Figure 2-1E**). Overall, the number of significantly changed RNAs (($|\log_2[\text{fold-change}]| \geq 1$ and FDR<0.05) in *Nab2*^{ex3} females and male heads represents a small fraction of RNAs detected in heads (2.2% and 3.7% in males and females, respectively), suggesting that Nab2 normally contributes to RNA-specific regulatory mechanisms in *Drosophila* head tissue.

Nab2 loss alters levels of transcripts linked to mRNA processing

To screen Nab2-regulated RNAs for enriched functions, Gene Set Enrichment Analysis (GSEA) (Mootha et al., 2003; Subramanian et al., 2005) was carried to identify enriched gene ontology (GO) terms (Ashburner et al., 2000; The Gene Ontology Consortium, 2019) among the significantly changed female and male RNAs identified by DESeq2. This filtering uncovers significant enrichment (p<0.05) for "RNA splicing" GO (GO:0008380) within the upregulated group of RNAs in both sexes (**Figure 2-2A**). In *Nab2*^{ex3} females, 32 of 155 genes annotated under this term are present among upregulated RNAs; whereas in males, 75 of 159 genes annotated under this term are present among upregulated RNAs (**Figure 2-2A**). This enrichment for upregulated splicing-related factors indicates that Nab2 loss could shift splicing patterns in the adult head. Consistent with this hypothesis, MISO (mixture of isoforms) analysis (Katz et al., 2010) of

annotated alternative splicing events confirms that Nab2 loss significantly alters splicing patterns within a small number of transcripts in female (48) and male (50) heads (**Table 2-S2**) that fall into a variety of GO terms (**Figure 2-S2**). These MISO-called alternative splicing events include 5' and 3' alternative-splice site usage, intron retention events, and previously annotated exon skipping events, some of which are detected in the same transcripts (**Figure 2-2B**).

To test whether Nab2 loss results in unannotated or aberrant splicing events, DEXSeq analysis (Anders et al., 2012) was performed to scan for differential abundance of individual exons relative to other exons within the same transcript. This analysis detects 151 affected RNAs in $Nab2^{ex3}$ females and 114 in $Nab2^{ex3}$ males (**Table 2-1**), with many top-ranked transcripts encoding factors with roles in behavior, neurodevelopment, and/or neural function (**Table 2-S3**).

The most statistically significant exon usage change in either sex is female-specific inclusion of exon 3 in the *Sex lethal* (*Sxl*) mRNA (2.86-fold increase, p=3.08x10^{-235}). This effect on *Sxl* mRNA in $Nab2^{ex3}$ females is followed in rank order of significance by enhanced inclusion of exons 1 and 2 of the MIF4GD homolog transcript *CG13124*, exons 1 and 2 of the voltage-gated ion channel transcript *I_h channel* (*I_h*), and exon 1 of the synaptic enzyme transcript *Acetylcholine esterase* (*Ace)*. In $Nab2^{ex3}$ males, the top four events are enhanced inclusion of exon 1 of the *Ace* transcript*,* exon 1 of the *Protein kinase C at 53E* (*Pkc53E*) transcript, exons 1 and 2 of the Rab GTPase *pollux* (*plx*) transcript, and exons 1 and 2 of *Protein kinase N* (*Pkn*) transcript. In some cases, identical exons are affected in both $Nab2^{ex3}$ sexes and accompanied by retention of the intervening intron (e.g. see *CG13124* and *I_h* traces in **Figure 2-S2**). The robust increase in *Sxl* exon 3 in $Nab2^{ex3}$ females is noteworthy both for the central role that differential inclusion of exon 3 plays in *Drosophila* sex determination (Harrison, 2007), but also because DEXSeq did not detect changes in exon 3 inclusion or abundance in $Nab2^{ex3}$ males. In light of this sex-specific effect of

Nab2 loss on alternative splicing of *Sxl* exon 3, subsequent analyses focused on the role of Nab2 in *Sxl* mRNA splicing in female heads.

Nab2^{ex3} females exhibit masculinized *Sxl* splicing in neuron-enriched tissues

The Sex lethal (Sxl) protein is a female-specific, U-rich RNA binding protein that acts through the *tra-dsx* and *msl-2* pathways to promote female somatic and germline identity (Gawande et al., 2006; Penalva and Sanchez, 2003). *Sxl* pre-mRNA is expressed in both males and females, but alternative splicing regulated by m^{6}A RNA methylation and several RBPs leads to female-specific skipping of exon 3 during splicing (Haussmann et al., 2016; Lence et al., 2016; Sakamoto et al., 1992). Because exon 3 includes an in-frame translation 'stop' codon, full-length Sxl protein is only made and active in female cells (Bell et al., 1988). The inclusion of *Sxl* exon 3 in *Nab2*^{ex3} mutants would thus implicate Nab2 as a novel component of molecular machinery that controls *Sxl* pre-mRNA splicing in female heads.

Visualizing *Sxl* RNA-Seq reads with IGV Viewer (Robinson et al., 2017) confirms a large increase in exon 3 reads in *Nab2*^{ex3} females (*Nab2*^{ex3}-F) relative to control females (control-F), and also shows retention of ~500 bases of intron 3 sequence in *Nab2*^{ex3} females (**Figure 2-3A**). Quantification of reads across the entire *Sxl* locus detects an ~1.5-fold increase in the overall abundance of the *Sxl* mRNA in *Nab2*^{ex3} females compared to control females. Normal splicing patterns are detected across all other *Sxl* intron-exon junctions in both genotypes of males and females, including female-specific exon 9 inclusion (**Figure 2-3A**). Reverse transcription polymerase chain reaction (RT-PCR) on fly heads using *Sxl* primers (see arrows in **Figure 2-3A** schematic) that detect exon 2-exon 4 (control females) and exon 2-exon 3-exon 4 (control males) confirms the presence of the mis-spliced exon 2-exon 3-exon 4 mRNA transcript in *Nab2*^{ex3} females (**Figure 2-3B**). The exon 2-exon 3-exon 4 mRNA transcript appears to be more abundant

in *Nab2*^{ex3} female heads than in female heads lacking *Mettl3*, which encodes the catalytic component of an m^{6}A methyltransferase complex that promotes exon 3 skipping in nervous system tissue (Haussmann et al., 2016; Kan et al., 2017; Lence et al., 2016). RT-PCR also reveals a ~1kb band in *Nab2*^{ex3} females (arrowhead, **Figure 2-3B**) that sequencing identifies as aberrantly spliced transcript that incorporates 503 bases of intron 3 leading up to a cryptic 5' splice site (i.e. exon 2-exon 3-intron 3^{503}-exon 4); this matches the *Sxl* intron 3 sequencing reads observed in IGV (see **Figure 2-3A**). Significantly, RT-PCR analysis of *Sxl* mRNA in dissected control and *Nab2*^{ex3} females detects exon 3 retention in *Nab2*^{ex3} thoraxes, but not in abdomens or ovaries (**Figure 2-3C**). This result implies that Nab2 is only necessary to direct *Sxl* exon 3 exclusion in specific tissues or cell types such as neurons, which are enriched in the head (brain) and thorax (ventral nerve cord). In sum, these data reveal a tissue-specific role for Nab2 in blocking *Sxl* exon 3 inclusion in females and regulating 5'-splice site utilization at the exon 3-exon 4 junction.

Sxl exon 3 inclusion in *Nab2*^{ex3} female head RNAs suggests that insufficient levels of the exon 2-exon 4 splice variant contribute to *Nab2*^{ex3} phenotypes in females. To test this hypothesis, the constitutively female-spliced *Sxl*^{M8} allele (Barbash and Cline, 1995) was placed as a heterozygote into the background of *Nab2*^{ex3} animals. *Sxl*^{M8} contains a 110 bp deletion covering the 5'-end of intron 2 and 3'-end of exon 3 and consequently undergoes constitutive splicing to the feminized exon 2-exon 4 variant regardless of sex (top panel, **Figure 2-3D**). Heterozygosity for this *Sxl*^{M8} allele produces strong rescue of *Nab2*^{ex3} mutant female viability from ~4% to 71% (*Sxl*^{M8}*/+;;Nab2*^{ex3}) (**Figure 2-3D**). Female *Nab2*^{ex3} siblings that did not inherit the *Sxl*^{M8} allele also exhibit elevated viability (64%), perhaps due to maternal loading of *Sxl* mRNA (**Figure 2-3D**). Surviving *Sxl*^{M8}*/+;;Nab2*^{ex3} females also show improved locomotion in a negative geotaxis assay (**Figure 2-3E**) and lengthened lifespan (**Figure 2-3F**) relative to *Nab2*^{ex3} females. Consistent with

the original report describing *Sxl*^{M8} (Barbash and Cline, 1995), the allele is male-lethal in control (*Nab2*^{pex41}) and *Nab2*^{ex3} backgrounds. This female-specific rescue of *Nab2*^{ex3} by *Sxl*^{M8} indicates that restoring Sxl expression can compensate for Nab2 loss in some developing tissues

As Sxl is itself an RBP with roles in alternative splicing (Bell et al., 1988; Penalva and Sanchez, 2003), the rescuing effect of the *Sxl*^{M8} allele prompted a bioinformatic scan for RBP motifs enriched in proximity to the Nab2-dependent alternative splicing events identified by MISO analysis (see **Figure 2-2B**). Input sequences were composed of retained introns plus 25bp extending into each flanking exon, and alternative splice sites with 25bp of exon plus 1kb of adjacent intron (see schematic, **Figure 2-3G**). This unbiased scan detected predicted Sxl binding sites as the single most abundant RBP motif within the Nab2-regulated MISO events in females (**Figure 2-3G**). Notably, Sxl motifs were not detected as enriched in the male *Nab2*^{ex3} MISO dataset, which otherwise strongly resembles the remaining group of female-enriched RBP motifs (e.g. the HNRNPL homolog *smooth* (*sm*), *RNA binding protein-9* (*Rbp9*), the U1-SNRNPA homolog *sans fille* (*snf*), and the U2-SNRNP component *U2AF50*). The female-specific enrichment for Sxl binding sites suggests that Nab2 may regulate alternative splicing events indirectly via control of a *Sxl*-regulated splicing program. Intriguingly, the Sxl target *transformer* (*tra*) and the Tra target *double-sex* (*dsx*) (Horabin and Schedl, 1993; Sanchez et al., 2001) were not recovered in the *Nab2*^{ex3} MISO or DESeq2 datasets, and IGV reads show no evidence of altered structure of their RNAs relative to *Nab2*^{pex41} controls (**Figure 2-S4**). Together these data suggest that Sxl may not control the *tra-dsx* pathway in the adult head, or that *tra* and *dsx* splicing are only altered in a subset of *Nab2*^{ex3} head cells and thus not detectable by bulk RNA-Seq analysis.

The dosage compensation complex contributes to phenotypes in *Nab2^{ex3}* mutant females

The lack of evidence that *tra* and *dsx* mRNAs are affected by *Nab2* loss prompted analysis of the other major role of Sxl, which is to bind to the *male-specific lethal-2* (*msl-2*) mRNA and inhibit its translation in female somatic and germline tissues (Keller and Akhtar, 2015; Lucchesi and Kuroda, 2015). As a result, Msl-2 protein is only expressed in male cells, where it promotes assembly of a chromatin modifying complex termed the Dosage Compensation Complex (DCC; composed of Msl-1, Msl-2, Msl-3, Mof, Mle and *roX1* and *roX2* non-coding RNAs), which is recruited to the male X chromosome to equalize X-linked gene expression between males and females (Keller and Akhtar, 2015; Lucchesi and Kuroda, 2015). A number of DCC components are expressed highly in the adult nervous system (Amrein and Axel, 1997), which correlates with the tissue-restricted link between Nab2 and *Sxl* splicing (as in **Figure 2-3B**). As a functional test of interactions between Nab2 and the DCC pathway, a loss-of-function allele of *msl-2* (*msl-2$^{killer\ of\ males\text{-}A}$* or *msl-2^{kmA}*) (Bevan, 1993) was tested for dominant effects on *Nab2^{ex3}* female phenotypes. Remarkably, a single copy of *msl-2^{kmA}* significantly rescues defects in viability (**Figure 2-4A**), lifespan (**Figure 2-4B**), and locomotion (**Figure 2-4C**) among *Nab2^{ex3}* females. *roX1* and *mle* loss-of-function alleles were also able to rescue *Nab2^{ex3}* phenotypes (**Figure 2-S5**). Given that Msl-2 is not normally active in adult female tissues (Amrein and Axel, 1997; Meller et al., 1997) and that forced *msl*-2 expression reduces female viability (Kelley et al., 1995), rescue by *msl-2^{kmA}* heterozygosity provides strong evidence that the DCC pathway is inappropriately activated in *Nab2^{ex3}* females. Of note, the *msl-2* and *mle* RNAs appear similar in IGV reads from control and *Nab2^{ex3}* adults (**Figure 2-S4**), indicating that genetic interactions between these loci are not likely due to direct effects of Nab2 loss on abundance and structure of these RNAs.

Nab2-regulated splicing of *Sxl* exon3 is dependent upon the Mettl3 m^{6}A methyltransferase

Genetic interactions between *Nab2*, *Sxl*, and *msl-2* alleles are consistent with a role for Nab2 protein in regulating sex-specific splicing of *Sxl* exon 3. One mechanism that promotes exon 3 exclusion in females is based on N^6-methylation of adenosines (m^{6}A) in *Sxl* pre-mRNA by the Methyltransferase like-3 (Mettl3)-containing methyltransferase complex (reviewed in Lence et al., 2017). Inactivating mutations in components of this m^{6}A 'writer' complex masculinize the pattern of exon 3 splicing in female flies (Haussmann et al., 2016; Kan et al., 2017; Lence et al., 2016) in a manner similar to *Nab2^{ex3}*. Molecular studies indicate that the Mettl3 complex promotes exon 3 exclusion in females by depositing m^{6}A within *Sxl* exon 3 and flanking introns (Haussmann et al., 2016; Kan et al., 2017; Lence et al., 2016).

To assess Nab2-Mettl3 functional interactions, the null allele *Mettl3^{null}* (formerly known as *Ime4^{null})* (Lence et al., 2016) was recombined into the *Nab2^{ex3}* background (**Figure 2-S6**; the loci are 281kb apart on chr3R), and then used to test for effects on phenotypes in *Nab2^{ex3},Mettl3^{null}* double mutant females. As described previously (Haussmann et al., 2016; Kan et al., 2017; Lence et al., 2016), loss of Mettl3 in an otherwise *wildtype* genetic background reduces adult viability, shortens lifespan and decreases locomotion in a negative geotaxis assay (**Figure 2-5A-C**). However, removing *Mettl3* has the inverse effect of suppressing each of these defects in *Nab2^{ex3}* females (**Figure 2-5A-C**): *Nab2^{ex3},Mettl3^{null}* double mutant females show approximately 5-fold higher viability, 1.5-fold longer lifespan, and 2-fold greater locomotion activity (at the 30sec time point; **Figure 2-5C**) than *Nab2^{ex3}* mutants alone. Significantly, qPCR analysis confirms that *Mettl3* loss causes aberrant *Sxl* exon 3-exon 4 splicing (as reported in Haussmann et al., 2016; Kan et al., 2017; Lence et al., 2016) but reduces it in *Nab2^{ex3},Mettl3^{null}* double mutant females relative to *Nab2^{ex3}* females (**Figure 2-5D-E**). Within the adult brain, removing *Mettl3* also rescues structural

defects in α- and β-lobes in the mushroom bodies (MBs) that are otherwise highly penetrant in *Nab2*^{ex3} adults (**Figure 2-5F**). *Nab2*^{ex3} brains normally show 60-80% penetrance of thinned or missing α-lobes and fused β-lobes (Bienkowski et al., 2017; Kelly et al., 2016), but *Nab2*^{ex3},*Mettl3*^{null} double mutants exhibit a reduction of α-lobe defects and complete suppression of the β-lobe fusion defect (**Figure 2-5F**). As Nab2 and Mettl3 each act autonomously within MB neurons to pattern α/β-lobe structure (Kelly et al., 2016; Soldano et al., 2020), these genetic interactions imply that Nab2 and Mettl3 may co-regulate pathways which guide axon projection.

Nab2 binds *Sxl* pre-mRNA and modulates its m^{6}A methylation

The ability of the *Mettl3*^{null} allele to promote appropriate sex-specific exon 2-exon 4 splicing of *Sxl* in *Nab2*^{ex3} females is significant, both because it identifies the m^{6}A 'writer' Mettl3 as required for *Sxl* mis-splicing in heads lacking Nab2, and because this same *Mettl3* allele normally results in hypomethylation of *Sxl* mRNA and exon 3 inclusion in female flies (Haussmann et al., 2016; Kan et al., 2017; Lence et al., 2016). This paradox could be explained if exon 3 inclusion in *Nab2*^{ex3} females is due to hypermethylation of the *Sxl* pre-mRNA, which is then suppressed by removing *Mettl3*. To test this hypothesis, a series of primer sets was designed to examine *Sxl* pre-mRNA and mRNA transcripts by RNA-immunoprecipitation (RIP) and anti-m^{6}A-RIP (MeRIP) (**Figure 2-6A**). As illustrated in **Figure 2-6A**, the *Sxl* transcript contains candidate binding sites for both Sxl protein (polyuridine tracts=**red** ticks) and Nab2 protein (polyadenosine tracts=**green** ticks), and approximate sites of m^{6}A methylation (**yellow** ticks) (mapped in Kan et al., 2017) (see **Figure 2-S7** for a complete schematic). To assess the m^{6}A status of total *Sxl* RNA, MeRIP precipitates from female head lysates (control, *Nab2*^{ex3}, *Mettl3*^{null}, and *Nab2*^{ex3},*Mettl3*^{null}) were analyzed by reverse transcription-real time quantitative PCR (RT-qPCR) with the exon 2-exon 2 (E2-E2) primer pair, which amplifies both pre-mRNA and mature mRNA (*Sxl*$^{E2\text{-}E2}$ in **Figure 2-6B**). This approach

detects reduced *Sxl* m^{6}A in *Mettl3^{null}* heads relative to controls, which is consistent with prior studies (Haussmann et al., 2016; Kan et al., 2017; Lence et al., 2016), and an increase in *Sxl* transcript recovered from MeRIP of *Nab2^{ex3}* heads, consistent with *Sxl* hypermethylation. This apparent increase in *Sxl* m^{6}A methylation in *Nab2^{ex3}* heads requires Mettl3, as *Sxl* mRNA recovery in MeRIP is strongly reduced in *Nab2^{ex3},Mettl3^{null}* double mutant heads. Two m^{6}A-methylated candidate Mettl3-target RNAs, *Act5c* and *Usp16* (Kan et al., 2017; Lence et al., 2016) were analyzed as additional positive controls for m^{6}A status. MeRIP-qPCR indicates that both mRNAs are hypomethylated in *Mettl3^{null}* and hypermethylated in *Nab2^{ex3}* (**Figure 2-S8**). For *Act5c*, this *Nab2^{ex3}* hypermethylation requires *Mettl3* (**Figure 2-6B**). Shifting this analysis to qPCR with the *Sxl* E2-E4 primer set (*Sxl$^{E2\text{-}E4}$* in **Figure 2-6B**), which is predicted to selectively detect spliced *Sxl* mRNAs, supports a very similar pattern of elevated *Sxl* m^{6}A in *Nab2^{ex3}* heads that requires *Mettl3*. These MeRIP-qPCR data argue that Nab2 either inhibits Mettl3-mediated m^{6}A deposition or promotes m^{6}A removal on *Sxl* mRNAs, which in turn controls patterns of exon 3 retention/skipping. A prediction of this model is that Nab2 loss should result in hypermethylation of the *Sxl* pre-mRNA. Testing this hypothesis in MeRIP precipitates with the I3-E3 primer pair (*Sxl$^{I2\text{-}E3}$* in **Figure 2-6C**) or the I3-E4 primer pair (*Sxl$^{I3\text{-}E4}$* in **Figure 2-6C**) reveals moderate (1.5-fold) enrichment for intron 2-containing *Sxl* RNAs in *Nab2^{ex3}* heads, and stronger (4.5-fold) enrichment for intron 3-containing RNAs, consistent with elevated m^{6}A on *Sxl* pre-mRNAs that still contain introns 2 and 3. A parallel anti-Flag IP from head lysates of adult females expressing N-terminally tagged Nab2 specifically in neurons (*elav>Flag:Nab2*), coupled with RT-qPCR with I3-E4 primers, indicates that Nab2 associates with unspliced *Sxl* pre-mRNA (**Figure 2-6D**). In sum, these data provide a molecular framework to interpret *Nab2-Mettl3-Sxl* interactions in which Nab2 associates with the *Sxl* pre-mRNA, perhaps via the poly(A) sites located in I2 and I3 (**green**

ticks; **Figure 2-6A**), and prevents its Mettl3-dependent hypermethylation, thus ensuring a level of m^6A necessary to guide *Sxl* exon 3 in the developing female nervous system.

DISCUSSION

Here we have employed an unbiased high-throughput RNA sequencing approach to identify head-enriched RNAs whose levels or structure are significantly affected by Nab2 loss. Bioinformatic filtering of this high read-depth dataset reveals changes in levels and structure of a relatively small set of transcripts, with the latter effect on RNA structure traced to splicing defects - intron retention, alternative 5' and 3' splice site usage, and exon skipping - in a small group of approximately 150 mRNAs. Among these, the most significant change is female-specific inclusion of exon 3 in the *Sxl* mRNA and use of a cryptic 5' splice site within the downstream intron. Because *Sxl* exon 3 contains a stop codon, its inclusion is predicted to disrupt female-specific expression of Sxl protein, a U-rich RNA binding protein that controls somatic and germline sexual identity via effects on splicing and translation of target mRNAs (rev. in Moschall et al., 2017; Penalva and Sanchez, 2003). Bioinformatic and genetic data indicate that *Sxl* mRNA may be an especially significant target of Nab2 in neurons: mis-spliced RNAs in *Nab2* mutant female heads are highly enriched for predicted Sxl binding motifs, and an allele of *Sxl* that constitutively skips exon 3 (Barbash and Cline, 1995) substantially reverses neurodevelopmental and behavioral defects in *Nab2* null females. Moving downstream of Sxl, alleles of male-specific dosage compensation complex (DCC) components, including the direct Sxl target *msl-2* (Bashaw and Baker, 1995, 1997), also rescue phenotypic defects in *Nab2* mutant females. Given that Msl-2 is not normally expressed or active in females, these data provide evidence that masculinized *Sxl* splicing and *msl-2*/DCC activation are important contributors to phenotypes in *Nab2* mutant female flies. These results imply a fairly specific link between Nab2 and the *Sxl* exon 3 splicing machinery, which is confirmed by strong genetic interactions between *Nab2* and the *Mettl3* methyltransferase that deposits m^6A on *Sxl* pre-mRNA and promotes exon 3 skipping (Haussmann et al., 2016; Kan et al., 2017; Lence et al., 2016). Molecular assays provide key insight into these *Nab2*:*Sxl*

interactions. The Nab2 protein associates with unspliced *Sxl* pre-mRNA in head lysates, and its loss results in Mettl3-dependent hypermethylation of mature *Sxl* mRNA and the unspliced *Sxl* pre-mRNA. Given the known role of m^6A in regulating *Sxl* exon 3 splicing, these data imply that Nab2 interacts with the *Sxl* pre-mRNA in the nucleus and opposes excessive m^6A methylation by the Mettl3 complex, thus ensuring a level of m^6A necessary to guide *Sxl* exon 3 skipping in the developing female nervous system.

Our finding are consistent with a fairly specific role for nuclear Nab2 in control of exon-specific splicing patterns within a small subset of head RNAs, most of which are shared between males and females. One Nab2-regulated transcript, the sex determination factor *Sxl*, is a sex-specific target of Nab2 in the female nervous system, and evidence indicates that altered *Sxl* splicing contributes to contributes to their phenotypic defects. As Sxl is itself an RBP that can control splicing, some fraction of the mis-sliced mRNAs detected in our HTS approach may not be direct Nab2 targets, but rather Sxl targets. This hypothesis is supported by the enrichment for predicted Sxl-binding sites among mis-spliced mRNAs in *Nab2* mutant female heads, and by the substantial rescue conferred by the Sxl^{M8} allele. However, splicing of the Sxl target *tra* is unaffected in the *Nab2* mutant RNA-Seq datasets. This could be due to lack of read depth, although this does not seem to be the case (see **Figure 2-S4**), or to Sxl-independent *tra* splicing in adult heads. Unbiased screens for Sxl target RNAs have carried out in ovaries (Primus et al., 2019) and primordial germ cells (Ota et al., 2017), but a similar approach has not been taken in the post-mitotic nervous system, where Sxl targets may differ from other tissue types. In this regard, the subgroup of Nab2-regulated head RNAs that also contain predicted U-rich Sxl binding motifs may be enriched for Sxl targets that contribute to developmental phenotypes in *Nab2* mutants.

The evidence for a *Drosophila* Nab2 role in splicing parallels evidence of accumulation of ~100 intron-containing pre-mRNAs in *S. cerevisiae* lacking the *Nab2* homolog (Soucek et al., 2016), with only a few transcripts affected in yeast, similar to what is observed in the current *Drosophila* study. Rescue of *Nab2* mutants by neuron-restricted expression of human ZC3H14 (Kelly et al., 2014) implies that this specificity may be a conserved element of Nab2/ZC3H14 proteins in higher eukaryotes. Indeed, knockdown of ZC3H14 in cultured vertebrate cells results in pre-mRNA processing defects and intron-specific splicing defects in the few RNAs that have been examined (Morris and Corbett, 2018; Wigington et al., 2016). The basis for Nab2 specificity in *Drosophila* heads is not clear, but it could reflect a high degree of selectivity in binding to nuclear pre-mRNAs (e.g. *Sxl*), or to interactions between Nab2 and a second mechanism that defines splicing targets. The convergence of Mettl3 and Nab2 on the *Sxl* pre-mRNA represents the first evidence that Nab2 can modulate m^6A-dependent control of pre-mRNA splicing. Hypermethylation of *Sxl* that results from Nab2 loss could reflect a requirement to bind A-rich sequences and block access of the Mettl3 complex or to recruitment of an m^6A 'eraser'. Intriguingly the human homolog of *Drosophila* Virilizer, a m^6A methyltransferase subunit and splicing cofactor (Hilfiker et al., 1995; Niessen et al., 2001), was recovered in an IP/mass-spectrometry screen for nuclear interactors of ZC3H14 (Morris and Corbett, 2018), suggesting a potential functional interaction between these proteins on shared target RNAs. Additional evidence that Nab2 restricts m^6A methylation of targets beyond *Sxl* (e.g. *Act5c* and *Usp16*; **Figs. 2-6B and 2-S8**) highlights the possibility that Nab2 may have a broader role in modulating m^6A-dependent RNA processing events, such as splicing, turnover, trafficking and translation.

The robust $Mettl3^{null}$ suppression of $Nab2^{ex3}$ mushroom body (MB) defects is unlikely to be mediated solely by effects on *Sxl*, which has no reported role in MB development. This

observation suggests that Nab2 and Mettl3 have an overlapping set of target RNAs that extends beyond *Sxl*. As almost all *Nab2* mutant phenotypes originate from a Nab2 role in central nervous system neurons (Kelly et al., 2016; Kelly et al., 2014; Pak et al., 2011), suppression by $Mettl3^{null}$ also implies that the Nab2-Mettl3 functional interaction is likely to play out in neurons. The broad phenotypic rescue of $Nab2^{ex3}$ afforded by $Mettl3^{null}$ is consistent with a model in which loss of Nab2 leads to m^6A hypermethylation of Nab2-Mettl3 shared targets, which is then suppressed by removing Mettl3. This 'goldilocks' model is consistent with the *Sxl* data presented here and implies that excessive m^6A caused by loss of Nab2 perturbs neuronal mRNA processing and/or expression in a manner similar to m^6A hypomethylation caused by loss of Mettl3. The precise effect of excess m^6A is unknown, but it could result in excessive recruitment of m^6A 'reader' proteins that overwhelm the specificity of downstream regulatory steps. Significantly, the ability of human *ZC3H14* to rescue $Nab2^{ex3}$ viability and locomotion when expressed in fly neurons indicates that this new m^6A inhibitory role of Nab2 may be conserved within the Nab2/ZC3H14 family of RBPs, and that excessive m^6A methylation of key RNAs also contributes to neurological deficits in *ZC3H14* mutant mice and patients.

MATERIALS AND METHODS

Drosophila stocks and genetics

Drosophila melanogaster stocks and crosses were maintained in humidified incubators at 25ºC with 12hr light-dark cycles. The alleles $Nab2^{ex3}$ (null), $Nab2^{pex41}$ (*precise excision 41*; control) and *UAS-Flag-Nab2* have been described previously (Kelly et al., 2014; Pak et al., 2011). Lines from Bloomington *Drosophila* Stock Center (BDSC): *GMR-Gal4 (*#1350), $elav^{C155}$*-Gal4* (#458), $msl\text{-}2^{227}$ (#5871), $msl\text{-}2^{kmA}$ (#25158), mle^{9} (#5873), $roX1^{ex6}$ (#43647). The $Mettl3^{null}$ allele was a kind gift of J-Y. Roignant. The $Nab2^{ex3}$,$Mettl3^{null}$ chromosome was generated by meiotic recombination and confirmed by genomic PCR (**Figure 2-S6**).

RNA Sequencing (RNA-Seq) on *Drosophila* heads

RNA-Seq was performed on three biological replicates of 60 newly-eclosed adult female and male *Drosophila* heads genotype (control and $Nab2^{ex3}$ mutants). Heads were collected on dry ice, lysed in TRIzol (ThermoFisher), phase-separated with chloroform, and ran through a RNeasy Mini Kit purification column (QIAGEN). Samples were treated with DNase I (QIAGEN) to remove DNA contamination and transported to the University of Georgia's Genomics and Bioinformatics Core for sequencing. rRNA was depleted using a Ribo-Zero Gold Kit (Illumina) and cDNA libraries were prepared using a KAPA Stranded RNA-Seq Kit (Roche). Quality control steps included initial Qubit quantification along with RNA fragment size assessment on an Agilent 2100 Bioanalzyer before and after rRNA depletion. The cDNA libraries were then sequenced for 150 cycles on a NextSeq 500 High Output Flow Cell (Illumina) set to generate paired-end, 75 base-pair (bp) reads. Total sequencing yield across all samples was 81.48 Gbp, equivalent to about 1.1 billion reads in total and 91 million reads per sample. Sequencing accuracy was high; 93.52% of reported bases have a sequencing quality (Q) score greater than or equal to 30.

Read mapping, differential expression, and visualization

Raw read FASTA files were analyzed on the Galaxy web platform (usegalaxy.org Afgan et al., 2018). The BDGP6 release *Drosophila melanogaster* genome (dos Santos et al., 2015) from release 92 of the Ensembl database (Yates et al., 2020) was used as input for subsequent read mapping, annotation, and visualization. Briefly, reads from all four NextSeq500 flow cell lanes were concatenated using the Galaxy *Concatenate datasets tail-to-head (cat)* tool and mapped using RNA STAR (Dobin et al., 2013) with default parameters with some modifications. For each Galaxy tool, version numbers and exact parameters used are detailed in the Table below:

Galaxy software and parameters:

Tool	Concatenate datasets tail-to-head (cat)	Default parameters
	Galaxy Version 0.1.0	
Tool	RNA STAR	Default parameters with the following exceptions:
	Galaxy Version 2.5.2b-0	read type: *paired*
		reference genome: *from history (using Ensembl FASTA and GTF referenced in text)*
Tool	featureCounts	Default parameters with the following exceptions:
	Galaxy Version 1.6.0.3	gene annotation file: *history (Ensembl GTF referenced in text)*
		count fragments instead of reads: *enabled*
		GFF gene identifier: *gene_name*
		strand specificity: *stranded-reverse*
Tool	DESeq2	Default parameters with the following exceptions:
	Galaxy Version 2.11.40.1	factors: *4 levels, each a group of three biological replicates*
		output normalized counts table-*true*
		output all levels vs all levels-*true*
Tool	DEXSeq-Count	Default parameters with the following exceptions:
	Galaxy Version 1.20.1	In 'read count' mode: strand specific library-*yes, reverse*
Tool	DEXSeq	Default parameters with the following exception:
	Galaxy Version 1.20.1	visualize results? - *no*

Gene Ontology (GO) software and parameters

Tool	GO2MSIG	Parameters:
	web interface	data source: *NCBI gene2go*
		taxon ID- *7227*
		evidence codes: *include—EXP, IDA, IEP, IGI, IMP, IPI, ISS, TAS*
		propagate associations - *true*
		use gene- *symbol*
		repress IDs - *no*
		create genesets for - *[1 top level domain only]*
		max. geneset size - *700*
		min. geneset size - *15*
		output format - *gmt*
		database release - *April 2015*
Tool	GSEA Desktop for Windows	Default parameters with the following exceptions:
	v4.0.3	*For up- and downregulated transcripts in Nab2^{ex3} vs. control:*
	GSEA-Preranked	zip-report - *true*
		plot top x - *100*
		create svgs - *true*
		collapse - *No collapse*
		For alternatively spliced transcripts in Nab2^{ex3} vs. control:
		zip-report - *true*
		minimum gene set size - *5*
		create svgs - *true*
		collapse - *No collapse*
Tool	AmiGO 2	Default parameters
	web interface	

Mapped reads were assigned to exons and tallied using featureCounts (Liao et al., 2014) default parameters with some modifications noted above. Differential expression analysis was conducted for all 12 samples using DESeq2 (Love et al., 2014) (Galaxy Version 2.11.40.1) and default parameters with some modifications noted above. Differential exon usage was analyzed using Galaxy Version 1.20.1 of DEXSeq (Anders et al., 2012) and the associated Galaxy tool

DEXSeq-Count in both "*prepare annotation*" and "*count reads*" modes. Both tools were run with the Ensembl GTF with default parameters with some modifications noted above. Unlike with DESeq2, female samples and male samples were compared in independent DEX-Seq analyses. Outputs from all of these tools were downloaded from Galaxy for local analysis, computation, and visualization.

Custom R scripts were written to generate volcano plots and heatmaps. Additional R packages used include ggplot2 (Wickham, 2016) and ggrepel (Slowikowski, 2019). R scripts were written and compiled in RStudio (Team, 2018). Principal component analysis was conducted on Galaxy. Mapped reads were visualized in the Integrative Genomics Viewer (IGV) (Robinson et al., 2017) and annotated based on data available on Flybase (Thurmond et al., 2019). Significant fold change values in either male or female from DESeq2 (adj. p-val<0.05 and $|\log_2 FC|>1$) were plotted, with the color indicating the fold change threshold reached in either males or females. Significantly DE genes (adj. p-val<0.05 and $|\log_2 FC|>1$) were classified by type, as indicated by their gene ID.

Mixtures of Isoforms (MISO) Analysis

Mixtures of isoforms (MISO) (Katz et al., 2010) version 0.5.4 was used to determine percent spliced in (PSI) PSI values for annotated alternative 3' splice sites, alternative 5' splice sites, and retained introns for each sample separately as follows. Alternative splicing annotations were generated using the rnaseqlib (a direct link to script is listed here) (https://rnaseqlib.readthedocs.io/en/clip/) script, gff_make_annotation.py, with flags--flanking-rule commonshortest --genome-label dm6. Replicates for each sample were pooled, and only full-length, mapped reads (76 bp) were used for the MISO analysis since MISO requires all reads input to be of the same length. MISO was run with the flag –prefilter, and the output was then input into

the script, summarize_miso, with the flag --summarize-samples. Next, differential, alternative 5' and 3' splice sites, and differential retained introns, were determined between *Nab2*^{ex3} and control for males and females, separately, using the script, compare_miso, with flag --compare-samples. The output of compare miso was then input into the script, filter_events, with the flags --filter --num-inc 10 --num-exc 10 --num-sum-inc-exc 50 --delta-psi 0.3 --bayes-factor 10, to obtain the final differential PSI values.

Gene ontology (GO) analysis

Gene Set Enrichment Analysis (GSEA) software (Subramanian et al., 2005) was employed for Gene Ontology (GO) analysis (The Gene Ontology Consortium, 2019). For clarity, analyses were conducted separately for each of the three top-level GO domains: *molecular function*, *biological process*, and *cellular component*. GSEA-compatible GO term gene sets for *Drosophila melanogaster* were acquired using the GO2MSIG web interface (Powell, 2014). GSEA Desktop for Windows, v4.0.3 (Broad Institute) was then used to identify two distinct classes of GO terms, independently for females and for males: (1) terms enriched among up- and downregulated transcripts in *Nab2*^{ex3} compared to controls, and (2) terms enriched among transcripts alternatively spliced in *Nab2*^{ex3} compared to controls. For the first class, inputs consisted of all genes whose expression could be compared by DESeq2 (i.e. adjusted *p*-value ≠ NA). For the second class, inputs consisted of all genes with previously annotated alternative splicing events according to MISO. To identify the first class of GO terms, genes were ranked by $\log_2$ (fold change) calculated by DESeq2 and analyzed by the GSEA-Pre-ranked tool. To identify the second class of GO terms, genes with were ranked by the absolute value of the difference in PSI (percent spliced in) between *Nab2*^{ex3} and control calculated by MISO. This second ranking was analyzed by the GSEA-Preranked tool. Enriched GO terms (nominal *p*-value<0.05) identified for the first class were

evaluated manually, surfacing multiple terms directly related to splicing. Enriched GO terms (nominal p-value<0.05) for the second class were ordered by normalized enrichment score (NES) and evaluated to identify the top "independent" GO terms. Terms were defined as "independent" by reference to their position in the GO hierarchy as reported on each term's "Inferred Tree View" page of the AmiGO2 GO database web tool (Carbon et al., 2009). "Independent" terms had no parent, child, or sibling terms in the GO hierarchy associated with a higher NES than their own.

RBPs Motif Enrichment Analysis using Mixture of Isoforms (MISO) Analysis

RNA sequences were taken at differentially retained introns and alternative 3' and 5' splice sites obtained from the MISO analysis on males and females separately (*Nab2*^{ex3} mutants vs. control). The sequence for each of these went 25 bp into the exon(s) of interest and 1 kb into the intron of interest. In the case of alternative 3' and 5' splice sites, the sequences went 25 bp into the exon starting from the alternative spice site that is closest to the center of the exon (i.e. the inner-most splice site), and 1 kb into the intron starting from that inner-most spice site. To convert these to RNA sequences, DNA sequences were first obtained using fastaFromBed (Quinlan and Hall, 2010), and then all T's were converted to U's with a custom script. To obtain putative binding sites for RBPs at these sequences, they were then input into fimo using the flags --text --max-strand and the "Ray2013_rbp_Drosophila_melanogaster.meme" file (Grant et al., 2011).

RNA isolation for reverse transcription (RT) PCR and real-time qPCR

Total RNA was isolated from adult tissues with TRIzol (Invitrogen) and treated with DNase I (Qiagen). For RT-PCR, cDNA was generated using SuperScript III First Strand cDNA Synthesis (Invitrogen) from 2µg of total RNA, and PCR products were resolved and imaged on 2% agarose gels (BioRad Image). Quantitative real-time PCR (qPCR) reactions were carried out in biological triplicate with QuantiTect SYBR Green Master Mix using an Applied Biosystems StepOne Plus

real-time machine (ABI). Results were analyzed using the ΔΔCT method, normalized as indicated (e.g. to *Act5C*), and plotted as fold-change relative to control.

Primers used for RT and qPCR analysis:

Name	Sequence	Detects
***Sxl* pre-mRNA**	Fwd: AGAACCAAAACTCCCTTACAGC Rev: GTGAGTGTCTTTCGCTTTTCG	intron2-exon3
***Sxl* pre-mRNA**	Fwd: ACCAATAACCGACAACACAATC Rev: ACATCCCAAATCCACGCCCACC	intron3-exon4
***Sxl* mRNA** ***Sxl* RT-PCR**	Fwd: GCTGAGCGCCAAAACAATTG Rev: AGGTGAGTTTCGGTTTTACAGG Fwd: ACACAAGAAAGTTGAACAGAGG Rev: CATTCCGGATGGCAGAGAATGG	exon2-exon2 exon 2-3-4
***Sxl* mRNA** **exon 2-4 transcript**	Fwd: GATTGAATCTCGATCATCGTTC Rev: CATTCCGGATGGCAGAGAATGG	exon2-exon4
***Sxl* mRNA** **exon 2-3 transcript**	Fwd: CGAAAAGCGAAAGACACTCACTG Rev: CATTCCGGATGGCAGAGAATGG	exon3-exon4
Act5C	Fwd: GAGCGCGGTTACTCTTTCAC Rev: ACTTCTCCAACGAGGAGCTG	*Actin5C*
USP-16-45-RF	Fwd: ACACTTGGTCACGTCGTTCA Rev: GGGCGCGCTCTTGAATTTAC	*USP-16*

Viability and lifespan analysis

Viability at 25°C was measured by assessing eclosion rates of among 100 wandering L3 larvae collected for each genotype and sex, and then reared in a single vial. Hatching was recorded for 5-6 days. At least 3 independents biological replicates per sex/genotype were tested and significance was calculated using grouped analysis on GraphPad (Prism). Lifespan was assessed at 25°C as described previously (Morton et al., 2020). In brief, newly eclosed animals were collected, separated by sex, placed in vials (10 per vial), and transferred to fresh vials weekly. Survivorship was scored daily. At least 3 independents biological replicates per vials of each genotype was tested and significance was calculated using grouped analysis on GraphPad (Prism).

Locomotion assays

Negative geotaxis was tested as previously described (Morton et al., 2020). Briefly, newly eclosed flies (day 0) were collected, divided into groups of 10 male or females, and kept in separate vials for 2-5days. Cohorts of age-matched flies were then transferred to a 25-ml graduated cylinder for analysis. At least three biological replicates per sex were analyzed per genotype on GraphPad (Prism).

Brain dissection and mushroom body (MB) imaging

Brain dissections were performed essentially as previously described in (Kelly et al., 2016). Briefly, adult brains were dissected in PBT (1xPBS, 0.1% TritonX-100) and collected in PBS at 4ºC. Brains were then fixed in 4% paraformaldehyde at RT, washed 3x in PBS, and incubated in 0.3% PBS-T (1xPBS, 0.3% TritonX-100). Following blocking for 1hr (0.1% PBS-T, 5% normal goat serum), brains were stained overnight in block+primary antibodies. After 5x washes in PBT, brains were incubated in block for 1hr and transferred into in block+secondary antibody for 3hrs. Brains were then washed 5x in PBT and mounted in Vectashield (Vector Labs). The FasII antibody clone 1D4 (Developmental Studies Hybridoma Bank) was used to label MBs at a 1:50 dilution. Whole brain images were captured with a 20x objective. Maximum intensity projections were obtained by combining serial optical sections (Z-stacks) with Nikon A1R HD25 software using Fiji. The number of α-lobe and β-lobe defects (e.g. thin, missing or fused) were scored analyzed using GraphPad (Prism).

Flag and m^{6}A RNA immunoprecipitation (Flag-RIP and MeRIP)

The FLAG-RIP and MeRIP protocols were performed using previously described protocols in (Bienkowski et al., 2017) and (Lence et al., 2016) with some modification. Briefly, three replicates of 30 newly eclosed female flies were collected in 1.5 ml Eppendorf tubes and frozen in dry ice.

Heads were removed with a 5.5 Dumont tweezer and homogenized with a mortar/pestle in Isolation buffer (50 mM Tris-HCl pH 8.1, 10 mM EDTA, 150 mM NaCl, and 1% SDS, 50 mM NaCl). This was diluted into IP buffer (50 mM HEPES, 150 mM NaCl, 5 mM EDTA, 0.5 mM DTT, 0.1% NP-40) supplemented with protease inhibitors (Roche) and RNasin Plus Inhibitor (Promega). Lysates were incubated with anti-Flag (M2 clone; Sigma) or anti-m^6A (Synaptic Systems) antibodies and recovered on magnetic Protein G Dynabeads (Invitrogen). After overnight incubation at 4ºC with rocking. Beads were washed 5x in IP buffer and RNA was isolated from antibody-bead precipitates, or controls (input samples) using TRIzol (ThermoFisher). Samples were treated with DNase-I and RNA was purified using RNeasy Kit (Qiagen).

Statistical Analysis

Group analysis on biological triplicate experiments was done using Two-way ANOVA (Turkey's multiple comparison test) on GraphPad (Prism) Version 8.4.2(464). Sample sizes (n) and *p*-values are denoted in the text or figures and noted by asterisks (for example, $*p<0.05$).

ACKNOWLEDGMENTS

Stocks obtained from the Bloomington Drosophila Stock Center/BDSC (NIH P40OD018537) were used in this study. We thank members of the Moberg and Corbett Labs for helpful discussions and advice, and B. Bixler, J. Tanquary, and C. Bowen for their contributions. We also thank M. Alabady (Georgia Genomics and Bioinfomatics Core) for technical support, and T. Lence and J.-Y. Roignant (Lausanne) for the gift of the *Mettl3* allele, and T. Cline (Berkeley) for discussions and insights on the *Sxl[M8]* allele. This work was funded by grants from the National Institute of Health to K.H.M. and A.H.C (R01 MH10730501), J.C.R. (F31 HD088043), and B.J. (F31 NS103595). B.J. and B.E.B were also supported during portions of the study by The Emory Initiative to Maximize Student Development (NIH R25 GM125598).

Competing Interests

The authors declare no competing interests.

REFERENCES

Afgan, E., Baker, D., Batut, B., van den Beek, M., Bouvier, D., Cech, M., Chilton, J., Clements, D., Coraor, N., Gruning, B.A., *et al.* (2018). The Galaxy platform for accessible, reproducible and collaborative biomedical analyses: 2018 update. Nucleic Acids Res *46*, W537-W544

Amrein, H., and Axel, R. (1997). Genes expressed in neurons of adult male Drosophila. Cell *88*, 459-469

Anders, S., Reyes, A., and Huber, W. (2012). Detecting differential usage of exons from RNA-seq data. Genome Res *22*, 2008-2017

Armstrong, J.D., de Belle, J.S., Wang, Z., and Kaiser, K. (1998). Metamorphosis of the mushroom bodies; large-scale rearrangements of the neural substrates for associative learning and memory in Drosophila. Learn Mem *5*, 102-114

Ashburner, M., Ball, C.A., Blake, J.A., Botstein, D., Butler, H., Cherry, J.M., Davis, A.P., Dolinski, K., Dwight, S.S., Eppig, J.T., *et al.* (2000). Gene ontology: Tool for the unification of biology (NIH Public Access), pp. 25-29.

Barbash, D.A., and Cline, T.W. (1995). Genetic and molecular analysis of the autosomal component of the primary sex determination signal of Drosophila melanogaster. Genetics *141*, 1451-1471

Bashaw, G.J., and Baker, B.S. (1995). The msl-2 dosage compensation gene of Drosophila encodes a putative DNA-binding protein whose expression is sex specifically regulated by Sex-lethal. Development *121*, 3245-3258

Bashaw, G.J., and Baker, B.S. (1997). The regulation of the Drosophila msl-2 gene reveals a function for Sex-lethal in translational control. Cell *89*, 789-798

Bell, L.R., Maine, E.M., Schedl, P., and Cline, T.W. (1988). Sex-lethal, a Drosophila sex determination switch gene, exhibits sex-specific RNA splicing and sequence similarity to RNA binding proteins. Cell *55*, 1037-1046

Bevan, C., Roote, J., Russell, S., Ashburner, M. (1993). On the allelism of killer-of-male and male-specific lethal mutations. Drosophila Information Service *72*, 125

Bienkowski, R.S., Banerjee, A., Rounds, J.C., Rha, J., Omotade, O.F., Gross, C., Morris, K.J., Leung, S.W., Pak, C., Jones, S.K., *et al.* (2017). The Conserved, Disease-Associated RNA Binding Protein dNab2 Interacts with the Fragile X Protein Ortholog in Drosophila Neurons. Cell Rep *20*, 1372-1384

Brinegar, A.E., and Cooper, T.A. (2016). Roles for RNA-binding proteins in development and disease. Brain research *1647*, 1-8

Carbon, S., Ireland, A., Mungall, C.J., Shu, S., Marshall, B., Lewis, S., Ami, G.O.H., and Web Presence Working, G. (2009). AmiGO: online access to ontology and annotation data. Bioinformatics *25*, 288-289

Conlon, E.G., and Manley, J.L. (2017). RNA-binding proteins in neurodegeneration: mechanisms in aggregate. Genes Dev *31*, 1509-1528

Darnell, J.C., and Richter, J.D. (2012). Cytoplasmic RNA-binding proteins and the control of complex brain function. Cold Spring Harb Perspect Biol *4*, a012344

Dobin, A., Davis, C.A., Schlesinger, F., Drenkow, J., Zaleski, C., Jha, S., Batut, P., Chaisson, M., and Gingeras, T.R. (2013). STAR: ultrafast universal RNA-seq aligner. Bioinformatics *29*, 15-21

dos Santos, G., Schroeder, A.J., Goodman, J.L., Strelets, V.B., Crosby, M.A., Thurmond, J., Emmert, D.B., Gelbart, W.M., and FlyBase, C. (2015). FlyBase: introduction of the Drosophila melanogaster Release 6 reference genome assembly and large-scale migration of genome annotations. Nucleic Acids Res *43*, D690-697

Fasken, M.B., Corbett, A.H., and Stewart, M. (2019). Structure-function relationships in the Nab2 polyadenosine-RNA binding Zn finger protein family. Protein Sci *28*, 513-523

Gawande, B., Robida, M.D., Rahn, A., and Singh, R. (2006). Drosophila Sex-lethal protein mediates polyadenylation switching in the female germline. EMBO J *25*, 1263-1272

Gerstberger, S., Hafner, M., and Tuschl, T. (2014). A census of human RNA-binding proteins. Nature Reviews Genetics *15*, 829-845

Grant, C.E., Bailey, T.L., and Noble, W.S. (2011). FIMO: scanning for occurrences of a given motif. Bioinformatics *27*, 1017-1018

Harrison, D.A. (2007). Sex determination: controlling the master. Curr Biol *17*, R328-330

Haussmann, I.U., Bodi, Z., Sanchez-Moran, E., Mongan, N.P., Archer, N., Fray, R.G., and Soller, M. (2016). m(6)A potentiates Sxl alternative pre-mRNA splicing for robust Drosophila sex determination. Nature

Heisenberg, M. (2003). Mushroom body memoir: from maps to models. Nature reviews Neuroscience *4*, 266-275

Hilfiker, A., Amrein, H., Dubendorfer, A., Schneiter, R., and Nothiger, R. (1995). The gene virilizer is required for female-specific splicing controlled by Sxl, the master gene for sexual development in Drosophila. Development *121*, 4017-4026

Horabin, J.I., and Schedl, P. (1993). Regulated splicing of the Drosophila sex-lethal male exon involves a blockage mechanism. Molecular and cellular biology *13*, 1408-1414

Kan, L., Grozhik, A.V., Vedanayagam, J., Patil, D.P., Pang, N., Lim, K.S., Huang, Y.C., Joseph, B., Lin, C.J., Despic, V.*, et al.* (2017). The m(6)A pathway facilitates sex determination in Drosophila. Nat Commun *8*, 15737

Katz, Y., Wang, E.T., Airoldi, E.M., and Burge, C.B. (2010). Analysis and design of RNA sequencing experiments for identifying isoform regulation. Nat Methods *7*, 1009-1015

Keller, C.I., and Akhtar, A. (2015). The MSL complex: juggling RNA-protein interactions for dosage compensation and beyond. Curr Opin Genet Dev *31*, 1-11

Kelley, R.L., Solovyeva, I., Lyman, L.M., Richman, R., Solovyev, V., and Kuroda, M.I. (1995). Expression of msl-2 causes assembly of dosage compensation regulators on the X chromosomes and female lethality in Drosophila. Cell *81*, 867-877

Kelly, S.M., Bienkowski, R., Banerjee, A., Melicharek, D.J., Brewer, Z.A., Marenda, D.R., Corbett, A.H., and Moberg, K.H. (2016). The Drosophila ortholog of the Zc3h14 RNA binding protein acts within neurons to pattern axon projection in the developing brain. Dev Neurobiol *76*, 93-106

Kelly, S.M., Leung, S.W., Apponi, L.H., Bramley, A.M., Tran, E.J., Chekanova, J.A., Wente, S.R., and Corbett, A.H. (2010). Recognition of polyadenosine RNA by the zinc finger domain of nuclear poly(A) RNA-binding protein 2 (Nab2) is required for correct mRNA 3'-end formation. J Biol Chem *285*, 26022-26032

Kelly, S.M., Leung, S.W., Pak, C., Banerjee, A., Moberg, K.H., and Corbett, A.H. (2014). A conserved role for the zinc finger polyadenosine RNA binding protein, ZC3H14, in control of poly(A) tail length. RNA *20*, 681-688

Lence, T., Akhtar, J., Bayer, M., Schmid, K., Spindler, L., Ho, C.H., Kreim, N., Andrade-Navarro, M.A., Poeck, B., Helm, M.*, et al.* (2016). m(6)A modulates neuronal functions and sex determination in Drosophila. Nature *540*, 242-247

Lence, T., Soller, M., and Roignant, J.Y. (2017). A fly view on the roles and mechanisms of the m(6)A mRNA modification and its players. RNA Biol *14*, 1232-1240

Leung, S.W., Apponi, L.H., Cornejo, O.E., Kitchen, C.M., Valentini, S.R., Pavlath, G.K., Dunham, C.M., and Corbett, A.H. (2009). Splice variants of the human ZC3H14 gene generate multiple isoforms of a zinc finger polyadenosine RNA binding protein. Gene *439*, 71-78

Liao, Y., Smyth, G.K., and Shi, W. (2014). featureCounts: an efficient general purpose program for assigning sequence reads to genomic features. Bioinformatics *30*, 923-930

Love, M.I., Huber, W., and Anders, S. (2014). Moderated estimation of fold change and dispersion for RNA-seq data with DESeq2. Genome Biology *15*, 550-550

Lucchesi, J.C., and Kuroda, M.I. (2015). Dosage compensation in Drosophila. Cold Spring Harb Perspect Biol *7*

Meller, V.H., Wu, K.H., Roman, G., Kuroda, M.I., and Davis, R.L. (1997). roX1 RNA paints the X chromosome of male Drosophila and is regulated by the dosage compensation system. Cell *88*, 445-457

Mootha, V.K., Lindgren, C.M., Eriksson, K.F., Subramanian, A., Sihag, S., Lehar, J., Puigserver, P., Carlsson, E., Ridderstråle, M., Laurila, E.*, et al.* (2003). PGC-1α-responsive genes involved in oxidative phosphorylation are coordinately downregulated in human diabetes. Nature Genetics *34*, 267-273

Morris, K.J., and Corbett, A.H. (2018). The polyadenosine RNA-binding protein ZC3H14 interacts with the THO complex and coordinately regulates the processing of neuronal transcripts. Nucleic Acids Res *46*, 6561-6575

Morton, D.J., Jalloh, B., Kim, L., Kremsky, I., Nair, R.J., Nguyen, K.B., Rounds, J.C., Sterrett, M.C., Brown, B., Le, T.*, et al.* (2020). A Drosophila model of Pontocerebellar Hypoplasia reveals a critical role for the RNA exosome in neurons. PLoS Genet *16*, e1008901

Moschall, R., Gaik, M., and Medenbach, J. (2017). Promiscuity in post-transcriptional control of gene expression: Drosophila sex-lethal and its regulatory partnerships. FEBS Lett *591*, 1471-1488

Niessen, M., Schneiter, R., and Nothiger, R. (2001). Molecular identification of virilizer, a gene required for the expression of the sex-determining gene Sex-lethal in Drosophila melanogaster. Genetics *157*, 679-688

Ota, R., Morita, S., Sato, M., Shigenobu, S., Hayashi, M., and Kobayashi, S. (2017). Transcripts immunoprecipitated with Sxl protein in primordial germ cells of Drosophila embryos. Dev Growth Differ *59*, 713-723

Pak, C., Garshasbi, M., Kahrizi, K., Gross, C., Apponi, L.H., Noto, J.J., Kelly, S.M., Leung, S.W., Tzschach, A., Behjati, F.*, et al.* (2011). Mutation of the conserved polyadenosine RNA binding protein, ZC3H14/dNab2, impairs neural function in Drosophila and humans. Proc Natl Acad Sci U S A *108*, 12390-12395

Penalva, L.O., and Sanchez, L. (2003). RNA binding protein sex-lethal (Sxl) and control of Drosophila sex determination and dosage compensation. Microbiol Mol Biol Rev *67*, 343-359, table of contents

Powell, J.A. (2014). GO2MSIG, an automated GO based multi-species gene set generator for gene set enrichment analysis. BMC Bioinformatics *15*, 146

Primus, S., Pozmanter, C., Baxter, K., and Van Doren, M. (2019). Tudor-domain containing protein 5-like promotes male sexual identity in the Drosophila germline and is repressed in females by Sex lethal. PLoS Genet *15*, e1007617

Quinlan, A.R., and Hall, I.M. (2010). BEDTools: a flexible suite of utilities for comparing genomic features. Bioinformatics *26*, 841-842

Rha, J., Jones, S.K., Fidler, J., Banerjee, A., Leung, S.W., Morris, K.J., Wong, J.C., Inglis, G.A.S., Shapiro, L., Deng, Q.*, et al.* (2017). The RNA-binding Protein, ZC3H14, is Required for Proper Poly(A) Tail Length Control, Expression of Synaptic Proteins, and Brain Function in Mice. Hum Mol Genet

Robinson, J.T., Thorvaldsdottir, H., Wenger, A.M., Zehir, A., and Mesirov, J.P. (2017). Variant Review with the Integrative Genomics Viewer. Cancer Res *77*, e31-e34

Sakamoto, H., Inoue, K., Higuchi, I., Ono, Y., and Shimura, Y. (1992). Control of Drosophila Sex-lethal pre-mRNA splicing by its own female-specific product. Nucleic Acids Res *20*, 5533-5540

Sanchez, L., Gorfinkiel, N., and Guerrero, I. (2001). Sex determination genes control the development of the Drosophila genital disc, modulating the response to Hedgehog, Wingless and Decapentaplegic signals. Development *128*, 1033-1043

Slowikowski, K. (2019). ggrepel: Automatically Position Non-Overlapping Text Labels with 'ggplot2'.
Smith, R.W., Blee, T.K., and Gray, N.K. (2014). Poly(A)-binding proteins are required for diverse biological processes in metazoans. Biochem Soc Trans *42*, 1229-1237

Soldano, A., Worpenberg, L., Paolantoni, C., Longhi, S., Mulorz, M.M., Lence, T., Wessels, H.-H., Aiello, G., Notarangelo, M., and Sutandy, F.R. (2020). The m6A reader Ythdf restricts axonal growth in Drosophila through target selection modulation of the Fragile X mental retardation protein. bioRxiv

Soucek, S., Zeng, Y., Bellur, D.L., Bergkessel, M., Morris, K.J., Deng, Q., Duong, D., Seyfried, N.T., Guthrie, C., Staley, J.P.*, et al.* (2016). The Evolutionarily-conserved Polyadenosine RNA Binding Protein, Nab2, Cooperates with Splicing Machinery to Regulate the Fate of pre-mRNA. Molecular and cellular biology *36*, 2697-2714

Subramanian, A., Tamayo, P., Mootha, V.K., Mukherjee, S., Ebert, B.L., Gillette, M.A., Paulovich, A., Pomeroy, S.L., Golub, T.R., Lander, E.S.*, et al.* (2005). Gene set enrichment analysis: a knowledge-based approach for interpreting genome-wide expression profiles. Proc Natl Acad Sci U S A *102*, 15545-15550

Team, R.S. (2018). RStudio: Integrated Development Environment for R (Boston, MA: RStudio, Inc.).

The Gene Ontology Consortium (2019). The Gene Ontology Resource: 20 years and still GOing strong. Nucleic Acids Research *47*, D330-D338

Thurmond, J., Goodman, J.L., Strelets, V.B., Attrill, H., Gramates, L.S., Marygold, S.J., Matthews, B.B., Millburn, G., Antonazzo, G., Trovisco, V.*, et al.* (2019). FlyBase 2.0: the next generation. Nucleic Acids Res *47*, D759-D765

Wan, L., Dockendorff, T.C., Jongens, T.A., and Dreyfuss, G. (2000). Characterization of dFMR1, a Drosophila melanogaster homolog of the fragile X mental retardation protein. Molecular and cellular biology *20*, 8536-8547

Wickham, H. (2016). ggplot2 : Elegant Graphics for Data Analysis. In Use R!, (Cham: Springer International Publishing : Imprint: Springer,), pp. 1 online resource (XVI, 260 pages 232 illustrations, 140 illustrations in color.
Wigington, C.P., Morris, K.J., Newman, L.E., and Corbett, A.H. (2016). The Polyadenosine RNA-binding Protein, Zinc Finger Cys3His Protein 14 (ZC3H14), Regulates the Pre-mRNA Processing of a Key ATP Synthase Subunit mRNA. J Biol Chem *291*, 22442-22459

Yates, A.D., Achuthan, P., Akanni, W., Allen, J., Allen, J., Alvarez-Jarreta, J., Amode, M.R., Armean, I.M., Azov, A.G., Bennett, R.*, et al.* (2020). Ensembl 2020. Nucleic Acids Res *48*, D682-D688

FIGURES AND TABLES

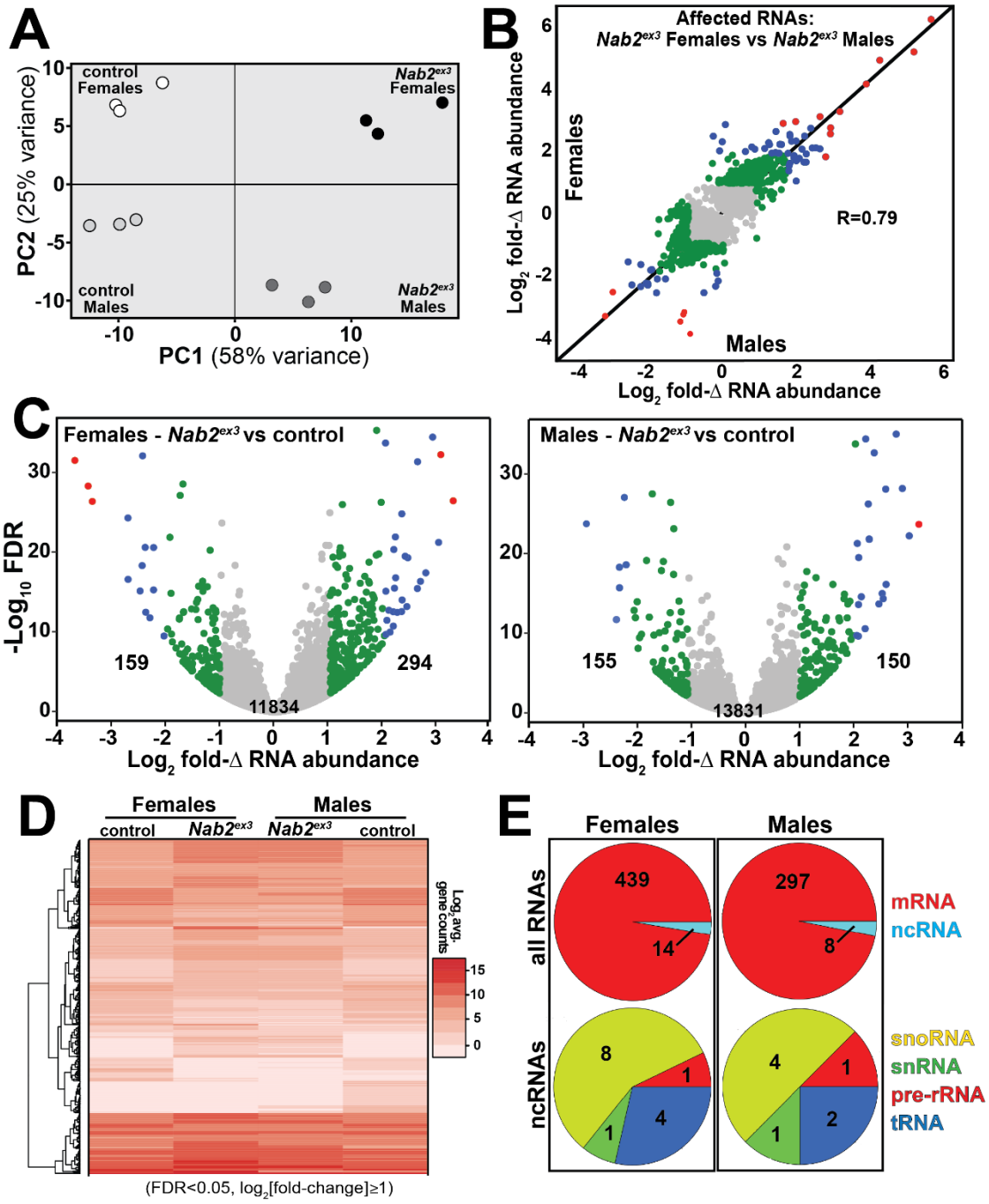

Figure 2-1. RNA sequencing detects effects of Nab2 loss on the head transcriptome. (A) Principal component analysis (PCA) of RNA-seq data from three biological replicates of control and *Nab2* mutant (*Nab2*^{ex3}) male and female heads. **(B)** Correlation scatter plot of $\log_2$ fold-change

(Δ) in abundance of affected RNAs in males and females (log_2 average gene counts: **grey**<1, 1≤**green**<2, 2≤**blue**<3, **red**≥3). **(C)** Volcano plots of fold-Δ in abundance vs. false discovery rate (FDR -log_{10}) of affected RNAs in *Nab2*^{ex3} females and males (dot plot color coding as in B). Elevated (≥1), reduced (≤-1), and total RNAs are indicated. **(D)** Heatmap comparison of significantly changed gene counts (FDR<0.05; |log_2 fold-Δ|≥1) in *Nab2*^{ex3} females and males vs. sex-matched controls. **(E)** Pie chart shows distribution of RNA classes among significantly affected RNAs detected in **C** and **D**.

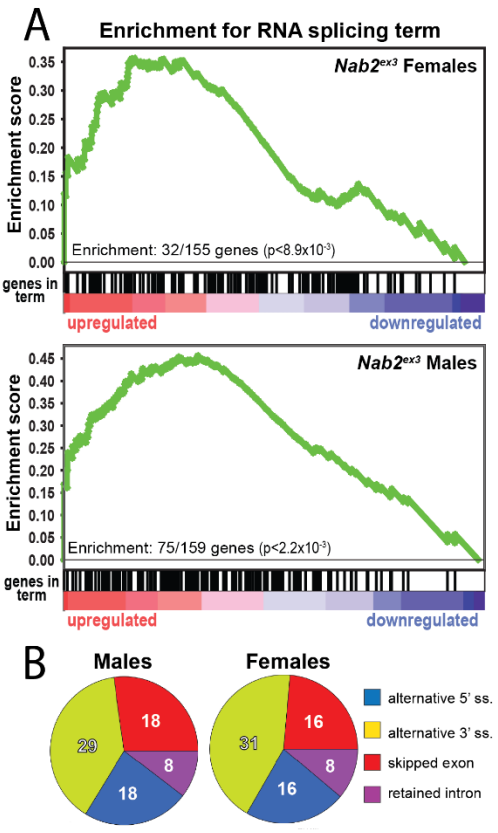

Figure 2-2. Significantly up/down-regulated RNAs in *Nab2*^{ex3} heads are enriched for predicted splicing factors. (A) Gene set enrichment analysis (GSEA) detects enrichment for the 'RNA splicing' GO term in up- and down-regulated gene sets in both female (top) and male (bottom) *Nab2*^{ex3} datasets. Gene enrichments are indicated with corresponding p-values. **(B)** Pie chart illustrating the distribution of previously annotated alternative splicing RNA splicing events that are significantly altered in *Nab2*^{ex3} mutant female and male heads (ss=splice site).

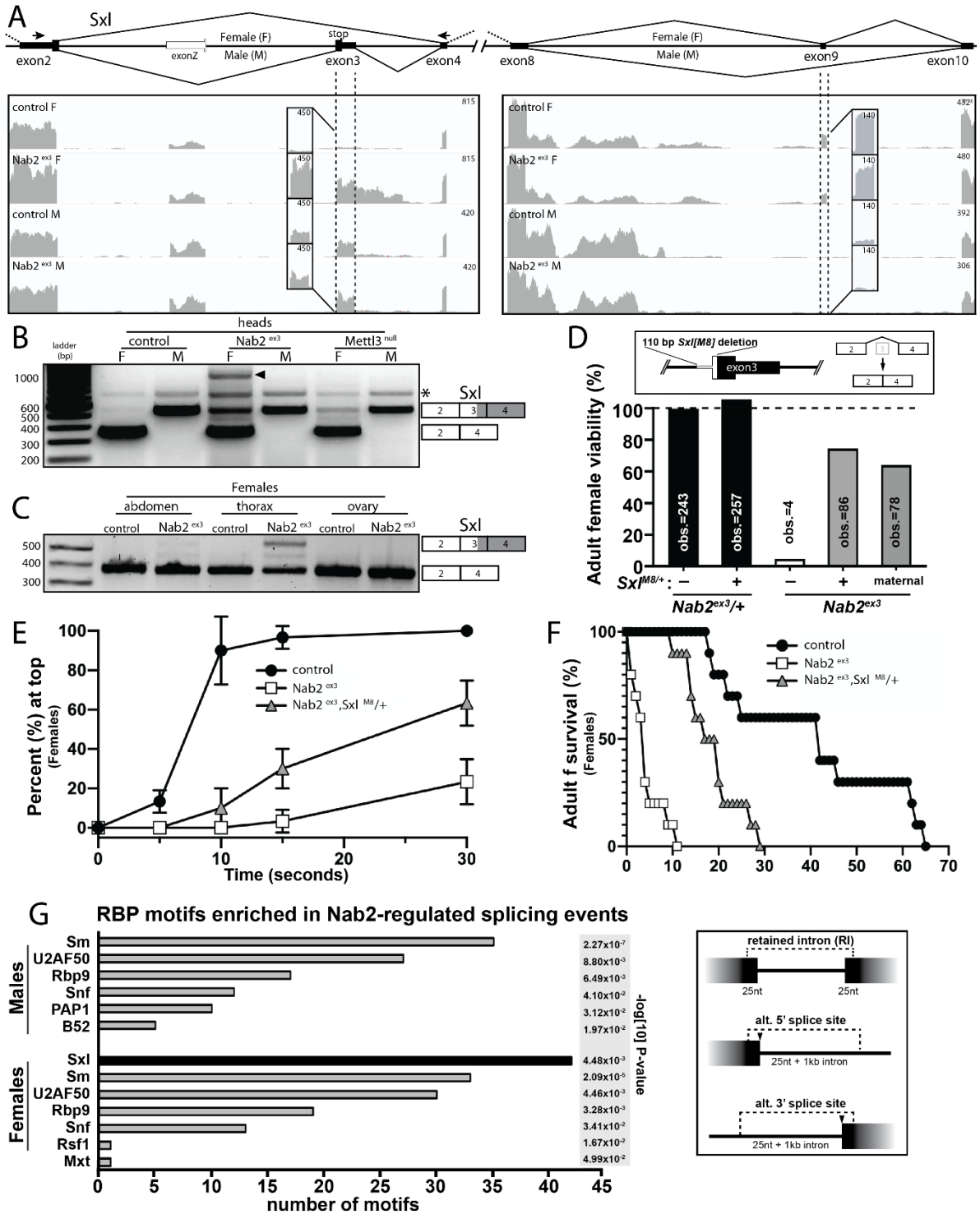

Figure 2-3. Alternative splicing of *Sxl* is disrupted in *Nab2^{ex3}* female heads. **(A) Top panel**: normal *Sxl* alternative splicing patterns across the exon 2-4 and exon 8-10 regions in females (F) and males (M). Arrows indicate location of primers used in **B**. **Bottom panel**: corresponding

sequencing reads across the *Sxl* locus in the indicated sexes and genotypes. Dotted lines and boxed insets highlight exon 3 and exon 9 reads. **(B)** RT-PCR analysis of *Sxl* mRNA in control, $Nab2^{ex3}$ and $Mettl3^{null}$ male (M) and female (F) heads. Exon 2-3-4 and exon 2-4 bands are indicated. Arrowhead denotes exon 2-3-intron-4 product noted in text. Asterisk (*) is non-specific product. **(C)** RT-PCR analysis of *Sxl* mRNA in adult female (F) control and $Nab2^{ex3}$ tissues using the same primers as in **B** and with exon 2-3-4 and 2-4 bands indicated. **(D)** A single copy of the Sxl^{M8} allele, which harbors a 110 bp deletion that causes constitutive exon2-4 splicing, partially suppresses lethality of $Nab2^{ex3}$ females, both zygotically and maternally. **(E-F)** Sxl^{M8} dominantly (i.e. *M8/+*) suppresses previously defined locomotion (as assessed by negative-geotaxis) and life-span defects among age-matched $Nab2^{e3}$ females. **(G)** RNA binding protein (RBM) motif enrichment analysis detects predicted Sxl binding sites as the most frequent motif among Nab2-regulated splicing events in female heads. Other enriched motifs are similar between male and female heads. Regions used for motif analysis (retained introns, and alternative 5' or 3' splice sites plus flanking sequence) are shown in the schematic.

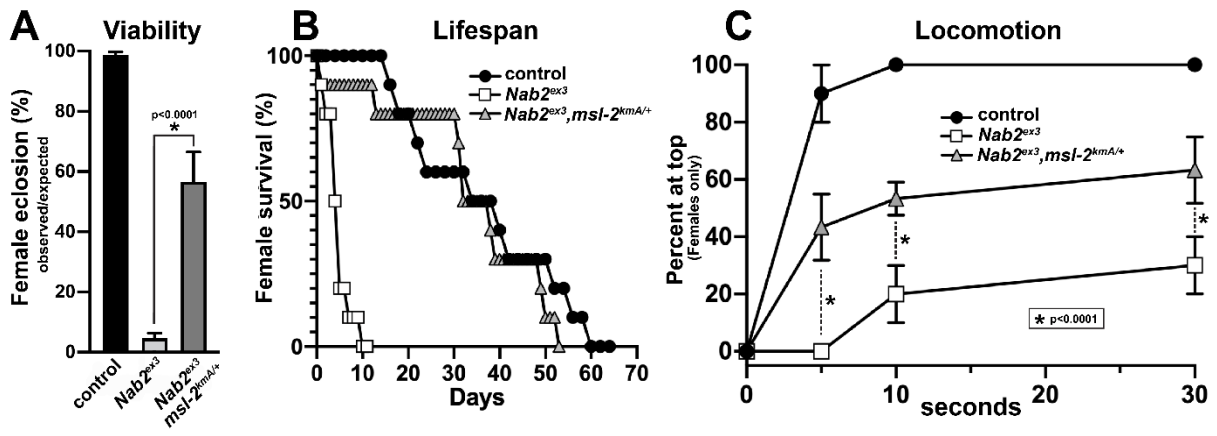

Figure 2-4. An allele of the DCC component *male-specific lethal-2* (*msl*-2) rescues *Nab2* phenotypes in females. (A) Percent of control, $Nab2^{ex3}$, and $msl\text{-}2^{kmA}/+;;Nab2^{ex3}$ (*msl*-2 is on the X chromosome) females eclosing as viable adults (calculated as #observed/#expected). **(B)** Survival of age-matched adult female flies of the same genotypes. **(C)** Negative geotaxis of age-matched adult females of the same genotypes at 5sec, 10sec and 30 sec timepoints. Significance values are indicated (*p<0.0001).

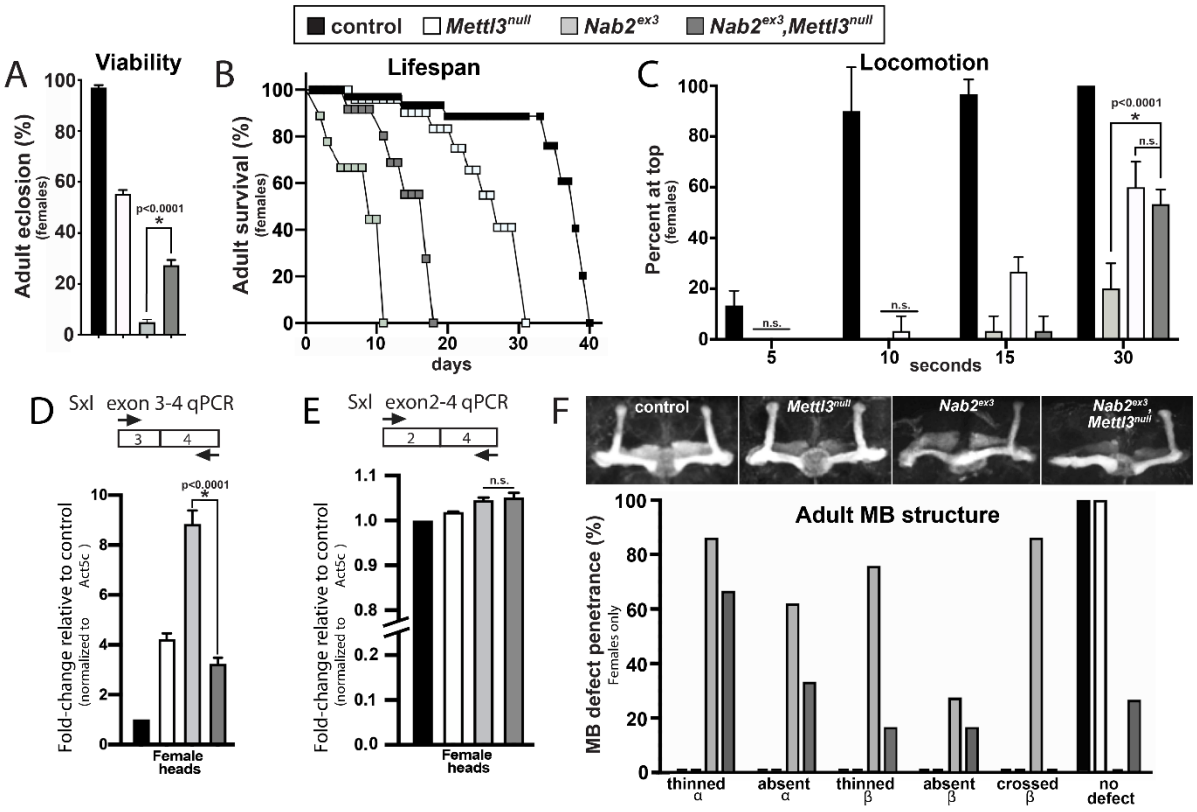

Figure 2-5. Removing the Mettl3 m^{6}A transferase suppresses viability, behavioral, neuroanatomical and *Sxl* splicing defects in *Nab2* mutant females. Color coding as indicated: control (**black** fill), *Mettl3*$^{null/null}$ (white fill), *Nab2*$^{ex3/3x3}$ (light grey fill), and *Nab2*$^{ex3/ex3}$,*Mettl3*$^{null/null}$ (**dark grey** fill). **(A)** Percent of control, *Nab2*^{ex3} and *Nab2*^{ex3},*Mettl3*^{null} females eclosing as viable adults (calculated as #observed/#expected). **(B)** Survival of age-matched adult female flies of the indicated genotypes. **(C)** Negative geotaxis of adult females of the indicated genotypes at indicated timepoints. Significance values are indicated at the 30sec timepoint (* p<0.0001; n.s.=not significant). **(D-E)** Quantitative real-time PCR analysis of the abundance of *Sxl* mRNA variants containing **(D)** the E3-E4 (exon3-exon4) or **(E)** the E2-E4 splice forms in female heads of the indicated genotypes. Primers denoted by arrows in the cartoon schematic. CT values are relative to control (*Nab2*^{pex41}) and normalized to *Act5c* control (*p<0.0001; n.s.=not significant). **(F) Top panel:** representative Z-stacked confocal images of

anti-Fas2 staining to visualize MBs in female brains of indicated genotypes. **Bottom panel:** penetrance of MB phenotypes (thinned/absent α-lobes, thinned/absent β-lobes, and β-lobes mid-line crossing) in adult females of indicated genotypes (n=30 per genotype). Note that β-lobe crossing characteristic of *Nab2* nulls (>80% penetrance, light grey bar) is completely suppressed by loss of *Mettl3* (dark grey bar).

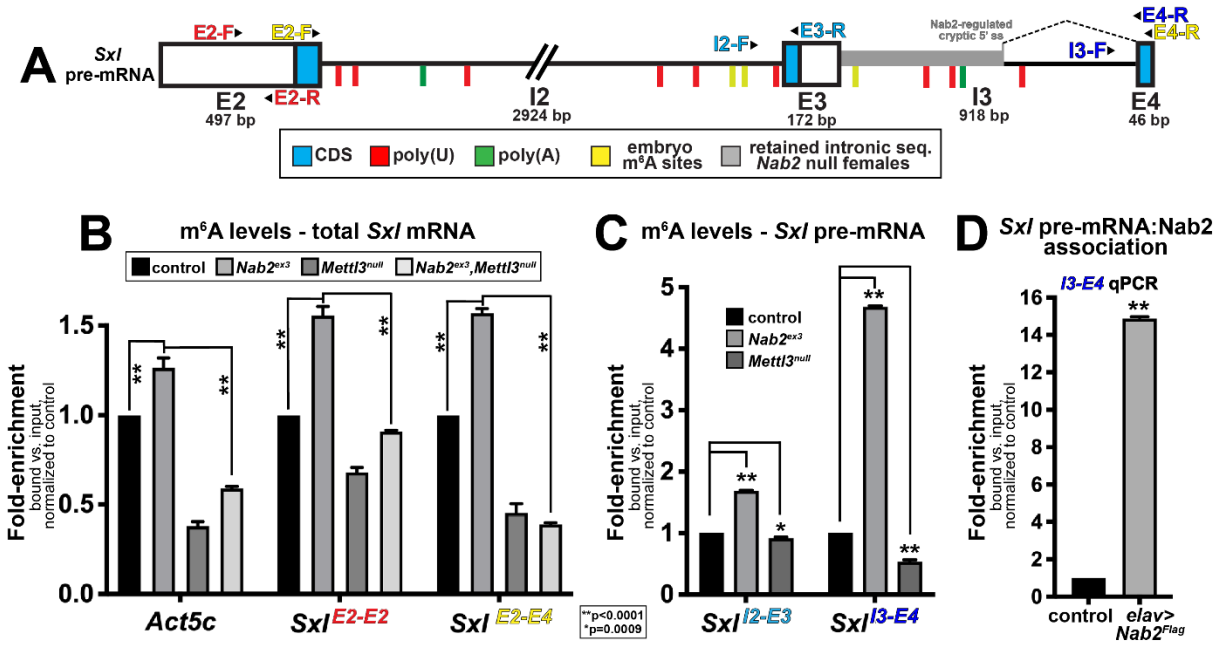

Figure 2-6. Nab2 associates with the *Sxl* mRNA and inhibits its m^{6}A methylation. (A) Diagram of (E2, E3, E4) and introns (I2, I3) of the *Sxl* pre-mRNA annotated to show coding sequence (CDS; **blue**), the retained intronic region in *Nab2^{ex3}* females (**grey**), and locations of color-coded primer pairs (**E2-F** and **E2-R**, **E2-F** and **E4-R**, **I2-F** and **E3-R**, **I3-F** and **E4-R**), poly(U) sites **red lines**, poly(A) sites **green lines**, and mapped m^{6}A locations in *Drosophila* embryos **yellow lines** (Kan et al., 2017). **(B)** Quantitative real-time PCR analysis of *Act5c* and *Sxl* mRNAs present in anti-m^{6}A precipitates of control (*Nab2^{pex41}*; black), *Nab2^{ex3}* (**grey**), *Mettl3^{null}* (**dark grey**), or *Nab2^{ex3},Mettl3^{null}* (**light grey**) female heads. *Sxl* primer pairs are indicated (**E2-F**+**E2-R** and **E2-F**+**E4-R**). **(C)** Similar analysis as in **B** using **I2-F**+**E3-R** and **I3-F**+**E4-R** primer pairs to detect unspliced variants of *Sxl* mRNA in anti-m^{6}A precipitates of control (black), *Nab2^{ex3}* (**grey**) and *Mettl3^{null}* (**dark grey**) female heads. **(D)** Quantitative real-time PCR analysis with the **I3-F**+**E4-R** primer pair in anti-Flag precipitates from control (*Nab2^{pex41}*) and *elav-Gal4,UAS-Nab2:Flag* female heads. For all panels, 1-day old female heads were used in three biological

replicates, and data represent bound vs. input ratios normalized to control (*Nab2*^{pex41}). Significance values are indicated (**p<0.0001, *p=0.0009).

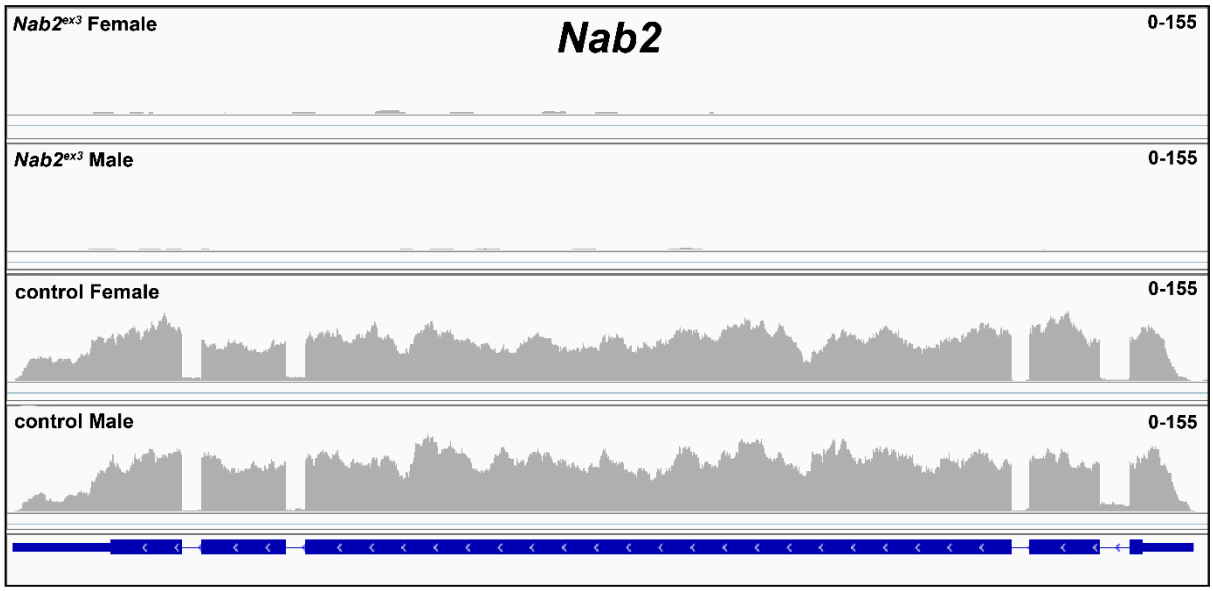

Figure 2-S1. RNA sequencing reads across the *Nab2* locus. IGV image of RNA sequencing reads across the *Nab2* locus in $Nab2^{ex3}$ (top tracks) and control ($Nab2^{pex41}$) adult female and male heads. Intron-exon structure is indicated at bottom. Read depth scale is indicated (0-155).

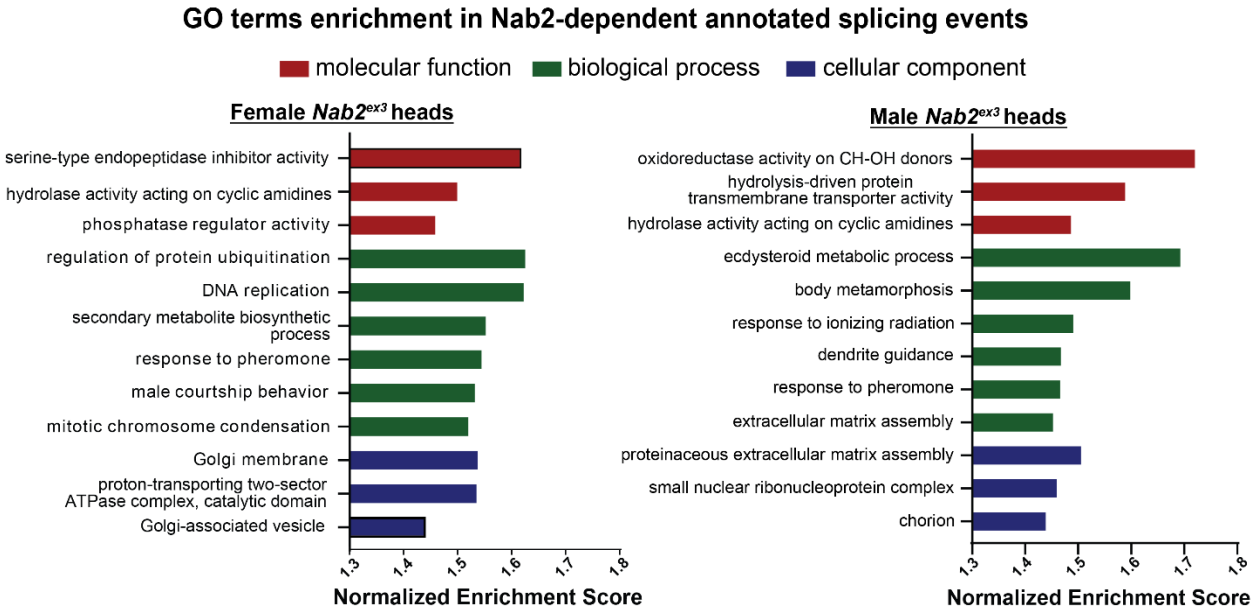

Figure 2-S2. GO term enrichment among Nab2-regulated alternative splicing events. Chart illustrating gene ontology (GO) terms enriched in the 'molecular function', 'biological process' and 'cellular component' categories among altered alternative splicing events detected by MISO in female and male *Nab2*^{ex3} head RNAs.

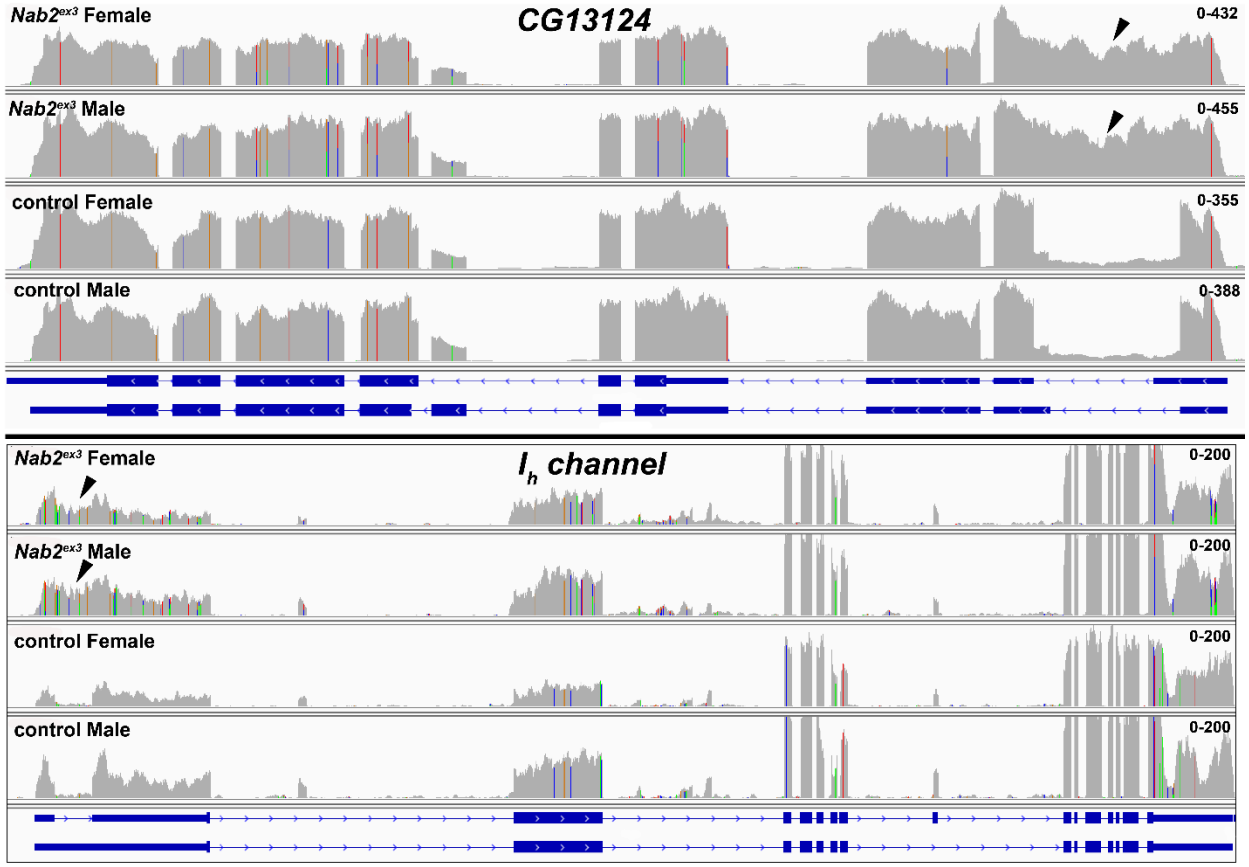

Figure 2-S3. RNA sequencing reads across the *CG13124* and *I_h channel* loci. IGV images of RNA sequencing reads across *CG13124* and *I_h channel* in *Nab2^{ex3}* (top tracks) and control (*Nab2^{pex41}*) adult female and male heads. Intron-exon structure is indicated at bottom. Read depth scales are indicated. Arrowheads indicate reads across the first intron of each gene, consistent with intron-retention.

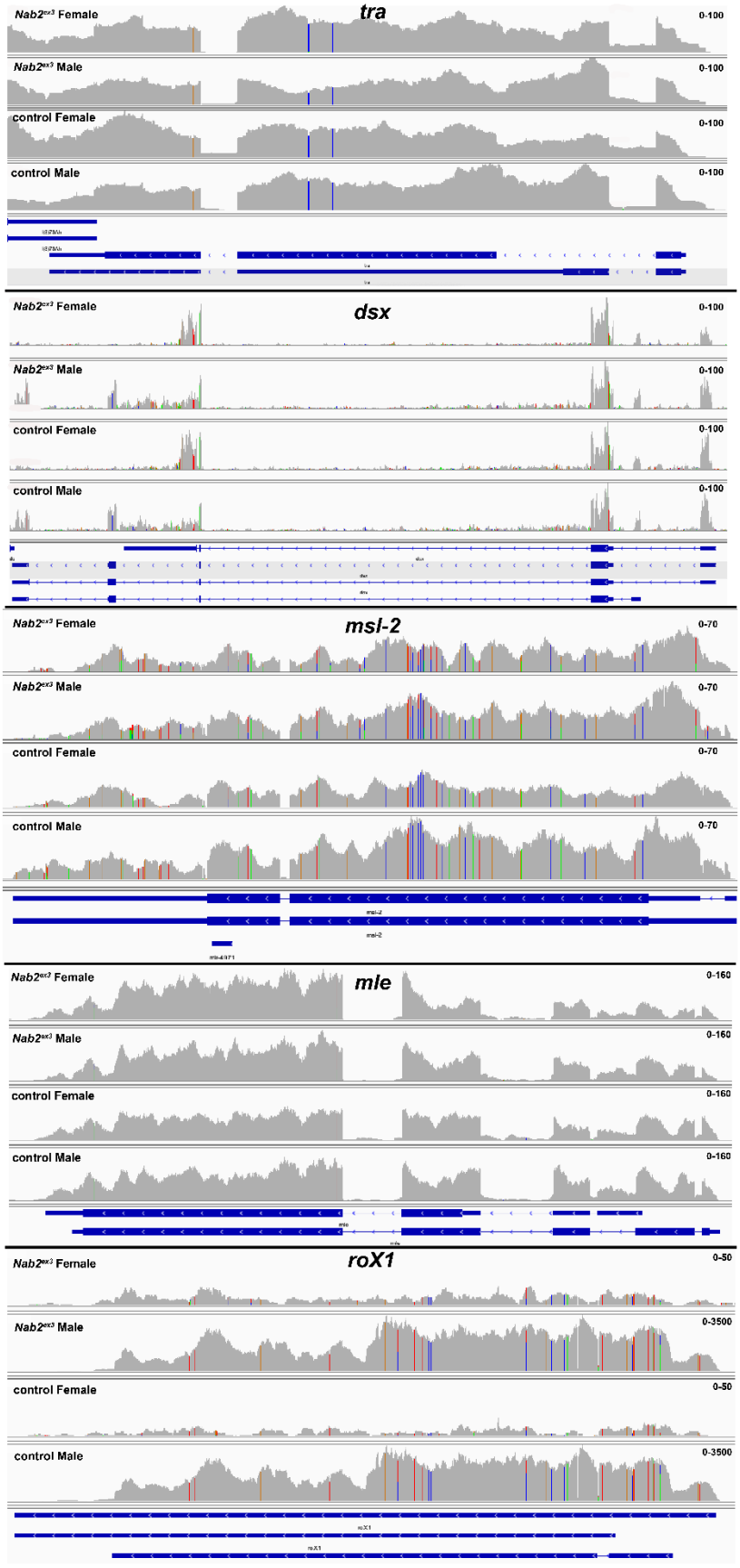
tra
Nab2ex3 Female
Nab2ex3 Male
control Female
control Male
0-100
dsx
Nab2ex3 Female
Nab2ex3 Male
control Female
control Male
0-100
msl-2
Nab2ex3 Female
Nab2ex3 Male
control Female
control Male
0-70
mle
Nab2ex3 Female
Nab2ex3 Male
control Female
control Male
0-160
roX1
Nab2ex3 Female
Nab2ex3 Male
control Female
control Male
0-50
0-3500

Figure 2-S4. RNA sequencing reads across the *tra* and *dsx* loci. IGV images of RNA sequencing reads across *tra*, *dsx*, *msl-2*, and *mle* in $Nab2^{ex3}$ (top tracks) and control ($Nab2^{pex41}$) adult female and male heads. Intron-exon structure is indicated at bottom. Read depth scales are indicated.

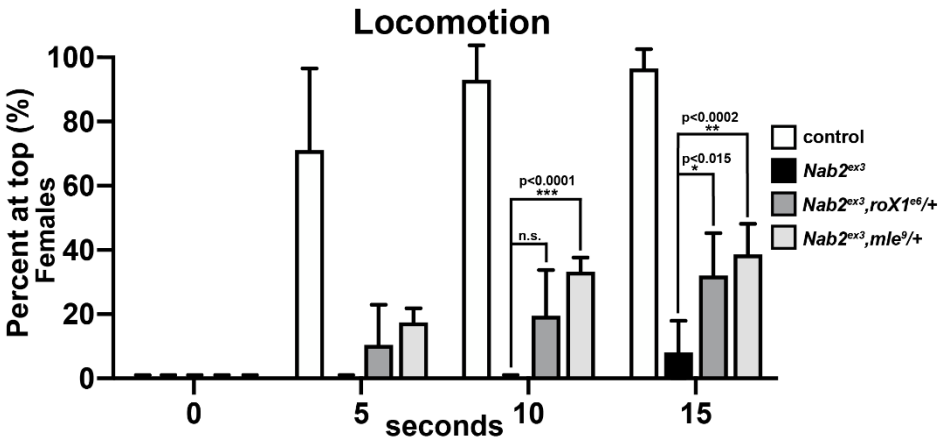

Figure 2-S5. Modification of *Nab2^{ex3}* locomotor defect by *roX1* and *mle* alleles. Negative geotaxis of age-matched adult female controls (*Nab2^{pex41}*), *Nab2^{ex3}* mutants, or *Nab2^{ex3}* mutants carrying single copies of the *roX1^{e6}* or *mle^{9}* loss-of-function alleles at 5sec, 10sec, and 15 sec timepoints. Significance values between indicated groups are indicated at the 30sec timepoint (p-values are indicated; n.s.=not significant).

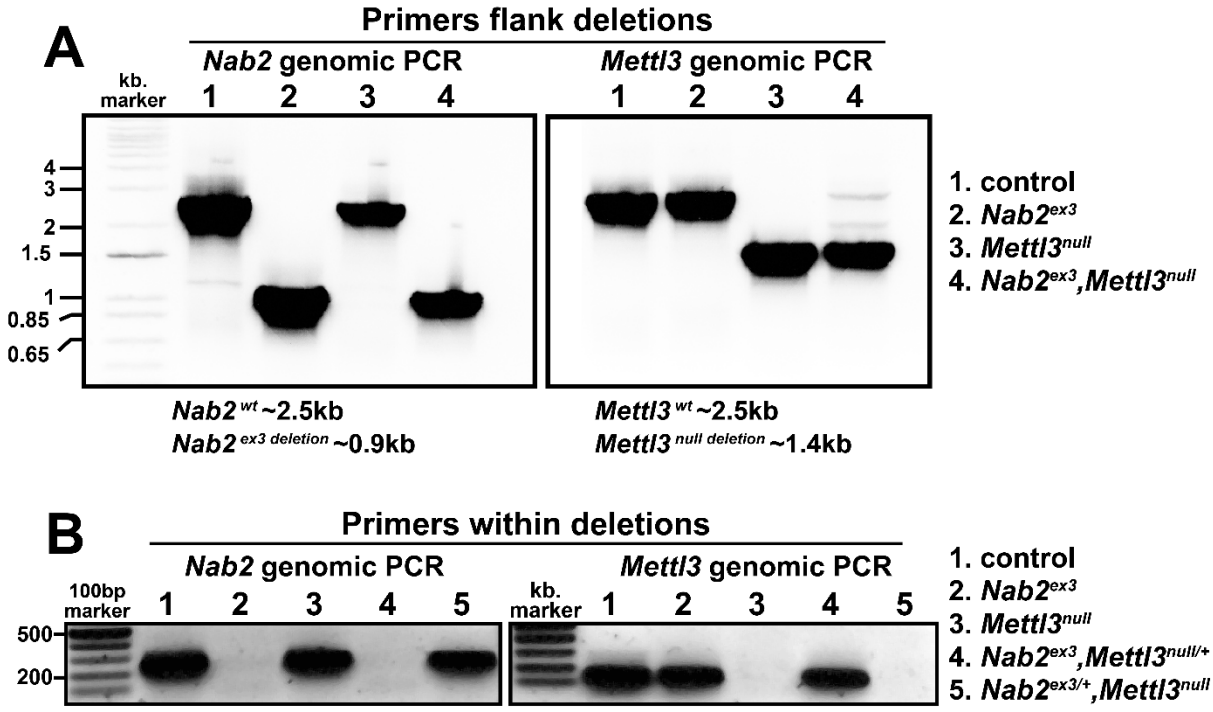

Figure 2-S6. Genomic PCR confirms the *Nab2^{ex3},Mettl3^{null}* recombinant. Genomic PCR on the indicated genotypes using primer pairs that either flank **(A, top panel)** or lie within **(B, bottom panel)** the *ex3* deletion in *Nab2* (left half of each gel) or the *null* crispr deletion in *Mettl3* (right half of each gel). Approximate product sizes are indicated.

Sxl Exon-2-3-4
ChrX: 7,087,614..7,092,170 (complement)_4557 bp
To scale: 1bp = 0.005 cm

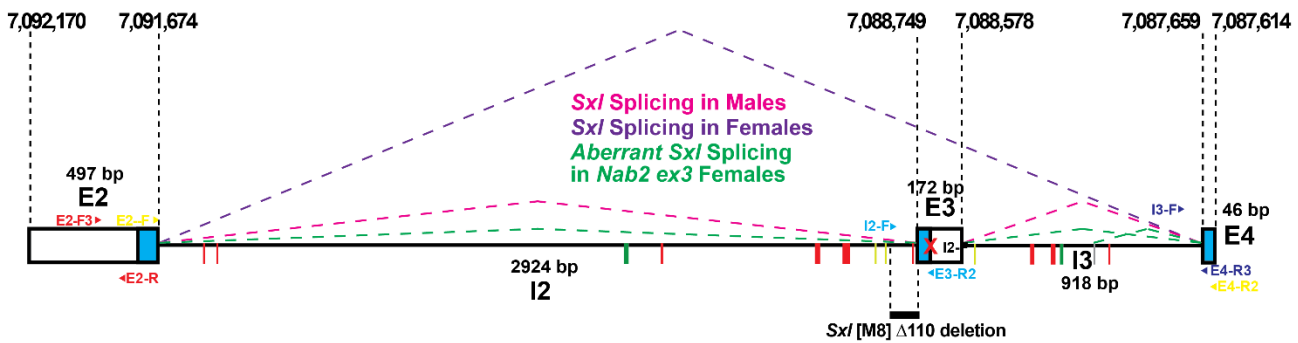

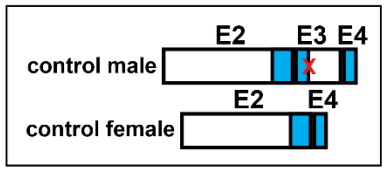

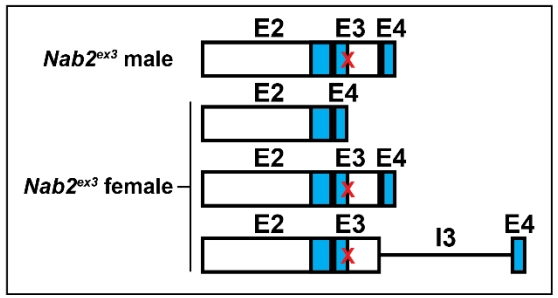

Key

- CDS
- poly(U)
- poly(A)
- site of cryptic 5'ss in I3 503 bp downstream of E3
- approximate positions of T3 m^{6}A sites in I2 and I3 with consensus motif A/G-A/G-AC-A/T (Kan et al, *Nat. Comm.*, 2017)

qPCR Primer Set	Target	Detection
Sxl E2-F + E4-R	*Sxl* E2-E4	Female *Sxl*
Sxl I2-F + E3-R2	*Sxl* I2-E3	Unspliced *Sxl*
Sxl I3-F + E4-R3	*Sxl* I3-E4	Unspliced *Sxl*
Sxl E2-F3+E2-R	*Sxl* E2-E2	Total *Sxl*

Figure 2-S7. Genomic PCR confirms a *Nab2^{ex3},Mettl3^{null}* recombinant. Detailed schematic of the exon 2-3-4 *Sxl* locus with annotated locations of introns and exons annotated to show coding sequence (CDS; blue), the retained intronic region in *Nab2^{ex3}* females (grey), and locations of color-coded primer pairs (E2-F and E2-R, E2-F and E4-R, I2-F and E3-R, I3-F and E4-R), poly(U) sites red lines, poly(A) sites green lines, and mapped m^{6}A locations in *Drosophila* embryos yellow lines (Kan et al., 2017). Colored dotted lines indicated sex-specific splicing in wildtype adults and the altered splicing documented in this study. Boxed areas below summarize exon-intron structure in wild type heads and *Nab2^{ex3}* heads. Base pair coordinates are indicated (Dm Release 6).

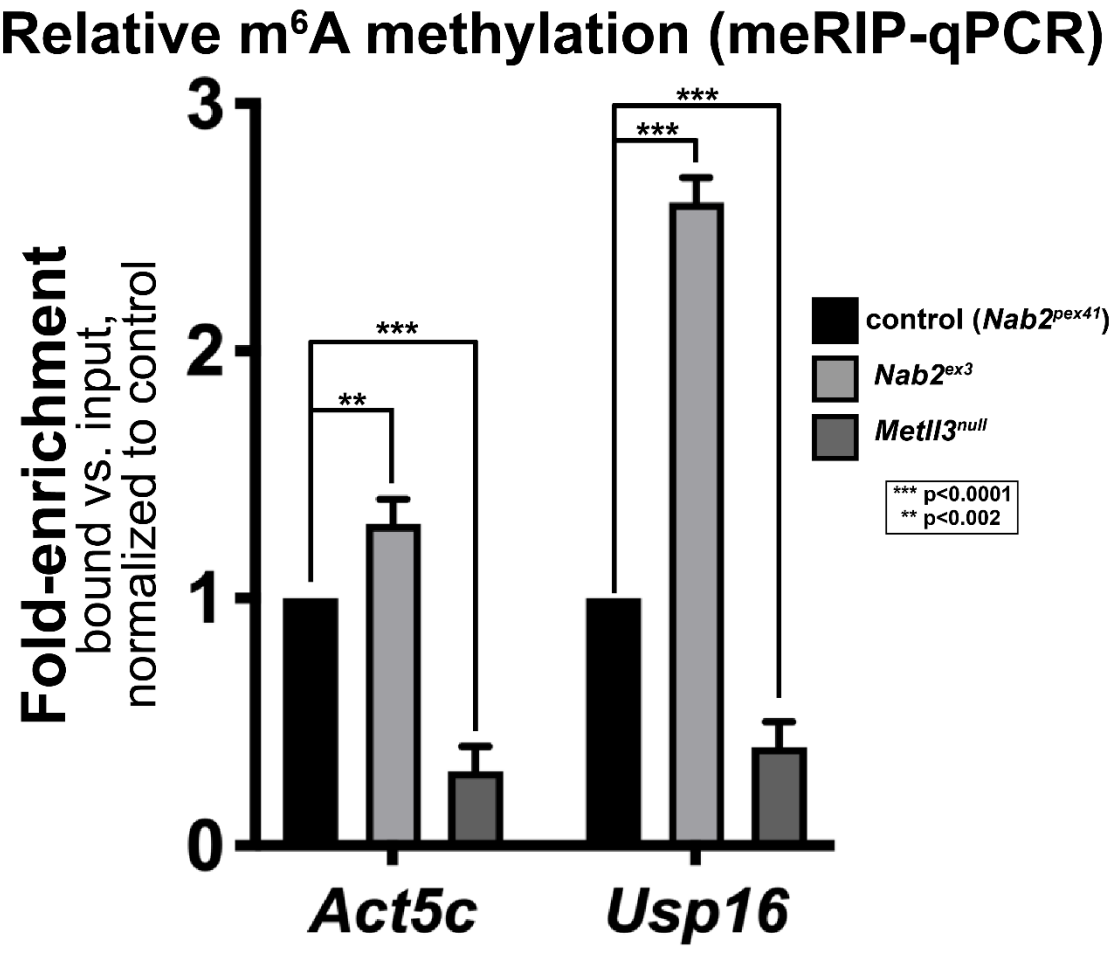

Figure 2-S8. Nab2 limits m^{6}A methylation of additional Mettl3 target RNAs. Quantitative real-time PCR analysis of *Act5c* and *Usp16* mRNAs present in anti-m^{6}A precipitates of control (*Nab2*^{pex41}; black), *Nab2*^{ex3} (grey), *Mettl3*^{null} (dark grey) adult female heads. 1-day old female heads were used in three biological replicates, and data represent bound vs. input ratios normalized to control (*Nab2*^{pex41}). p-values are indicated (n.s.=not significant).

Table 1

Alternative exon usage (DEXSeq) in *Nab2*^{ex3} head transcriptomes

	Females	Males
# of alternatively used exons *	**151**	**114**

* |(exon usage fold change)| > ~1.75 BH Adj. p < 0.05

Top misspliced transcripts

Females	foldΔ exon usage	BH adj. p-value
Sex lethal (Sxl)	2.86	3.08×10^{-235}
CG13124	2.45	1.09×10^{-81}
Ih channel	2.29	3.28×10^{63}
Ace	1.81	1.02×10^{-59}
Males	**foldΔ exon usage**	**BH adj. p-value**
Ace	2.02	1.88×10^{-169}
Pkc53E	1.74	6.12×10^{-102}
plx	2.12	9.03×10^{-67}
Pkn	1.84	9.04×10^{-67}

TABLE 2-1. Alternative exon usage (DEXSeq) in *Nab2*^{ex3} head transcriptomes.

TABLE 2-S1 contains 35,476 rows, TABLE 2-S2 contains 147 rows, and TABLE 2-S3 contains 266 rows. Thus, these tables are too large for direct inclusion in this dissertation document. To view TABLES 2-S1,2-S2, and 2-S3, please refer to Supplemental Tables 1-3 within the Supplemental Materials associated with Jalloh et al., 2020, the in-revision manuscript associated with this dissertation chapter. These Supplemental Materials are available in bioRxiv, the online preprint repository, at https://www.biorxiv.org/content/10.1101/2020.11.13.382168v3.supplementary-material. The titles associated with TABLES 2-S1, 2-S2, and 2-S3 are listed below.

TABLE 2-S1. DESeq2 results for all genes.

TABLE 2-S2. All significantly different annotated alternative splicing events (quantified by change in percent-spliced-in or Δ-PSI) identified in *Nab2*^{ex3} null females and males by MISO.

TABLE 2-S3. DEXSeq-called differential exon usage in *Nab2* mutant heads.

CHAPTER 3: THE DISEASE-ASSOCIATED PROTEINS *DROSOPHILA* NAB2 AND ATAXIN-2 INTERACT WITH SHARED RNAS AND COREGULATE NEURONAL MORPHOLOGY

This chapter has been submitted for consideration for publication as an Investigation in the Neurogenetics Series in *Genetics*. This chapter, representing a manuscript on which J. Christopher Rounds is first author, has been submitted as:

The Disease-Associated Proteins *Drosophila* Nab2 and Ataxin-2 Interact with Shared RNAs and Coregulate Neuronal Morphology

J. Christopher Rounds*, Edwin B. Corgiat*, Changtian Ye*, Joseph A. Behnke*, Seth M. Kelly‡, Anita H. Corbett†[1], Kenneth H. Moberg*[1,2]

*Department of Cell Biology, Emory University School of Medicine, Atlanta, GA 30322;
†Department of Biology, Emory University, Atlanta, GA 30322;
‡Department of Biology, The College of Wooster, Wooster, OH 44691

[1]Co-corresponding authors

J. Christopher Rounds served as the lead researcher and first author on the contents of this chapter. He performed the genetic, biochemical, and bioinformatic experiments and analyses described within, as well as most of the included microscopy and imaging experiments. He authored and performed the experiments underlying Figures 3-1, 3-2, 3-3B, 3-4, 3-5, 3-6, and 3-7; Table 3-1; Figures 3-S1, 3-S3, and 3-S4; and Tables 3-S1, 3-S2, and 3-S3. He wrote the R and PRISM scripts described in the subsection "Custom Software Code." Finally, he authored the text of this chapter, writing the original and all subsequent drafts and actively incorporating and interpreting edits from authors Anita H. Corbett and Kenneth H. Moberg.

Figures 3-3A and 3-S2 represent a collaboration between Changtian Ye, Joseph A. Behnke, and J. Christopher Rounds. Changtian Ye performed the rounds of genetic crosses, dissection, and immunostaining to generate samples for microscopic imaging, which all three authors performed led by Changtian Ye. Edwin B. Corgiat and Seth M. Kelly provided sustained, essential intellectual contributions throughout the planning and execution of the research reported here. Each also performed valuable related experiments ultimately not reported herein.

For RNA immunoprecipitation-sequencing (RIP-Seq), the Georgia Genomics and Bioninformatics core prepared cDNA libraries and performed sequencing; J. Christopher Rounds performed all preceding biochemical RIP experiments and sample collection, administratively coordinated the sequencing project with the core, and performed all bioinformatic analyses that followed.

Anita H. Corbett and Kenneth H. Moberg mentored J. Christopher Rounds and Edwin B. Corgiat, provided sustained intellectual contributions and administrative support, supplied financial support along with J. Christopher Rounds, and edited the text.

ABSTRACT

Nab2 encodes a conserved polyadenosine RNA-binding protein (RBP) with broad roles in post-transcriptional regulation, including in poly(A) RNA export, poly(A) tail length control, transcription termination, and mRNA splicing. Mutation of the *Nab2* human ortholog *ZC3H14* gives rise to an autosomal recessive intellectual disability, but understanding of Nab2/ZC3H14 function in metazoan nervous systems is limited, in part because no comprehensive identification of metazoan Nab2/ZC3H14-associated RNA transcripts has yet been conducted. Moreover, many Nab2/ZC3H14 functional protein partnerships likely remain unidentified. Here we present evidence that *Drosophila melanogaster* Nab2 interacts with the RBP Ataxin-2 (Atx2), a neuronal translational regulator, and implicate these proteins in coordinate regulation of neuronal morphology and adult viability. We then present the first high-throughput identifications of Nab2- and Atx2-associated RNAs in *Drosophila* brain neurons using an RNA immunoprecipitation-sequencing (RIP-Seq) approach. Critically, the RNA interactomes of each RBP overlap, and Nab2 exhibits high specificity in its RNA associations in neurons *in vivo*, associating with a small fraction of all polyadenylated RNAs. The identities of shared associated transcripts (e.g. *drk*, *me31B*, *stai*) and of transcripts specific to Nab2 or Atx2 (e.g. *Arpc2*, *tea*, respectively) promise insight into neuronal functions of and interactions between each RBP. Significantly, Nab2-associated RNAs are overrepresented for internal A-rich motifs, suggesting these sequences may partially mediate Nab2 target selection. Taken together, these data demonstrate that Nab2 opposingly regulates neuronal morphology and shares associated neuronal RNAs with Atx2, and that *Drosophila* Nab2 associates with a more specific subset of polyadenylated mRNAs than its polyadenosine affinity alone may suggest.

INTRODUCTION

Intellectual disability refers to a broad group of neurodevelopmental disorders affecting approximately 1% of the world population (Maulik *et al.* 2011) and defined by significant limitations in intellectual functioning and adaptive behavior (Tassé *et al.* 2016; Vissers *et al.* 2016). Intellectual disabilities are etiologically diverse and in some cases genetically complex, yet many exhibit overlapping molecular dysfunctions in a comparatively limited set of fundamental neurodevelopmental pathways (reviewed in Chelly *et al.* 2006; van Bokhoven 2011; and Verma *et al.* 2019). Thus, monogenic intellectual disabilities represent experimentally tractable avenues for understanding both these disorders more broadly and neurodevelopment in general (Najmabadi *et al.* 2011; Agha *et al.* 2014). One set of such informative monogenic intellectual disabilities is caused by mutations affecting genes encoding RNA-binding proteins (RBPs) (reviewed in Bardoni *et al.* 2012) such as *ZC3H14* (*zinc finger CCCH-type containing 14*). Specifically, loss-of-function mutations in *ZC3H14*, which encodes a ubiquitously expressed polyadenosine RBP, cause a non-syndromic form of autosomal recessive intellectual disability (Pak *et al.* 2011; Al-Nabhani *et al.* 2018). However, the molecular functions and developmental roles of human ZC3H14 are largely unknown; defining these functions and roles provides an opportunity to better understand intellectual disability and human neurodevelopment.

Drosophila melanogaster has proven a powerful model system to understand the molecular functions of proteins encoded by many intellectual disability genes (Inlow and Restifo 2004; Oortveld *et al.* 2013), and ZC3H14 is no exception—its functions have begun to be dissected in part through study of its *Drosophila* ortholog Nab2 (Pak *et al.* 2011; Kelly *et al.* 2014). *Drosophila* Nab2, like ZC3H14, is a polyadenosine RNA-binding protein that induces neurological defects when its expression is altered; deletion or overexpression of *Nab2* causes neuronal morphological defects in the eye, axon projection defects in the developing brain, and memory impairments (Pak

et al. 2011; Kelly *et al.* 2016; Bienkowski *et al.* 2017; Corgiat *et al.* 2020). The function of Nab2 is particularly important in *Drosophila* neurons, as pan-neuronal expression of Nab2 or an isoform of human ZC3H14 is sufficient to rescue the severe limitation in adult viability and locomotor defects caused by zygotic Nab2 deficiency (Pak *et al.* 2011; Kelly *et al.* 2014). Crucially, Nab2 physically and functionally interacts with Fmr1, the *Drosophila* homolog of the Fragile X Syndrome RBP FMRP (Verkerk *et al.* 1991; Ashley *et al.* 1993; Wan *et al.* 2000), to support axonal morphology and olfactory memory (Bienkowski *et al.* 2017). Previous data suggest functions of *Drosophila* Nab2 in poly(A) tail length control, translational regulation, and mRNA splicing, but mechanistic demonstrations of its molecular function on individual, endogenous transcripts have yet to emerge (Pak *et al.* 2011; Kelly *et al.* 2014; Bienkowski *et al.* 2017; Jalloh *et al.* 2020). Such demonstrations have been prevented in large part because very few *Drosophila* Nab2-associated RNAs have been identified (Bienkowski *et al.* 2017; Jalloh *et al.* 2020), and a comprehensive accounting of Nab2-associated RNAs has yet to be conducted.

While the precise molecular function of *Drosophila* Nab2 on its associated transcripts is unknown, informed hypotheses may be drawn by synthesizing research on *Drosophila* Nab2 and orthologs murine ZC3H14, human ZC3H14, and *S. cerevisiae* Nab2, the most well-studied Nab2/ZC3H14 ortholog (reviewed in Fasken *et al.* 2019). In *S. cerevisiae*, Nab2 functions pervasively across many RNAs in transcript stability and transcription termination, and it likely acts similarly broadly in poly(A) tail length control and poly(A) RNA export (Schmid *et al.* 2015; Fasken *et al.* 2019; Alpert *et al.* 2020). Mutation of *S. cerevisiae* Nab2 induces dramatic increases in bulk poly(A) tail length and disrupts bulk poly(A) export from the nucleus (Green *et al.* 2002; Kelly *et al.* 2010). Consistent with its pervasive effects on many transcripts, *S. cerevisiae* Nab2 exhibits a broad binding target profile and is essential for cellular viability (Anderson *et al.* 1993;

Tuck and Tollervey 2013). By contrast, mutant analyses of metazoan Nab2/ZC3H14 imply increased RNA target specificity for these proteins. Unlike Nab2 in *S. cerevisiae*, full-length ZC3H14 in mice and humans is not essential for viability—instead, loss of ZC3H14 decreases viability in mice and causes neurological or neurodevelopmental defects in both organisms (Pak *et al.* 2011; Rha *et al.* 2017b; Al-Nabhani *et al.* 2018). Bulk poly(A) tail lengths increase upon Nab2 loss in *Drosophila* or full-length ZC3H14 loss in mice *in vivo*, but this increase is not observed across all mouse tissues or all individual *Drosophila* mRNAs tested, and it is less pronounced than the effects observed in *S. cerevisiae* (Kelly *et al.* 2010; Bienkowski *et al.* 2017; Rha *et al.* 2017b). Moreover, in *Drosophila* and mouse cells, respectively, a pervasive nuclear poly(A) export defect is not observed upon Nab2 loss or ZC3H14 knockdown (Farny *et al.* 2008; Pak *et al.* 2011; Kelly *et al.* 2014). *Drosophila* Nab2 is required for proper splicing of individual introns and exons, but in a small, specific set of transcripts, including *Sex lethal* (Jalloh *et al.* 2020). Taken together, these data are consistent with a focused role for *Drosophila* Nab2 in regulating poly(A) tail length, splicing, stability, and nuclear export crucial for certain transcripts, cell types, and developmental contexts (Bienkowski *et al.* 2017; Rha *et al.* 2017b; Jalloh *et al.* 2020). Crucially however, the theme of *Drosophila* Nab2 RNA target specificity implied by these data has not been tested and remains an important open question, especially as the polyadenosine affinity of *Drosophila* Nab2 (Pak *et al.* 2011) makes it theoretically capable of associating with all polyadenylated transcripts through their poly(A) tails. Thus, a comprehensive identification of *Drosophila* Nab2-associated RNAs is necessary to determine the potential scope of Nab2 function and provide sets of transcripts on which the molecular consequences of Nab2-RNA association may be systematically evaluated. In the present study, in response we define the first neuronal RNA interactome for Nab2.

Contextualizing Nab2-RNA associations requires further definition of the molecular pathways and proteins, particularly other RBPs, that Nab2 interacts with or regulates. Notably, the *Nab2* modifier eye screen that initially linked Nab2 and Fmr1 (Bienkowski *et al.* 2017) also recovered an allele of *Ataxin-2* (*Atx2*), which encodes a conserved RBP and regulatory partner of Fmr1 in *Drosophila* neurons (Sudhakaran *et al.* 2014; Jiménez-López and Guzmán 2014). The shared connection of Nab2 and Atx2 with Fmr1 raised the possibility of cooperation or competition between these two proteins. Underscoring the value of this approach, Atx2 is a protein of particular importance for human health and neuronal function. Expansion of a polyglutamine tract within ATXN2, the human Atx2 ortholog, gives rise to the autosomal dominant neurodegenerative disease spinocerebellar ataxia type 2 (SCA2) (Imbert *et al.* 1996; Pulst *et al.* 1996; Sanpei *et al.* 1996). Expansions of the same tract are also associated with parkinsonism and amyotrophic lateral sclerosis (ALS) (Gwinn-Hardy *et al.* 2000; Elden *et al.* 2010; Park *et al.* 2015). Functionally, *Atx2* encodes a conserved RNA-binding protein that regulates protein translation, mRNA stability, and mRNP granule formation and plays roles in memory, cellular metabolism, and circadian rhythms (reviewed in Ostrowski *et al.* 2017; Lee *et al.* 2018). Among the most well-studied molecular roles of Atx2 are its contributions to regulation of mRNA translation in the cytoplasm. Specifically, Atx2 suppresses the translation of some target RNAs through RNP granule formation and interactions with the RNAi machinery (McCann *et al.* 2011; Sudhakaran *et al.* 2014; Bakthavachalu *et al.* 2018) and supports the translation of other targets by promoting RNA circularization (Lim and Allada 2013; Zhang *et al.* 2013; Lee *et al.* 2017). Intriguingly Atx2, like Nab2, contributes to poly(A) tail length control in *S. cerevisiae*—the yeast Atx2 ortholog Pbp1 promotes poly(A) tail length, likely by inhibiting the activity of poly(A) nuclease (PAN) (Mangus *et al.* 1998, 2004). The shared connections of Nab2 and Atx2 to Fmr1, neuronal translation, and

poly(A) tail length control emphasize the potential for and need to test whether these RBPs functionally interact beyond the initial eye screen link.

Here, after expanding the genetic link previously identified between Nab2 and Atx2 in our modifier screen, we used genetic and molecular approaches to probe the functional connections between these two RBPs. We show that Nab2 and Atx2 functionally interact to control neuronal morphology of the mushroom bodies (MBs), a learning and memory center of the *Drosophila* brain (Heisenberg 2003; Kahsai and Zars 2011; Yagi *et al.* 2016; Takemura *et al.* 2017). We then present the first high-throughput identification of Nab2- and Atx2-associated RNAs in *Drosophila*; in fact, such accounting has been performed for Nab2 only in *S. cerevisiae*, not in any metazoan (Guisbert *et al.* 2005; Batisse *et al.* 2009; Tuck and Tollervey 2013; Baejen *et al.* 2014). This approach demonstrates Nab2 and Atx2 associate with an overlapping set of RNA transcripts in fly brains and provides insight into the functions of each protein individually and in concert with one another. Considering these data as a whole, we propose a model in which the genetic interactions between Nab2 and Atx2 are explained by their counterbalanced regulation of shared associated RNAs. Our data represent a valuable resource for understanding the neuronal roles of Nab2 and Atx2 in *Drosophila* and, potentially, for understanding links between each RBP and human disease.

Materials and Methods

Drosophila genetics and husbandry

Genetic crosses of *Drosophila melanogaster* were raised on standard media and maintained at 25°C in humidified incubators (SRI20PF, Shel Lab) with 12-hour light-dark cycles unless otherwise specified. Cultures were often supplemented with granular yeast (Red Star Yeast) to encourage egg laying. Parental stocks were maintained at either at room temperature (RT) or 18°C

to control virgin eclosion timing. Stocks used include $Nab2^{ex3}$ (a *Nab2* null), $Nab2^{pex41}$ (a P-element excision control serving as a *Nab2* wild type), and *UAS>Nab2-FLAG*, all first described in (Pak *et al.* 2011). Additional stocks used include *GMR-Gal4* (on chromosome 2), $Atx2^{X1}$ (an *Atx2* null, gift of N. Bonini) (Satterfield *et al.* 2002), and *UAS>Atx2-3xFLAG* (gift of R. Allada) (Lim and Allada 2013). Finally, stocks sourced from the Bloomington Drosophila Stock Center (BDSC) include: *elav>Gal4* ($elav^{c155}$, BL458) (Lin and Goodman 1994), *OK107-Gal4* (BL854) (Connolly *et al.* 1996), *Df(3R)Exel6174* (BL7653) (Parks *et al.* 2004), *UAS>Nab2* ($Nab2^{EP3716}$, BL17159) (Rørth *et al.* 1998; Bellen *et al.* 2004), and $Atx2^{DG08112}$. The $Atx2^{DG08112}$ stock (Huet *et al.* 2002) was mapped as part of the Gene Disruption Project (GDP) (Bellen *et al.* 2004) and is no longer available from the BDSC; copies provided upon request.

***Drosophila* eye imaging**

Drosophila eyes were imaged using a Leica MC170 HD digital camera mounted on a Nikon SMZ800N stereo microscope at 8X magnification. To prepare subjects for imaging, flies were flash frozen (−80°C, 1 minute), fixed in place on a clear Slygard pad using minutien pins (26002-10, Fine Science Tools), and submerged in 70% ethanol to diffuse light and reduce glare. Subjects were illuminated with a fiber optic ring light (Dolan-Jenner) and LED illuminator (Nikon Instruments Inc.) and image acquisition was performed using the Leica Application Suite (v4.12) for Windows under the following parameters: 140 ms exposure; automatic white balance; highest available resolution; and default values for gain, saturation, gamma, and hue. Each subject was imaged at multiple focal planes (often ≥ 10), and these were subsequently combined using the *Auto-Align* and *Auto-Blend* functions in Photoshop CS5.1 Extended (Adobe) to generate final, merged images in which the entire subject is in-focus. These “focus stacking” processing steps (Patterson) combine only in-focus regions of an image series into a single, merged image.

Immunofluorescence

For mushroom body morphology experiments, *Drosophila* brains were dissected using methods similar to those in (Williamson and Hiesinger 2010; Kelly *et al.* 2016, 2017). Briefly, using #5 Dumont fine forceps (Ted Pella, Inc.), for each dissection a *Drosophila* head was isolated in PBS (often supplemented with 0.1% Triton X-100), the proboscis was removed to provide a forceps grip point, and the remaining cuticle and trachea were peeled away from the brain within. On wet ice, dissected brains were fixed in 4% paraformaldehyde for 30 minutes and then permeabilized in 0.3% PBS-Triton (PBS-T) for 20 minutes. For both primary and secondary antibody incubations, brains were left rocking at 4°C for 1-3 nights in 0.1% PBS-T supplemented with blocking agent normal goat serum (Jackson ImmunoResearch) at a 1:20 dilution. Immunostained brains were mounted on SuperFrost Plus slides (12-550-15, Fisher Scientific) in Vectashield (H-1000, Vector Laboratories) using a cover slip "bridge" method (Kelly *et al.* 2017). Brains were imaged on a Zeiss LSM 510 confocal microscope. Exclusively female flies were dissected for practicality, given that $Nab2^{ex3}$ nulls were analyzed in this experiment and $Nab2^{ex3}$ adult viability skews towards females (Jalloh *et al.* 2020).

For Nab2-Atx2 localization experiments, whole animals were fixed in 4% paraformaldehyde, 0.008% PBS-T, shaking, for 3 hours at RT and then washed in PBS and stored at 4°C overnight. Brains were dissected in 0.008% PBS-T using similar methods as described above, permeabilized by shaking in 0.5% PBS-T overnight at 4°C, and blocked by shaking in 0.5% PBS-T, 5% NGS for 2 hours at RT. For both primary and secondary antibody/Hoechst incubations, brains were left shaking at 4°C for 2-3 nights in 0.5% PBS-T, 5% NGS. After washing with 0.5% PBS-T followed by PBS, brains were mounted in SlowFade Gold Antifade Mountant (S36936, Invitrogen), surrounded by an adhesive imaging spacer (GBL654002, Sigma-Aldrich) to prevent

sample compression, and finally cover-slipped and sealed with clear nail polish. Brains were imaged on an A1R HD25 confocal microscope (Nikon) and a multi-photon FV1000 laser-scanning microscope (Olympus).

Primary antibodies and dilutions used are as follows: mouse α-Fasciclin 2 (1:50) (1D4, Developmental Studies Hybridoma Bank), rabbit α-GFP (1:400) (A11122, Invitrogen), and mouse α-FLAG (1:500) (F1804, Sigma-Aldrich). Secondary antibodies and dilutions used are as follows: goat α-mouse Cy3 (1:100) (Jackson ImmunoResearch), goat α-mouse Alexa 594 (1:400) (A11032, Invitrogen) and goat α-rabbit Alexa 488 (1:400) (A11008, Invitrogen). To fluoresce DNA and mark nuclei in localization experiments, brains were also incubated with a Hoechst 33342 stain (1:1,000) (H21492, Invitrogen) during secondary antibody incubation.

Further brain image analysis and processing, including generating maximum intensity projections and focus stacks and adjusting brightness and contrast, was performed with Photoshop CS5.1 Extended (Adobe) and Fiji (Schindelin *et al.* 2012), a distribution of ImageJ (Schneider *et al.* 2012; Rueden *et al.* 2017).

Immunoprecipitation

This immunoprecipitation protocol was developed through optimization guided by the protocols presented in (Yang *et al.* 2005; Banerjee *et al.* 2017; Bienkowski *et al.* 2017; Morris and Corbett 2018). Nuclear Isolation Buffer (NIB; 10 mM Tris HCl pH 7.4, 10 mM NaCl, 3 mM $MgCl_2$, 0.5% NP-40) and Immunoprecipitation Buffer (IP Buffer; 50 mM HEPES, 150 mM NaCl, 5 mM EDTA, 0.1% NP-40) were prepared ahead of the experiment and stored indefinitely at 4°C. Both buffers, and the glycine and PBS solutions below, were prepared primarily in 0.1% diethyl pyrocarbonate (DEPC)-treated and autoclaved ultrapure Milli-Q water to limit RNase contamination. Both NIB and IP Buffer were supplemented with an EDTA-free cOmplete protease inhibitor cocktail tablet

(1 tablet/28 ml; 11873580001, Roche) and RNasin Plus RNase inhibitor (0.2%; N2615, Promega) freshly before each experiment. Additionally, before each experiment Protein G-coupled magnetic Dynabeads (10003D, Thermo Fisher) were conjugated to glycerol-free (Domanski *et al.* 2012) monoclonal α-FLAG (F3165, Sigma-Aldrich) in aliquots of 1.5 mg beads/9 μg antibody by incubation for 45 minutes at room temperature. Throughout the experiment, beads were magnetized using DynaMag-Spin magnets (e.g. 12320D, Thermo Fisher) as necessary. Exclusively female flies were used for consistency with MB experiments and for practicality, as both *elav>Nab2-FLAG* and *elav>Atx2-3xFLAG* prohibitively decreased relative male viability (data not shown), presumably due to deleterious effects in males likely driven by dosage compensation of the X-chromosome-linked *elav>Gal4* construct leading to enhanced epitope-tagged protein overexpression.

300 female *Drosophila* heads each of the genotypes *elav>Gal4* alone, *elav>Nab2-FLAG*, and *elav>Atx2-3xFLAG*, previously isolated in bulk (see *Supplemental Materials and Methods*), were fixed in 1% formaldehyde, 0.1% NP-40 in PBS for 30 minutes at 4°C. Fixation was quenched by adding glycine to a final concentration of 250 mM and rocking for 10 minutes at 4°C. Heads were washed in 0.1% NP-40 in PBS and then manually homogenized with a smooth Teflon pestle for 5 minutes in 250 μL of NIB in a size AA glass tissue grinder at 4°C (3431D70, Thomas Scientific). Homogenates were spun through 35 μm cell strainer caps into round-bottom tubes (352235, Falcon) to remove exoskeletal debris, transferred, and then centrifuged for 5 minutes at 500×g at 4°C to separate an insoluble fraction. Twenty percent of the soluble supernatant volume was isolated and defined as Input; the remaining eighty percent was used for immunoprecipitation. Both Input and IP samples were diluted to final concentrations of 0.8x IP Buffer to ensure comparable and efficient sample lysis. IP samples were transferred onto the α-FLAG-conjugated

magnetic Dynabeads, and both sample types were incubated, rotating, for 10 minutes at room temperature. Next, IP sample supernatant was collected as the Unbound fraction, and IP sample beads were washed three times in IP Buffer. Finally, IP sample beads were resuspended in IP Buffer, transferred to clean tubes, and stored along with Input samples overnight at 4°C to allow passive hydrolysis to partially reverse formaldehyde crosslinks. This protocol was applied for both protein co-immunoprecipitation and RNA immunoprecipitation.

For protein co-immunoprecipitation, harsh elution of protein from IP sample beads was accomplished the next day—IP samples were diluted in modified Laemmli Sample Buffer (Laemmli 1970), incubated at 98°C for 5 minutes, centrifuged at 16,100×g for 5 minutes at room temperature, and magnetized to collect beads. Sample supernatants were then collected as IP samples. In parallel, Input samples were concentrated using an acetone-based method; this step was required for subsequent immunoblot analysis. Input samples were diluted to generate 80% chilled acetone solutions, vortexed for 15 seconds, and incubated at −20°C for 60 minutes. Samples were centrifuged at 14,000×g for 10 minutes at room temperature, resulting supernatants were discarded, and most remaining acetone was evaporated by air drying protein pellets in open tubes for 30 seconds at room temperature. To solubilize these dried protein pellets, samples were suspended in a solution equal parts modified Laemmli Sample Buffer (Laemmli 1970) and IP Buffer, vortexed, sonicated for 3x5 minutes in a 4°C Bioruptor ultrasonicator (UCD-200, Diagenode), vortexed, and heated at 98°C for 10 minutes. Finally, remaining insoluble material was collected by centrifugation at 16,100×g for 5 minutes at room temperature. Associated supernatants were isolated as concentrated Input protein samples. For RNA immunoprecipitation, harsh elution of RNA from IP sample beads was accomplished the next day with Trizol—both IP and Input samples were subjected to the RNA extraction protocol detailed below.

RNA Extraction

Following immunoprecipitation, RNA was isolated from IP and Input samples using a TRIzol-column hybrid approach adapted from (Rodriguez-Lanetty). To account for volume differences, samples were vigorously homogenized in TRIzol reagent (15596018, Thermo Fisher) at a ratio of either 1:10 (IP sample:TRIzol) or 1:3 (Input sample:TRIzol) and then incubated for 5 minutes at room temperature. All homogenized samples were clarified by centrifugation at 12,000×g at 4°C for 5 minutes, IP samples were magnetized to collect beads, and supernatant was isolated from all samples. After adding chloroform at a ratio of 0.2:1 (choloroform:TRIzol), samples were manually shaken and incubated at room temperature for 3 minutes. Samples were phase separated by centrifugation at 12,000×g at 4°C for 15 minutes, after which the aqueous layer was carefully isolated and mixed with an equal volume of 100% ethanol. RNA was further purified using an RNeasy Mini Kit (74106, QIAGEN) according to the manufacturer's instructions (RNeasy Mini Handbook, 4th Ed., June 2012) with the following deviations: for each sample, a final 30 µL elution was performed twice, isolating 60 µL of RNA in total into each collection tube. An on-column DNase digestion step was also performed under the same instructions using an RNase-Free DNase Set (79254, QIAGEN). Final RNA concentration and sample purity were determined via a NanoDrop 1000 spectrophotometer (Thermo Fisher).

RNA Sequencing

RNA from twelve samples of 300 adult female *Drosophila* heads each was isolated via the immunoprecipitation and extraction protocols described above, generating twelve pairs of IP and Input samples, or twenty-four samples in total. These samples were composed of four biological replicates each of *elav>Gal4* alone, *elav>Nab2-FLAG*, and *elav>Atx2-3xFLAG*. Once obtained, RNA samples were transferred on dry ice to the Georgia Genomics and Bioinformatics Core at

UGA for library preparation and sequencing. There, IP samples were first concentrated using solid phase reversible immobilization (SPRI) beads. Then, the TruSeq Stranded Total RNA Library Prep Gold kit (20020598, Illumina) was used to deplete rRNA and prepare stranded cDNA libraries from all twenty-four samples. These uniquely barcoded cDNA libraries were then pooled by sample type, forming one IP library pool and one Input library pool. Each pool was sequenced on a separate NextSeq High Output Flow Cell (Illumina) for 150 cycles to generate paired-end, 75 base-pair (bp) reads. Total non-index sequencing yield across all IP samples was 88.49 Gbp, equivalent to about 1.2 billion reads in total and 98 million reads per sample. Total non-index sequencing yield across all Input samples was 83.25 Gbp, equivalent to about 1.1 billion reads in total and 93 million reads per sample. Sequencing accuracy was high; 87.83% and 91.38% of non-index reads for IP and Input samples, respectively, have a sequencing quality (Q) score greater than or equal to 30.

RNA Sequencing Analysis—Read Mapping, Differential Expression, Visualization

Following sequencing, raw read FASTA files were transferred to Emory for bioinformatic analysis. To start, analyses were conducted on the Galaxy web platform, specifically using the public server at usegalaxy.org (Afgan *et al.* 2018). This analysis was supported by the BDGP6.22 release of the *Drosophila melanogaster* genome (Hoskins *et al.* 2015)—both the raw sequence FASTA and the gene annotation GTF were downloaded from release 97 of the Ensembl database (Yates *et al.* 2020) and used as inputs in subsequent read mapping, annotation, and visualization steps. For each Galaxy tool described below, exact parameters and version numbers used are detailed in Table 3-S1. For each sample, reads from across all four NextSeq flow cell lanes were concatenated using the Galaxy *Concatenate datasets tail-to-head* tool and mapped using RNA STAR (Dobin *et al.* 2013). Mapped reads were then assigned to exons/genes and tallied using

featureCounts (Liao *et al.* 2014). To enable inter-sample read count comparisons, count normalization and differential expression analysis was conducted using *DESeq2* (Love *et al.* 2014). Importantly, *DESeq2* analysis was performed twice, once on the 12 IP samples and once on the 12 Input samples; see *Supplemental Materials and Methods* for discussion of this sample separation method.

Outputs from all of the above tools were downloaded from Galaxy for local analysis, computation, and visualization. Custom R scripts were written to generate the scatterplots and hypergeometric test reported here and are available in File S3. Scripts in the R programming language (R Core Team 2019) were written and compiled in RStudio (R Studio Team 2018). Additional R packages used in these scripts include ggplot2 (Wickham 2016), ggrepel (Slowikowski 2019), BiocManager (Morgan 2018), and DESeq2 (Love *et al.* 2014). Analyses were supported by bulk data downloads along with extensive gene-level annotation, sequence information, and references provided by Flybase (Thurmond *et al.* 2018). Principal component analysis was conducted by and reported from the above *DESeq2* assessment on Galaxy. Mapped reads were visualized in the Integrative Genomics Viewer (IGV) (Robinson *et al.* 2011) on the same version of the *D. melanogaster* genome used above.

Gene-by-gene one-way ANOVAs to identify significantly enriched (i.e. RBP-associated) transcripts

Gene-by-gene ANOVAs and post-hoc tests for the 5,760 genes identified in the "testable" set, along with bar graphs of IP/Input values, were generated in Prism 8 for Windows 64-bit (GraphPad Software). Custom R and PRISM scripts were written to generate and label the 5,760 PRISM data tables, one per testable gene, required for this analysis, and custom R scripts were written to extract and combine the outputs from each test; these scripts are all available in File S3. See *Results* for a

summary and below for a further detailed discussion of the statistical testing used to define the testable transcript set and identify significantly enriched (i.e. RBP-associated) transcripts in our RIP-Seq results.

To identify RNA targets of Nab2 and Atx2—that is, RNAs enriched in either Nab2 RIP or Atx2 RIP samples relative to control RIP—directly comparing normalized read counts between RIP samples is insufficient. Differences in RNA expression between samples must be accounted for, as these differences can partially or wholly explain differences in the amount of RNA isolated by IP. We employed a common solution to this problem used in RIP- and ChIP-qPCR (Zhao *et al.* 2010; Aguilo *et al.* 2015; Li *et al.* 2019), scaling normalized RIP reads for each gene in each sample by the corresponding number of normalized Input reads. For clarity, we describe these values as "IP/Input"—they are commonly referred to as "Percent Input" or "% Input." These IP/Input values could then be compared between samples, further normalizing them to *elav-Gal4* alone controls. In this way, RIP fold enrichment, appropriately normalized to library size/composition *and* gene expression, were calculated for each gene in each sample. To promote the reliability of our analyses and increase our statistical power to detect differences in fold enrichment, we limited further analyses to a testable set of 5,760 genes out of the 17,753 total genes annotated in the BDGP6.22 genome. The testable gene set was defined as having detectable expression in all twelve Input samples and an average normalized read count in either Nab2 or Atx2 RIP samples greater than 10. These criteria were based on those used in (Lu *et al.* 2014; Malmevik *et al.* 2015). In this defined gene set, differences in fold enrichment were statistically tested using gene-by-gene one-way ANOVAs (Li *et al.* 2019) in Prism 8 (GraphPad software), applying Dunnett's post-hoc test to calculate significance *p*-values only for the comparison of each experimental sample to the control sample (Dunnett 1955). In each case, *p*-values were adjusted

to correct for multiple hypothesis testing only within each gene-by-gene ANOVA. We identified a small, focused set of statistically significantly enriched RNAs using this approach and concluded that additional corrections across all genes to control type I error (i.e. false positives) are not necessary (Rothman 1990). In fact, in the analyses above we determined that rRNA depletion during our RIP-Seq library preparation was incomplete, resulting in comparatively low read depth. Thus, rather than failing to adequately control type I error, we strongly suspect the RBP-associated transcripts we identified through this approach represent an undercount, to be expanded in future studies by methods with higher sensitivity (e.g. CLIP-Seq).

RNA Sequencing Analysis—Sequence Motif Analyses

Sequence motif analyses were conducted using the MEME Suite of software tools, accessed through the web interface at meme-suite.org (Bailey *et al.* 2009). For each MEME Suite tool described below, exact parameters and version numbers used are detailed in Table 3-S1. Within the MEME Suite, we used MEME itself (Bailey and Elkan 1994) to scan all Nab2-associated transcripts, regardless of their association with Atx2, to 1) identify sequence motifs shared across multiple transcripts and 2) evaluate the frequency and statistical significance of the discovered sequence motifs. Next, FIMO (Grant *et al.* 2011) was used to quantify the frequency among 1) Nab2-associated transcripts and 2) non-Nab2 associated transcripts of user-provided sequences, specifically i) a 41-bp A-rich motif identified in Nab2-associated transcripts by MEME, ii) A_{12}, and iii) $A_{11}G$. Non-Nab2-associated transcripts are defined as all 5,619 transcripts in the testable set found to not be statistically significantly associated with Nab2 by RIP-Seq. Sequence logos (i.e. visual representations of weighted sequence motifs) were generated by MEME and by WebLogo 3.7.4, available at weblogo.threeplusone.com (Crooks *et al.* 2004).

Importantly, for any Nab2-associated or non-Nab2 associated transcripts annotated with multiple splice variants, all variant sequences were included as inputs in our motif analyses. This inclusion reflects an inherent limitation of standard shotgun—that is, short-read—sequencing, as most reads cannot be unambiguously assigned to one splice variant of a given gene, only to given exon(s) encoded by that gene. We therefore chose this inclusion strategy to avoid introducing any bias associated with attempting to call single splice variants for RBP association, and for analytical simplicity. Full sequences of Nab2-associated and non-Nab2 associated transcripts were obtained using the FlyBase Sequence Downloader at flybase.org/download/sequence/batch/ (database release FB2020_04).

Data Availability

The authors affirm that all data necessary for confirming the conclusions of the article are present within the article and associated figures, tables, supplemental materials, and database accessions. File S1 contains *Supplemental Materials and Methods*, including those focused on bulk *Drosophila* head isolation, immunoblotting, *DESeq2*-based count normalization, and Gene Ontology analyses. File S2 contains detailed legends for all supplemental tables. File S3 contains all custom code—both R and PRISM scripts—written to generate, analyze, or visualize data in this article and associated figures, tables, and supplemental materials. Sequencing data, including raw reads, processed counts, and statistical analyses for each individual RIP-Seq sample, are available at the Gene Expression Omnibus (GEO) under accession: GSE165677. *Drosophila* stocks are available upon request. Supplemental materials, including files, figures, and tables, are available at figshare: https://figshare.com/s/6f28676d7119624b3105.

RESULTS

Atx2 loss-of-function alleles suppress Nab2 overexpression phenotypes in the adult eye

Previous work has established a Gal4-driven Nab2 overexpression system in the *Drosophila* eye as an effective screening platform to identify potential regulatory partners and targets of Nab2 (Pak *et al.* 2011; Bienkowski *et al.* 2017; Lee *et al.* 2020). This approach uses the *Glass Multimer Reporter* (*GMR*) construct (Ellis *et al.* 1993; Hay *et al.* 1994) to drive expression of the *S. cerevisiae* Gal4 transcription factor in fated eye cells (Freeman 1996). In turn, Gal4 binds to *Upstream Activating Sequence* (*UAS*) sites within an EP-type P-element (Rørth 1996) inserted upstream of the endogenous *Nab2* gene (*EP3716*) and induces eye-specific overexpression of endogenous Nab2 protein (a genotype hereafter referred to as *GMR>Nab2*). *GMR>Nab2* produces a consistent array of eye morphological defects compared to the *GMR-Gal4* transgene control (Pak *et al.* 2011; Bienkowski *et al.* 2017; Lee *et al.* 2020) and (Figure 3-1A,B). Specifically, this misexpression causes loss of posterior eye pigment, sporadic blackened patches, and disruptions to ommatidial organization lending the surface of the eye a "rough" appearance. Notably, *GMR>Nab2*-induced pigment loss increases in severity along the anterior-to-posterior axis of the eye, likely because *GMR* activation occurs behind the morphogenetic furrow, the posterior-to-anterior wave of eye morphogenesis observed in the larval eye disc (Wolff and Ready 1991; Hay *et al.* 1994). As a result, posterior *GMR>Nab2* eye cells experience the longest period of Nab2 overexpression.

Using the *GMR>Nab2* modifier screen as a foundation, we previously identified the *Drosophila* Fragile X Syndrome RBP and neuronal translational regulator Fmr1 as a physical and functional interactor of Nab2 (Bienkowski *et al.* 2017). An allele of the *Ataxin-2* (*Atx2*) gene, which encodes an RNA binding protein that is a regulatory partner of Fmr1 in *Drosophila* (Sudhakaran *et al.* 2014), was also detected in eye this screen as a candidate *GMR>Nab2* modifier

(Bienkowski *et al.* 2017). To pursue this potential Nab2-Atx2 link, we tested two *Atx2* alleles for genetic interactions with *GMR>Nab2*. The first allele, $Atx2^{DG08112}$, is caused by the insertion of a 15.6 kb *{wHy}* P-element near the 5' end of *Atx2* (Huet *et al.* 2002; Bellen *et al.* 2004) and is lethal *in trans* to *Df(3R)Exel6174*, a deletion that completely removes the *Atx2* locus and nearby genes (Parks *et al.* 2004). That is, crossing balanced $Atx2^{DG08112}$ and *Df(3R)Exel6174* alleles produces no *trans* heterozygotes among other F1 progeny (n=54). Based on these data, we interpret $Atx2^{DG08112}$ to be a strong hypomorph. The second *Atx2* allele, $Atx2^{X1}$, is a 1.4 kb imprecise-excision-based deletion that removes the first 22 codons of the *Atx2* coding sequence and that has been characterized as a null (Satterfield *et al.* 2002). In part because Nab2 loss induces some sex-specific defects (Jalloh *et al.* 2020), we analyzed each sex individually. In adult females, heterozygosity for either of these two loss-of-function alleles, $Atx2^{DG08112}$ (Figure 3-1C) or $Atx2^{X1}$ (Figure 3-1D), dominantly suppresses the pigment loss and blackened patches caused by *GMR>Nab2*. In contrast, both *Atx2* alleles have limited impact on ommatidial organization or "roughness". In males, *GMR>Nab2* induces morphological eye defects (Figure 3-1 E,F) comparable to those in females, and similarly heterozygosity for either $Atx2^{DG08112}$ (Figure 3-1G) or $Atx2^{X1}$ (Figure 3-1H) dominantly suppresses the pigment loss and blackened patch defects.

Atx2 loss-of-function alleles suppress _Nab2_ null effects on adult viability and brain morphology

Misexpression of Nab2 induces dramatic phenotypes in domains beyond the eye; homozygosity for the null allele $Nab2^{ex3}$ causes a dramatic reduction in adult viability (Pak *et al.* 2011). Thus, to explore whether modifying effects of *Atx2* loss-of-function alleles extend to the endogenous *Nab2* locus, we analyzed the effect of *Atx2* heterozygosity on low adult viability in $Nab2^{ex3}$ homozygotes (Figure 3-S1). As in the eye, both the $Atx2^{DG08112}$ and $Atx2^{X1}$ alleles dominantly suppress the

viability defects observed in *Nab2*^{ex3} females, elevating adult viability from 17% to 39% and 82%, respectively (Figure 3-1I). The corresponding effect in males is not as penetrant; only the null *Atx2*^{X1} allele dominantly suppresses the viability defect in *Nab2*^{ex3} males (Figure 3-1J). Taken together, these data establish gross similarities in *Nab2-Atx2* genetic interactions in females and males. Thus, for practicality we focused further experiments exclusively on female flies, given the more prohibitive impact on male viability of changes in Nab2 expression (Jalloh *et al.* 2020 and see *Materials and Methods*).

That *Atx2* loss-of-function alleles improve adult viability of *Nab2*^{ex3} homozygotes suggests Atx2 and Nab2 coregulate processes or transcripts important for adult development or survival. However, these genetic interactions do not reveal in what cell types or tissues this coregulation may occur. We therefore focused further investigations of *Nab2-Atx2* interaction in the brain, given the established and important roles of each protein in brain neurons (Lim and Allada 2013; Sudhakaran *et al.* 2014; Kelly *et al.* 2016; Bienkowski *et al.* 2017). *Nab2*^{ex3} homozygous flies develop morphological defects in the axon tracts—lobes—of the mushroom body (MB) brain structure, a principal olfactory learning and memory center of the insect brain (Heisenberg 2003; Kahsai and Zars 2011; Yagi *et al.* 2016; Takemura *et al.* 2017). Specifically, the MBs of surviving *Nab2*^{ex3} homozygous null adults exhibit two highly penetrant structural defects: thinning or absence of the dorsally-projecting α lobes and over-projection or "fusion" of the medially-projecting β lobes (Kelly *et al.* 2016). We found that heterozygosity for either *Atx2*^{DG08112} or *Atx2*^{X1} also causes defects in MB morphology—specifically β lobe fusion—with no apparent effects on α lobe morphology as compared to controls (Figure 3-2A-C). Importantly, in the background of *Nab2*^{ex3} nulls (Figure 3-2D), heterozygosity for either *Atx2*^{DG08112} (Figure 3-2E) or *Atx2*^{X1} (Figure 3-2F) suppresses the thinning or absence of α lobes, decreasing the penetrance of this phenotype

from 62% of α lobes to 30% or 36%, respectively (Figure 3-2G). In contrast, neither *Atx2* allele significantly affects the penetrance of β lobe fusion in $Nab2^{ex3}$ nulls, demonstrating the effect of each mutation is not additive to the effect of $Nab2^{ex3}$ homozygosity in this context (Figure 3-2H). A similar α-lobe-specific interaction occurs between alleles of *Nab2* and *Fmr1* (Bienkowski *et al.* 2017). Notably, as α and β lobes are composed of tracts of bifurcated axons from single cells (Takemura *et al.* 2017), this α-lobe-specific suppression by *Atx2* alleles demonstrates a *Nab2-Atx2* genetic interaction at subcellular resolution. Moreover, that *Atx2* loss-of-function alleles suppress defects of a *Nab2* null allele implies that Atx2 and Nab2 proteins may coregulate, but in opposing ways, pathways guiding α lobe morphology during development.

Nab2 and Atx2 primarily localize to independent compartments in mushroom body neurons

The genetic links between *Nab2* and *Atx2* could reflect a physical interaction between their encoded proteins (e.g. as shared components of mRNP complexes), as has been observed for both Nab2 and Atx2 with Fmr1 (Sudhakaran *et al.* 2014; Bienkowski *et al.* 2017). Alternatively, these genetic links could reflect functional but not physical interactions between Nab2 and Atx2 on common RNAs or neurodevelopmental processes. The latter hypothesis aligns with the localization patterns of each protein—Nab2 localizes primarily to neuronal nuclei with a small fraction in the cytoplasm in some contexts (Kelly *et al.* 2016; Bienkowski *et al.* 2017), while Atx2 is exclusive to the neuronal cytoplasm except under certain pathogenic conditions (Lessing and Bonini 2008; Elden *et al.* 2010). To begin to differentiate between these hypotheses, we evaluated the localization profiles of each protein in MBs *in vivo*. We expressed both *UAS-Nab2-YFP* and *UAS-Atx2-3xFLAG* transgenes in adult MB Kenyon cells using the pan-MB driver *OK107-Gal4* (Figure 3-3A). Similar to observations in human cerebral cortex tissues (Huynh *et al.* 2003), Atx2 is nearly excluded from nuclei and localizes strongly to the soma cytoplasm of MB Kenyon cells

in adults *in vivo*. In contrast, Nab2 localizes predominantly to the nuclei of these neurons *in vivo*. This distinction extends beyond the soma and into the α and β lobe axon tracts; Atx2 localizes robustly to these cytoplasmic compartments while Nab2 does not (Figure 3-S2).

To more rigorously assess Nab2-Atx2 protein interactions across all cell compartments, we expressed a FLAG-tagged Nab2 transgene (*UAS-Nab2-FLAG*) (Pak *et al.* 2011) using the pan-neuronal driver *elav-Gal4* (Lin and Goodman 1994) and subjected brain-neuron-enriched head lysates to immunoprecipitation with α-FLAG-conjugated beads to recover Nab2-associated proteins. Probing with specific antibodies confirms that Fmr1 is enriched in Nab2 immunoprecipitates as previously reported (Bienkowski *et al.* 2017), but reveals weak enrichment of Atx2 (Figure 3-3B). These results indicate complexes containing Nab2 and Atx2 may form in neurons but are rare relative to Nab2-Fmr1 complexes. Taken together, these subcellular localization and biochemical data suggest Nab2 and Atx2 do not generally co-occupy the same RNA or mRNP complexes throughout the post-transcriptional life of an RNA in adult mushroom body neurons. Therefore, we considered the possibility that *Nab2-Atx2* genetic interactions instead reflect roles in post-transcriptional control of shared RNA targets at different points in time or different locations in the cell.

The Nab2 and Atx2 RNA interactomes in brain neurons overlap

Neither Nab2- nor Atx2-associated RNAs have been identified by a high-throughput method in *Drosophila*—such accounting has been conducted for Atx2 in human cells (Yokoshi *et al.* 2014) and for Nab2 only in *S. cerevisiae*, not in any metazoan (Guisbert *et al.* 2005; Batisse *et al.* 2009; Tuck and Tollervey 2013; Baejen *et al.* 2014). To test the hypothesis that Nab2 and Atx2 share RNA targets, we identified transcripts stably associated with epitope-tagged versions of each protein in adult brain neurons using an RNA immunoprecipitation-sequencing (RIP-Seq)

approach. In this approach, protein products of *UAS-Nab2-FLAG* or *UAS-Atx2-3xFLAG* transgenes are robustly expressed under *elav-Gal4* control and are efficiently immunoprecipitated from adult head lysates (Figure 3-4A). Briefly, four biological replicates each of *elav-Gal4*, *elav>Nab2-FLAG*, and *elav>Atx2-3xFLAG* adult female *Drosophila* heads were lysed and immunoprecipitated with α-FLAG-conjugated beads. Then, RNA from both IP and Input samples was rRNA depleted, reverse transcribed into stranded cDNA libraries, and sequenced. Using the Galaxy web platform through the public server at usegalaxy.org (Afgan *et al.* 2018), reads were mapped using STAR (Dobin *et al.* 2013) to the BDGP6.22 release of the *Drosophila melanogaster* genome (sourced through Ensembl, Yates *et al.* 2020), assigned to exons/genes and tallied using *featureCounts* (Liao *et al.* 2014), and normalized for inter-library count comparisons using *DESeq2* (Love *et al.* 2014). A principal component analysis (PCA) generated as part of *DESeq2* demonstrates the high inter-genotype reproducibility among RNA IP (RIP) samples and shows that samples expressing Nab2-FLAG or Atx2-3xFLAG differ more from *elav-Gal4* controls than from one another (Figure 3-4B).

To identify Nab2-associated and Atx2-associated RNAs, we calculated percent input (IP/Input) enrichment values (Zhao *et al.* 2010; Aguilo *et al.* 2015; Li *et al.* 2019) for each of the 5,760 genes in the testable set defined by 1) detectable expression in all twelve Inputs and 2) an average normalized Nab2- or Atx2-IP read count greater than 10 (Lu *et al.* 2014; Malmevik *et al.* 2015). Fold enrichment differences were statistically tested by performing gene-by-gene one-way ANOVAs (Li *et al.* 2019), applying Dunnett's post-hoc test (Dunnett 1955), and calculating adjusted *p*-values corrected for multiple hypothesis testing within each gene-by-gene ANOVA (values hereafter referred to as *Dun. Adj. p*; see *Materials and Methods* for more detail). Using this approach, we identify 141 and 103 RNAs significantly enriched in α-FLAG IPs of *elav>Nab2-*

FLAG and *elav>Atx2-3xFLAG* female heads, respectively (Table 3-S2, Figure 3-S3). The size and focus of these sets of statistically significantly enriched RNAs suggests type I (i.e. false positive) error is sufficiently controlled and additional corrections between genes are not necessary (Rothman 1990). Comparing the Nab2- and Atx2-IP groups strongly supports our hypothesis, revealing 28 transcripts shared between Nab2- and Atx2-associated *Drosophila* neuronal RNAs (Figure 3-4C). This overlap is highly significant according to the hypergeometric test—it is extremely unlikely to occur by random selection from the total tested gene set. The full list of transcripts associated with both Nab2 and Atx2 (Table 1) includes multiple mRNAs that encode proteins with functions in neuronal domains in which *Nab2* and *Atx2* genetically interact, raising the possibility that coregulation of these RNAs by Nab2 and Atx2 partially explains these *Nab2-Atx2* genetic links. These shared transcripts include *drk* (*downstream of receptor kinase*), *me31B* (*maternal expression at 31B*), *sm* (*smooth*), and *stai* (*stathmin*). The protein encoded by *drk* is a receptor tyrosine kinase (RTK) adaptor that regulates growth and development by binding activated RTKs, such as sevenless in R7 retinal cells (Almudi *et al.* 2010), and contributes to, among other processes, cell survival in the eye (Schoenherr *et al.* 2012) and olfactory learning and memory in the MB (Moressis *et al.* 2009). The protein encoded by *me31B* is a DEAD-box RNA helicase expressed in many cellular contexts, including the MB Kenyon cells (Hillebrand *et al.* 2010) and the oocyte (Nakamura *et al.* 2001), that physically associates with Atx2 (Lee *et al.* 2017) and serves as a central player in miRNA-mediated translational repression (Barbee *et al.* 2006) and assembly of some RNP granules (Eulalio *et al.* 2007). Finally, the proteins encoded by *sm* and *stai* are respectively an hnRNP linked to defects in axon termination (Layalle *et al.* 2005) and a tubulin binding protein linked to natural variation in the size of MB α and β lobes (Lachkar *et al.* 2010; Zwarts *et al.* 2015).

The 28 shared transcripts represent approximately 20% and 24% of the total transcripts identified as Nab2- and Atx2-associated, respectively, underscoring that these proteins also associate with RNA sets independent from one another. From these independent sets, we defined the top Nab2-specific and Atx2-specific associated transcripts as the top 20 most significantly associated transcripts (by *Dun. Adj. p*) and top 20 most strongly enriched transcripts (by IP/Input) in each set. As with shared RNAs, multiple RBP-specific RNAs with links to *Nab2* or *Atx2* functions or mutant phenotypes are identified among these top transcripts, raising the possibility that regulation of these RNAs by Nab2 or Atx2 partially explains the mechanism of action of these RBPs (Figure 3-4D,E). For example, the top Nab2-specific associated RNAs include *Arpc2* (*Actin-related protein 2/3 complex, subunit 2*), *side-II* (*sidestep II*), and *Cpsf160* (C*leavage and polyadenylation specificity factor 160*). These transcripts respectively encode proteins with proposed functions in neuronal growth cone advance (Yang *et al.* 2012), synapse formation between certain neuronal subtypes (Tan *et al.* 2015), and mRNA poly(A)-tail formation based on orthology to mammalian *Cpsf1* (Mandel *et al.* 2008). The top Atx2-specific associated RNAs include *dj-1β*, *mtm* (*myotubularin*), and *Snx16* (*Sorting nexin 16*). These transcripts respectively encode proteins with proposed functions in ATP synthesis and motor neuron synaptic transmission (Hao *et al.* 2010; Oswald *et al.* 2018), endosomal trafficking regulation via phosphatase activity (Velichkova *et al.* 2010; Jean *et al.* 2012), and neuromuscular junction synaptic growth (Rodal *et al.* 2011).

Gene Ontology terms enriched in Nab2 and Atx2 RNA interactomes emphasize additional RBP-associated transcripts

Evaluating Nab2- and Atx2-associated RNAs individually provides valuable but incomplete insight, allowing larger trends to be missed. To complement these analyses, we holistically

evaluated the shared and specific Nab2- and Atx2-associated transcripts by subjecting each gene list to PANTHER Gene Ontology (GO) analysis, revealing the identities and members of enriched GO terms in each transcript set (Ashburner *et al.* 2000; Mi *et al.* 2019; The Gene Ontology Consortium 2019). Critically, GO term enrichment was calculated by comparing term abundance between these lists and the testable set of 5,760 head-enriched genes rather than the entire genome. In this way, these analyses did not identify GO terms as enriched simply because of their overrepresentation in *Drosophila* heads. Among shared Nab2- and Atx2-associated RNAs, we identify overrepresented GO terms and RBP-associated transcripts within them that highlight crucial functions and processes Nab2 and Atx2 may coregulate (Figure 3-4F). Among these GO terms are 'microtubule binding', which includes *apolpp* (*apolipophorin*) and *shi* (*shibire*); 'sensory perception of taste', which includes *Gαo* and *Gγ30A*; 'gene silencing by miRNA', which includes *AGO2* (*Argonaute 2*) and *me31B*; and 'short-term memory', which includes *shi* and *drk*. Survey of the associated RNAs specific to either RBP reveals overrepresented GO terms and transcripts within them which may mediate processes Nab2 and Atx2 regulate independently of one another, including respectively the GO terms 'exosomal secretion', which includes *Rab35* and *Rab7*; and 'regulation of ATP metabolic process', which includes *Dg* (*Dystroglycan*) and *dj-1β* (Figure 3-S4).

To combine and summarize the individual transcript and GO analyses, we highlight groups of seven transcripts found within the shared (Figure 3-5A) and RBP-specific (Figure 3-5B,C) associated transcript sets. These highlights were selected from the combined set of transcripts 1) demonstrating a fold enrichment (IP/Input) greater than 1.5 and/or 2) included in the most overrepresented GO terms (fully defined in Table 3-S3). Beyond transcripts already described, this summary includes the shared transcript *HmgZ* (*HMG protein Z*), Nab2-specific transcripts *fwe*

(*flower*) and *SLC22A* (*SLC22A family member*), and Atx2-specific transcripts *tea* (*telomere ends associated*) and *Xpc* (*Xeroderma pigmentosum, complementation group C*). A group of functionally diverse transcripts in the testable set that did not associate with either RBP is shown for comparison and as evidence of the specificity of the RIP-Seq assay (Figure 3-5D).

Polyadenosine sequence motifs are enriched in Nab2-associated RNAs

The diversity of RNAs that do not associate with Nab2 and Atx2 in the RIP assay (Figure 3-5D) underscores a key finding—both of these RBPs exhibit specific RNA-association patterns within brain neurons. This observation is not surprising for Atx2 given, for example, the sequence specificity of its human homolog in HEK293T cells (Yokoshi *et al.* 2014), but it represents a valuable insight for Nab2. The extent of the metazoan Nab2/ZC3H14 RNA target pool has been an enduring question (Rha *et al.* 2017a), given the breadth of the *S. cerevisiae* Nab2 target pool (Batisse *et al.* 2009; Tuck and Tollervey 2013) and the ability of Nab2/ZC3H14 across eukaryotes to bind polyadenosine RNA *in vitro* (Kelly *et al.* 2007; Pak *et al.* 2011), raising the possibility for very broad binding of mRNAs via their poly(A) tails *in vivo*. We found a relatively focused set of RNAs co-precipitate with Nab2-FLAG from fly brain neurons, indicating Nab2 may indeed exhibit greater specificity in *Drosophila* than would be observed if the protein bound all or most polyadenylated transcripts via their poly(A) tails.

Thus, we sought to determine what additional RNA sequence features may drive the association of Nab2 with its target transcripts if not only the presence of a poly(A) tail. We used MEME (Bailey and Elkan 1994) to scan all Nab2-associated transcripts to identify shared sequence motifs that may represent Nab2 binding sites and partially explain Nab2 specificity. Strikingly, this analysis identifies a 41-bp long, internal-A-rich stretch among the first ten 6-50-bp motifs shared among Nab2-associated transcripts. Importantly, each of these 10 sequence motifs are

shared across overlapping sets of many but not all Nab2-associated RNAs. Using FIMO (Grant *et al.* 2011), another part of the MEME Suite (Bailey *et al.* 2009), we quantified the frequency of close and exact matches to the consensus version of this motif among Nab2-associated RNAs. Occurrences of this A-rich motif are significantly more common in Nab2-associated transcripts compared to non-Nab2 associated transcripts, respectively appearing once every 135 bases and once every 845 bases on average, a 6.3-fold enrichment (Figure 3-6A). The high frequency of this motif in Nab2-associated transcripts is consistent with data from *S. cerevisiae* that Nab2 does not associate with RNAs exclusively through the poly(A) tail and also binds to upstream UTRs and coding sequences, likely through other A-rich sequences (Guisbert *et al.* 2005; González-Aguilera *et al.* 2011; Tuck and Tollervey 2013; Baejen *et al.* 2014; Aibara *et al.* 2017). Importantly, that this A-rich motif is enriched in but not exclusive to Nab2-associated RNAs is consistent with results for other RBPs—linear sequence motifs alone are generally insufficient to explain RBP specificity (Dominguez *et al.* 2018) and RBPs do not generally occupy all of their available binding motifs throughout the transcriptome (Li *et al.* 2010; Taliaferro *et al.* 2016).

As a complement to these analyses, we used FIMO to scan Nab2-associated RNAs for the presence of the smallest canonical binding motifs sufficient for Nab2 association in *S. cerevisiae*—A_{12} and $A_{11}G$ (Guisbert *et al.* 2005; Aibara *et al.* 2017). This approach reveals that in *Drosophila* brain neurons A_{12} and $A_{11}G$ sites are significantly but moderately more common in Nab2-associated transcripts compared to non-Nab2 associated transcripts. These A_{12} and $A_{11}G$ sites appear respectively once every 1,553 and 687 bases on average among Nab2-associated transcripts and once every 1,901 and 935 bases on average among non-Nab2-assoicated transcripts, a 1.2- and 1.4-fold enrichment (Figure 3-6B,C). Taken together, the findings that Nab2 associates with a specific subset of all RNAs with poly(A) tails, and that these three A-rich motifs are not exclusive

to Nab2-associated RNAs, strongly argues that the polyadenosine sequence affinity of Nab2 alone is insufficient to explain Nab2-RNA association specificity in *Drosophila* brain neurons. Other mechanisms must also contribute to Nab2 target choice, such as RNA secondary structure, protein-protein interactions, subnuclear localization, and binding site competition. That said, the significant enrichment of a 41-bp A-rich motif, A_{12}, and $A_{11}G$ observed in Nab2-associated RNAs suggests Nab2-RNA association is partially mediated through these genetically encoded RNA sequence motifs as well as or instead of through the poly(A) tail.

DISCUSSION

Mutation of either *ZC3H14 or ATXN2* gives rise to human disease, and the Nab2 and Atx2 RNA-binding proteins encoded by their *Drosophila* orthologs are linked by a shared association with Fmr1 (Sudhakaran *et al.* 2014; Bienkowski *et al.* 2017). Here we show that *Nab2* and *Atx2* interact in multiple contexts in *Drosophila*, specifically in fated eye cells, adult viability, and mushroom body neuronal morphology. Notably, these interactions are dose-sensitive, as heterozygosity for *Atx2* loss-of-function alleles is sufficient to suppress *Nab2* null phenotypes in adult viability and MB morphology. That is, loss of Nab2 may sensitize these domains to reduced Atx2 activity, suggesting these RBPs regulate some common processes. We find that these *Nab2-Atx2* interactions are likely not explained by extended, simultaneous co-occupancy of Nab2 and Atx2 in common RNP complexes on shared RNA transcripts. Each protein is concentrated in distinct subcellular compartments in adult mushroom body neurons *in vivo*, and Nab2 and Atx2 weakly associate by co-IP from brain neurons. Thus, to explore an alternative possibility—sequential regulation of shared RNA transcripts—we have carried out the first high-throughput identification of Nab2- and Atx2-associated RNAs in *Drosophila*. We find these proteins associate with

overlapping sets of transcripts in *Drosophila* neurons, consistent with their shared and distinct functions and supporting the model of sequential regulation. Identification of these protein-transcript associations promises further insight into the functions shared between and unique to each RBP. In addition, the identification of *Drosophila* Nab2-associated RNAs begins to address longstanding questions about Nab2 function and the particular sensitivity of neurons to Nab2 loss, revealing that Nab2 associates with a specific subset of polyadenylated RNAs *in vivo* despite the theoretical potential to bind across all polyadenylated transcripts suggested by its high polyadenosine affinity *in vitro* (Pak *et al.* 2011).

A model of opposing regulatory roles for Nab2 and Atx2

We show that Nab2 and Atx2 share associated RNAs in *Drosophila* neurons (Figures 3-4,3-5) and that *Atx2* loss-of-function alleles suppress phenotypes of Nab2 loss (Figures 3-1,3-2). Taken together, these findings imply that, at least for transcripts crucial for adult survival and MB α lobe morphology, Nab2 and Atx2 exert opposing regulatory roles on their shared associated RNAs. This opposing role possibility aligns with some of the known functions of each protein. Namely, in *S. cerevisiae* Nab2 contributes to proper nuclear processing events including protection from enzymatic degradation, poly(A) tail length control, splicing, and transcriptional termination while also facilitating poly(A) RNA export from the nucleus (Green *et al.* 2002; Hector *et al.* 2002; Kelly *et al.* 2010; Schmid *et al.* 2015; Soucek *et al.* 2016; Alpert *et al.* 2020). If *Drosophila* Nab2 also performs some or all of these nuclear processing roles on its associated RNAs, then Nab2 binding should contribute to transcript stability, nuclear export, and ultimately protein expression. Atx2, in contrast, is a key regulator of translational efficiency in the cytoplasm, suppressing the translation of some target RNAs and activating the translation of others (reviewed in Lee *et al.* 2018). As our data suggest Nab2 and Atx2 act in functional opposition on a shared transcript set,

we propose Atx2 primarily functions as a translational inhibitor rather than activator on shared Nab2- and Atx2-associated RNAs. In this model (Figure 3-7), Nab2 and Atx2 would act in temporal and spatial sequence to balance protein expression from their shared associated RNAs in neurons, with Nab2 promoting proper nuclear RNA processing, stability, and export and Atx2 inhibiting RNA translation, respectively.

This model of sequential temporal and spatial regulation aligns with evidence that Nab2 and Atx2 primarily localize to different subcellular compartments in adult MBs at steady state and exhibit a low level of co-precipitation from brain neurons (Figure 3-3). Potential explanations for the combination of distinct localization profiles and limited physical association between Nab2 and Atx2 are found in proposals that *S. cerevisiae* Nab2 shuttles out of the nucleus with bound RNAs during export before releasing them and returning to the nucleus (Aitchison *et al.* 1996; Lee and Aitchison 1999; Duncan *et al.* 2000). Thus, Nab2 and Atx2 may physically share associated RNAs briefly if neuronal *Drosophila* Nab2 similarly shuttles and both RBPs are present during the nuclear-cytoplasmic handoff of mRNP remodeling that follows mRNA export from the nucleus (reviewed in Müller-McNicoll and Neugebauer 2013; Chen and Shyu 2014). Functional and physical links between Nab2 and an RBP with a prominent cytoplasmic localization pattern like Atx2 have been observed previously, specifically with Fmr1 (Bienkowski *et al.* 2017). However, the physical associations observed between Fmr1 and Nab2 are more robust than that observed between Atx2 and Nab2 in the present study (Figure 3-3B)—this distinction may be partially explained by the different localization patterns of Atx2 and Fmr1. Atx2 is exclusively cytoplasmic in neurons except under certain pathogenic conditions (Huynh *et al.* 2003; Lessing and Bonini 2008; Elden *et al.* 2010), while Fmr1 shuttles between the two compartments, associating with at least some of its target RNAs in the nucleus (Tamanini *et al.* 1999; Kim *et al.* 2009). Thus, Nab2

and Fmr1 may theoretically co-occupy and coregulate shared transcripts in both cellular compartments while Nab2 and Atx2 sequentially regulate shared transcripts exchanged during a nuclear-cytoplasmic handoff, representing two distinct modes of functional interaction between Nab2 and a cytoplasmic RBP.

This model provides a firm foundation and raises many readily testable hypotheses to be explored in future research. The model predicts that for shared Nab2- and Atx2-associated RNAs, loss of Nab2 decreases transcript stability, impedes proper nuclear processing events including poly(A) tail length control, and impairs poly(A) RNA export from the nucleus, ultimately leading to decreases in protein product. Conversely, we predict partial loss of Atx2 releases translational inhibition on these shared transcripts and induces increases in protein product. Finally, loss of both proteins would balance these effects, resulting in steady-state levels of protein product more similar to the wild-type condition. With the identity of Nab2- and Atx2-associated RNAs in hand, future research is enabled to test these predictions.

Prominent Nab2- and Atx2-associated transcripts provide links to brain development and function

Of all the RBP-associated transcripts identified here, we defined the prominent shared and RBP-specific associated transcripts as those annotated within overrepresented GO terms (Figure 3-4F, Figure 3-S4) and/or passing a 1.5-fold enrichment threshold. The identities and functional roles of these prominent RBP-associated transcripts (examples in Figure 3-5) provide potential mechanistic explanations for the biological roles of each RBP. For example, the effects of Nab2 and Atx2 on MB morphology may be mediated in part through regulation of shared mRNAs *sm* and *stai*, which respectively encode an hnRNP and a tubulin binding protein both linked to axonal morphology and development (Layalle *et al.* 2005; Lachkar *et al.* 2010; Zwarts *et al.* 2015). The

effects of Nab2 and Atx2 on memory (Sudhakaran *et al.* 2014; Kelly *et al.* 2016) may be due in part to regulation of shared transcripts *drk*, *shi*, *Gαo*, and *me31B*, all of which encode proteins with roles in memory formation or retrieval (Dubnau *et al.* 2001; Ferris *et al.* 2006; Moressis *et al.* 2009; Sudhakaran *et al.* 2014). Both Nab2 and Atx2 may be involved in RNAi at multiple levels, regulating *me31B* RNA in neurons in addition to associating, in the case of Atx2, with me31B protein (Lee *et al.* 2017; Bakthavachalu *et al.* 2018). Finally, the suppression of *GMR>Nab2* by *Atx2* alleles in the eye may be explained in part by the shared association of Nab2 and Atx2 with *HmgZ* (*HMG protein Z*) RNA, which encodes a chromatin remodeler linked to survival of R7 retinal photoreceptor neurons (Kanuka *et al.* 2005; Ragab *et al.* 2006).

Among the associated RNAs specific to each RBP, we found only Nab2 associated with *fwe* (*flower*), *Arpc2*, *side-II*, and *SLC22A* RNA, connections which may further explain the role of Nab2 in guiding MB morphology and regulating learning and memory. These transcripts respectively encode a transmembrane mediator of neuronal culling in development (Merino *et al.* 2013), a component of the neuronal growth cone advance-regulating Arp2/3 complex (Hudson and Cooley 2002; Yang *et al.* 2012), an immunoglobulin superfamily member potentially contributing to axon guidance and synapse formation in the optic lobe (Tan *et al.* 2015), and a transmembrane acetylcholine transporter localized to MB dendrites and involved in suppressing memory formation (Gai *et al.* 2016). On the other hand, the association of Atx2 with Atx2-specific RNAs *Xpc* and *tea*, which respectively encode players in the fundamental cellular processes of DNA repair and telomere protection (Henning *et al.* 1994; Goosen 2010; Zhang *et al.* 2016), may partially explain why Atx2 genomic loss, unlike Nab2 genomic loss, is larval lethal (Satterfield *et al.* 2002). In summary, defining the potential functional impact of Nab2- and Atx2-RNA

associations like these will provide critical insight into the roles of Nab2 and Atx2 in neurodevelopment and *Drosophila* disease models.

Nab2 associates with a more specific set of RNAs in metazoans than in *S. cerevisiae*

The degree of RNA association specificity metazoan Nab2/ZC3H14 exhibits has been a longstanding question, in part because competing answers are suggested by the functional similarities and differences between metazoan Nab2/ZC3H14 and the *S. cerevisiae* Nab2 ortholog. In *S. cerevisiae*, Nab2 is essential for viability (Anderson *et al.* 1993) and is a central player in post-transcriptional regulation of many transcripts, serving as a nuclear poly(A)-binding-protein regulating transcript stability (Schmid *et al.* 2015), poly(A) tail length, and poly(A) RNA export from the nucleus among other processes (reviewed in Moore 2005; Chen and Shyu 2014; and Stewart 2019). However, in metazoans Nab2 or the full-length form of ZC3H14 is dispensable for cellular viability, and the effects of either protein on poly(A) tail length and poly(A) RNA export from the nucleus are either less pronounced and likely exerted on fewer transcripts than in *S. cerevisiae* or are not detected (Farny *et al.* 2008; Kelly *et al.* 2010; Wigington *et al.* 2016; Bienkowski *et al.* 2017; Rha *et al.* 2017b; Morris and Corbett 2018). Consistently, Nab2/ZC3H14 have not been found to associate with all polyadenylated RNAs tested in metazoans so far (Wigington *et al.* 2016; Bienkowski *et al.* 2017; Morris and Corbett 2018), but the possibility has remained that these few identified non-Nab2/ZC3H14-associated transcripts are outliers and metazoan Nab2/ZC3H14 associates with a large majority of polyadenylated RNAs similarly to *S. cerevisiae* Nab2 (Tuck and Tollervey 2013), likely in part by binding poly(A) tails. Indeed, the identities of Nab2- or ZC3H14-associated RNAs in metazoans had never previously been addressed with a comprehensive, high-throughput method.

Our results identify a specific set of transcripts that neuronal Nab2 associates with in *Drosophila*. Of the 5,760 transcripts tested in the RIP-Seq, only about 2.5% were found to associate with Nab2 in *Drosophila* neurons (Figure 3-4), a much smaller percentage of the transcriptome than associates with Nab2 in *S. cerevisiae* (Guisbert *et al.* 2005; Batisse *et al.* 2009; Tuck and Tollervey 2013). Importantly, this likely represents an undercount of all Nab2-associated transcripts in neurons *in vivo*—some RNAs associated with Nab2 in prior studies are absent from our Nab2-associated transcript set (Bienkowski *et al.* 2017; Jalloh *et al.* 2020), and technical limitations impacted our sequencing read depth (see *Methods*). Higher sensitivity approaches (e.g. CLIP-Seq) could reveal a broader set of Nab2-associated transcripts in *Drosophila* than we define here. Nonetheless, in the present study the majority of both RNAs (Figure 3-4) and tested polyadenosine-rich sequence motifs (Figure 3-6) were not found to be associated with Nab2, strongly supporting a model in which Nab2 associates with a specific subset of RNAs in *Drosophila* neurons. Perhaps for this more select group of transcripts Nab2 still plays a key role in transcript stability, poly(A) tail length control, transcription termination, and poly(A) RNA export from the nucleus, such that defects will only be observed in targeted examinations of single transcripts and not in bulk assays—one does not always reflect the other (Kelly *et al.* 2014; Bienkowski *et al.* 2017). This model of Nab2 specificity in *Drosophila* aligns well with the knowledge that Nab2/full-length ZC3H14 is essential for cellular viability in *S. cerevisiae* (Anderson *et al.* 1993) but not in *Drosophila* (Bienkowski *et al.* 2017), mice (Rha *et al.* 2017b), or, seemingly, humans (Pak *et al.* 2011; Al-Nabhani *et al.* 2018). This diminished global requirement for Nab2/ZC3H14 in metazoans may be due, at least in part, to functional overlap with PABPN1, an evolutionarily distinct nuclear polyadenosine RNA-binding protein that is

absent in *S. cerevisiae* (Mangus *et al.* 2003) but controls poly(A) tail length and is essential in *Drosophila* (Benoit *et al.* 2005), mice (Vest *et al.* 2017), and humans (Hart *et al.* 2015).

The model of Nab2 specificity in *Drosophila* does not conflict with its affinity for polyadenosine, which could theoretically allow Nab2 to bind all transcripts with a poly(A) tail. Even in *S. cerevisiae*, the broad binding profile of Nab2 (Batisse *et al.* 2009) and central role in poly(A) tail length control (Kelly *et al.* 2010), poly(A) RNA export from the nucleus (Green *et al.* 2002), and protection of poly(A) RNA from degradation (Schmid *et al.* 2015) does not translate to binding the poly(A) tails of all transcripts (Guisbert *et al.* 2005; Tuck and Tollervey 2013). More broadly, linear sequence motifs alone are insufficient to explain RBP specificity—RBPs do not generally occupy all of their available binding motifs throughout the transcriptome (Li *et al.* 2010; Taliaferro *et al.* 2016). Moreover, non-paralog RBPs with substantially overlapping or identical linear target motifs still bind distinct RNA target sets, demonstrating that linear motifs are only one of a set of RNA features that direct RBP-RNA associations (Dominguez *et al.* 2018). Based on the present study, these general features of RBPs hold for Nab2 as well. MEME and FIMO motif analyses reveal a long A-rich motif and the canonical Nab2 binding motifs A_{12} and $A_{11}G$ are enriched in but not exclusive to Nab2-associated RNAs (Figure 3-6). Given the behavior of other RBPs, it is consistent that *Drosophila* Nab2 exhibits this binding specificity and, given our RIP-Seq data and previous studies, likely binds some but almost certainly does not bind not all poly(A) tails in *Drosophila* despite its high affinity for polyadenosine RNA *in vitro* (Pak *et al.* 2011).

Taken together, these data align with the model that in metazoans Nab2/ZC3H14 is more specific in its transcript associations than in *S. cerevisiae*. With this model in mind and the Nab2-associated transcripts identified in this study in hand, future research will be enabled to focus on how Nab2 functions on these particular transcripts in *Drosophila*, and why this function is so

crucial for adult viability, neuronal morphology, locomotion, and learning and memory. Given that a polyadenosine-rich motif along with A_{12} and $A_{11}G$ motifs are correlated with but are not sufficient for Nab2-RNA association, future research must also focus on what additional features of transcripts or their associated proteins promote or prevent Nab2 association.

Conclusion

In sum, the data we present here identify functional interactions between Nab2 and Atx2 in *Drosophila* brain morphology and adult viability and define a set of RNA transcripts associated with each protein in brain neurons. Crucially, theses RNA sets overlap—some associated transcripts are shared between Nab2 and Atx2 and some are specific to each RBP. Identifying these RBP-associated transcripts provides potential mechanistic links between the roles in neuronal development and function their encoded proteins perform, Nab2, and Atx2. This foundation will be especially important for Nab2, as the exact molecular function of metazoan Nab2/ZC3H14 on the vast majority of its associated RNAs in any cell type remains largely unknown. The identity of many *Drosophila* Nab2-associated transcripts, now revealed, will be required to define Nab2/ZC3H14 function in metazoans and enable our understanding of why loss of this largely nuclear polyadenosine RNA-binding protein results in neurological or neurodevelopmental deficits in flies and mice and in intellectual disability in humans.

ACKNOWLEDGEMENTS

The authors would like to thank current and past members of the Moberg and Corbett lab groups, especially Drs. Ayan Banerjee, Rick Bienkowski, Daniel Barron, Binta Jalloh, Stephanie Jones, Annie McPherson-Davie, Milo Fasken, and Sara Leung for their support of, instruction in, and enlightening discussions of this work. We would also like to thank Drs. Bing Yao, Jingjing Yang, Michael Christopher, and Carlos Moreno for initial bioinformatics advice and the Georgia Genomics and Bioinformatics Core (GGBC) at the University of Georgia, especially Tyler James Simmonds and Dr. Magdy S. Alabady, for essential library preparation, sequencing, and assistance in sequencing experiment design and preparation.

We would like to thank Drs. Nancy Bonini and Michael Parisi for the gift of a *Atx2*^{X1} stock; Dr. Ravi Allada, Khadijah Hamid, and Dr. Satya Surabhi for the gift of a *UAS>Atx2-3xFLAG* stock; Dr. Chunghun Lim and for the gift of rabbit α-Atx2; Dr. Corey S. Goodman for the contribution of 1D4 Anti-Fas2 to the DSHB; Drs. Gary Bassell, Roger Deal, Steven Warren, James Q. Zheng, and their respective labs for assistance and use of their equipment; Laura Fox-Goharioon for confocal microscope training; Dr. Michael I. Love for extensive public online instruction in the methodology and use of *DESeq2*; Dr. Mauricio Rodriguez-Lanetty for a public TRIzol-column hybrid RNA extraction protocol; and Eileen Chow for public video instruction in bulk *Drosophila* head isolation.

The authors would also like to thank with particular enthusiasm the authors, contributors, and ongoing maintainers of the incredible public resources supporting this work and without which it would not have been possible, including Flybase (NIH U41HG000739, UK MRC MR/N030117/1), the Galaxy Project (NIH 2U41HG006620), the R Project, the Developmental Studies Hybridoma Bank (University of Iowa, NIH), and the Bloomington Drosophila Stock Center (NIH P40OD018537). This research was funded by grants from the National Institutes of

Health, specifically from the National Institute of Child Health and Human Development (F31 HD088043) to J.C.R. and from the National Institute of Mental Health (R01 MH107305) to A.H.C. and K.H.M. The authors declare no conflicts of interest.

LITERATURE CITED

Afgan E., D. Baker, B. Batut, M. van den Beek, D. Bouvier, *et al.*, 2018 The Galaxy platform for accessible, reproducible and collaborative biomedical analyses: 2018 update. Nucleic Acids Res. 46: 537–544. https://doi.org/10.1093/nar/gky379

Agha Z., Z. Iqbal, M. Azam, H. Ayub, L. E. L. M. Vissers, *et al.*, 2014 Exome Sequencing Identifies Three Novel Candidate Genes Implicated in Intellectual Disability, (O. R. Bandapalli, Ed.). PLoS One 9: e112687. https://doi.org/10.1371/journal.pone.0112687

Aguilo F., F. Zhang, A. Sancho, M. Fidalgo, S. Di Cecilia, *et al.*, 2015 Coordination of m6A mRNA Methylation and Gene Transcription by ZFP217 Regulates Pluripotency and Reprogramming. Cell Stem Cell 17: 689–704. https://doi.org/10.1016/j.stem.2015.09.005

Aibara S., J. M. B. Gordon, A. S. Riesterer, S. H. McLaughlin, and M. Stewart, 2017 Structural basis for the dimerization of Nab2 generated by RNA binding provides insight into its contribution to both poly(A) tail length determination and transcript compaction in Saccharomyces cerevisiae. Nucleic Acids Res. 45: 1529–1538. https://doi.org/10.1093/nar/gkw1224

Aitchison J. D., G. Blobel, and M. P. Rout, 1996 Kap104p: A karyopherin involved in the nuclear transport of messenger RNA binding proteins. Science (80-.). 274: 624–627. https://doi.org/10.1126/science.274.5287.624

Al-Nabhani M., S. Al-Rashdi, F. Al-Murshedi, A. Al-Kindi, K. Al-Thihli, *et al.*, 2018 Reanalysis of exome sequencing data of intellectual disability samples: Yields and benefits. Clin. Genet. https://doi.org/10.1111/cge.13438

Almudi I., M. Corominas, and F. Serras, 2010 Competition between SOCS36E and Drk modulates sevenless receptor tyrosine kinase activity. J. Cell Sci. 123: 3857–3862. https://doi.org/10.1242/jcs.071134

Alpert T., K. Straube, F. Carrillo Oesterreich, and K. M. Neugebauer, 2020 Widespread Transcriptional Readthrough Caused by Nab2 Depletion Leads to Chimeric Transcripts with Retained Introns. Cell Rep. 33: 108324. https://doi.org/10.1016/j.celrep.2020.108324

Anderson J. T., S. M. Wilson, K. V Datar, and M. S. Swanson, 1993 NAB2: a yeast nuclear polyadenylated RNA-binding protein essential for cell viability. Mol. Cell. Biol. 13: 2730–2741. https://doi.org/10.1128/mcb.13.5.2730

Ashburner M., C. A. Ball, J. A. Blake, D. Botstein, H. Butler, *et al.*, 2000 Gene ontology: Tool for the unification of biology. Nat. Genet. 25: 25–29.

Ashley C. T., K. D. Wilkinson, D. Reines, and S. T. Warren, 1993 FMR1 protein: Conserved RNP family domains and selective RNA binding. Science (80-.). 262: 563–566. https://doi.org/10.1126/science.7692601

Baejen C., P. Torkler, S. Gressel, K. Essig, J. Söding, *et al.*, 2014 Transcriptome Maps of mRNP Biogenesis Factors Define Pre-mRNA Recognition. Mol. Cell 55: 745–757. https://doi.org/10.1016/j.molcel.2014.08.005

Bailey T. L., and C. Elkan, 1994 Fitting a mixture model by expectation maximization to

discover motifs in biopolymers. Proceedings. Int. Conf. Intell. Syst. Mol. Biol. 2: 28–36.

Bailey T. L., M. Boden, F. A. Buske, M. Frith, C. E. Grant, *et al.*, 2009 MEME Suite: Tools for motif discovery and searching. Nucleic Acids Res. 37: W202–W208. https://doi.org/10.1093/nar/gkp335

Bakthavachalu B., J. Huelsmeier, I. P. Sudhakaran, J. Hillebrand, A. Singh, *et al.*, 2018 RNP-Granule Assembly via Ataxin-2 Disordered Domains Is Required for Long-Term Memory and Neurodegeneration Article RNP-Granule Assembly via Ataxin-2 Disordered Domains Is Required for Long-Term Memory and Neurodegeneration. Neuron 98: 754-766.e4. https://doi.org/10.1016/j.neuron.2018.04.032

Banerjee A., K. E. Vest, G. K. Pavlath, and A. H. Corbett, 2017 Nuclear poly(A) binding protein 1 (PABPN1) and Matrin3 interact in muscle cells and regulate RNA processing. Nucleic Acids Res. 45: 10706–10725. https://doi.org/10.1093/nar/gkx786

Barbee S. A., P. S. Estes, A. M. Cziko, J. Hillebrand, R. A. Luedeman, *et al.*, 2006 Staufen- and FMRP-Containing Neuronal RNPs Are Structurally and Functionally Related to Somatic P Bodies. Neuron 52: 997–1009. https://doi.org/10.1016/j.neuron.2006.10.028

Bardoni B., S. Abekhoukh, S. Zongaro, and M. Melko, 2012 Intellectual disabilities, neuronal posttranscriptional RNA metabolism, and RNA-binding proteins: Three actors for a complex scenario, pp. 29–51 in *Progress in Brain Research*, Elsevier B.V.

Batisse J., C. Batisse, A. Budd, B. Bö ttcher, and E. Hurt, 2009 Purification of Nuclear Poly(A)-binding Protein Nab2 Reveals Association with the Yeast Transcriptome and a Messenger Ribonucleoprotein Core Structure. J. Biol. Chem. 284: 34911–34917. https://doi.org/10.1074/jbc.M109.062034

Bellen H. J., R. W. Levis, G. Liao, Y. He, J. W. Carlson, *et al.*, 2004 The BDGP gene disruption project: Single transposon insertions associated with 40% of Drosophila genes. Genetics 167: 761–781. https://doi.org/10.1534/genetics.104.026427

Benoit B., G. Mitou, A. Chartier, C. Temme, S. Zaessinger, *et al.*, 2005 An essential cytoplasmic function for the nuclear poly(A) binding protein, PABP2, in poly(A) tail length control and early development in Drosophila. Dev. Cell 9: 511–522. https://doi.org/10.1016/j.devcel.2005.09.002

Bienkowski R. S., A. Banerjee, J. C. Rounds, J. Rha, O. F. Omotade, *et al.*, 2017 The Conserved, Disease-Associated RNA Binding Protein dNab2 Interacts with the Fragile X Protein Ortholog in Drosophila Neurons. Cell Rep. 20: 1372–1384. https://doi.org/10.1016/j.celrep.2017.07.038

Bokhoven H. van, 2011 Genetic and epigenetic networks in intellectual disabilities. Annu. Rev. Genet. 45: 81–104. https://doi.org/10.1146/annurev-genet-110410-132512

Chelly J., M. Khelfaoui, F. Francis, B. Chérif, and T. Bienvenu, 2006 Genetics and pathophysiology of mental retardation. Eur. J. Hum. Genet. 14: 701–713.

Chen C. Y. A., and A. Bin Shyu, 2014 Emerging mechanisms of mRNP remodeling regulation. Wiley Interdiscip. Rev. RNA 5: 713–722. https://doi.org/10.1002/wrna.1241

Connolly J. B., I. J. H. Roberts, J. D. Armstrong, K. Kaiser, M. Forte, *et al.*, 1996 Associative learning disrupted by impaired Gs signaling in Drosophila mushroom bodies. Science (80-.). 274: 2104–2107. https://doi.org/10.1126/science.274.5295.2104

Corgiat E. B., S. M. List, J. C. Rounds, A. H. Corbett, and K. H. Moberg, 2020 The RNA binding protein Nab2 regulates the proteome of the developing Drosophila brain. bioRxiv 2020.12.10.419846. https://doi.org/10.1101/2020.12.10.419846

Crooks G. E., G. Hon, J. M. Chandonia, and S. E. Brenner, 2004 WebLogo: A sequence logo generator. Genome Res. 14: 1188–1190. https://doi.org/10.1101/gr.849004

Dobin A., C. A. Davis, F. Schlesinger, J. Drenkow, C. Zaleski, *et al.*, 2013 STAR: ultrafast universal RNA-seq aligner. Bioinformatics 29: 15–21. https://doi.org/10.1093/bioinformatics/bts635

Domanski M., K. Molloy, H. Jiang, B. T. Chait, M. P. Rout, *et al.*, 2012 Improved methodology for the affinity isolation of human protein complexes expressed at near endogenous levels. Biotechniques 0: 1–6. https://doi.org/10.2144/000113864

Dominguez D., P. Freese, M. S. Alexis, A. Su, M. Hochman, *et al.*, 2018 Sequence, Structure, and Context Preferences of Human RNA Binding Proteins. Mol. Cell 70: 854-867.e9. https://doi.org/10.1016/j.molcel.2018.05.001

Dubnau J., L. Grady, T. Kitamoto, and T. Tully, 2001 Disruption of neurotransmission in Drosophila mushroom body blocks retrieval but not acquisition of memory. Nature 411: 476–480. https://doi.org/10.1038/35078077

Duncan K., J. G. Umen, and C. Guthrie, 2000 A putative ubiquitin ligase required for efficient mRNA export differentially affects hnRNP transport. Curr. Biol. 10: 687–696. https://doi.org/10.1016/S0960-9822(00)00527-3

Dunnett C. W., 1955 A Multiple Comparison Procedure for Comparing Several Treatments with a Control. J. Am. Stat. Assoc. 50: 1096–1121. https://doi.org/10.1080/01621459.1955.10501294

Elden A. C., H.-J. Kim, M. P. Hart, A. S. Chen-Plotkin, B. S. Johnson, *et al.*, 2010 Ataxin-2 intermediate-length polyglutamine expansions are associated with increased risk for ALS. Nature 466: 1069–1075. https://doi.org/10.1038/nature09320

Ellis M. C., E. M. O'Neill, and G. M. Rubin, 1993 Expression of Drosophila glass protein and evidence for negative regulation of its activity in non-neuronal cells by another DNA-binding protein. Development 119: 855–865.

Eulalio A., I. Behm-Ansmant, D. Schweizer, and E. Izaurralde, 2007 P-Body Formation Is a Consequence, Not the Cause, of RNA-Mediated Gene Silencing. Mol. Cell. Biol. 27: 3970–3981. https://doi.org/10.1128/mcb.00128-07

Farny N. G., J. A. Hurt, and P. A. Silver, 2008 Definition of global and transcript-specific mRNA export pathways in metazoans. Genes Dev. 22: 66–78. https://doi.org/10.1101/gad.1616008

Fasken M. B., A. H. Corbett, and M. Stewart, 2019 Structure-function relationships in the Nab2

polyadenosine-RNA binding Zn finger protein family. Protein Sci. 28: 513–523. https://doi.org/10.1002/pro.3565

Ferris J., H. Ge, L. Liu, and G. Roman, 2006 G(o) signaling is required for Drosophila associative learning. Nat. Neurosci. 9: 1036–1040. https://doi.org/10.1038/nn1738

Freeman M., 1996 Reiterative use of the EGF receptor triggers differentiation of all cell types in the Drosophila eye. Cell 87: 651–660. https://doi.org/10.1016/S0092-8674(00)81385-9

Gai Y., Z. Liu, I. Cervantes-Sandoval, and R. L. Davis, 2016 Drosophila SLC22A Transporter Is a Memory Suppressor Gene that Influences Cholinergic Neurotransmission to the Mushroom Bodies. Neuron 90: 581–595. https://doi.org/10.1016/j.neuron.2016.03.017

González-Aguilera C., C. Tous, R. Babiano, J. de la Cruz, R. Luna, *et al.*, 2011 Nab2 functions in the metabolism of RNA driven by polymerases II and III. Mol. Biol. Cell 22: 2729–40. https://doi.org/10.1091/mbc.E11-01-0055

Goosen N., 2010 Scanning the DNA for damage by the nucleotide excision repair machinery. DNA Repair (Amst). 9: 593–596. https://doi.org/10.1016/j.dnarep.2010.02.015

Grant C. E., T. L. Bailey, and W. S. Noble, 2011 FIMO: Scanning for occurrences of a given motif. Bioinformatics 27: 1017–1018. https://doi.org/10.1093/bioinformatics/btr064

Green D. M., K. A. Marfatia, E. B. Crafton, X. Zhang, X. Cheng, *et al.*, 2002 Nab2p is required for poly(A) RNA export in Saccharomyces cerevisiae and is regulated by arginine methylation via Hmt1p. J. Biol. Chem. 277: 7752–7760. https://doi.org/10.1074/jbc.M110053200

Guisbert K. K., K. Duncan, H. Li, and C. Guthrie, 2005 Functional specificity of shuttling hnRNPs revealed by genome-wide analysis of their RNA binding profiles. RNA 11: 383–393. https://doi.org/10.1261/rna.7234205

Gwinn-Hardy K., J. Y. Chen, H. C. Liu, T. Y. Liu, M. Boss, *et al.*, 2000 Spinocerebellar ataxia type 2 with parkinsonism in ethnic Chinese. Neurology 55: 800–805. https://doi.org/10.1212/WNL.55.6.800

Hao L. Y., B. I. Giasson, and N. M. Bonini, 2010 DJ-1 is critical for mitochondrial function and rescues PINK1 loss of function. Proc. Natl. Acad. Sci. U. S. A. 107: 9747–9752. https://doi.org/10.1073/pnas.0911175107

Hart T., M. Chandrashekhar, M. Aregger, Z. Steinhart, K. R. Brown, *et al.*, 2015 High-Resolution CRISPR Screens Reveal Fitness Genes and Genotype-Specific Cancer Liabilities. Cell 163: 1515–1526. https://doi.org/10.1016/j.cell.2015.11.015

Hay B. A., T. Wolff, and G. M. Rubin, 1994 Expression of baculovirus P35 prevents cell death in Drosophila. Development 120: 2121–2129.

Hector R. E., K. R. Nykamp, S. Dheur, J. T. Anderson, P. J. Non, *et al.*, 2002 Dual requirement for yeast hnRNP Nab2p in mRNA poly(A) tail length control and nuclear export. EMBO J. 21: 1800–10. https://doi.org/10.1093/emboj/21.7.1800

Heisenberg M., 2003 Mushroom body memoir: From maps to models. Nat. Rev. Neurosci. 4:

266–275. https://doi.org/10.1038/nrn1074

Henning K. A., C. Peterson, R. Legerski, and E. C. Friedberg, 1994 Cloning the Drosophila homolog of the xeroderma pigmentosum complementation group C gene reveals homology between the predicted human and drosophila polypeptides and that encoded by the yeast RAD4 gene. Nucleic Acids Res. 22: 257–261. https://doi.org/10.1093/nar/22.3.257

Hillebrand J., K. Pan, A. Kokaram, S. Barbee, R. Parker, *et al.*, 2010 The Me31B DEAD-Box Helicase Localizes to Postsynaptic Foci and Regulates Expression of a CaMKII Reporter mRNA in Dendrites of Drosophila Olfactory Projection Neurons. Front. Neural Circuits 4: 121. https://doi.org/10.3389/fncir.2010.00121

Hoskins R. A., J. W. Carlson, K. H. Wan, S. Park, I. Mendez, *et al.*, 2015 The Release 6 reference sequence of the Drosophila melanogaster genome. Genome Res. 25: 445–458. https://doi.org/10.1101/gr.185579.114

Hudson A. M., and L. Cooley, 2002 A subset of dynamic actin rearrangements in Drosophila requires the Arp2/3 complex. J. Cell Biol. 156: 677–687. https://doi.org/10.1083/jcb.200109065

Huet F., J. T. Lu, K. V. Myrick, L. R. Baugh, M. A. Crosby, *et al.*, 2002 A deletion-generator compound element allows deletion saturation analysis for genomewide phenotypic annotation. Proc. Natl. Acad. Sci. U. S. A. 99: 9948–9953. https://doi.org/10.1073/pnas.142310099

Huynh D. P., H.-T. Yang, H. Vakharia, D. Nguyen, and S. M. Pulst, 2003 Expansion of the polyQ repeat in ataxin-2 alters its Golgi localization, disrupts the Golgi complex and causes cell death. Hum. Mol. Genet. 12: 1485–1496. https://doi.org/10.1093/hmg/ddg175

Imbert G., F. Saudou, G. Yvert, D. Devys, Y. Trottier, *et al.*, 1996 Cloning of the gene for spinooerebellar ataxia 2 reveals a locus with high sensitivity to expanded CAG/glutamine repeats. Nat. Genet. 14: 285–291. https://doi.org/10.1038/ng1196-285

Inlow J. K., and L. L. Restifo, 2004 Molecular and Comparative Genetics of Mental Retardation. Genetics 166: 835–881. https://doi.org/10.1534/genetics.166.2.835

Jalloh B., J. C. Rounds, B. E. Brown, I. J. Kremsky, A. Banerjee, *et al.*, 2020 The Nab2 RNA binding protein promotes sex-specific splicing of Sex lethal in Drosophila neuronal tissue. bioRxiv 2020.11.13.382168. https://doi.org/10.1101/2020.11.13.382168

Jean S., S. Cox, E. J. Schmidt, F. L. Robinson, and A. Kiger, 2012 Sbf/MTMR13 coordinates PI(3)P and Rab21 regulation in endocytic control of cellular remodeling. Mol. Biol. Cell 23: 2723–2740. https://doi.org/10.1091/mbc.E12-05-0375

Jiménez-López D., and P. Guzmán, 2014 Insights into the evolution and domain structure of ataxin-2 proteins across eukaryotes. BMC Res. Notes 7: 453. https://doi.org/10.1186/1756-0500-7-453

Kahsai L., and T. Zars, 2011 Learning and memory in drosophila: Behavior, genetics, and neural systems, pp. 139–167 in *International Review of Neurobiology*, Academic Press Inc.

Kanuka H., T. Hiratou, T. Igaki, H. Kanda, E. Kuranaga, *et al.*, 2005 Gain-of-function screen

identifies a role of the Sec61α translocon in Drosophila postmitotic neurotoxicity. Biochim. Biophys. Acta - Gen. Subj. 1726: 225–237. https://doi.org/10.1016/j.bbagen.2005.06.020

Kelly S. M., S. A. Pabit, C. M. Kitchen, P. Guo, K. A. Marfatia, *et al.*, 2007 Recognition of polyadenosine RNA by zinc finger proteins. Proc. Natl. Acad. Sci. U. S. A. 104: 12306–12311. https://doi.org/10.1073/pnas.0701244104

Kelly S. M., S. W. Leung, L. H. Apponi, A. M. Bramley, E. J. Tran, *et al.*, 2010 Recognition of polyadenosine RNA by the zinc finger domain of nuclear poly(A) RNA-binding protein 2 (Nab2) is required for correct mRNA 3'-end formation. J. Biol. Chem. 285: 26022–32. https://doi.org/10.1074/jbc.M110.141127

Kelly S. M., S. W. Leung, C. Pak, A. Banerjee, K. H. Moberg, *et al.*, 2014 A conserved role for the zinc finger polyadenosine RNA binding protein, ZC3H14, in control of poly(A) tail length. RNA 20: 681–8. https://doi.org/10.1261/rna.043984.113

Kelly S. M., R. Bienkowski, A. Banerjee, D. J. Melicharek, Z. A. Brewer, *et al.*, 2016 The Drosophila ortholog of the Zc3h14 RNA binding protein acts within neurons to pattern axon projection in the developing brain. Dev. Neurobiol. 76: 93–106. https://doi.org/10.1002/dneu.22301

Kelly S. M., A. Elchert, and M. Kahl, 2017 Dissection and immunofluorescent staining of mushroom body and photoreceptor neurons in adult Drosophila melanogaster brains. J. Vis. Exp. 2017: e56174. https://doi.org/10.3791/56174

Kim M., M. Bellini, and S. Ceman, 2009 Fragile X Mental Retardation Protein FMRP Binds mRNAs in the Nucleus. Mol. Cell. Biol. 29: 214–228. https://doi.org/10.1128/mcb.01377-08

Lachkar S., M. Lebois, M. O. Steinmetz, A. Guichet, N. Lal, *et al.*, 2010 Drosophila stathmins bind tubulin heterodimers with high and variable stoichiometries. J. Biol. Chem. 285: 11667–11680. https://doi.org/10.1074/jbc.M109.096727

Laemmli U. K., 1970 Cleavage of structural proteins during the assembly of the head of bacteriophage T4. Nature 227: 680–685. https://doi.org/10.1038/227680a0

Layalle S., E. Coessens, A. Ghysen, and C. Dambly-Chaudière, 2005 Smooth, a hnRNP encoding gene, controls axonal navigation in Drosophila. Genes to Cells 10: 119–125. https://doi.org/10.1111/j.1365-2443.2005.00822.x

Lee D. C. Y., and J. D. Aitchison, 1999 Kap104p-mediated nuclear import. Nuclear localization signals in mRNA- binding proteins and the role of Ran and RNA. J. Biol. Chem. 274: 29031–29037. https://doi.org/10.1074/jbc.274.41.29031

Lee J., E. Yoo, H. Lee, K. Park, J.-H. Hur, *et al.*, 2017 LSM12 and ME31B/DDX6 Define Distinct Modes of Posttranscriptional Regulation by ATAXIN-2 Protein Complex in Drosophila Circadian Pacemaker Neurons. Mol. Cell 66: 129-140.e7. https://doi.org/10.1016/j.molcel.2017.03.004

Lee J., M. Kim, T. Q. Itoh, and C. Lim, 2018 Ataxin-2: A versatile posttranscriptional regulator and its implication in neural function. Wiley Interdiscip. Rev. RNA 9: e1488. https://doi.org/10.1002/wrna.1488

Lee W.-H., E. B. Corgiat, J. C. Rounds, Z. Shepherd, A. H. Corbett, *et al.*, 2020 A Genetic Screen Links the Disease-Associated Nab2 RNA-Binding Protein to the Planar Cell Polarity Pathway in Drosophila melanogaster. G3 GENES, GENOMES, Genet. https://doi.org/10.1534/g3.120.401637

Lessing D., and N. M. Bonini, 2008 Polyglutamine Genes Interact to Modulate the Severity and Progression of Neurodegeneration in Drosophila, (H. Y. Zoghbi, Ed.). PLoS Biol. 6: e29. https://doi.org/10.1371/journal.pbio.0060029

Li X., G. Quon, H. D. Lipshitz, and Q. Morris, 2010 Predicting in vivo binding sites of RNA-binding proteins using mRNA secondary structure. RNA 16: 1096–1107. https://doi.org/10.1261/rna.2017210

Li J., Y. Chen, X. Xu, J. Jones, M. Tiwari, *et al.*, 2019 HNRNPK maintains epidermal progenitor function through transcription of proliferation genes and degrading differentiation promoting mRNAs. Nat. Commun. 10: 1–14. https://doi.org/10.1038/s41467-019-12238-x

Liao Y., G. K. Smyth, and W. Shi, 2014 featureCounts: an efficient general purpose program for assigning sequence reads to genomic features. Bioinformatics 30: 923–930. https://doi.org/10.1093/bioinformatics/btt656

Lim C., and R. Allada, 2013 ATAXIN-2 Activates PERIOD Translation to Sustain Circadian Rhythms in Drosophila. Science (80-.). 340. https://doi.org/10.1126/science.1234785

Lin D. M., and C. S. Goodman, 1994 Ectopic and increased expression of fasciclin II alters motoneuron growth cone guidance. Neuron 13: 507–523. https://doi.org/10.1016/0896-6273(94)90022-1

Love M. I., W. Huber, and S. Anders, 2014 Moderated estimation of fold change and dispersion for RNA-seq data with DESeq2. Genome Biol. 15: 550. https://doi.org/10.1186/s13059-014-0550-8

Lu Z., X. Guan, C. A. Schmidt, and A. G. Matera, 2014 RIP-seq analysis of eukaryotic Sm proteins identifies three major categories of Sm-containing ribonucleoproteins. Genome Biol. 15: 1–23. https://doi.org/10.1186/gb-2014-15-1-r7

Malmevik J., R. Petri, T. Klussendorf, P. Knauff, M. Åkerblom, *et al.*, 2015 Identification of the miRNA targetome in hippocampal neurons using RIP-seq. Sci. Rep. 5: 12609. https://doi.org/10.1038/srep12609

Mandel C. R., Y. Bai, and L. Tong, 2008 Protein factors in pre-mRNA 3′-end processing. Cell. Mol. Life Sci. 65: 1099–1122.

Mangus D. A., N. Amrani, and A. Jacobson, 1998 Pbp1p, a Factor Interacting withSaccharomyces cerevisiae Poly(A)-Binding Protein, Regulates Polyadenylation. Mol. Cell. Biol. 18: 7383–7396. https://doi.org/10.1128/mcb.18.12.7383

Mangus D. A., M. C. Evans, and A. Jacobson, 2003 Poly(A)-binding proteins: Multifunctional scaffolds for the post-transcriptional control of gene expression. Genome Biol. 4: 1–14. https://doi.org/10.1186/gb-2003-4-7-223

Mangus D. A., M. M. Smith, J. M. McSweeney, and A. Jacobson, 2004 Identification of Factors

Regulating Poly(A) Tail Synthesis and Maturation. Mol. Cell. Biol. 24: 4196–4206. https://doi.org/10.1128/mcb.24.10.4196-4206.2004

Maulik P. K., M. N. Mascarenhas, C. D. Mathers, T. Dua, and S. Saxena, 2011 Prevalence of intellectual disability: A meta-analysis of population-based studies. Res. Dev. Disabil. 32: 419–436.

McCann C., E. E. Holohan, S. Das, A. Dervan, A. Larkin, *et al.*, 2011 The Ataxin-2 protein is required for microRNA function and synapse-specific long-term olfactory habituation. Proc. Natl. Acad. Sci. U. S. A. 108: E655-62. https://doi.org/10.1073/pnas.1107198108

Merino M. M., C. Rhiner, M. Portela, and E. Moreno, 2013 "Fitness fingerprints" mediate physiological culling of unwanted neurons in drosophila. Curr. Biol. 23: 1300–1309. https://doi.org/10.1016/j.cub.2013.05.053

Mi H., A. Muruganujan, D. Ebert, X. Huang, and P. D. Thomas, 2019 PANTHER version 14: more genomes, a new PANTHER GO-slim and improvements in enrichment analysis tools. Nucleic Acids Res. 47: 419–426. https://doi.org/10.1093/nar/gky1038

Moore M. J., 2005 From birth to death: The complex lives of eukaryotic mRNAs. Science (80-.). 309: 1514–1518. https://doi.org/10.1126/science.1111443

Moressis A., A. R. Friedrich, E. Pavlopoulos, R. L. Davis, and E. M. C. Skoulakis, 2009 A dual role for the adaptor protein DRK in Drosophila olfactory learning and memory. J. Neurosci. 29: 2611–2625. https://doi.org/10.1523/JNEUROSCI.3670-08.2009

Morgan M., 2018 BiocManager: Access the Bioconductor Project Package Repository

Morris K. J., and A. H. Corbett, 2018 The polyadenosine RNA-binding protein ZC3H14 interacts with the THO complex and coordinately regulates the processing of neuronal transcripts. Nucleic Acids Res. 46: 6561–6575. https://doi.org/10.1093/nar/gky446

Müller-McNicoll M., and K. M. Neugebauer, 2013 How cells get the message: Dynamic assembly and function of mRNA-protein complexes. Nat. Rev. Genet. 14: 275–287. https://doi.org/10.1038/nrg3434

Najmabadi H., H. Hu, M. Garshasbi, T. Zemojtel, S. S. Abedini, *et al.*, 2011 Deep sequencing reveals 50 novel genes for recessive cognitive disorders. Nature 478: 57–63. https://doi.org/10.1038/nature10423

Nakamura A., R. Amikura, K. Hanyu, and S. Kobayashi, 2001 Me31B silences translation of oocyte-localizing RNAs through the formation of cytoplasmic RNP complex during Drosophila oogenesis. Development 128: 3233–3242.

Oortveld M. A. W., S. Keerthikumar, M. Oti, B. Nijhof, A. C. Fernandes, *et al.*, 2013 Human Intellectual Disability Genes Form Conserved Functional Modules in Drosophila, (J. Flint, Ed.). PLoS Genet. 9: e1003911. https://doi.org/10.1371/journal.pgen.1003911

Ostrowski L. A., A. C. Hall, and K. Mekhail, 2017 Ataxin-2: From RNA control to human health and disease. Genes (Basel). 8: 2–21.

Oswald M. C. W., P. S. Brooks, M. F. Zwart, A. Mukherjee, R. J. H. West, *et al.*, 2018 Reactive

oxygen species regulate activity- dependent neuronal plasticity in Drosophila. Elife 7. https://doi.org/10.7554/eLife.39393

Pak C., M. Garshasbi, K. Kahrizi, C. Gross, L. H. Apponi, *et al.*, 2011 Mutation of the conserved polyadenosine RNA binding protein, ZC3H14/dNab2, impairs neural function in Drosophila and humans. Proc. Natl. Acad. Sci. U. S. A. 108: 12390–5. https://doi.org/10.1073/pnas.1107103108

Park H., H. J. Kim, and B. S. Jeon, 2015 Parkinsonism in spinocerebellar ataxia. Biomed Res. Int. 2015.

Parks A. L., K. R. Cook, M. Belvin, N. A. Dompe, R. Fawcett, *et al.*, 2004 Systematic generation of high-resolution deletion coverage of the Drosophila melanogaster genome. Nat. Genet. 36: 288–292. https://doi.org/10.1038/ng1312

Patterson S., How To Focus Stack Images In Photoshop. photoshopessentials.com.

Pulst S. M., A. Nechiporuk, T. Nechiporuk, S. Gispert, X. N. Chen, *et al.*, 1996 Moderate expansion of a normally biallelic trinucleotide repeat in spinooerebellar ataxia type. Nat. Genet. 14: 269–276. https://doi.org/10.1038/ng1196-269

R Core Team, 2019 R: A Language and Environment for Statistical Computing

R Studio Team, 2018 RStudio: Integrated Development Environment for R

Ragab A., E. C. Thompson, and A. A. Travers, 2006 High mobility group proteins HMGD and HMGZ interact genetically with the Brahma chromatin remodeling complex in Drosophila. Genetics 172: 1069–1078. https://doi.org/10.1534/genetics.105.049957

Rha J., S. K. Jones, and A. H. Corbett, 2017a ZC3H14, pp. 1–7 in *Encyclopedia of Signaling Molecules*, edited by Choi S. Springer New York, New York, NY.

Rha J., S. K. Jones, J. Fidler, A. Banerjee, S. W. Leung, *et al.*, 2017b The RNA-binding protein, ZC3H14, is required for proper poly(A) tail length control, expression of synaptic proteins, and brain function in mice. Hum. Mol. Genet. 26: 3663–3681. https://doi.org/10.1093/hmg/ddx248

Robinson J. T., H. Thorvaldsdóttir, W. Winckler, M. Guttman, E. S. Lander, *et al.*, 2011 Integrative genomics viewer. Nat. Biotechnol. 29: 24–26.

Rodal A. A., A. D. Blunk, Y. Akbergenova, R. A. Jorquera, L. K. Buhl, *et al.*, 2011 A presynaptic endosomal trafficking pathway controls synaptic growth signaling. J. Cell Biol. 193: 201–217. https://doi.org/10.1083/jcb.201009052

Rodriguez-Lanetty M., *Trizol/RNeasy hybrid RNA extraction protocol*.

Rørth P., 1996 A modular misexpression screen in Drosophila detecting tissue-specific phenotypes. Proc. Natl. Acad. Sci. U. S. A. 93: 12418–12422. https://doi.org/10.1073/pnas.93.22.12418

Rørth P., K. Szabo, A. Bailey, T. Laverty, J. Rehm, *et al.*, 1998 Systematic gain-of-function genetics in Drosophila. Development 125: 1049–1057.

Rothman K. J., 1990 No adjustments are needed for multiple comparisons. Epidemiology 1: 43–6.

Rueden C. T., J. Schindelin, M. C. Hiner, B. E. DeZonia, A. E. Walter, *et al.*, 2017 ImageJ2: ImageJ for the next generation of scientific image data. BMC Bioinformatics 18: 529. https://doi.org/10.1186/s12859-017-1934-z

Sanpei K., H. Takano, S. Igarashi, T. Sato, M. Oyake, *et al.*, 1996 Identification of the spinocerebellar ataxia type 2 gene using a direct identification of repeat expansion and cloning technique, DIRECT. Nat. Genet. 14: 277–284. https://doi.org/10.1038/ng1196-277

Satterfield T. F., S. M. Jackson, and L. J. Pallanck, 2002 A Drosophila Homolog of the Polyglutamine Disease Gene SCA2 Is a Dosage-Sensitive Regulator of Actin Filament Formation. Genetics 162: 1687–1702.

Schindelin J., I. Arganda-Carreras, E. Frise, V. Kaynig, M. Longair, *et al.*, 2012 Fiji: An open-source platform for biological-image analysis. Nat. Methods 9: 676–682.

Schmid M., P. Olszewski, V. Pelechano, I. Gupta, L. M. Steinmetz, *et al.*, 2015 The Nuclear PolyA-Binding Protein Nab2p Is Essential for mRNA Production. Cell Rep. 12: 128–139. https://doi.org/10.1016/j.celrep.2015.06.008

Schneider C. A., W. S. Rasband, and K. W. Eliceiri, 2012 NIH Image to ImageJ: 25 years of image analysis. Nat. Methods 9: 671–675.

Schoenherr J. A., J. M. Drennan, J. S. Martinez, M. R. Chikka, M. C. Hall, *et al.*, 2012 Drosophila Activated Cdc42 Kinase Has an Anti-Apoptotic Function, (H. Steller, Ed.). PLoS Genet. 8: e1002725. https://doi.org/10.1371/journal.pgen.1002725

Slowikowski K., 2019 ggrepel: Automatically Position Non-Overlapping Text Labels with "ggplot2"

Soucek S., Y. Zeng, D. L. Bellur, M. Bergkessel, K. J. Morris, *et al.*, 2016 The Evolutionarily-conserved Polyadenosine RNA Binding Protein, Nab2, Cooperates with Splicing Machinery to Regulate the Fate of pre-mRNA. Mol. Cell. Biol. 36: 2697–2714. https://doi.org/10.1128/MCB.00402-16

Stewart M., 2019 Polyadenylation and nuclear export of mRNAs. J. Biol. Chem. 294: 2977–2987. https://doi.org/10.1074/jbc.REV118.005594

Sudhakaran I. P., J. Hillebrand, A. Dervan, S. Das, E. E. Holohan, *et al.*, 2014 FMRP and Ataxin-2 function together in long-term olfactory habituation and neuronal translational control. Proc Natl Acad Sci U S A 111: E99–E108. https://doi.org/10.1073/pnas.1309543111

Takemura S. ya, Y. Aso, T. Hige, A. Wong, Z. Lu, *et al.*, 2017 A connectome of a learning and memory center in the adult Drosophila brain. Elife 6. https://doi.org/10.7554/eLife.26975

Taliaferro J. M., N. J. Lambert, P. H. Sudmant, D. Dominguez, J. J. Merkin, *et al.*, 2016 RNA Sequence Context Effects Measured In Vitro Predict In Vivo Protein Binding and Regulation. Mol. Cell 64: 294–306. https://doi.org/10.1016/j.molcel.2016.08.035

Tamanini F., C. Bontekoe, C. E. Bakker, L. Van Unen, B. Anar, *et al.*, 1999 Different targets for the fragile X-related proteins revealed by their distinct nuclear localizations. Hum. Mol. Genet. 8: 863–869. https://doi.org/10.1093/hmg/8.5.863

Tan L., K. X. Zhang, M. Y. Pecot, S. Nagarkar-Jaiswal, P. T. Lee, *et al.*, 2015 Ig Superfamily Ligand and Receptor Pairs Expressed in Synaptic Partners in Drosophila. Cell 163: 1756–1769. https://doi.org/10.1016/j.cell.2015.11.021

Tassé M. J., R. Luckasson, and R. L. Schalock, 2016 The relation between intellectual functioning and adaptive behavior in the diagnosis of intellectual disability. Intellect. Dev. Disabil. 54: 381–390. https://doi.org/10.1352/1934-9556-54.6.381

The Gene Ontology Consortium, 2019 The Gene Ontology Resource: 20 years and still GOing strong. Nucleic Acids Res. 47: D330–D338. https://doi.org/10.1093/nar/gky1055

Thurmond J., J. L. Goodman, V. B. Strelets, H. Attrill, L. S. Gramates, *et al.*, 2018 FlyBase 2.0: the next generation. Nucleic Acids Res. 47: 759–765. https://doi.org/10.1093/nar/gky1003

Tuck A. C., and D. Tollervey, 2013 A transcriptome-wide atlas of RNP composition reveals diverse classes of mRNAs and lncRNAs. Cell 154: 996–1009. https://doi.org/10.1016/j.cell.2013.07.047

Velichkova M., J. Juan, P. Kadandale, S. Jean, I. Ribeiro, *et al.*, 2010 Drosophila Mtm and class II PI3K coregulate a PI(3)P pool with cortical and endolysosomal functions. J. Cell Biol. 190: 407–425. https://doi.org/10.1083/jcb.200911020

Verkerk A. J. M. H., M. Pieretti, J. S. Sutcliffe, Y. H. Fu, D. P. A. Kuhl, *et al.*, 1991 Identification of a gene (FMR-1) containing a CGG repeat coincident with a breakpoint cluster region exhibiting length variation in fragile X syndrome. Cell 65: 905–914. https://doi.org/10.1016/0092-8674(91)90397-H

Verma V., A. Paul, A. A. Vishwanath, B. Vaidya, and J. P. Clement, 2019 Understanding intellectual disability and utism spectrum disorders from common mouse models: Synapses to behaviour. Open Biol. 9. https://doi.org/10.1098/rsob.180265

Vest K. E., B. L. Phillips, A. Banerjee, L. H. Apponi, E. B. Dammer, *et al.*, 2017 Novel mouse models of oculopharyngeal muscular dystrophy (OPMD) reveal early onset mitochondrial defects and suggest loss of PABPN1 may contribute to pathology. Hum. Mol. Genet. 26: 3235–3252. https://doi.org/10.1093/hmg/ddx206

Vissers L. E. L. M., C. Gilissen, and J. A. Veltman, 2016 Genetic studies in intellectual disability and related disorders. Nat. Rev. Genet. 17: 9–18.

Wan L., T. C. Dockendorff, T. A. Jongens, and G. Dreyfuss, 2000 Characterization of dFMR1, a Drosophila melanogaster Homolog of the Fragile X Mental Retardation Protein. Mol. Cell. Biol. 20: 8536–8547. https://doi.org/10.1128/mcb.20.22.8536-8547.2000

Wickham H., 2016 *ggplot2: Elegant Graphics for Data Analysis*. Springer-Verlag New York.

Wigington C. P., K. J. Morris, L. E. Newman, and A. H. Corbett, 2016 The Polyadenosine RNA-binding Protein, Zinc Finger Cys 3 His Protein 14 (ZC3H14), Regulates the Pre-mRNA Processing of a Key ATP Synthase Subunit mRNA * □ S. Publ. JBC Pap. Press.

https://doi.org/10.1074/jbc.M116.754069

Williamson W. R., and P. R. Hiesinger, 2010 Preparation of developing and adult Drosophila brains and retinae for live imaging. J. Vis. Exp. e1936. https://doi.org/10.3791/1936

Wolff T., and D. F. Ready, 1991 *The beginning of pattern formation in the Drosophila compound eye: the morphogenetic furrow and the second mitotic wave*.

Yagi R., Y. Mabuchi, M. Mizunami, and N. K. Tanaka, 2016 Convergence of multimodal sensory pathways to the mushroom body calyx in Drosophila melanogaster. Sci. Rep. 6. https://doi.org/10.1038/srep29481

Yang Z., H. J. Edenberg, and R. L. Davis, 2005 Isolation of mRNA from specific tissues of Drosophila by mRNA tagging. Nucleic Acids Res. 33: e148–e148. https://doi.org/10.1093/nar/gni149

Yang Q., X. F. Zhang, T. D. Pollard, and P. Forscher, 2012 Arp2/3 complex-dependent actin networks constrain myosin II function in driving retrograde actin flow. J. Cell Biol. 197: 939–956. https://doi.org/10.1083/jcb.201111052

Yates A. D., P. Achuthan, W. Akanni, J. Allen, J. Allen, *et al.*, 2020 Ensembl 2020. Nucleic Acids Res. 48. https://doi.org/10.1093/nar/gkz966

Yokoshi M., Q. Li, M. Yamamoto, H. Okada, Y. Suzuki, *et al.*, 2014 Direct Binding of Ataxin-2 to Distinct Elements in 3′ UTRs Promotes mRNA Stability and Protein Expression. Mol. Cell 55: 186–198. https://doi.org/10.1016/J.MOLCEL.2014.05.022

Zhang Y., J. Ling, C. Yuan, R. Dubruille, and P. Emery, 2013 A Role for Drosophila ATX2 in Activation of PER Translation and Circadian Behavior. Science (80-.). 340.

Zhang Y., L. Zhang, X. Tang, S. R. Bhardwaj, J. Ji, *et al.*, 2016 MTV, an ssDNA Protecting Complex Essential for Transposon-Based Telomere Maintenance in Drosophila, (G. Bosco, Ed.). PLOS Genet. 12: e1006435. https://doi.org/10.1371/journal.pgen.1006435

Zhao J., T. K. Ohsumi, J. T. Kung, Y. Ogawa, D. J. Grau, *et al.*, 2010 Genome-wide Identification of Polycomb-Associated RNAs by RIP-seq. Mol. Cell 40: 939–953. https://doi.org/10.1016/j.molcel.2010.12.011

Zwarts L., L. Vanden Broeck, E. Cappuyns, J. F. Ayroles, M. M. Magwire, *et al.*, 2015 The genetic basis of natural variation in mushroom body size in Drosophila melanogaster. Nat. Commun. 6: 1–11. https://doi.org/10.1038/ncomms10115

FIGURES AND TABLES

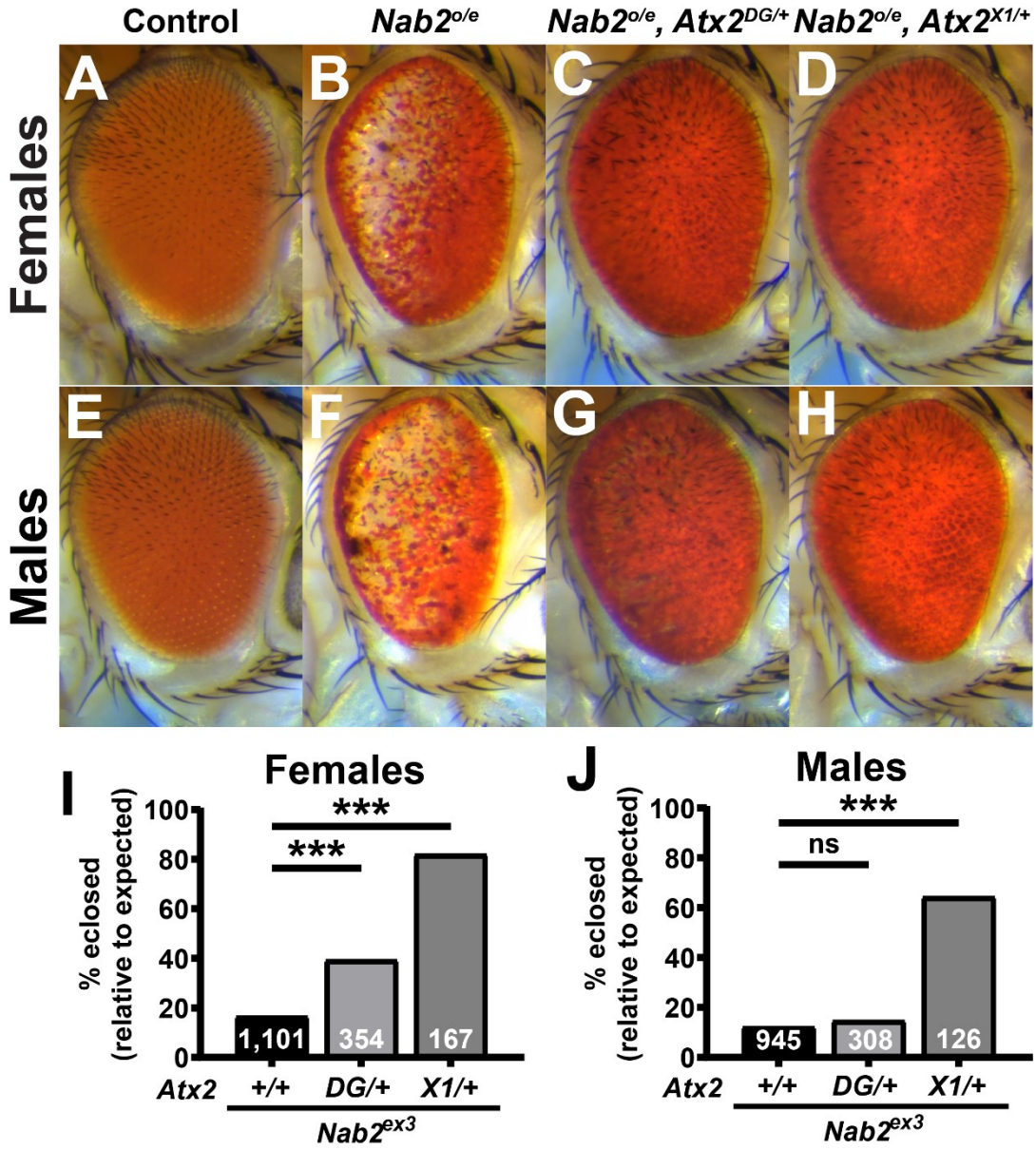

Figure 3-1. Loss-of-function alleles of *Atx2* suppress effects of *Nab2* misexpression in female and male *Drosophila*. Compared to (A) the uniform color and regimented ommatidial structure of the *Drosophila* eye in control females expressing the fated-eye-cell-specific *GMR-Gal4* driver alone, (B) overexpression of endogenous *Nab2* with *GMR-Gal4* (*Nab2*$^{o/e}$) induces posterior pigment loss, sporadic blackened patches, and ommatidial disorder or "roughness". Heterozygosity for either of two *Atx2* loss-of-function alleles, (C) *Atx2*$^{DG08112/+}$ or (D) *Atx2*$^{X1/+}$,

dominantly suppresses the pigment loss and blackened patch phenotype, with limited impact on roughness. (E-H) These genetic relationships are also observed in eyes in males. (I, J) Flies lacking functional endogenous *Nab2*, $Nab2^{ex3}$ homozygotes, demonstrate dramatically decreased adult viability, as quantified by the percentage of flies reaching pupal eclosion and adulthood out of the amount expected by Mendelian inheritance. (I) In females, both loss-of-function alleles of *Atx2* significantly suppress this effect, partially rescuing viability; (J) in males, only $Atx2^{XI/+}$ suppresses. Sample sizes (n) are reported in each bar and include all F1 progeny scored, including genetically distinct siblings of the genotype of interest used to calculate *% eclosed (relative to expected)*. Fisher's Exact Test (two-sided) was used to assess statistical significance. ns=not significant, ***=$p<0.001$.

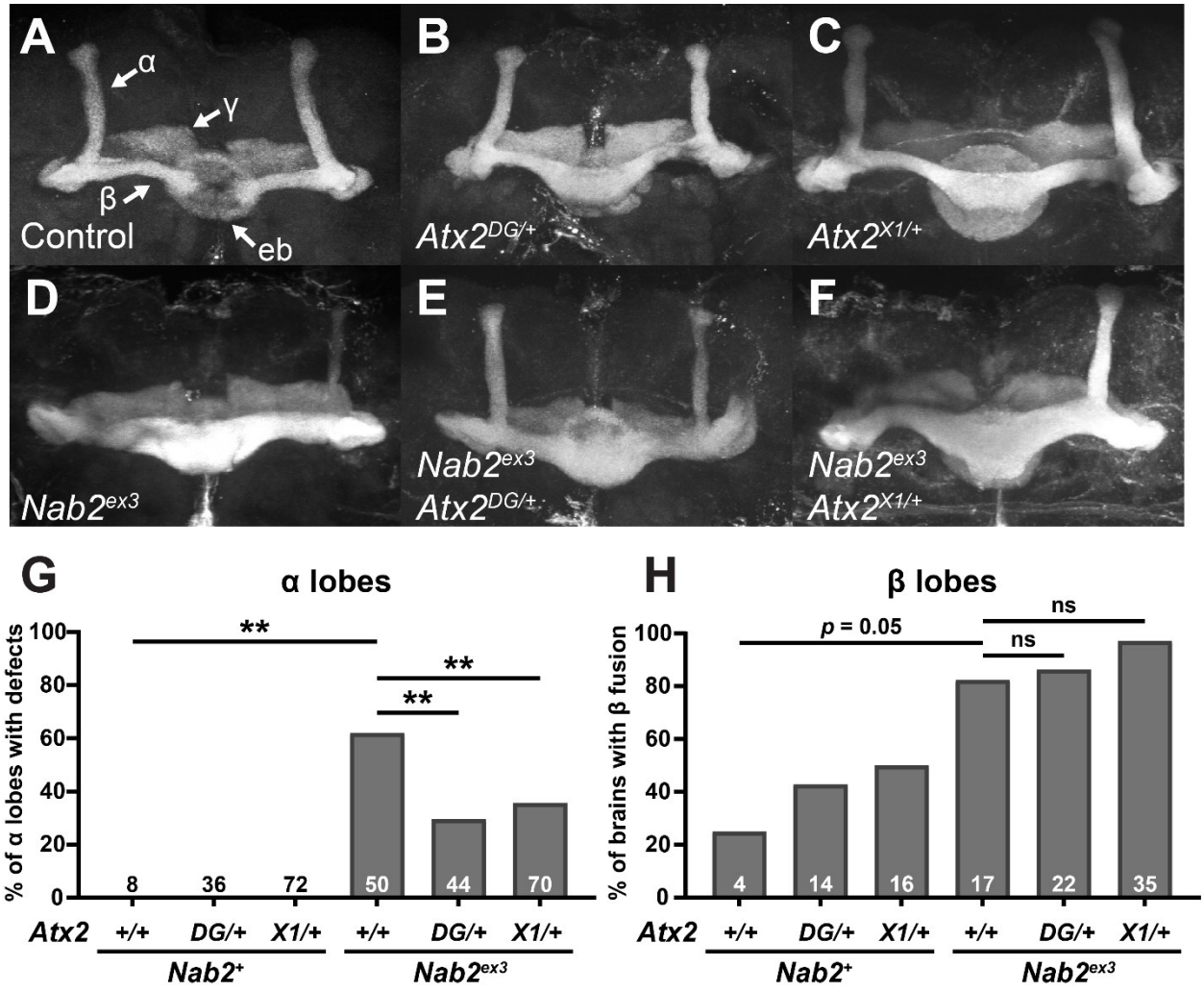

Figure 3-2. Loss-of-function alleles of *Atx2* specifically suppress axon morphology defects in *Nab2*^{ex3} mushroom body α, but not β, lobes. (A) In a representative *Nab2*^{pex41} control brain, Fasciclin 2 (Fas2)-marked axons from some Kenyon cells of the mushroom body bifurcate and project dorsally into α lobes and medially into β lobes. Fas2 also marks mushroom body γ lobes and the ellipsoid body (eb) (white arrows). Representative images show heterozygosity for (B) *Atx2*$^{DG08112/+}$ or (C) *Atx2*$^{X1/+}$ induces over-projection or "fusion" of β lobes, while (D) homozygosity for the *Nab2* null allele *Nab2*^{ex3} induces both β lobe fusion and the thinning or complete absence of α lobes. Heterozygosity for either (E) *Atx2*$^{DG08112/+}$ or (F) *Atx2*$^{X1/+}$ in combination with *Nab2*^{ex3} partially restores proper α lobe morphology and, as quantified in (G),

significantly suppresses the penetrance of α lobe defects compared to *Nab2*^{ex3} alone. (H) By comparison, as quantified in (H), these *Atx2* alleles neither suppress nor enhance the penetrance of β lobe defects compared to *Nab2*^{ex3} alone. Sample sizes (n) are reported in each bar and quantify, for each genotype, the total number of α lobes scored for defects and the total number of brains scored for β lobe fusion. Fisher's Exact Test (two-tailed) was used to assess statistical significance. ns=not significant, **=$p \leq 0.01$.

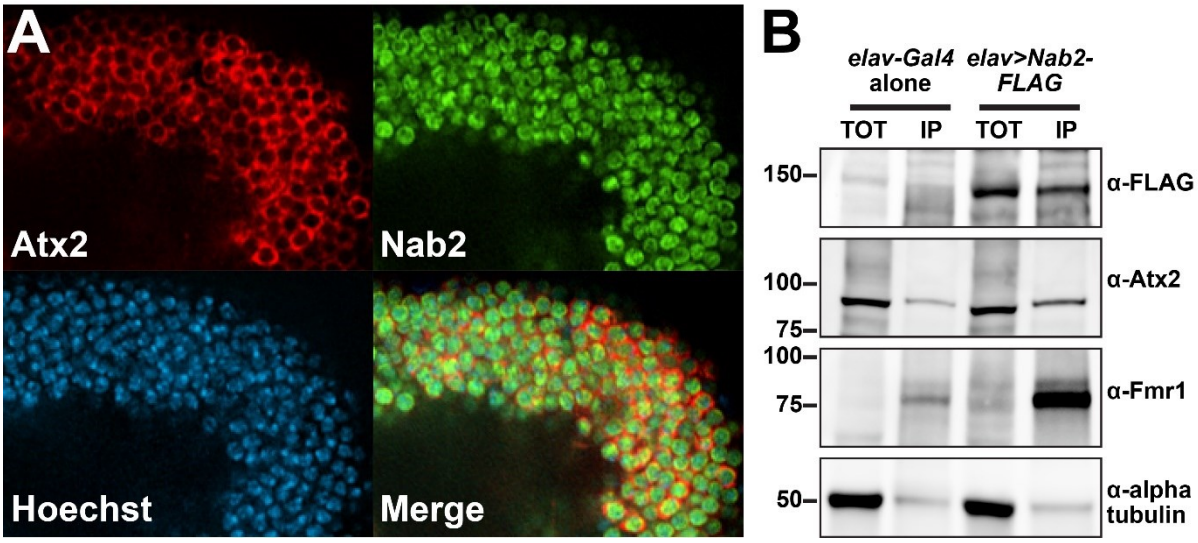

Figure 3-3. Nab2 and Atx2 primarily localize to different cellular compartments and show limited physical association in brain neurons. (A) To specifically assess protein localization in mushroom body neurons, tagged transgenic copies of Atx2 and Nab2 (Atx2-3xFLAG and Nab2-YFP) were expressed in female brains under the MB-specific *OK107-Gal4*. Kenyon cell soma, the cell bodies of the MBs, are shown for a representative brain. False-colored panels show fluorescence corresponding to α-FLAG (red, Atx2-3xFLAG), α-GFP (green, Nab2-YFP), Hoechst 33342 (blue, nuclei), and a merge of all three channels. Nab2 is localized primarily to the nuclei at steady state based on overlap with Hoechst 33342 signal, and Atx2 localizes primarily in the surrounding cytoplasm. (B) To test for physical association between Nab2 and Atx2 in brain neurons, lysates of female *Drosophila* heads, either *elav-Gal4* alone controls or *elav>Nab2-FLAG*, were subjected to co-immunoprecipitation using α-FLAG. For both genotypes, Input samples (TOT) represent 6.25% of assayed lysate and immunoprecipitation (IP) samples represent 25% of total samples eluted from α-FLAG beads. Samples were resolved via gel electrophoresis and analyzed by immunoblotting, probing with antibodies against FLAG, Atx2, Fmr1 (a positive control), or alpha tubulin (a negative control). Atx2 associates weakly with Nab2 based on its

enrichment in IP samples; this association is less robust than that between Nab2 and positive control Fmr1.

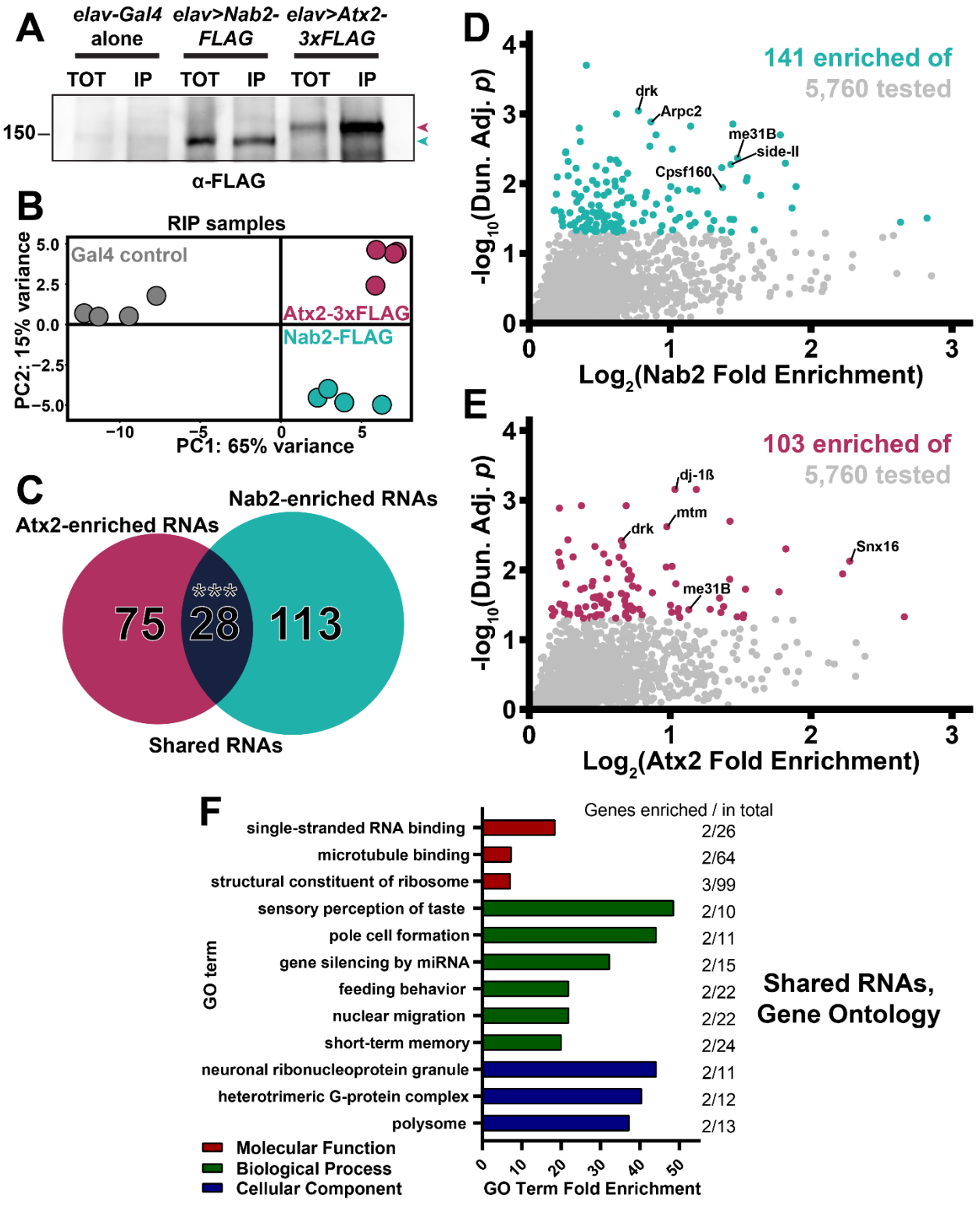

Figure 3-4. RIP-Seq reveals overlapping sets of transcripts associate with Nab2-FLAG and Atx2-3xFLAG in brain neurons. (A) Lysates from heads of female adult flies expressing either

pan-neuronal *elav-Gal4* alone as a control, *elav>Nab2-FLAG*, or *elav>Atx2-3xFLAG* were subjected to α-FLAG immunoprecipitation and immunoblotting to test IP efficacy. Input samples (TOT) represent ~6.25% of total assayed lysates and immunoprecipitation samples (IP) represent 25% of total samples eluted from α-FLAG beads. Both epitope-tag samples show robust immunoreactivity to α-FLAG in TOT and IP (arrowheads), indicating effective transgene expression and successful tagged-protein enrichment by IP. (B) Principal component analysis of 12 sequenced RNA IP samples reveals high intra-genotype reproducibility. Comparison of principal component 1 (PC1) and principal component 2 (PC2) demonstrates Nab-FLAG (teal) and Atx2-3xFLAG (maroon) samples differ more from Gal4 controls (gray) than from one another, as predicted. (C) Venn diagram of Nab2-enriched and Atx2-enriched RNAs identified by RIP-Seq, revealing that 28 shared transcripts associate with both RBPs, a significant overlap according to the hypergeometric test (***=$p<0.001$). (D-E) Scatter plot of all transcripts within the 5,760 of the testable set with positive (D) log_2*(Nab2 Fold Enrichment)* or (E) log_2*(Atx2 Fold Enrichment)* values. *Fold Enrichment* values quantify how effectively a transcript was enriched by IP and are derived by calculating IP/Input (i.e. percent input) values for control and epitope-tag samples and setting the average of control values to 1 (i.e. 0 on the logarithmic scale used here). Y-axes display results of significance testing, conducted by gene-by-gene one-way ANOVA, Dunnett's post-hoc test, and within-gene multiple hypothesis testing adjustment (*Dun. Adj. p*). Statistically significant transcripts (*Dun. Adj. p* < 0.05) are colored. On each plot, labels identify three transcripts among the "top" (see *Results* for details) RBP-specific RBP-associated transcripts and two transcripts (*drk*, *me31B*) among the shared RBP-associated transcripts. (F) The independent *Molecular Function* (red), *Biological Process* (green), and *Cellular Component* (blue) Gene Ontology (GO) terms most overrepresented among the shared Nab2- and Atx2-associated transcripts as compared

to the entire testable transcript set. GO term independence was determined by "Hierarchical Selection" (see *Methods*). The number of GO term members within the shared RBP-associated transcripts and within the entire testable transcript set (*Genes enriched / in total*) are reported to the right of each bar.

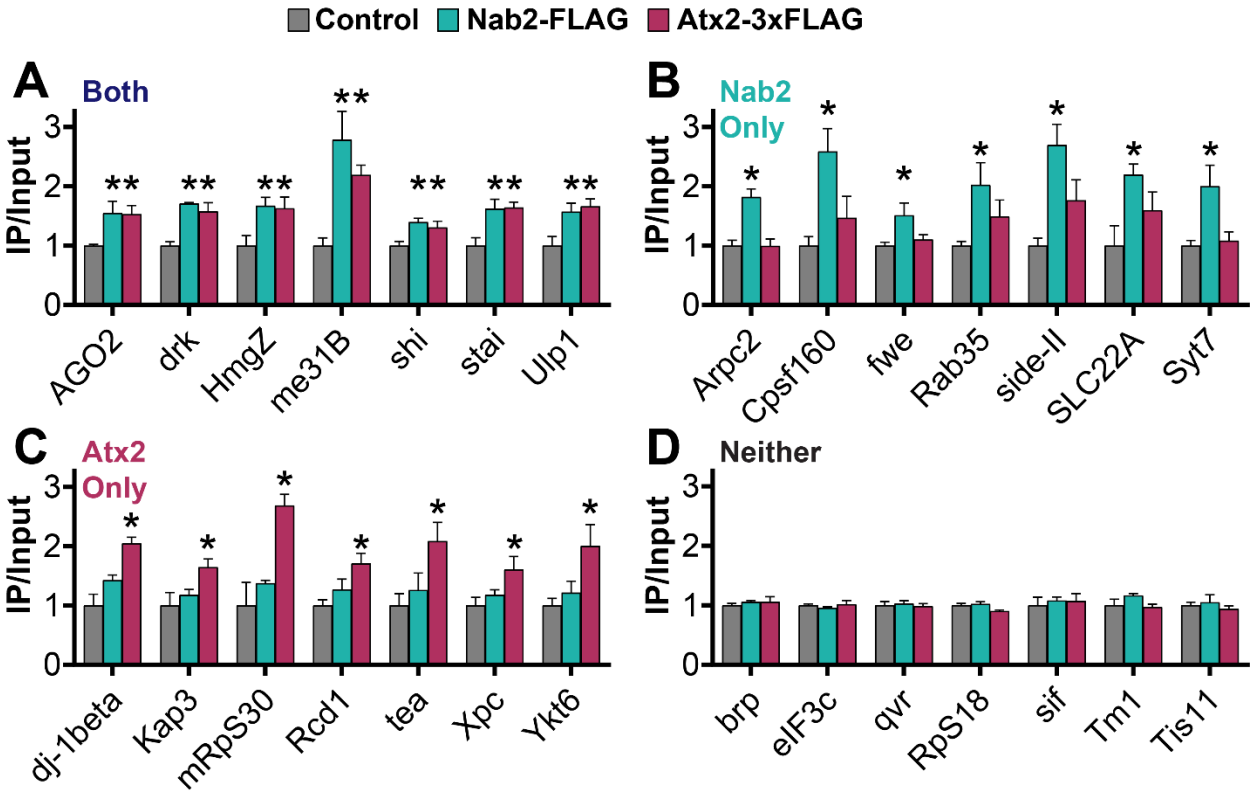

Figure 3-5. Potential functionally important RNA targets of Nab2 and Atx2 identified by combining individual transcript and holistic GO analyses of RIP-Seq results. For transcripts that associate with *Both* Nab2 and Atx2, *Nab2 Only*, *Atx2 Only*, or *Neither* RBP by RIP-Seq, seven transcripts of particular functional interest are presented as a summary of each category. (A-C) These transcripts met one or both of two criteria: 1) inclusion in an associated overrepresented GO term 2) an *IP/Input (*i.e. *Fold Enrichment*) value > 1.5. Given the functions of proteins encoded by these transcripts, these selections represent potential phenotypically important targets of post-transcriptional regulation by Nab2 and Atx2. (D) These transcripts, as a negative control, encode a functionally diverse set of proteins and do not associate with Nab2 or Atx2 (*Neither*), affirming the specificity of the RNA interactome of each RBP. Error bars represent standard errors of the mean (SEM). Gene-by-gene one-way ANOVA, Dunnett's post-hoc test, and within-gene multiple

hypothesis testing adjustment (*Dun. Adj. p*) was used to assess statistical significance. * = *Dun. Adj. p* < 0.05.

A

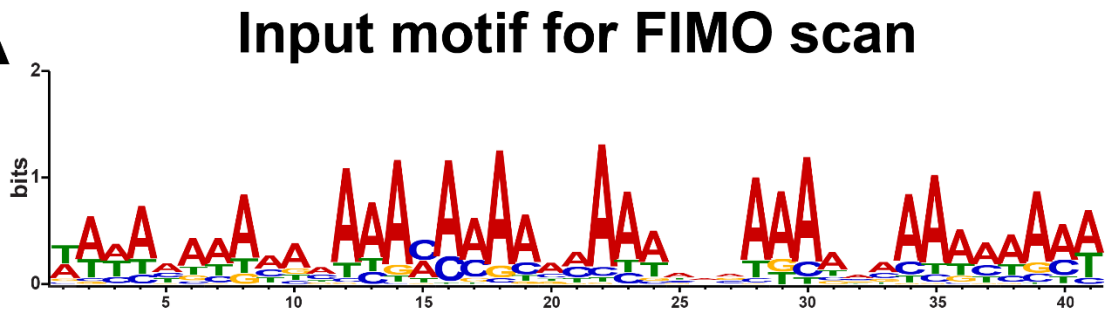

A-rich motif, 41-bp, identified in Nab2-associated transcripts by MEME			
Transcript Set	**Motif occurrences** ($p < 0.0001$)	**Motif frequency** (Occurrences/total bases in Set)	
Nab2-associated	**19,265**	**1 motif per 135 bases**	***
All others	**77,596**	**1 motif per 845 bases**	

B

A_{12}			
Transcript Set	**Motif occurrences** ($p < 0.0001$)	**Motif frequency** (Occurrences/total bases in Set)	
Nab2-associated	**1,674**	**1 motif per 1,553 bases**	***
All others	**34,465**	**1 motif per 1,901 bases**	

C

$A_{11}G$			
Transcript Set	**Motif occurrences** ($p < 0.0001$)	**Motif frequency** (Occurrences/total bases in Set)	
Nab2-associated	**3,786**	**1 motif per 687 bases**	***
All others	**70,103**	**1 motif per 935 bases**	

Figure 3-6. A broad A-rich motif and two specific, canonical Nab2 binding motifs are enriched in Nab2-associated RNAs. Output from transcript set scans by FIMO, which quantifies the occurrences in supplied sequence sets of motifs identical or highly similar to an input motif. Two transcript sets were scanned in each analysis: 1) all transcripts encoded by *Nab2-associated*

gene models and 2) all transcripts encoded by *All others*, shorthand for all non-Nab2-associated gene models in the RIP-Seq testable set. (A) A 41-bp A-rich motif, identified by MEME as one of the first ten 6-50 bp motifs within *Nab2-associated* transcripts, was used as input for FIMO. (B) A canonical Nab2 binding motif from *S. cerevisiae*, $A_{11}G$, was used as FIMO input. (C) A simple homopolymer stretch of A's for which Nab2 would have a very high affinity, A_{12}, was used as FIMO input. In all three cases, particularly in (A), the scanned motif is significantly enriched in the *Nab2-associated* transcript set compared to the *All others* transcript set. However, none of the three input motifs are exclusive or nearly exclusive to Nab2-associated transcripts—each is still notably abundant within *All others*. Statistical significance was assessed using the chi-square test (two-sided). ***=$p<0.001$.

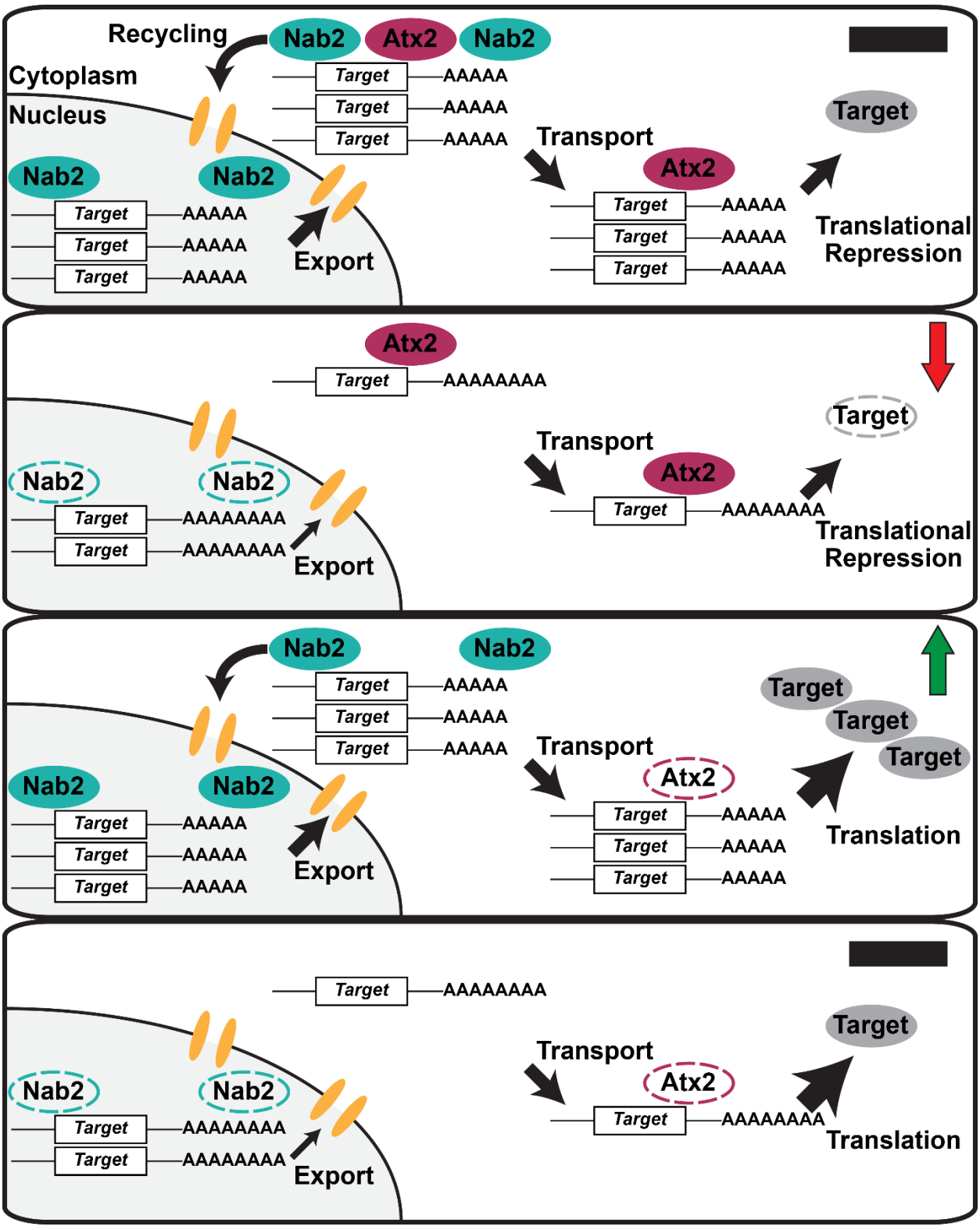

Figure 3-7. A model of opposing regulatory roles for Nab2 and Atx2 on shared associated RNA transcripts. Nab2 and Atx2 associate with a shared set of RNA transcripts in *Drosophila*

brain neurons but primarily localize to separate subcellular compartments and weakly physically associate. *S. cerevisiae* Nab2 regulates nuclear processing, including transcript stability, poly(A) tail length, and export, across a broad RNA transcript set—*Drosophila* Nab2 may perform similar functions on its comparatively limited associated RNA set. Atx2 serves numerous roles in post-transcriptional regulation, including as a miRNA-machinery linked translational repressor. Taken together, these data imply the following model. (*Top*) In the wild-type condition, Nab2 protects transcripts from degradation, limits poly(A) tail length, and contributes to *Target* RNA export from the nucleus, shuttling with its associated transcripts into the cytoplasm. Nab2 and Atx2 may co-occupy the same transcripts briefly or occasionally during nuclear-cytoplasmic mRNP remodeling and prior to Nab2 recycling into the nucleus. Atx2 accompanies *Target* transcripts through transport to their destinations (e.g. synaptic terminals) and contributes to miRNA-mediated translational repression, which is released under certain conditions (e.g. synaptic activity), ultimately contributing to regulated production of wild-type levels of Target protein (black —). (*Second panel*) In $Nab2^{ex3}$ nulls, *Target* mRNAs are less stable, exhibit longer poly(A) tails, and are exported less efficiently from the nucleus. As a result, less *Target* mRNA reaches its appropriate destination, resulting in a decrease in steady-state levels of Target protein (red ↓). (*Third panel*) In Atx2 loss-of-function heterozygotes (i.e. $Atx2^{DG08112/+}$ or $Atx2^{X1/+}$), less Atx2 protein is expressed and available to repress *Target* translation, resulting in less responsive, higher steady-state levels of Target protein (green ↑). (*Bottom*) Effects of the complete loss of Nab2 in $Nab2^{ex3}$ and the decrease of functional Atx2 in *Atx2* loss-of-function heterozygotes balance one another. While nuclear *Target* mRNA is less stable and less is exported from the nucleus successfully, these RNAs are also under less strict translational control in partial absence of Atx2, ultimately resulting in Target protein levels and corresponding phenotypes more similar to the

wild-type condition (black —). This model represents a prediction from our data and the published knowledge of the functions of each protein—it must be tested in future research, a task enabled by the identification of Nab2- and Atx2-associated transcripts in the current study.

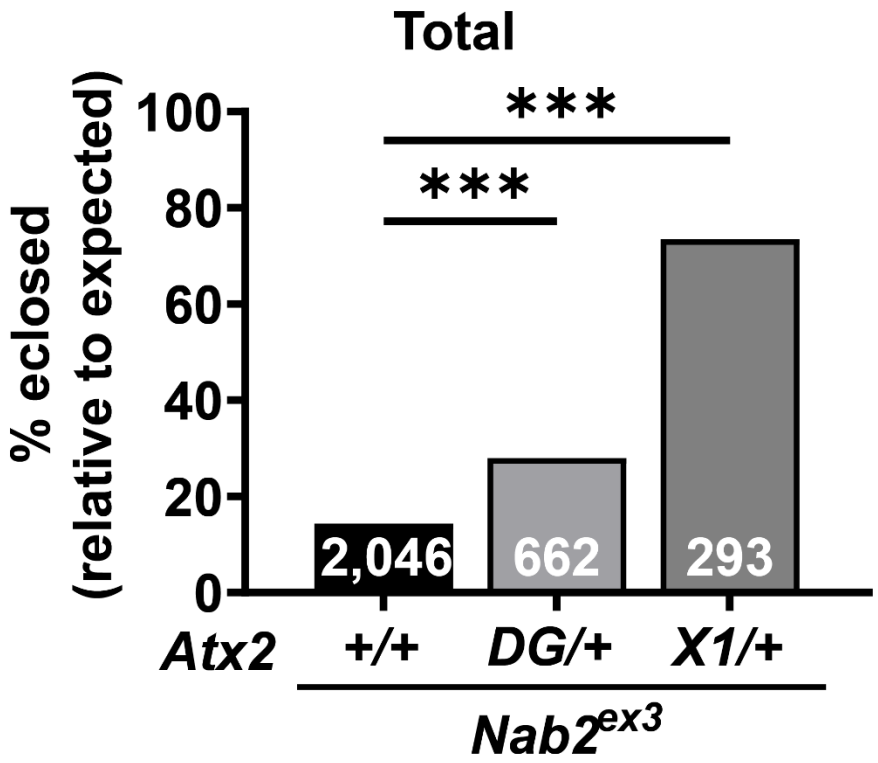

Figure 3-S1 (Associated with Figure 3-1). Heterozygosity for either *Atx2* loss-of-function allele suppresses effects of *Nab2*^{ex3} for the progeny population in total, partially restoring adult viability. Flies lacking functional endogenous *Nab2*, *Nab2*^{ex3} homozygotes, demonstrate dramatically decreased adult viability, as quantified by the percentage of flies reaching pupal eclosion and adulthood out of the amount expected by Mendelian inheritance. When flies are considered irrespective of sex, heterozygosity for either loss-of-function allele of *Atx2*—*Atx2*^{DG08112} or *Atx2*^{X1}—significantly suppresses this effect, partially rescuing viability. Sample sizes (n) are reported in each bar and include all F1 progeny scored, including genetically distinct siblings of the genotype of interest used to calculate *% eclosed (relative to expected)*. Fisher's Exact Test (two-sided) was used to assess statistical significance. ***=p<0.001.

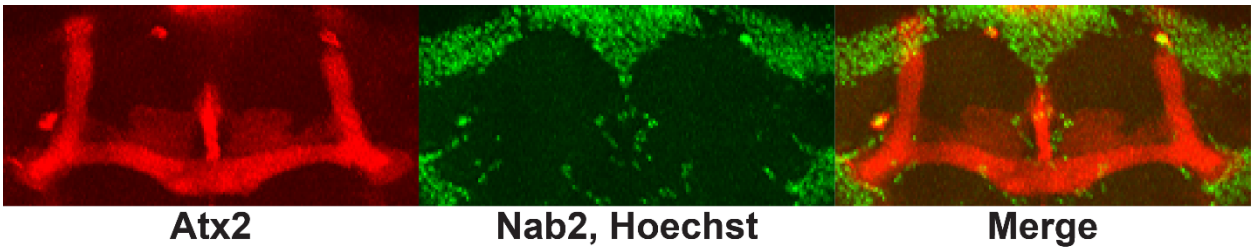

Figure 3-S2 (Associated with Figure 3-3). Atx2, but not Nab2, robustly localizes to axonal lobes of the mushroom body in adult brains. To specifically assess protein localization in mushroom body neurons, tagged transgenic copies of Atx2 and Nab2 (Atx2-3xFLAG and Nab2-YFP) were expressed in female brains under the MB-specific *OK107-Gal4*. The lobes or axon tracts of the MBs are shown for a representative brain. False-colored panels show fluorescence corresponding to α-FLAG (red, Atx2-3xFLAG), the combination of α-GFP and Hoechst 33342 (green, Nab2-YFP and nuclei), and a merge of both channels. Atx2 localizes robustly to the axon tracts comprising the MB lobes, consistent with its cytoplasmic roles in translational regulation and mRNP granule formation. Fluorescence corresponding to Nab2 and Hoechst 33342 primarily localizes to the brain cortex—the site of the vast majority of neuronal cell bodies—consistent with a nearly exclusive nuclear localization of Nab2 in adult MBs.

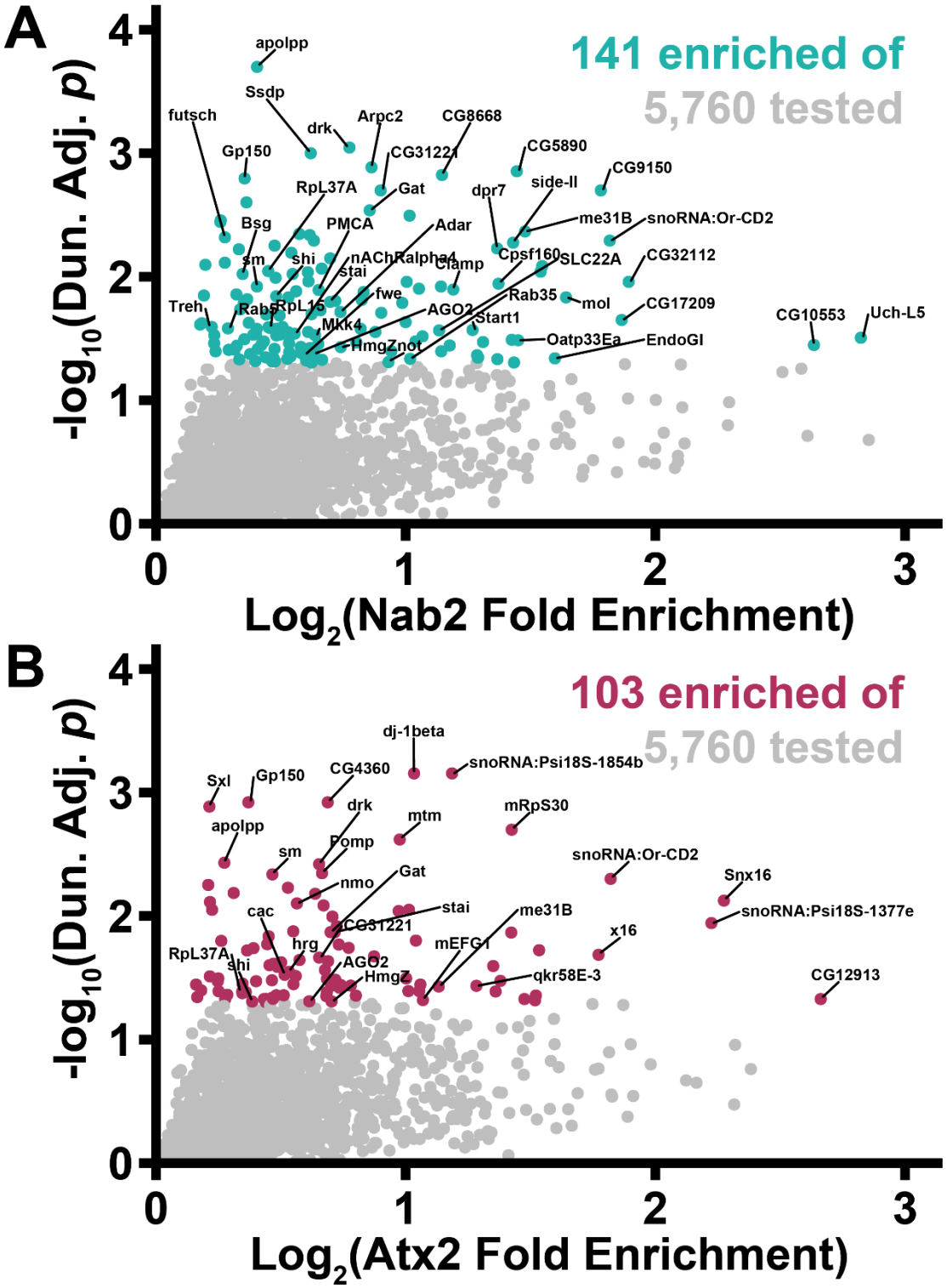

Figure 3-S3 (Associated with Figure 3-4). RIP-Seq analysis reveals diverse sets of overlapping transcripts associate with Nab2-FLAG and Atx2-3xFLAG. (A-B) Scatter plots of

all transcripts within the 5,760 of the testable set with positive (A) *log_2(Nab2 Fold Enrichment)* or (B) *log_2(Atx2 Fold Enrichment)* values. *Fold Enrichment* values quantify how effectively a transcript was enriched by IP and are derived by calculating IP/Input (i.e. percent input) values for control and epitope-tag samples and setting the average of control values to 1 (i.e. 0 on the logarithmic scale used here). Y-axes display results of significance testing, conducted by gene-by-gene one-way ANOVA, Dunnett's post-hoc test, and within-gene multiple hypothesis testing adjustment (*Dun. Adj. p*). Statistically significant transcripts (*Dun. Adj. p* < 0.05) are colored. On each plot, labels identify many transcripts of interest chosen by both objective and subjective means. Labels are shown for many transcripts among the "top" RBP-specific RBP-associated transcripts, the shared RBP-associated transcripts, the transcripts emphasized by GO analyses (see *Results* for details), and others of subjective interest. RBP-associated transcripts of interest not included in the main text include *Treh* and *Bsg* in (A), *qkr58E-3* and *cac* in (B), and *RpL37A* and *Gp150* in both panels.

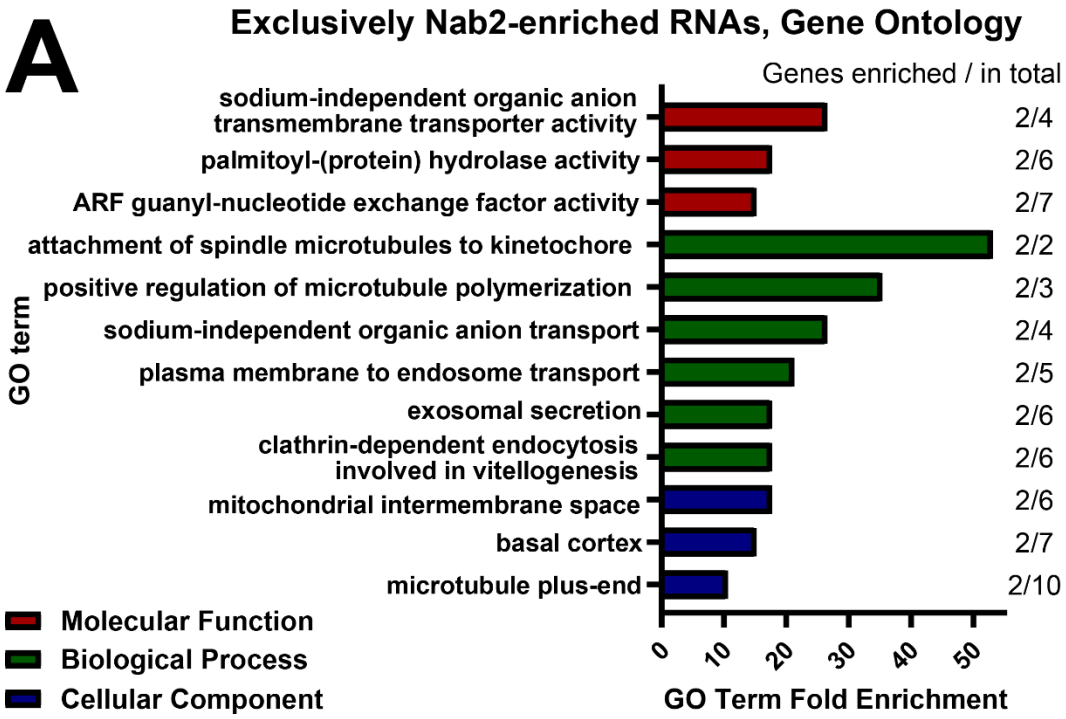

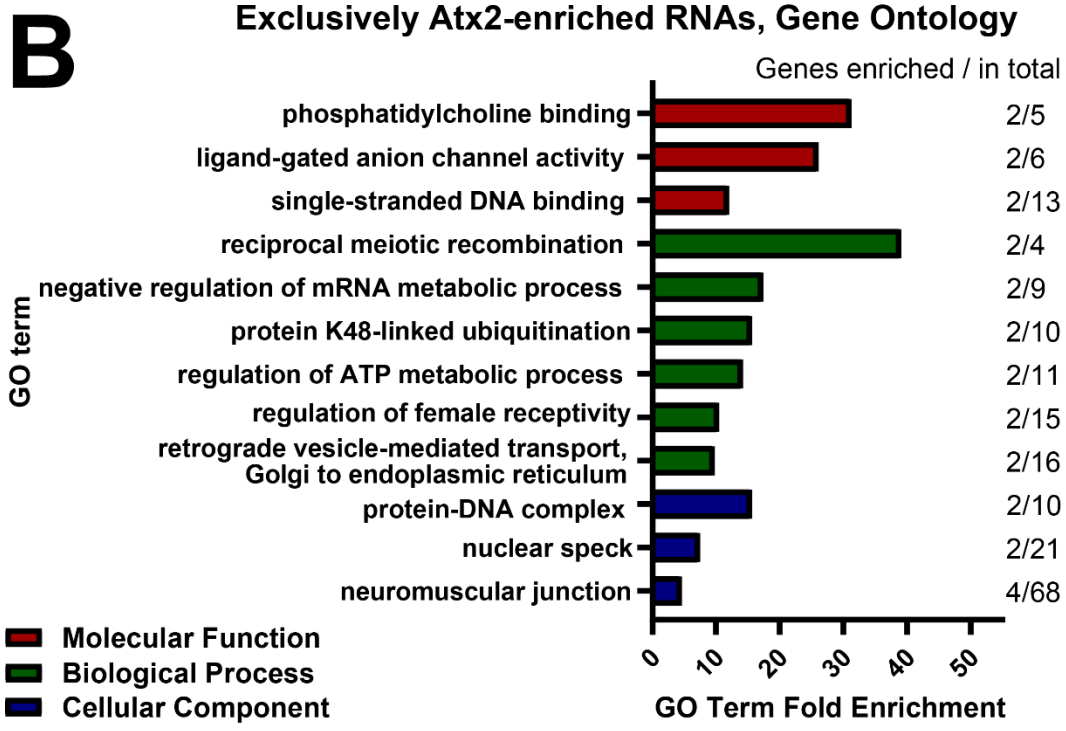

Figure 3-S4 (Associated with Figure 3-4). Holistic PANTHER GO analyses of transcripts associating only with Nab2-FLAG or Atx2-3xFLAG by RIP-Seq identify functions each RBP may regulate independent of the other. (A-B) The independent *Molecular Function* (red),

Biological Process (green), and *Cellular Component* (blue) Gene Ontology (GO) terms most overrepresented among the (A) Nab2-specifc or (B) Atx2-specific associated transcripts as compared to the entire testable transcript set. GO term independence was determined by "Hierarchical Selection" (see *Methods*). The number of GO term members within the RBP-associated transcripts and within the entire testable transcript set (*Genes enriched / Genes in total*) are reported to the right of each bar. Terms enriched among Nab2-associated transcripts include *positive regulation of microtubule polymerization* and *exosomal secretion*, while terms enriched among Atx2-associated transcripts include *regulation of ATP metabolic process* and *retrograde vesicle-mediated transport, Golgi to endoplasmic reticulum*. These GO terms may reflect processes within domains such as cytoskeletal organization, metabolism, and vesicle transport that Nab2 and Atx2 regulate independently of one another.

Shared Nab2- and Atx2-associated transcripts			
AGO2	***drk***	***me31B***	***shi***
apolpp	***Gαo***	***Msp300***	***sm***
CG31221	***Gat***	***mtd***	***snoRNA:Or-aca5***
CG42540	***Gγ30A***	***Rbp6***	***snoRNA:Or-CD2***
CG4360	***Gp150***	***RpL37A***	***snoRNA:Ψ18S-1854b***
CG6675	***HmgZ***	***RpS27A***	***Stai***
CG9813	***l(3)80Fg[a]***	***RpS29***	***Ulp1***

TABLE 3-1. Identities of the 28 transcripts overlapping between the Nab2 and Atx2 RNA interactomes. For all 5,760 genes in the RIP-Seq testable set, control-normalized IP/Input enrichment values were calculated followed by gene-by-gene one-way ANOVAs, Dunnett's post-hoc tests, and within-gene multiple hypothesis testing adjustment (*Dun. Adj. p*). All transcripts statistically significantly (*Dun. Adj. p* < 0.05) enriched in both Nab2- and Atx2-associated transcripts sets are listed here. Functional interactions between Nab2 and Atx2 in brain neurons may be explained by their coordinate regulation of these shared associated transcripts.

[a]Symbol updated from *CG40178* to current nomenclature in BDGP6.37.

A *Materials and Methods* Supplemental Table detailing RIP-Seq analysis pipeline software in 3 groups		
Group 1 - Galaxy software and parameters used for read mapping, count normalization, and other RNA-Seq analyses		
Tool	Concatenate datasets tail-to-head	
Version	Galaxy Version 1.0.0	
	This tool was used with default parameters.	
Tool	RNA STAR	
Version	Galaxy Version 2.6.0b-1	
	This tool was used with default parameters with the following exceptions:	
	read type	paired (as individual datasets)
	reference genome	from history (using the Ensembl FASTA and GTF referenced in text)
	length of the genomic sequence around annotated junctions	74
Tool	featureCounts	
Version	Galaxy Version 1.6.3+galaxy2	
	This tool was used with default parameters with the following exceptions:	
	specify strand information	Stranded(Reverse)
	gene annotation file	history (using the Ensembl GTF referenced in text)
	create gene-length file	—true
	count fragments instead of reads	enabled
	GFF gene identifier	gene_name
Tool	DESeq2	
Version	Galaxy Version 2.11.40.2	
	This tool was used with default parameters with the following exceptions:	
	factors	3 levels, each a dataset collection of four biological replicates
	output normalized counts table	—true
	output all levels vs all levels	—true
Group 2 - Gene Ontology (GO) software and parameters used to facilitate or perform GO analyses		
Tool	PANTHER	
Version	web interface	
Access Date	September, 2020	
	This tool was used with the following parameters:	
	Enter IDs	Appropriate RBP-associated transcript lists, referenced in text
	Select organism	Drosophila melanogaster
	Select analysis	Statistical overrepresentation test
	SELECT REFERENCE LIST, Select Organism	Drosophila melanogaster

	SELECT REFERENCE LIST, Upload List	Gene, Transcript, Protein and Alternate ID
	SELECT REFERENCE LIST, Choose list from your workspace	5,760 transcripts in the "testable set", referenced in text
	Analysis Type	PANTHER Overrepresentation Test (Released 20200728)
	Annotation Version and Release Date	GO Ontology database DOI: 10.5281/zenodo.3954044 Released 2020-07-16
	Annotation Data Set	GO molecular function complete *or* GO biological process complete *or* GO cellular component complete
	Test Type	Fisher's Exact
	***p*-value Correction**	No correction
Tool	AmiGO 2	
Version	web interface	
Access Dates	2020-2021	
Group 3 - Sequence Motif Analyses, MEME Suite		
Tool	MEME Suite	
Version	5.1.1	
Tool	MEME	
Version	5.1.1	
	This tool was used with the following parameters:	
	Motif discovery mode	Classic mode
	Sequence alphabet	DNA, RNA or Protein
	Input primary sequences	Upload sequences, referenced in text
	Site distirbution	Any Number of Repetitions (anr)
	Number of motifs	10
	Background model	0-order model of sequences
	Motif width (minimum)	6
	Motif width (maximum)	50
	Motif site count (minimum)	2
	Motif site count (maximum)	600
	Can motif be on both strands?	Select "search given strand only"
	Should MEME restrict the search to palindromes?	Leave "look for palindromes only" unchecked
	Should MEME shuffle the sequence?	Leave "Shuffle the sequences" unchecked
Tool	FIMO	
Version	5.1.1	
	This tool was used with the following parameters:	
	Input the motifs (to scan with)	"Submitted motifs" transferred from MEME output or motifs manually entered, sequences supplied are referenced in text

	Input the sequences (to scan for matches to input motif)	Upload sequences, referenced in text
	Enable tissue/cell-specific scanning	Leave unchecked
	How should matches be filtered before output?	Match *p*-value<0.0001 (default)
	Scan both strands?	Select "scan given strand only"

TABLE 3-S1. Software, version numbers, and exact parameters used in RIP-Seq analyses. As a supplement to the in-text *Materials and Methods*, this table details software names, version numbers, and exact parameters or settings used in our RIP-Seq analysis pipeline. Descriptions cover software used for, among other functions, read mapping, count normalization, gene ontology analysis, and sequence motif analysis. Tools are divided into three subcategories—*Galaxy software…*, *Gene Ontology (GO) software…*, and *Sequence Motif Analyses, MEME Suite*. For each software tool described, the tool name, version number, access data (where appropriate) is given in one column, and the exact parameters or settings used are given in a second.

TABLE 3-S2 contains 5,763 rows, and thus is too large for direct inclusion in this dissertation document. To view TABLE 3-S2, please refer to TABLE S2 within the Supplemental Materials associated with Rounds et al., 2021, the in-submission manuscript associated with this dissertation chapter. These Supplemental Materials are available in the online figshare repository at https://figshare.com/s/6f28676d7119624b3105. The legend associated with TABLE 3-S2 is included below.

TABLE 3-S2. Identities, enrichment values, and significance testing for *Both Nab2 and Atx2*-associated transcripts, *Only Nab2*-associated transcripts, *Only Atx2*-associated transcripts, and all other transcripts in the RIP-Seq testable set. The gene symbols, IP/Input control-normalized enrichment values, and results of statistical significance testing are provided for all 5,760 transcripts in the RIP-Seq testable set, including the 28 *Both Nab2 and Atx2*-associated transcripts, the 113 *Nab2 Only*-associated transcripts, and the 75 *Atx2 Only*-associated transcripts. For each transcript, the first three columns present *Control-normalized IP/Input* (i.e. Fold Enrichment) values, which quantify how effectively a transcript was enriched by IP. These are derived by calculating IP/Input values from *DESeq2*-normalized counts for each control and epitope-tag sample and then setting the average of control values to 1. The next two columns display results from significance testing by gene-by-gene one-way ANOVAs, Dunnett's post hoc tests, and within-gene multiple hypothesis testing adjustment. Transcripts with *Dun. Adj. p*-values < 0.05 are considered statistically significantly enriched by IP and thus were found to be associated with the relevant RBP. The next column categorizes the transcript by which RBP, if any, it was found to be significantly associated with. The next three columns detail the standard error of the mean (SEM) of the *Control-normalized IP/Input* values. The last two columns list Dunnett values calculated in the course of significance testing.

Both Nab2- and Atx2-associated **Transcript Set**	
Overrepresented GO Terms (GO Term Accession)	**GO Term Members in Transcript Set**
Molecular Function	
single-stranded RNA binding (GO:0003727)	*Rbp6* *AGO2*
microtubule binding (GO:0008017)	*shi* *apolpp*
structural constituent of ribosome (GO:0003735)	*RpL37A* *RpS29* *RpS27A*
Biological Process	
sensory perception of taste (GO:0050909)	*Ggamma30A* *Galphao*
pole cell formation (GO:0007279)	*AGO2* *me31B*
gene silencing by miRNA (GO:0035195)	*AGO2* *me31B*
feeding behavior (GO:0007631)	*sm* *shi*
nuclear migration (GO:0007097)	*Msp300* *AGO2*
short-term memory (GO:0007614)	*shi* *drk*
Cellular Component	
neuronal ribonucleoprotein granule (GO:0071598)	*AGO2* *me31B*
heterotrimeric G-protein complex (GO:0005834)	*Ggamma30A* *Galphao*
polysome (GO:0005844)	*RpS29* *Rbp6*
Only Nab2-associated **Transcript Set**	
Overrepresented GO Terms (GO Term Accession)	**GO Term Members in Transcript Set**
Molecular Function	
sodium-independent organic anion transmembrane transporter activity (GO:0015347)	*Oatp30B* *Oatp33Ea*
palmitoyl-(protein) hydrolase activity (GO:0008474)	*DmelCG18815* *DmelCG15111*
ARF guanyl-nucleotide exchange factor activity (GO:0005086)	*Efa6* *garz*
Biological Process	
attachment of spindle microtubules to kinetochore (GO:0008608)	*BuGZ* *chb*
positive regulation of microtubule polymerization (GO:0031116)	*msps* *chb*

sodium-independent organic anion transport (GO:0043252)	*Oatp30B*	*Oatp33Ea*		
plasma membrane to endosome transport (GO:0048227)	*Rab35*	*Rab5*		
exosomal secretion (GO:1990182)	*Rab35*	*Rab7*		
clathrin-dependent endocytosis involved in vitellogenesis (GO:0061883)	*Rab7*	*Rab5*		
Cellular Component				
mitochondrial intermembrane space (GO:0005758)	*Cyt-c-p*	*prel*		
basal cortex (GO:0045180)	*pros*	*chb*		
microtubule plus-end (GO:0035371)	*msps*	*chb*		
Only Atx2-associated **Transcript Set**				
Overrepresented GO Terms (GO Term Accession)	**GO Term Members in Transcript Set**			
Molecular Function				
phosphatidylcholine binding (GO:0031210)	*Pcyt1*	*rdgB*		
ligand-gated anion channel activity (GO:0099095)	*Rdl*	*DmelCG7589*		
single-stranded DNA binding (GO:0003697)	*Xpc*	*tea*		
Biological Process				
reciprocal meiotic recombination (GO:0007131)	*Xpc*	*Sxl*		
negative regulation of mRNA metabolic process (GO:1903312)	*mbf1*	*Sxl*		
protein K48-linked ubiquitination (GO:0070936)	*DmelCG17019*	*DmelCG2924*		
regulation of ATP metabolic process (GO:1903578)	*Dg*	*dj-1beta*		
regulation of female receptivity (GO:0045924)	*DmelCG10433*	*egh*		
retrograde vesicle-mediated transport, Golgi to endoplasmic reticulum (GO:0006890)	*deltaCOP*	*Ykt6*		
Cellular Component				
protein-DNA complex (GO:0032993)	*His4:CG33909*	*tea*		
nuclear speck (GO:0016607)	*x16*	*qkr58E-3*		
neuromuscular junction (GO:0031594)	*cac*	*Dg*	*unc-13*	*Snx16*

TABLE 3-S3. Identities of all RBP-associated transcripts annotated under the overrepresented GO terms reported herein. Figure 3-4 and Figure 3-S4 report the top 3 independent (see *Methods*) *Molecular Function* and *Cellular Component* GO terms, and the top 6 independent *Biological Process* GO terms, that among the three sets of RBP-associated transcripts (*Both Nab2 and Atx2*, *Nab2 Only*, and *Atx2 Only*) are most overrepresented by fold enrichment compared to the entire testable transcript set. The identities of a few RBP-associated transcripts annotated under these GO terms are reported in-text; all such transcripts are reported in this table. GO terms are categorized by RBP-associated transcript set (first column), further categorized by top-level GO term, and then listed in descending order of fold enrichment (second column). GO accessions are provided for each term to annotate and unambiguously identify it. RBP-associated transcripts within each set and annotated under each GO term are listed in the third through sixth columns. Some transcripts are listed multiple times, reflecting their annotation under multiple top independent GO terms.

Supplemental Materials and Methods

Bulk *Drosophila* Head Isolation

Thousands of isolated *Drosophila* heads were required to complete the immunoprecipitation experiments detailed in this study. To ensure feasibility, reproducibility, and efficiency, heads were isolated essentially as described in (Tian *et al.* 2013; Chow 2015). Briefly, whole adults were transferred from −80°C storage to a 15 ml conical tube and submerged in liquid nitrogen. Using a vortex mixer (02215365, Fisher Scientific), tubes were vortexed (speed 10, contact-activated) for six 3-second intervals, returning to liquid nitrogen between each. Resulting slurries were separated by a stack of stainless-steel sieves on dry ice. In this stack, a 710 µm U.S.A. standard No. 25 test sieve rested atop a 425 µm U.S.A. standard No. 40 test sieve (EW-59987-12 and EW-59987-16, Cole-Parmer). After brief, vigorous shaking on dry ice, only *Drosophila* heads remained on the smaller sieve, enabling exact counting and isolation on dry ice. Heads were returned to −80°C storage until further use.

Immunoblotting

Samples previously diluted in modified 2X Laemmli sample buffer (0.125 M Tris-HCl, 4% SDS, 20% glycerol, 0.2 M dithiothreitol (DTT), 0.02% bromophenol blue; final pH of 6.8) (Laemmli 1970) were again centrifuged at 16,100×g for 5 minutes at room temperature to clear insoluble material, magnetized as appropriate, and collected as supernatants. If the color of any Input sample solutions yellowed, indicating acidification by leftover acetone, all input samples were neutralized by an equal volume of 1 M Tris, pH 8.0. Samples were resolved on a 7.5% precast, "stain-free" polyacrylamide gel supplemented with UV-reactive trihalo compounds (456-8023, Bio-Rad). Then, these trihalo compounds were activated by 45-second UV exposure, covalently adding small, persistent fluorophores to sample proteins and allowing total protein visualization in all subsequent steps. Next, samples were transferred to a polyvinylidene difluoride (PVDF)

membrane (0.2 μm; 162-0177, Bio-Rad) and blocked at room temperature in 4% non-fat milk in TBS-T (0.1% Tween). Membranes were sequentially incubated in primary antibodies, secondary antibodies, and Clarity ECL (1705061, Bio-Rad) at room temperature, with each incubation separated by washes in TBS-T (0.1% Tween). Immune-reactive species, total protein loading, and Kaleidoscope protein ladder (161-0375, Bio-Rad) were then visualized with a ChemiDoc MP digital gel imager (Bio-Rad). Primary antibodies and dilutions used are as follows: rabbit α-Atx2 at 1:1,000 (gift of Dr. Chunghun Lim, (Lee *et al.* 2017)), rabbit α-alpha tubulin at 1:1,000 (ab52866, Abcam), rabbit α-Nab2 (1:4,000) (first described in (Pak *et al.* 2011)), mouse α-Fmr1 at 1:200 (sc-57005, Santa Cruz Biotechnology), and mouse α-FLAG at 1:500 (F1804, Sigma-Aldrich). Secondary antibodies and dilutions used are as follows: goat α-rabbit HRP at 1:4,000 (Jackson) and goat α-mouse HRP at 1:1,000.

Independent *DESeq2* normalization of IP and Input sample read counts

Importantly, we chose to perform two independent *DESeq2* analyses, once on the 12 IP samples and once on the 12 Input samples, to normalize sample read counts for inter-library comparisons, rather than performing a single *DESeq2* analysis on all 24 samples at once. In our view, this sample separation method produces the most properly normalized read counts for inter-sample comparison because, when considered as a whole group, samples from RNA IP experiments violate some of the assumptions underlying the *DESeq* median-of-ratios read normalization strategy (Anders and Huber 2010; Anders *et al.* 2012). Specifically, the *DESeq* software within *DESeq2* normalizes for library size and composition under the assumption that most genes are expressed similarly across samples. This is not expected to be true between IP and Input samples, but it is a reasonable assumption within these groups. Thus, *DESeq* represents a valid count normalization strategy within, but not across, each group. Further discussion on this subject may be found in the *DESeq2*

vignette (Love *et al.* 2020) available from Bioconductor (Gentleman *et al.* 2004; Huber *et al.* 2015). Notably, either normalization strategy produces broadly similar results (data not shown)—we argue those produced by independent normalization are only moderately more stringently, accurately normalized.

RNA Sequencing Analysis—Gene Ontology

The *Statistical overrepresentation test* tool in the PANTHER software web interface (Mi *et al.* 2019) was employed for Gene Ontology (GO) analysis (Ashburner *et al.* 2000; The Gene Ontology Consortium 2019). Exact parameters, GO database version information, and access dates used for this analysis are detailed in Supplemental Table 1. For PANTHER compatibility, prior to upload gene symbols were converted to FlyBase IDs (FBgnxxxxxxx) using the Flybase ID Validator at http://flybase.org/convert/id (database release FB2020_04). Critically, GO term enrichment in given gene lists was evaluated in reference to only the 5,760 genes in the testable set (see *Materials and Methods* and *Results*), not to the total 17,753 genes annotated in the BGDP6.22 release of the *Drosophila* genome described above. This restriction controls for the effect of sample type on GO term overrepresentation testing and prevents, for example, the mis-identification of GO terms enriched in all female *Drosophila* heads as being enriched specifically in Nab2-associated RNAs. Three gene lists were analyzed for GO term overrepresentation by PANTHER: transcripts significantly associated with *Both Nab2 and Atx2* (28), *Only Nab2* (113), and *Only Atx2* (75). On a technical note, 134 genes in the testable set, along with 5, 7, and 3 genes included in the *Both Nab2 and Atx2*, *Only Nab2*, and *Only Atx2* sets, respectively, are not protein-coding genes or are otherwise unannotated in the PANTHER database and were thus automatically excluded by PANTHER from these GO analyses and related enrichment calculations.

For each transcript set, analyses were conducted separately for each of the three top-level GO domains—molecular function, biological process, and cellular component—using the PANTHER "complete" GO term sets. For each gene list, overrepresented GO terms (nominal *p*-value<0.05) were identified and, to avoid redundancy and increase explanatory power, were filtered through a process of "Hierarchical Selection" to identify the top 3 or 6 "independent" GO terms. First, overrepresented terms were sorted hierarchically by PANTHER. That is, less specific parent terms in the GO hierarchy (e.g. "regulation of nervous system process") were grouped with their more specific child terms (e.g. "negative regulation of neuronal action potential"), and the resulting term families were rank-ordered by the fold enrichment of their most specific child term. Then, for each term family, the most specific term with at least two members in the given RBP-associated transcript list was kept; the remaining terms in each family were discarded. Within-family ties for term specificity in the GO hierarchy were resolved with fold enrichment, keeping only the most enriched term of each tie. The remaining GO terms were re-ordered by fold enrichment, and the top 3 or 6 were reported in the bar graphs presented here. GO term accession numbers and additional term information were obtained as necessary from the AmiGO 2 GO database web tool (Carbon *et al.* 2009).

Literature Cited in Supplemental Materials and Methods

Anders S., and W. Huber, 2010 Differential expression analysis for sequence count data. Genome Biol. 11: R106. https://doi.org/10.1186/gb-2010-11-10-r106

Anders S., A. Reyes, and W. Huber, 2012 Detecting differential usage of exons from RNA-seq data. Genome Res. 22: 2008–2017. https://doi.org/10.1101/gr.133744.111

Ashburner M., C. A. Ball, J. A. Blake, D. Botstein, H. Butler, *et al.*, 2000 Gene ontology: Tool for the unification of biology. Nat. Genet. 25: 25–29.

Carbon S., A. Ireland, C. J. Mungall, S. Shu, B. Marshall, *et al.*, 2009 AmiGO: online access to ontology and annotation data. BIOINFORMATICS 25: 288–289. https://doi.org/10.1093/bioinformatics/btn615

Chow E., 2015 How to separate Drosophila heads & bodies in bulk - YouTube

Gentleman R. C., V. J. Carey, D. M. Bates, B. Bolstad, M. Dettling, *et al.*, 2004 *Bioconductor: open software development for computational biology and bioinformatics*.

Huber W., V. J. Carey, R. Gentleman, S. Anders, M. Carlson, *et al.*, 2015 Orchestrating high-throughput genomic analysis with Bioconductor. Nat. Methods 12: 115–121. https://doi.org/10.1038/nmeth.3252

Laemmli U. K., 1970 Cleavage of structural proteins during the assembly of the head of bacteriophage T4. Nature 227: 680–685. https://doi.org/10.1038/227680a0

Lee J., E. Yoo, H. Lee, K. Park, J.-H. Hur, *et al.*, 2017 LSM12 and ME31B/DDX6 Define Distinct Modes of Posttranscriptional Regulation by ATAXIN-2 Protein Complex in Drosophila Circadian Pacemaker Neurons. Mol. Cell 66: 129-140.e7. https://doi.org/10.1016/j.molcel.2017.03.004

Love M., C. Ahlmann-Eltze, S. Anders, and W. Huber, 2020 Differential gene expression analysis based on the negative binomial distribution (DESeq2, Bioconductor Version, Release 3.11)

Mi H., A. Muruganujan, D. Ebert, X. Huang, and P. D. Thomas, 2019 PANTHER version 14: more genomes, a new PANTHER GO-slim and improvements in enrichment analysis tools. Nucleic Acids Res. 47: 419–426. https://doi.org/10.1093/nar/gky1038

Pak C., M. Garshasbi, K. Kahrizi, C. Gross, L. H. Apponi, *et al.*, 2011 Mutation of the conserved polyadenosine RNA binding protein, ZC3H14/dNab2, impairs neural function in Drosophila and humans. Proc. Natl. Acad. Sci. U. S. A. 108: 12390–5. https://doi.org/10.1073/pnas.1107103108

The Gene Ontology Consortium, 2019 The Gene Ontology Resource: 20 years and still GOing strong. Nucleic Acids Res. 47: D330–D338. https://doi.org/10.1093/nar/gky1055

Tian X., M. Zhu, L. Li, and C. Wu, 2013 Identifying Protein-protein Interaction in Drosophila Adult Heads by Tandem Affinity Purification (TAP). J. Vis. Exp. e50968–e50968. https://doi.org/10.3791/50968

Custom Software Code

All custom code written to generate, analyze, or visualize data in this chapter, associated supplemental materials, and associated database accessions represents dozens of pages of text when presented in this format, and is thus too large for direct inclusion in this dissertation document. Moreover, this code is of the most utility if presented and contextualized in a .txt file stylized closer its original format. To view this R and PRISM code, along with descriptions of the purpose and function of each individual script, please refer to File S3 within the Supplemental Materials associated with Rounds et al., 2021, the in-submission manuscript associated with this dissertation chapter. These Supplemental Materials are available in the online figshare repository at https://figshare.com/s/6f28676d7119624b3105.

CHAPTER 4: EXPANDED DATA | OTHER TESTS OF *NAB2-ATX2* INTERACTION, RIP-SEQ RRNA DEPLETION AND READ DEPTH LIMITATIONS, AND IMPROVEMENTS IN *NAB2*^{EX3} ADULT VIABILITY THROUGH ANGLED VIALS AND THE *NAB2*^{NEX3F42A} OUTCROSS.

This chapter has been written by J. Christopher Rounds specifically for inclusion in this dissertation.

J. Christopher Rounds served as lead researcher and first author on the contents of this chapter. He performed the majority of the genetic, biochemical, and bioinformatic experiments and analyses described within, as well as all of the included microscopy and imaging experiments. He authored and performed the experiments underlying Figures 4-1, 4-2, 4-4, 4-5, 4-6, and 4-7.

Seth M. Kelly authored and performed the experiments underlying Figure 4-3. The circadian behavior experiments detailed in this figure represent work by Seth M. Kelly over multiple years as part of a collaboration with J. Christopher Rounds—he wishes to express his gratitude for this hard work by his fellow author here.

For RNA immunoprecipitation-sequencing (RIP-Seq), the Georgia Genomics and Bioninformatics core prepared cDNA libraries and performed sequencing; J. Christopher Rounds performed all preceding biochemical RIP experiments and sample collection, administratively coordinated the sequencing project with the core, and performed all bioinformatic analyses that followed.

Anita H. Corbett and Kenneth H. Moberg mentored J. Christopher Rounds, provided sustained intellectual contributions and administrative support, and supplied financial support along with J. Christopher Rounds.

RESULTS AND DISCUSSION

Heterozygosity for a third *Atx2* loss-of-function allele, $Atx2^{06490}$, suppresses phenotypes of Nab2 loss but not Nab2 overexpression

In Chapter 3, we used two *Atx2* loss-of-function alleles, $Atx2^{DG08112}$ and $Atx2^{X1}$, to establish *Nab2-Atx2* functional, genetic interactions in fated eye cells, adult viability, and mushroom body axonal morphology (see Figures 3-1, 3-2, 3-S1). To complement and expand these analyses, we tested whether a third *Atx2* loss-of-function allele, $Atx2^{06490}$ (Satterfield *et al.* 2002), similarly suppresses phenotypes of Nab2 dysfunction in these domains. Intriguingly, we find general agreement between the effects of these three *Atx2* alleles, but we also observe some differences—namely, $Atx2^{06490}$ suppresses fewer phenotypes of Nab2 dysfunction than either $Atx2^{DG08112}$ or $Atx2^{X1}$. Notably, for the following analyses, we use the same control and Nab2 overexpression or loss samples, images, and quantifications as we used in Chapter 3, enabling more direct comparisons of the effects of the three *Atx2* loss-of-function alleles under study. To wit, heterozygosity for $Atx2^{06490}$ does not suppress the pigment loss and blackened patch phenotypes of Nab2 overexpression in fated eye cells described in Chapter 3 (i.e. *GMR>Nab2*). This lack of suppression is observed in both females (Figure 4-1A-C) and males (Figure 4-1D-F). However, heterozygosity for $Atx2^{06490}$ robustly, significantly suppresses the effects of Nab2 loss on adult viability (Figure 4-1G). That is, heterozygosity for the $Atx2^{06490}$ loss-of-function allele when combined with $Nab2^{ex3}$ null homozygosity results in adult viability values of 72% and 68% in females and males, respectively, of the values expected by Mendelian inheritance (Figure 4-1H,I). We show these values represent a significant suppression from adult viability values of and 17% and 12% in $Nab2^{ex3}$ null females and males, respectively.

Similarly, we find heterozygosity for the $Atx2^{06490}$ loss-of-function allele suppresses axonal morphology defects associated with loss of Nab2. Specifically, as described in Chapter 3 (see

Figure 3-2), some Kenyon cells of the mushroom bodies, a principal center of olfactory learning and memory in the insect brain (Heisenberg 2003; Kahsai and Zars 2011; Yagi *et al.* 2016; Takemura *et al.* 2017), bifurcate and project into two axon tracts or lobes, the α and β lobes (Figure 4-2A). Homozygosity for the $Nab2^{ex3}$ null allele results in characteristic morphological defects in these axons at a high penetrance—specifically, loss or thinning of α lobes and over-projection or "fusion" of β lobes (Kelly *et al.* 2016; Bienkowski *et al.* 2017; and Figure 4-2B). As with the loss-of-function alleles $Atx2^{DG08112}$ and $Atx2^{X1}$, heterozygosity for the loss-of-function allele $Atx2^{06490}$ suppresses α, but not β, lobe defects in $Nab2^{ex3}$ homozygous nulls, partially restoring proper α lobe morphology (Figure 4-2C). Quantification of these results illustrates the α lobe suppression by $Atx2^{06490}$ in $Nab2^{ex3}$ homozygous nulls is statistically significant and reveals this allele suppresses the penetrance of defective α lobes to 37% from 62% in $Nab2^{ex3}$ nulls alone (Figure 4-2D). In contrast $Atx2^{06490}$ heterozygosity does not significantly affect the penetrance of β lobe fusion in $Nab2^{ex3}$ homozygous nulls (Figure 4-2E).

Taken together, these results with $Atx2^{06490}$ heterozygosity demonstrate the robustness of the *Nab2-Atx2* genetic interaction in the context of loss-of-function alleles. This third *Atx2* allele recapitulates the suppression observed with $Atx2^{DG08112}$ and $Atx2^{X1}$, the *Atx2* alleles described in Chapter 3 (see Figures 3-1, 3-2, and 3-S1), by suppressing $Nab2^{ex3}$ null adult viability and axonal morphology defects. Thus, these results generally align with and strengthen the case for our model of counterbalanced regulation by Nab2 and Atx2, as Atx2 loss-of-function again suppresses effects of Nab2 loss. Intriguingly though, $Atx2^{06490}$ heterozygosity does not recapitulate the suppression observed for the other *Atx2* alleles of Nab2 overexpression in fated eye cells (*GMR>Nab2*). This contrast is particularly notable as both Atx^{06490} and $Atx2^{DG08112}$ alleles are characterized by a P-element transposon insertion in the 5'UTR of *Atx2* (Satterfield *et al.* 2002; Huet *et al.* 2002; Bellen

et al. 2004)—*a priori* expectations would predict decreases in Atx2 expression and/or function would be similar between these alleles. Thus, the distinction in the effects of these *Atx2* alleles suggests an unappreciated difference between Atx2 expression, structure, or genetic background between Atx^{06490} and $Atx2^{DG08112}$. These results may also reflect subtleties in Atx2 interactions with the molecular effects of Nab2 overexpression, which are very poorly understood. Future research will be needed to address these gaps in knowledge and explain why all tested *Atx2* loss-of-function alleles suppress phenotypes of Nab2 loss in $Nab2^{ex3}$ homozygous nulls but do not all suppress phenotypes of Nab2 overexpression in *GMR>Nab2*.

Nab2-Atx2 functional interactions extend into circadian behaviors, expanding the scope of processes potentially coregulated by these RBPs

In Chapter 3 and above in this Chapter, we demonstrated heterozygosity for *Atx2* loss-of-function alleles generally suppresses many canonical phenotypes of Nab2 dysfunction in fated eye cells, adult viability, and mushroom body axonal morphology (Pak *et al.* 2011; Kelly *et al.* 2016). To better understand Nab2-Atx2 functional relationships, we also inverted this approach, testing whether depletion of Nab2 alters a canonical phenotype of Atx2 depletion—circadian behavior deficits (Lim and Allada 2013; Zhang *et al.* 2013). These experiments employ a range of powerful *Drosophila* genetic tools, including *timeless-Gal4* (*tim-Gal4*), a construct which expresses Gal4 across neurons regulating circadian behavior (Emery *et al.* 1998). These experiments also make use of flies carrying a null allele of *period*, per^{01}, which induces arrhythmicity in circadian behavior (Konopka and Benzer 1971; Yu *et al.* 1987) and thus serves as a positive control for circadian behavior defects. To establish and study circadian behaviors, we determine and quantify "free-running" circadian behaviors in single *Drosophila* subjects—that is, we capture the circadian behavior subjects exhibit when relying only on intrinsic biological rhythms, not on any external

light, dark, or environmental cues (for a review of and detailed protocol similar to what we describe here, see Chiu *et al.* 2010). To experimentally evaluate these rhythms, subjects are raised for three controlled 24-hour cycles of 12 hours lights ON and 12 hours lights OFF each to "entrain" or provide cues to standardize and synchronize circadian behavioral rhythms. Then, lights are left OFF for seven consecutive 24-hour cycles; the activity patterns exhibited during this period are the free-running circadian behaviors of interest. Across all nine 24-hour cycles, each individual subject is housed in a unit of a *Drosophila* Activity Monitor (DAM) (e.g. from Trikinetics, Inc.), comprised of multiple small tubes each divided by infrared lasers. Each instance of a subject passing through this laser—a beam break—is recorded and, when summed, used to quantify activity for an individual subject over a given time period. These data are pooled for subjects of the same genotype to produce graphs of activity called actograms and to quantify the degree and features of rhythmic behaviors. We used rethomics software (Geissmann *et al.* 2019) to perform this data analysis.

We evaluated the free-running circadian rhythms of eight genotypes using these methods. Five genotypes represent necessary controls: w^{1118} negative controls; per^{01} positive controls; two RNAi-construct-alone controls, *UAS-Nab2-IR* and *UAS-Atx2-IR*; and a *timeless-Gal4* alone control. The three experimental genotypes were: *tim-Gal4>UAS-Nab2-IR* or Nab2 knockdown, *tim-Gal4>UAS-Atx2-IR* or Atx2 knockdown, and *tim-Gal4>UAS-Nab2-IR + UAS-Atx2-IR* or double knockdown. Actograms demonstrate each control generally exhibits expected free-running rhythms (Figure 4-3A). Each transgenic construct alone demonstrates peaks of activity centered the start of every 12-hour period, characteristic of normal *Drosophila* behavior (see Chiu *et al.* 2010), though with more activity during the "day" than when in the presence of light/dark cues. In contrast and as expected (Konopka and Benzer 1971; Yu *et al.* 1987), per^{01} positive controls

exhibit nearly complete loss of rhythmic circadian activity during the free-running period. The behaviors of these controls validate our experimental protocol accurately observes and quantifies free-running rhythms, allowing reliable conclusions to be drawn from the experimental samples. Actograms show that, similarly to previous reports (Lim and Allada 2013; Zhang *et al.* 2013), knockdown of Atx2 in circadian neurons induces a loss in free-running rhythms similar to that observed in per^{01}. In contrast, knockdown of Nab2 in these neurons appears to leave free-running rhythms largely intact, though potentially with broader peaks of activity, while double knockdown may produce an intermediate phenotype, appearing to demonstrate moderately more rhythmicity than Atx2 knockdown alone but less than Nab2 knockdown alone.

Quantifying the free-running rhythms represented by the actograms in Figure 4-3A confirms the implications of these visualizations for the experimental samples—Nab2 knockdown in circadian neurons suppresses the loss in rhythmic behavior caused by Atx2 knockdown in these cells (Figure 4-3B). When combined with Atx2 knockdown, Nab2 knockdown induces an increase in the percentage of flies exhibiting free-running circadian rhythms compared to Atx2 knockdown alone, quantified as the percentage of rhythmic flies in the sample group. Importantly, Nab2 knockdown alone does not reduce the percentage of rhythmic flies—in fact, in this context, Nab2 knockdown suppresses the slight percent rhythmicity defect seen in *tim-Gal4* alone. This suppression of a phenotype of Atx2 depletion by co-incident Nab2 depletion mirrors the suppression of Nab2 loss by heterozygosity for *Atx2* loss-of-function alleles in adult viability and mushroom body axonal morphology.

However, these analyses also reveal a novel type of *Nab2-Atx2* functional interaction—synergistic enhancement. Despite dramatically different effects on percent rhythmicity, individual knockdown of either Nab2 or Atx2 in circadian neurons does not alter the length of a complete

circadian period from the approximately 24-hour period seen in *tim-Gal4* alone controls (Figure 4-3C). In contrast, double knockdown of both Nab2 and Atx2 significantly lengthens circadian periods to a broad range centered near 25.5 hours. This synergistic effect implies depletion of either Nab2 or Atx2 sensitizes circadian neurons to loss of the other RBP as observed for these proteins in other phenotypes and contexts, but that Nab2 and Atx2 may cooperatively control period length rather than counterbalancing one another in this context. Alternatively, this synergistic effect may reflect nuances in molecular regulation of circadian rhythms, allowing for the possibility Nab2 and Atx2 also counterbalance one another in regulating circadian protein levels, but that disruption of this regulation throughout the molecular fluctuations in a circadian cycle ultimately results in increased circadian period lengths. Finally, with respect to power, a measure of the amplitude or strength of circadian behaviors (see Chiu *et al.* 2010), Nab2 knockdown in circadian neurons is unable to suppress the dramatic decrease caused by At2 knockdown in these cells (Figure 4-3D).

In total, these data establish circadian behaviors as another biological process potentially coregulated by Nab2 and Atx2 along with adult viability and axonal morphology. These results are in some respects consistent with our model of counterbalanced regulation of shared transcripts by Nab2 and Atx2 (see percent rhythmicity data, Figure 4-2B), but synergistic effects of double knockdown of these RBPs on period lengths also suggest the possibility of greater nuance or an alternative Nab2-Atx2 functional relationship in regulating circadian behavioral rhythms.

Absence of Nab2 in *Nab2* nulls may not induce axonal morphology defects in circadian Pdf neurons, unlike knockdown of Atx2

Neurons expressing Pigment-dispersing factor (Pdf) are involved in circadian rhythm regulation—specifically, in “govern[ing] free-running locomotor rhythms”—and exhibit altered axonal

morphology when Atx2 is knocked down by RNAi in circadian neurons by *timeless-Gal4* (hereafter referred to as *tim>Atx2*^{RNAiKK}) (Lim and Allada 2013). Under *tim>Atx2*^{RNAiKK}, both the dorsal and lateral projections (the posterior optic tract or POT) of these cells exhibit "modest outgrowth" or "extra branching/targeting" to a penetrance of approximately 50-60%. Given the functional, genetic interactions between *Nab2* and *Atx2* in regulating mushroom body axon morphology (Chapter 3), a known domain of Nab2 function, we explored whether Nab2 may also contribute to regulation of Pdf neuron morphology, a known domain of Atx2 function (Lim and Allada 2013). Preliminary experiments indicate that *Nab2-Atx2* relationship may not be reciprocal in this way in this case—loss of Nab2 in *Nab2*^{ex3} null homozygotes did not appear to induce dramatic axonal outgrowth deficits in Pdf neurons in adult female brains at our level of detection (Figure 4-4A,B). Importantly, limited success in immunostaining the POT, as compared to robust immunostaining of the dorsal projections, may have masked morphological changes in Pdf neuron axon projections in *Nab2*^{ex3} nulls. Further examination is warranted, but based on these data alone, loss of Nab2 may not alter Pdf neuron axon projection morphology. Whether Nab2 suppresses or enhances effects of Atx2 knockdown on the morphology of these cells remains an open question and should be explored in future research.

Comparative analysis, detailed investigation, and attempted response on the unexpectedly unsuccessful rRNA depletion underlying analysis-limiting, low RIP-Seq read depth

The research we report in Chapters 2 and 3 heavily features high-throughput RNA-sequencing (RNA-Seq) experiments along with extensive, detailed analyses of the results of each. In Chapter 2, we performed an RNA-Seq experiment to characterize the effects of Nab2 loss on RNA abundance and structure in neuron-enriched fly head tissues of female and male samples. In Chapter 3, we performed an RNA immunoprecipitation-sequencing (RIP-Seq) experiment to

identify RNAs associated with Nab2 and Atx2 in fly brain neurons. For consistency, reproducibility, feasibility, efficiency, and result comparability, we applied many of the same or very similar RNA extraction, cDNA library generation, and bioinformatic tools and analyses to characterize, map, annotate, quantify, and statistically compare the abundance of our sequencing reads. For example, in both cases for read mapping we used a release of the read mapping software STAR (Dobin *et al.* 2013) available through the Galaxy project on the public server at usegalaxy.org (Afgan *et al.* 2018). Through these analyses, we discovered an unanticipated explanation for the unexpectedly low read depth we observed in our RIP-Seq but not RNA-Seq results—a broad failure in rRNA depletion as part of cDNA library preparation of our RIP-Seq samples. See Chapter 3 for complementary discussion of the effects of this rRNA depletion setback on our RIP-Seq results. In brief, we suspect many Nab2- and Atx2-associated RNAs remain to be discovered in *Drosophila* neurons as a complement to our analyses. Low read depth and attendant noisiness impeded our ability to reliably detect RNA-RBP association for a given transcript in the context of low read counts and expected inter-sample variability.

Here, we explore the analyses and data which identify and characterize this rRNA depletion setback. We also describe an ultimately unsuccessful attempt to apply an alternative rRNA depletion method to our RIP-Seq samples, a method applied with the intention to have performed a second sequencing run on these samples if depletion proved successful. First, we demonstrate the overall quality (i.e. base-call reliability) of our RNA-Seq (Chapter 2) and RIP-Seq (Chapter 3) experiments is comparable (Figure 4-5A,B). Over 87% of nucleotide base calls for the RNA-Seq and RIP-Seq IP samples carried a quality (Q) score greater than or equal to 30, indicating these calls are each 99.9% accurate (i.e. each call possesses only a 1 in 1,000 chance of inaccuracy) (Illumina 2011) (Figure 4-5A). In each case, over 77 billion bases meet this criterion. Through the

Galaxy project on the public server at usegalaxy.org (Afgan *et al.* 2018), we performed FastQC (Andrews and Babraham Bioinformatics) analysis of two representative samples, *Nab2*^{ex3} null male sample 3 (RNA-Seq) and *elav>Nab2-FLAG* IP sample 1 (RIP-Seq). These analyses show these high-quality base calls are appropriately distributed across the length of reads in aggregate, with quality dipping gradually in both cases along read length, as expected (Figure 4-5B). The representative RIP-Seq sample demonstrates only a slightly greater dip in and variability of quality along the aggregated read length; the overwhelming majority of nucleotide base calls in both cases are of a very high quality and reliability, indicating comparable success in the sequencing event itself and likely comparable cDNA library purity across both samples, which would *a priori* be expected to produce read mapping data of similarly high depth.

Surprisingly, however, we observed dramatic differences in the percentage of reads STAR mapped to a single, unique location in the *Drosophila* genome between our RNA-Seq and RIP-Seq samples; three representative examples are detailed in Figure 4-5C. Sequencing of each of these three representative samples—*Nab2*^{pex41} control female sample 1, *elav>Nab2-FLAG* IP sample 1, and *elav>Nab2-FLAG* Input sample 1—produced over 40 million reads per sample, a robust collection in each case. Approximately 72% of reads for the representative RNA-Seq sample were mapped back to ta single, unique location in the genome, allowing in each case an unambiguous call of a single read count for a single gene, the process essential for comparing the relative abundance of a given transcript across sequencing samples. However, far, far fewer reads could be uniquely mapped for either representative RIP-Seq sample—only approximately 5% and 2.5% of reads for the IP and Input sample, respectively, could be mapped this way.

This low unique mapping translates to far fewer counts called for any given transcript in the RIP-Seq samples as compared to the RNA-Seq samples, despite the comparable number of

reads generated for each sample overall. For the RNA-Seq samples, many, many more individual transcripts were assigned hundreds of read counts as compared to only tens or single digit values assigned to transcripts in RIP-Seq samples. This discrepancy held enormous implications for the count comparisons, statistical testing, and conclusions that can be performed in or drawn from either data set. For example if, in the context of low inter-sample variability, for a given transcript 250 read counts are assigned in control samples on average compared to 500 read counts assigned in *Nab2*^{ex3} null samples on average, such a difference can reliably be interpreted as a true two-fold difference in transcript abundance between controls and *Nab2*^{ex3} nulls. In contrast, a difference of 2 compared to 4 assigned read counts between control and *elav>Nab2-FLAG* IP samples cannot be interpreted this way, and will by definition occur in the context of much greater inter-sample variability. Taken together, such low counts and high inter-sample variability will preclude a determination of whether this nominal two-fold count difference reflects true inter-sample differences or is simply a consequence of the unavoidable noisiness of repeated measurements of small amounts—differences of this sort simply lack the resolution to make such a determination.

Analysis of the locations to which our RIP-Seq sample reads do map provides a key additional detail—these reads are not unmappable to the *Drosophila* genome (due to, for example, sample degradation or contamination). Instead, over 80% of reads in both representative RIP-Seq samples map to multiple loci, much higher than the approximately 23% of reads which map this way in the representative RNA-Seq sample (Figure 4-5C). Closer analyses of the multi-mapping reads in the RIP-Seq were performed in multiple ways, for example by using BLAST to assess the highest frequency sequences identified in FastQC output or by visualizing read pileups in the Integrative Genomics Viewer or IGV (Robinson *et al.* 2011) (data not shown). Such analyses reveal very many of these multi-mapping reads in RIP-Seq samples map to genes encoding

ribosomal RNA (rRNA). The sequences of these genes as a group are highly repetitive, as they exist in multiple copies in the genome, such that short sequencing reads mapping to them often cannot be unambiguously assigned to a single location in the genome.

Upon this discovery, we concluded rRNA depletion, a key step in cDNA library preparation prior to sequencing given the extremely and prohibitively high abundance of rRNA transcripts *in vivo*, was unsuccessful in our RIP-Seq samples. This failure of rRNA depletion occurred despite our use of a protocol as similar as possible to that we previously used for RNA-Seq. To ensure resiliency and redundancy and prepare for unexpected externalities like this, we had supplied only approximately 50% of each RIP-Seq sample to be sequenced in our first sequencing run. For similar reasons, along with the RIP-Seq samples we describe in Chapter 3, we also supplied for sequencing IP and Input samples from separately-processed dense fractions isolated as a consequence of immunoprecipitation sample lysate filtration (by cell strainer) and centrifugation (see Chapter 3, *Materials and Methods* for detail on this step). We collected these Pilot Dense Fractions with intent for them to serve as nuclear fractions—subsequent analyses revealed both cytoplasmic and nuclear proteins are present in these samples and they do not represent a subcellular-compartment-specific lysate (data not shown). However, we determined these Dense Fractions could be used to test rRNA depletion methods without consuming our remaining precious RIP-Seq samples of interest. To that end, we requested application of a second rRNA depletion method by the sequencing core to these Pilot Dense Fraction samples, specifically the Low Input v2 RiboMinus Eukaryote kit (ThermoFisher Cat. No. A15027). We pursued this option to determine suitability of this second rRNA depletion method for use on our RIP-Seq samples of interest.

We found, ultimately, this second rRNA depletion method was similarly unsuccessful to the first (Figure 4-6A). As in our IP and Input samples proper, and as in the first rRNA depletion attempt with the Pilot Dense Fraction samples, this second rRNA depletion method on the Pilot Dense Fraction samples resulted in a bulk of reads mapping to multiple, often rRNA genomic loci, with a very small percentage of reads mapping to unique genomic locations (e.g. to protein coding genes). This second rRNA depletion method also produced similar transcript-level results, validating the reproducibility of our overall sequencing protocol and analysis pipeline (Figure 4-6B). For a representative sample, the *elav>Gal4* alone control Pilot Dense Fraction IP sample, transcript identities for the top 2,000 transcripts (by total read count) were highly overlapping between the original and the second rRNA depletion methods, with notable overlap extending through the ranked transcript list even into the identities of the bottom 2,000 transcripts (with read counts greater than 0). Finally, a view at the individual transcript level aligns with the conclusions implied by analyses of all transcripts. For *Nab2* and its neighboring genes *crb*, *asRNA:CR46093*, and *BRWD3* in the representative *elav>Gal4* alone control Pilot Dense Fraction IP sample, both rRNA depletion methods result in low read depth spread across exon-encoding genomic sequence (Figure 4-6C). The most pronounced differences between these depletion methods at this scale are often simply an even lower read depth in the second depletion method. This even lower read depth is presumably owed to the continued handling of unstable, sensitive RNA samples required to perform the second depletion and sequencing protocols. Ultimately then, given in part that the second rRNA depletion method was similarly unsuccessful as the first, we concluded further optimization work was essential before performing any additional IP-and-sequencing experiments in our research group to identify RNAs associated with Nab2 or any other RBP. We proceeded with analysis of the first rRNA depletion dataset as is, using it to make substantial contributions to

our knowledge of Nab2- and Atx2-associated transcripts and to our understanding of the functions of each of these RBPs. However, our results and experience detailed here also emphasize the necessity for future research to further expand scientific knowledge about and collect additional data on the associated transcripts and functions of these RBPs.

Fortunately, we ultimately were able to develop analytical methods to enable statistically sound comparisons and conclusions between our RIP-Seq samples, such that transcripts of sufficient read counts and reproducibility could be called as Nab2- or Atx2-associated. But, for many transcripts a nominal, normalized enrichment in Nab2-IP samples was not backed by high enough read counts or high enough consistency between samples for even our more lenient statistical methods to make a call of significant enrichment. Taken together, these findings guide our conviction that we identified Nab2- and Atx2-associated transcripts by our RIP-Seq, but that more RBP-associated transcripts remain to be identified than would otherwise be expected in a RIP-Seq experiment such as ours, especially one already optimized as ours was by the performance of a previous RNA-Seq using extremely similar or identical RNA extraction, rRNA depletion, cDNA library preparation, and bioinformatic analysis pipelines and protocols. We interpret the data presented in this subsection to indicate rRNA depletion was unsuccessful in our RIP-Seq but not our RNA-Seq samples. This discrepancy occurred despite the usage of nearly identical rRNA depletion kits for each sample set. However, the manufacturer of the depletion kit we used changed between our two sequencing experiments. In addition, the standard operating procedures and personnel at the sequencing core we collaborated with changed between these two experiments, though we did request and receive an exception from this core for our project to use the same depletion kit for our RIP-Seq as was employed for our RNA-Seq. Behind-the-scenes changes to the rRNA depletion kit (though correspondence with technical support indicated none occurred),

lack of prior experience by core personnel with the depletion kit we requested, or an unknown error or chance issue with preparation or handling of our samples are likely candidates to explain the unsuccessful rRNA depletion we observed. We are unable to differentiate between these possibilities with the data we have. The ultimate conclusion, however, is the same in any of these cases: an unsuccessful rRNA depletion step of cDNA library preparation severely limited read depth of all non-rRNA-encoding regions of the genome (e.g. of protein-coding genes) in our RIP-Seq. This low read depth curtailed the breadth of Nab2- and Atx2-associated transcripts we were able to identify. We identified over 100 transcripts statistically significantly enriched and thus associated with Nab2 and with Atx2 in *Drosophila* brain neurons, making major contributions to the study of each RBP. The low read depth caused by this unsuccessful rRNA depletion simply emphasizes a conclusion common to any single experiment to identify RBP-associated RNAs: additional high-throughput sequencing experiments will be necessary to identify the full repertoire of transcripts associated with these RBPs. Given the centrality and importance of associated transcript identities to illuminating the function of Nab2 and Atx2 and their mechanistic links to human health, development, and disease, such future high-throughput experiments must be carried out to complement and expand the foundation we lay here.

Outcrossing the historical *Nab2^{ex3}* allele improved *Nab2^{ex3}* null adult viability, dramatically increasing sample collection efficiency and experimental feasibility

The original *Nab2^{ex3}* stock experienced a period of unexplained, waning *Nab2^{ex3}* null adult viability, ultimately reaching nearly zero, or nearly 0% of expected viability by Mendelian inheritance. This was observed by most or all researchers using the *Nab2^{ex3}* stock in and around 2016 across two institutions in two states (specifically at Emory University in Georgia and The College of Wooster in Ohio). As a result of this decreased viability, many experiments which

required *Nab2*^{ex3} null adults grew practically prohibitive, as usable *Nab2*^{ex3} homozygous null samples from balanced *Nab2*^{ex3} stocks grew extremely rare. In response, we outcrossed the historical balanced *Nab2*^{ex3} stock to an isogenic control stock (*iso-1*) obtained from the Bloomington Drosophila Stock Center (BDSC), passaging the allele through many generations and ultimately recovering it in two independent stable, balanced outcrossed *Nab2*^{ex3} stocks.

The *Drosophila* crossing scheme for *Nab2*^{ex3} allele outcrossing and recovery, pictured in full in Figure 4-7A, began with crossing virgin *iso-1* females to males of the historical balanced *Nab2*^{ex3} stock. F1 progeny that did not inherit a recombination-suppressing *TM6B* balancer chromosome, and thus did inherit the *Nab2*^{ex3} allele, were mated to one another, establishing separate lines. In each line, successive rounds of progeny were collected and mated together until the F4 generation was reached. Six individual F4 males ("New *ex3* F4s" or *Nex3F4*) also carrying a w^- allele were separated into individual vials crossed to a separate set of double-balanced (*TM3/TM6B*) virgin females. In the progeny of these six independent crosses, individual *Nex3F4* chromosomes were now captured alone and *in trans* to a recombination-suppressing balancer third chromosome. However, by visual scoring alone, no two males could be known to have the *same Nex3F4* chromosome. So, individual male progeny from each of these six progeny sets were given a set and letter designation to code, identify, and differentiate them—the third male from progeny set 4 was identified as *4C* or *Nex3F4#4C*. Sixteen males were coded: *1A*, *1B*, *1C*, *1D*, *2A*, *2B*, *2C*, *3A*, *3B*, *3C*, *4A*, *4B*, *4C*, *5A*, *5B*, and *6A*. These males, now coded, were themselves each crossed to a separate set of double-balanced (*TM3/TM6B*) virgin females, securing each *Nex3F4#_ _* chromosome as the only non-balancer third chromosome in its respective line. For efficiency during screening, in each line the *Nex3F4#_ _* chromosome, *TM3*, and *TM6B* were allowed to "float" (i.e. the line produced all viable combinations of each of these three third chromosomes

over a few generations). *Nex3F4#_ _* chromosome capture and the suppression of recombination should have been equally or nearly equally effective in the presence of both, rather than only one, balancer third chromosome in these lines, at least in the short-term. Each individual *Nex3F4#_ _* line was screened for $Nab2^{ex3}$ null phenotypes, including defects in adult viability and an approximately five-fold skew in female:male viability towards females (Pak *et al.* 2011 and unpublished data). Progeny were also screened for the kinked large humeral or scutal thoracic bristles (i.e. macrochaetae) characteristic of $Nab2^{ex3}$ homozygous nulls, especially the anterior notopleural macrochaeta (aNP); for phenotypic examples in $Nab2^{ex3}$ homozygous nulls, see (Pak *et al.* 2011; Lee *et al.* 2020), for macrochaetae nomenclature, see (Takano 1998; Fig M113 in Rédei 2008; Usui *et al.* 2008). The following ten lines were screened: *Nex3F41A*, *Nex3F41B*, *Nex3F41C*, *Nex3F41D*, *Nex3F42A*, *Nex3F42B*, *Nex3F42C*, *Nex3F43A*, *Nex3F43C*, and *Nex3F45B* (data not shown). Two lines, *Nex3F42A* and *Nex3F45B*, scored as very likely carriers of the $Nab2^{ex3}$ allele, as no viable non-balanced adult homozygotes were observed in the small adult progeny sets screened. These chromosomes were then fully secured in a stable stock, placing each highly likely $Nab2^{ex3}$ chromosome *in trans* to *TM6B* carrying a mini-white construct (hereafter referred to as *TM6B,* w^+). To accomplish this final step, *Nex3F42A* and *Nex3F45B* males carrying the highly likely $Nab2^{ex3}$ chromosome balanced over either *TM3* or *TM6B* were independently crossed to *TM3/TM6B,* w^+ double-balanced females, and select progeny were interbred to generate stable outcrossed and recovered $Nab2^{ex3}$ stocks balanced with *TM6B,* w^+.

Next, we determined whether outcrossing and recovering the $Nab2^{ex3}$ allele, generating stocks $Nab2^{Nex3F42A}$ and $Nab2^{Nex3F45B}$, successfully restored homozygous adult viability of $Nab2^{ex3}$ to approximately 3% of the viability expected by Mendelian inheritance, or the levels observed for the historical $Nab2^{ex3}$ allele (Pak *et al.* 2011; Kelly *et al.* 2014) before its unexplained decline to

almost 0%. Thus, we carefully determined the adult viability of *Nab2*^{Nex3F42A} homozygous nulls, establishing 18 vials of *Nab2*^{Nex3F42A} stock at 25°C on "Day 0" and collecting F1 progeny daily over the six-day window in which all progeny are unambiguously F1s (i.e. lacking any occasional early-eclosing F2) at this temperature, Days 10-16. Moreover, stock vials were maintained using a novel angled method (Figure 4-7B) to limit opportunities for *Nab2*^{Nex3F42A} null adults to get stuck and perish in soggy food in the vial base. Thousands of F1 progeny were generated and scored using these methods, demonstrating that, indeed, the outcrossing and recovery process proved successful in restoring *Nab2*^{ex3} homozygous null adult viability —in fact, the adult viability of *Nab2*^{Nex3F42A} homozygous nulls was notably improved from the level of the historical *Nab2*^{ex3} null allele, reaching approximately 14% rather than 3% of the value expected by Mendelian inheritance (Figure 4-7C). While some of this improvement is almost certainly due to our use of the angled vial method (Figure 4-7B), the widespread reports of *Nab2*^{ex3} homozygous null adult viability declines reported from multiple *Drosophila Nab2* researchers, and the marked increase in adult viability of the outcrossed *Nab2*^{Nex3F42A} as compared to the historical *Nab2*^{ex3} null allele strongly argues that an acquired, unknown genetic or epigenetic background modifier partially explained the acquired low adult viability in historical *Nab2*^{ex3} null homozygotes. Our data argues the 14% value more accurately reflects the effects of genomic *Nab2* loss alone on adult viability, and that studies using the outcrossed *Nab2*^{Nex3F42A} null allele, as ours now do, more accurately and specifically identify the effects of Nab2 loss alone, and thus will more accurately define the function of Nab2.

The angled vial method (Figure 4-7B) is also an important innovation on its own, as its use likely improves *Nab2*^{ex3} null adult viability in any genetic or epigenetic background, presumably by lowering the threshold for coordination, strength, and/or perception *Nab2*^{ex3} null adults require

to avoid falling off vial walls and getting stuck in the soggy food in the vial base, or to avoid getting stuck while walking on that food while eating or laying eggs. In this method, vials are propped on their side at an approximately 30° angle, laying them on vial divider paperboard previously folded in half to construct a simple stand. Importantly, laying vials completely horizontally proves counterproductive and comparatively negatively impacts adult viability (data not shown). In a fully horizontal orientation, the food in the vial base, loosened by adults and larvae over time, sloughs down to fill the entire vial length, increasing the sogginess and surface area of the food in which flies may get stuck and perish.

The outcrossed *Nab2*^{ex3} allele *Nab2*^{Nex3F42A} also dramatically reduces the female:male sex skew observed in the historical *Nab2*^{ex3} stock (Figure 4-7D). The female:male ratio of viable *Nab2*^{ex3} adults in the historical *Nab2*^{ex3} stock is approximately 5.7:1, reflecting an unknown male-specific reduction in adult viability in *Nab2*^{ex3} null males compared to *Nab2*^{ex3} null females. The outcrossed allele demonstrates a substantial reduction in this skew, exhibiting a female:male ratio in viable adults of 1.6:1. This ratio is notably skewed as compared to heterozygous *Nab2*$^{ex3/+}$ sibling controls, which exhibit a female:male ratio in viable adults of 1.1:1, but is substantially suppressed as compared to the historical *Nab2*^{ex3} stock. The reduction in the skew of the female:male ratio in viable *Nab2*^{Nex3F42A} null adults as compared to the historical stock likely reflects separation-by-outcross from a background genetic or epigenetic modifier that exerted male-specific effects on adult viability. We also identified an potential additional contributing factor to, if not a wholly alternative explanation for, the extreme female:male sex skew observed in viable adults in the historical *Nab2*^{ex3} stock. As part of our careful determination of the *Nab2*^{ex3} null adult viability in the *Nab2*^{Nex3F42A} stock, we performed daily progeny collections from many parallel *Nab2*^{Nex3F42A} vials all established on the same day. We observed unexpected daily

variability in female:male eclosion frequency in *Nab2*^{Nex3F42A} null adults that was not observed in heterozygous *Nab2*$^{ex3/+}$ sibling controls (Figure 4-7E). Similar ratios of female and male heterozygous *Nab2*$^{ex3/+}$ adults eclosed on each day of the seven-day collection period; *Nab2*^{Nex3F42A} null adults demonstrate day-to-day variability in this ratio. On some collection days, many more *Nab2*^{Nex3F42A} null females eclosed than did males; on others, similar numbers of *Nab2*^{Nex3F42A} null females and males eclosed. Given the relatively short lifespans of *Nab2*^{ex3} null adults compared to controls (Jalloh *et al.* 2020), the female:male ratio in viable *Nab2*^{ex3} null adults observed in the historical *Nab2*^{ex3} stock may have been highly dependent on the exact timepoints and frequency of adult collection if daily collections were not performed. As with overall adult viability, separating the *Nab2*^{ex3} null allele from this unknown modifier enables future experiments to more accurately identify and explain why loss of Nab2 results in sex-specific impacts on adult viability. Moreover, results from the outcrossed *Nab2*^{Nex3F42A} allele reveal that the effects of genomic Nab2 loss on male adult viability are only moderately more severe than effects in females, compared to the extreme, nearly 6-to-1 ratio originally observed. Again, this will enable future experiments and experimenters to more accurately study and model the functions and sex-specific effects of Nab2 in *Drosophila*.

In summary, the outcrossed *Nab2*^{Nex3F42A} stock, when raised using the angled vial method (Figure 4-7B), demonstrates rates of adult viability substantially higher than those observed in this historical *Nab2*^{ex3} stock—14% compared to 3% of adults expected by Mendelian inheritance (Figure 4-7C). Moreover, the outcrossed *Nab2*^{Nex3F42A} stock exhibits only a moderate skew towards females —1.6:1—in the female:male ratio of viable *Nab2*^{ex3} null adults, a skew much less extreme than the nearly 6-to-1 ratio observed in the historical *Nab2*^{ex3} stock (Figure 4-7D). So, outcrossing brought both overall viability and female:male sex ratios of *Nab2*^{ex3} null adults closer to control

conditions. Thus, in the outcrossed *Nab2*^{Nex3F42A} stock, the effects of genomic Nab2 loss have very likely been separated from the effects of a background genetic or epigenetic modifier in the historical *Nab2*^{ex3} stock, improving the applicability, accuracy, and reliability of results using the *Nab2*^{Nex3F42A} stock as compared to the historical *Nab2*^{ex3} stock. Moreover, results produced using this outcrossed stock will improve upon our ability to report on Nab2 function specifically and with certainty, all while greatly improving experimental feasibility, making *Nab2*^{ex3} null adults much more practical and efficient to isolate, collect, and analyze in large quantities.

REFERENCES

Afgan E., D. Baker, B. Batut, M. van den Beek, D. Bouvier, *et al.*, 2018 The Galaxy platform for accessible, reproducible and collaborative biomedical analyses: 2018 update. Nucleic Acids Res. 46: 537–544. https://doi.org/10.1093/nar/gky379

Andrews S., and Babraham Bioinformatics, FastQC A Quality Control tool for High Throughput Sequence Data. https://www.bioinformatics.babraham.ac.uk/projects/fastqc/.

Bellen H. J., R. W. Levis, G. Liao, Y. He, J. W. Carlson, *et al.*, 2004 The BDGP gene disruption project: Single transposon insertions associated with 40% of Drosophila genes. Genetics 167: 761–781. https://doi.org/10.1534/genetics.104.026427

Bienkowski R. S., A. Banerjee, J. C. Rounds, J. Rha, O. F. Omotade, *et al.*, 2017 The Conserved, Disease-Associated RNA Binding Protein dNab2 Interacts with the Fragile X Protein Ortholog in Drosophila Neurons. Cell Rep. 20: 1372–1384. https://doi.org/10.1016/j.celrep.2017.07.038

Chiu J. C., K. H. Low, D. H. Pike, E. Yildirim, and I. Edery, 2010 Assaying locomotor activity to study circadian rhythms and sleep parameters in Drosophila. J. Vis. Exp. https://doi.org/10.3791/2157

Dobin A., C. A. Davis, F. Schlesinger, J. Drenkow, C. Zaleski, *et al.*, 2013 STAR: ultrafast universal RNA-seq aligner. Bioinformatics 29: 15–21. https://doi.org/10.1093/bioinformatics/bts635

Emery P., W. V. So, M. Kaneko, J. C. Hall, and M. Rosbash, 1998 Cry, a Drosophila clock and light-regulated cryptochrome, is a major contributor to circadian rhythm resetting and photosensitivity. Cell 95: 669–679. https://doi.org/10.1016/S0092-8674(00)81637-2

Geissmann Q., L. G. Rodriguez, E. J. Beckwith, and G. F. Gilestro, 2019 Rethomics: An R framework to analyse high-throughput behavioural data. PLoS One 14: e0209331. https://doi.org/10.1371/journal.pone.0209331

Heisenberg M., 2003 Mushroom body memoir: From maps to models. Nat. Rev. Neurosci. 4: 266–275. https://doi.org/10.1038/nrn1074

Huet F., J. T. Lu, K. V. Myrick, L. R. Baugh, M. A. Crosby, *et al.*, 2002 A deletion-generator compound element allows deletion saturation analysis for genomewide phenotypic annotation. Proc. Natl. Acad. Sci. U. S. A. 99: 9948–9953. https://doi.org/10.1073/pnas.142310099

Illumina, 2011 *Quality Scores for Next-Generation Sequencing*.

Jalloh B., J. C. Rounds, B. E. Brown, I. J. Kremsky, A. Banerjee, *et al.*, 2020 The Nab2 RNA binding protein promotes sex-specific splicing of Sex lethal in Drosophila neuronal tissue. bioRxiv 2020.11.13.382168. https://doi.org/10.1101/2020.11.13.382168

Kahsai L., and T. Zars, 2011 Learning and memory in drosophila: Behavior, genetics, and neural systems, pp. 139–167 in *International Review of Neurobiology*, Academic Press Inc.

Kelly S. M., S. W. Leung, C. Pak, A. Banerjee, K. H. Moberg, *et al.*, 2014 A conserved role for

the zinc finger polyadenosine RNA binding protein, ZC3H14, in control of poly(A) tail length. RNA 20: 681–8. https://doi.org/10.1261/rna.043984.113

Kelly S. M., R. Bienkowski, A. Banerjee, D. J. Melicharek, Z. A. Brewer, *et al.*, 2016 The Drosophila ortholog of the Zc3h14 RNA binding protein acts within neurons to pattern axon projection in the developing brain. Dev. Neurobiol. 76: 93–106. https://doi.org/10.1002/dneu.22301

Konopka R. J., and S. Benzer, 1971 Clock mutants of Drosophila melanogaster. Proc. Natl. Acad. Sci. U. S. A. 68: 2112–2116. https://doi.org/10.1073/pnas.68.9.2112

Lee W.-H., E. B. Corgiat, J. C. Rounds, Z. Shepherd, A. H. Corbett, *et al.*, 2020 A Genetic Screen Links the Disease-Associated Nab2 RNA-Binding Protein to the Planar Cell Polarity Pathway in Drosophila melanogaster. G3 GENES, GENOMES, Genet. https://doi.org/10.1534/g3.120.401637

Lim C., and R. Allada, 2013 ATAXIN-2 Activates PERIOD Translation to Sustain Circadian Rhythms in Drosophila. Science (80-.). 340. https://doi.org/10.1126/science.1234785

Pak C., M. Garshasbi, K. Kahrizi, C. Gross, L. H. Apponi, *et al.*, 2011 Mutation of the conserved polyadenosine RNA binding protein, ZC3H14/dNab2, impairs neural function in Drosophila and humans. Proc. Natl. Acad. Sci. U. S. A. 108: 12390–5. https://doi.org/10.1073/pnas.1107103108

Rédei G. P., 2008 Morphogenesis in Drosophila (See Fig. M113), pp. 1257–1264 in *Encyclopedia of Genetics, Genomics, Proteomics and Informatics*, Springer Netherlands.

Robinson J. T., H. Thorvaldsdóttir, W. Winckler, M. Guttman, E. S. Lander, *et al.*, 2011 Integrative genomics viewer. Nat. Biotechnol. 29: 24–26.

Satterfield T. F., S. M. Jackson, and L. J. Pallanck, 2002 A Drosophila Homolog of the Polyglutamine Disease Gene SCA2 Is a Dosage-Sensitive Regulator of Actin Filament Formation. Genetics 162: 1687–1702.

Takano T. S., 1998 *Loss of Notum Macrochaetae as an Interspecific Hybrid Anomaly Between Drosophila melanogaster and D. simulans*.

Takemura S. ya, Y. Aso, T. Hige, A. Wong, Z. Lu, *et al.*, 2017 A connectome of a learning and memory center in the adult Drosophila brain. Elife 6. https://doi.org/10.7554/eLife.26975

Usui K., C. Goldstone, J. M. Gibert, and P. Simpson, 2008 Redundant mechanisms mediate bristle patterning on the Drosophila thorax. Proc. Natl. Acad. Sci. U. S. A. 105: 20112–20117. https://doi.org/10.1073/pnas.0804282105

Yagi R., Y. Mabuchi, M. Mizunami, and N. K. Tanaka, 2016 Convergence of multimodal sensory pathways to the mushroom body calyx in Drosophila melanogaster. Sci. Rep. 6. https://doi.org/10.1038/srep29481

Yu Q., A. C. Jacquier, Y. Citri, M. Hamblen, J. C. Hall, *et al.*, 1987 Molecular mapping of point mutations in the period gene that stop or speed up biological clocks in Drosophila melanogaster. Proc. Natl. Acad. Sci. U. S. A. 84: 784–788. https://doi.org/10.1073/pnas.84.3.784

Zhang Y., J. Ling, C. Yuan, R. Dubruille, and P. Emery, 2013 A Role for Drosophila ATX2 in Activation of PER Translation and Circadian Behavior. Science (80-.). 340.

FIGURES

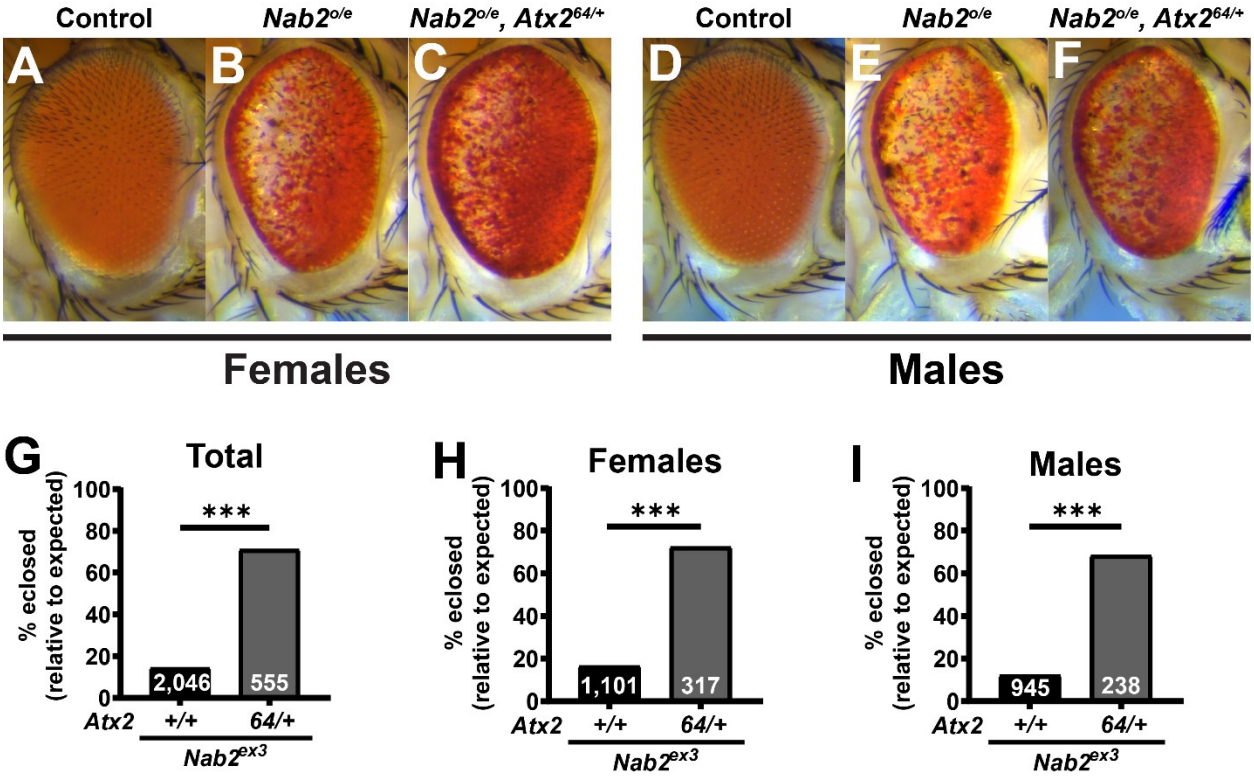

Figure 4-1. Heterozygosity for the *Atx2*^{06490} loss-of-function allele suppresses adult viability defects but not eye morphology defects of Nab2 misexpression in females and males. (A) A control female *Drosophila* heterozygous for the fated-eye-cell driver *GMR-Gal4* demonstrates the uniform color and regimented ommatidial structure characteristic of the fly eye. (B) Females overexpressing Nab2 under control of *GMR-Gal4* (*Nab2*$^{o/e}$) display posterior pigment loss, a disorganized or "rough" ommatidial lattice, and sporadic blackened patches. (C) Heterozygosity for the *Atx2*^{06490} loss-of-function allele (*Atx2*$^{64/+}$) does not suppress any of the three eye phenotypes associated with *Nab2*$^{o/e}$. This lack of suppression contrasts with the effects of heterozygosity for the *Atx2*^{DG08112} and *Atx2*^{X1} loss-of-function alleles (see Figure 3-1). (D-F) Male *Drosophila* of identical genotypes as A-C produce similar results—*Atx2*$^{64/+}$ does not suppress eye phenotypes of *Nab2*$^{o/e}$ in males. (G) However, heterozygosity for *Atx2*^{06490} strongly and significantly suppresses the adult viability defects caused by Nab2 loss in *Nab2*^{ex3} homozygous nulls. Adult viability is

quantified as the percentage of flies eclosed compared to the number expected by Mendelian inheritance. (H-I) As in the overall population in (G), $Atx2^{64/+}$ significantly suppresses $Nab2^{ex3}$ null adult viability defects when only females or males are considered. Sample sizes (n) are reported in each bar and include all F1 progeny scored, including the genetically distinct siblings of each genotype of interest used to calculate the number of flies expected by Mendelian inheritance. Fisher's Exact Test (two-sided) was used to assess statistical significance. ns=not significant, ***=$p<0.001$. Importantly, panels A, B, D, and E, along with the $Nab2^{ex3}$ null adult viability values are reproduced from Figure 3-1, enabling direct comparisons between effects of all three *Atx2* loss-of-function alleles under study.

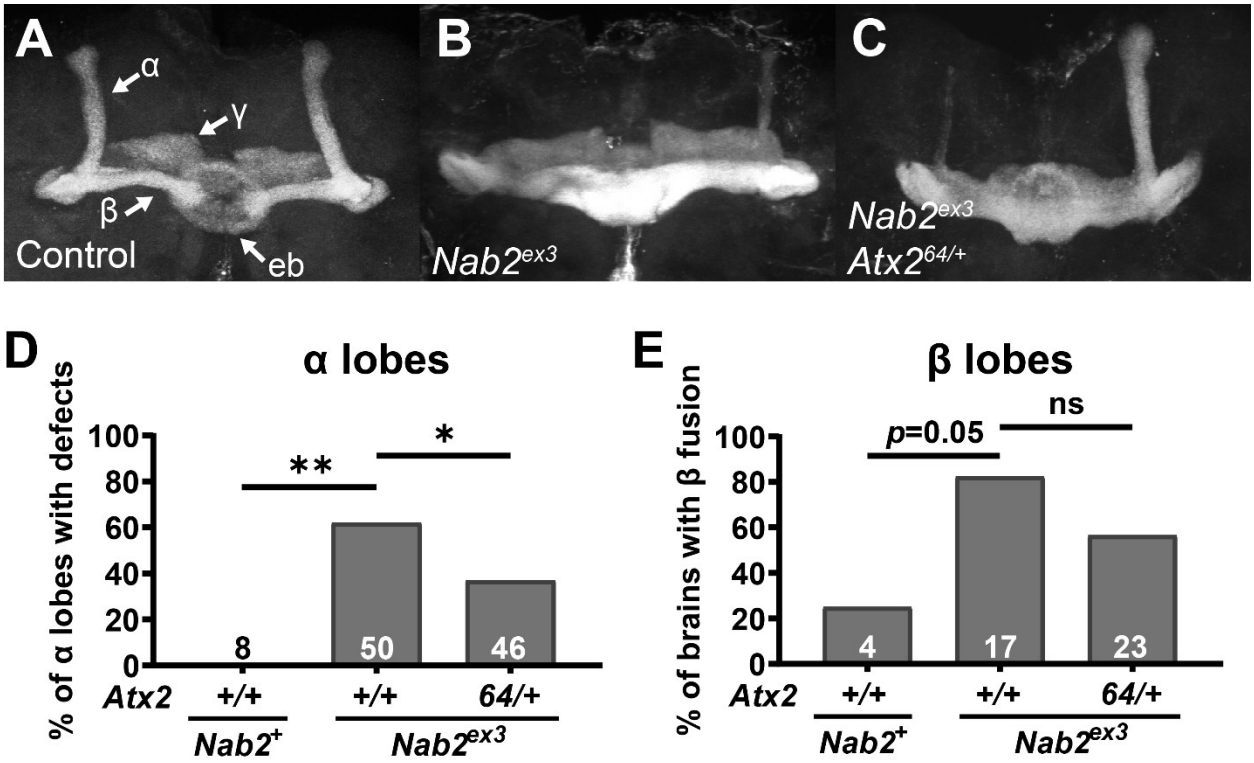

Figure 4-2. Heterozygosity for the *Atx2*^{06490} loss-of-function allele suppresses axonal morphology defects in *Nab2*^{ex3} null mushroom body α, but not β, lobes. (A) A representative *Nab2*^{pex41} control brain demonstrates the morphology of the α and β lobes, Fasciclin 2 (Fas2)-marked dorsally and medially projecting axon tracts or lobes, respectively, of the mushroom bodies (white arrows and labels). Fas2 also detects the γ lobes of the mushroom bodies and the ellipsoid body (eb) (white arrows and labels). (B) A representative *Nab2*^{ex3} homozygous null brain displays characteristic defects in mushroom body morphology, namely thinning or missing α lobes and over-projecting or "fused" β lobes. (C) Heterozygosity for the *Atx2*^{06490} loss-of-function allele (*Atx2*$^{64/+}$) suppresses α but not β lobe morphology defects of *Nab2*^{ex3} nulls, partially restoring proper α lobe morphology in this representative brain. (D) Quantification of α lobe defects illustrates this suppression by *Atx2*^{06490} and demonstrates its statistical significance. (E) Quantification of β lobe defects, showing *Atx2*$^{64/+}$ does not statistically significantly affect the penetrance of *Nab2*^{ex3} null β lobe fusion, though an intriguing trend towards suppression is

observed. Sample sizes (n) are reported in each bar and quantify, for each genotype, the total number of α lobes scored for defects or the total number of brains scored for β lobe fusion. Fisher's Exact Test (two-tailed) was used to assess statistical significance. ns=not significant, *=$p<0.05$, **=$p\leq0.01$. Importantly, panels A and B, and quantification data for associated genotypes within panels D and E, are reproduced from Figure 3-2, enabling direct comparisons between the effects of all three *Atx2* loss-of-function alleles under study.

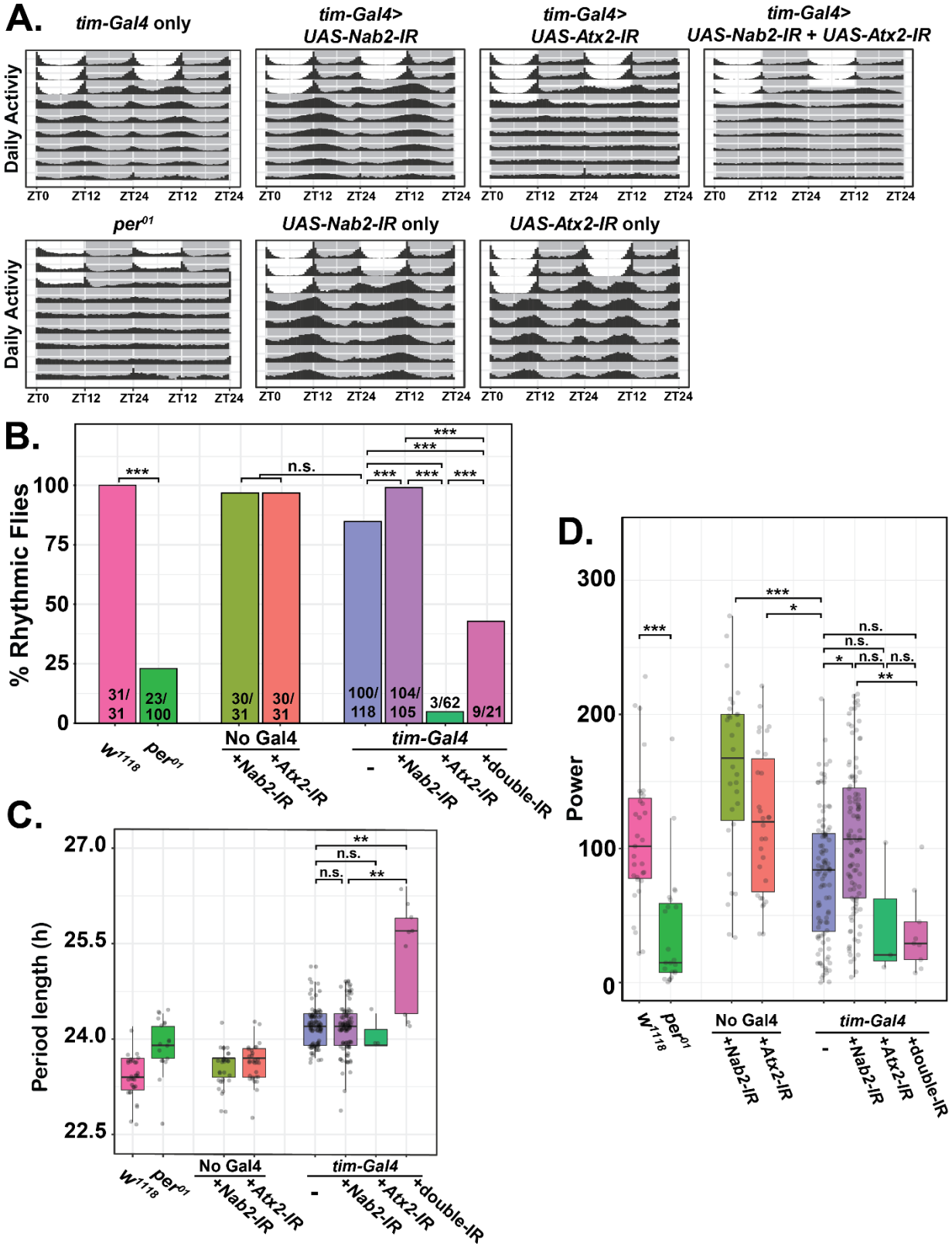
A.
tim-Gal4 only
tim-Gal4> UAS-Nab2-IR
tim-Gal4> UAS-Atx2-IR
tim-Gal4> UAS-Nab2-IR + UAS-Atx2-IR
per01
UAS-Nab2-IR only
UAS-Atx2-IR only
Daily Activiy
ZT0 ZT12 ZT24 ZT12 ZT24
B.
% Rhythmic Flies
31/ 31
23/ 100
30/ 31
30/ 31
100/ 118
104/ 105
3/62
9/21
n.s.
***
No Gal4
tim-Gal4
w1118
per01
+Nab2-IR
+Atx2-IR
-
+double-IR
C.
Period length (h)
27.0
25.5
24.0
22.5
n.s.
**
D.
Power
300
200
100
0
*

Figure 4-3. RNAi-induced knockdown of Nab2 in circadian neurons suppresses a circadian rhythmicity defect of Atx2 knockdown while synergistically enhancing circadian period length. (A) Actograms displaying daily activity as assessed by a *Drosophila* Activity Monitor (DAM) for seven genotypes: *tim-Gal4* only controls, per^{01} positive controls, *UAS-Nab2-IR* and *UAS-Atx2-IR* only RNAi construct controls, and three experimental genotypes. The three experimental genotypes are: *tim-Gal4>UAS-Nab2-IR* (Nab2 knockdown), *tim-Gal4>UAS-Atx2-IR* (Atx2 knockdown), and *tim>Gal4>UAS-Nab2-IR + UAS-Atx2-IR* (double knockdown). Each line of each actogram displays two consecutive days, or two full cycles of Zeitgeber Time (ZT) beginning with lights ON at ZT0 and restarting at ZT24/ZT0 24 hours later. These representations are specifically double-plot actograms—that is, day displays repeat, as the second day shown on any given line is the first day displayed on the next line down. Shading indicates lights ON (white shading) or lights OFF (grey shading), while black, filled curves represent fly activity as measured by DAM beam breaks. Free-running (i.e. without environmental cues) circadian rhythms are assessed for seven days after three days of rhythm standardization or entrainment. All five control genotypes display expected free-running rhythms, and Atx2 knockdown alone leads to rapid loss of most rhythmic activity, as expected. Nab2 knockdown alone does not induce circadian rhythm loss, though activity peaks appear to broaden in this condition. The double knockdown actogram indicates Nab2 knockdown may moderately suppress rhythm loss caused by Atx2 knockdown, but low activity amplitudes make further characterization difficult without the quantitative analyses below. (B) The percentage of flies exhibiting rhythmic free-running circadian behavior are displayed for all seven genotypes in A) along with an additional negative control, w^{1118}. In general, this quantification confirms the actogram interpretations listed above, while revealing definitively that Nab2 knockdown indeed suppresses the rhythmicity loss observed under Atx2 knockdown, at

least with respect to the percentage of rhythmic flies. (C) Free-running circadian period lengths are quantified for the same genotypes as in B). In contrast to the relationship observed between Nab2 and Atx2 knockdown in percent rhythmicity, Nab2 and Atx2 knockdown appear to have no effect on period length alone and synergistically increase period length when induced together. (D) Power, a measure of circadian behavior amplitude (see Chiu *et al.* 2010), is displayed for the same eight genotypes as in B) and C). Atx2 knockdown does not significantly affect power but does induce a non-significant trend towards a decrease, double knockdown produces a similarly low power as Atx2 knockdown alone, and Nab2 knockdown does not decrease power. Rethomics software (Geissmann *et al.* 2019) was used to quantify circadian behavior and its attendant features, while pairwise chi-square tests with multiple hypothesis testing correction were used to assess statistical significance.

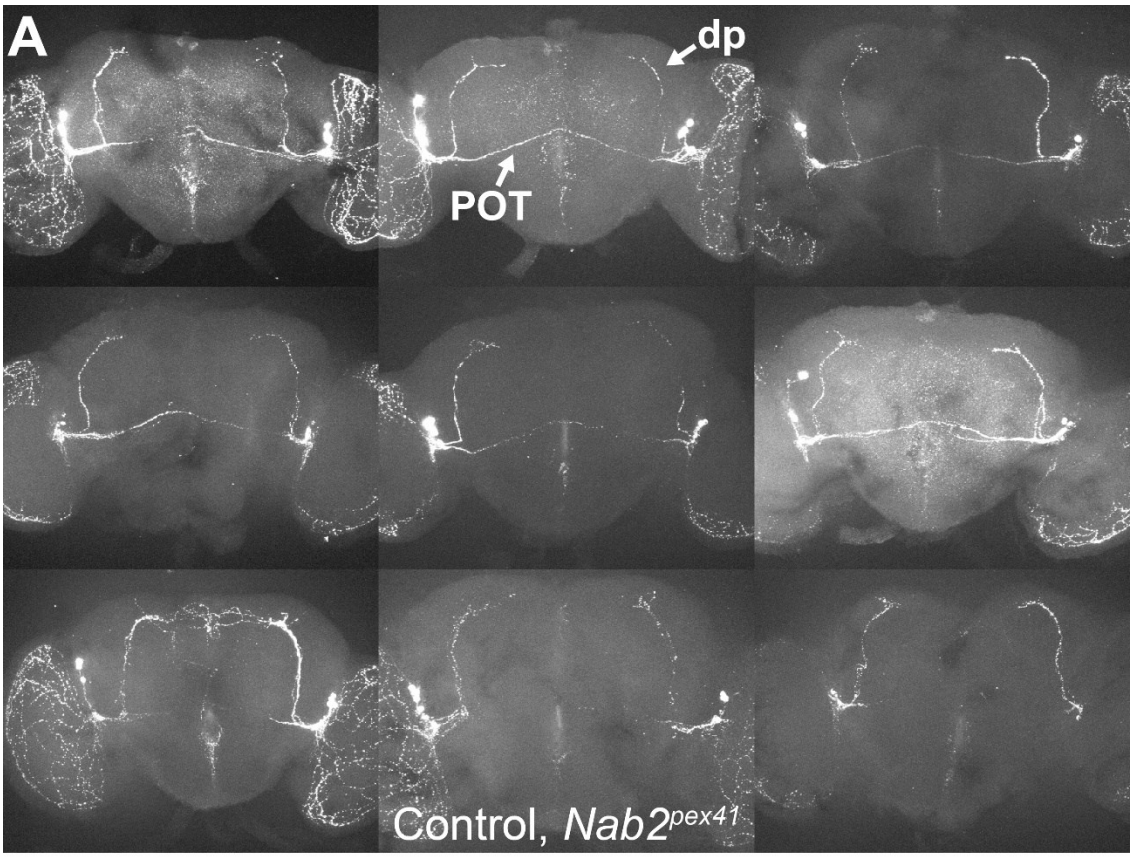
A
dp
POT
Control, Nab2pex41

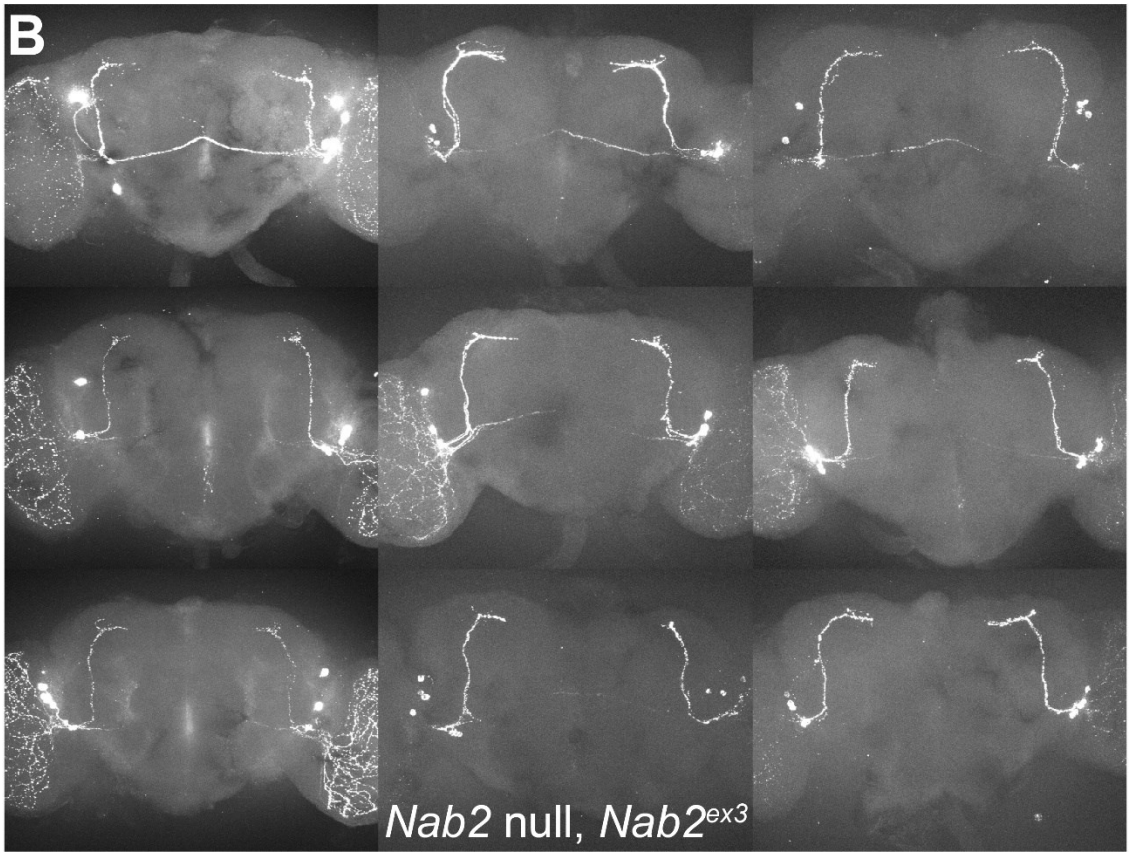
B
Nab2 null, Nab2ex3

Figure 4-4. Genomic loss of *Nab2* may not alter axonal morphology of circadian Pdf neurons, unlike knockdown of Atx2 by *tim>Gal4*. A selection of brains dissected from (A) control ($Nab2^{pex41}$) and (B) Nab2 homozygous null ($Nab2^{ex3}$) adult females, each immunostained with α-Pdf, are shown. Loss of Nab2 does not appear to induce in these cells the axonal outgrowth or extra branching/abnormal targeting phenotypes observed when Atx2 is knocked down in neurons regulating circadian rhythms by *timeless>Gal4* (Lim and Allada 2013). We cannot exclude the possibility that such morphological defects may occur in $Nab2^{ex3}$ Pdf neurons, but that these fell below the level of detection presented here, or that such defects may have been masked by limited immunostaining in these brains of the posterior optic tracts (POT), the medial projections from Pdf neurons. In (A), both dorsal projections (dp) and the POT are labeled for reference.

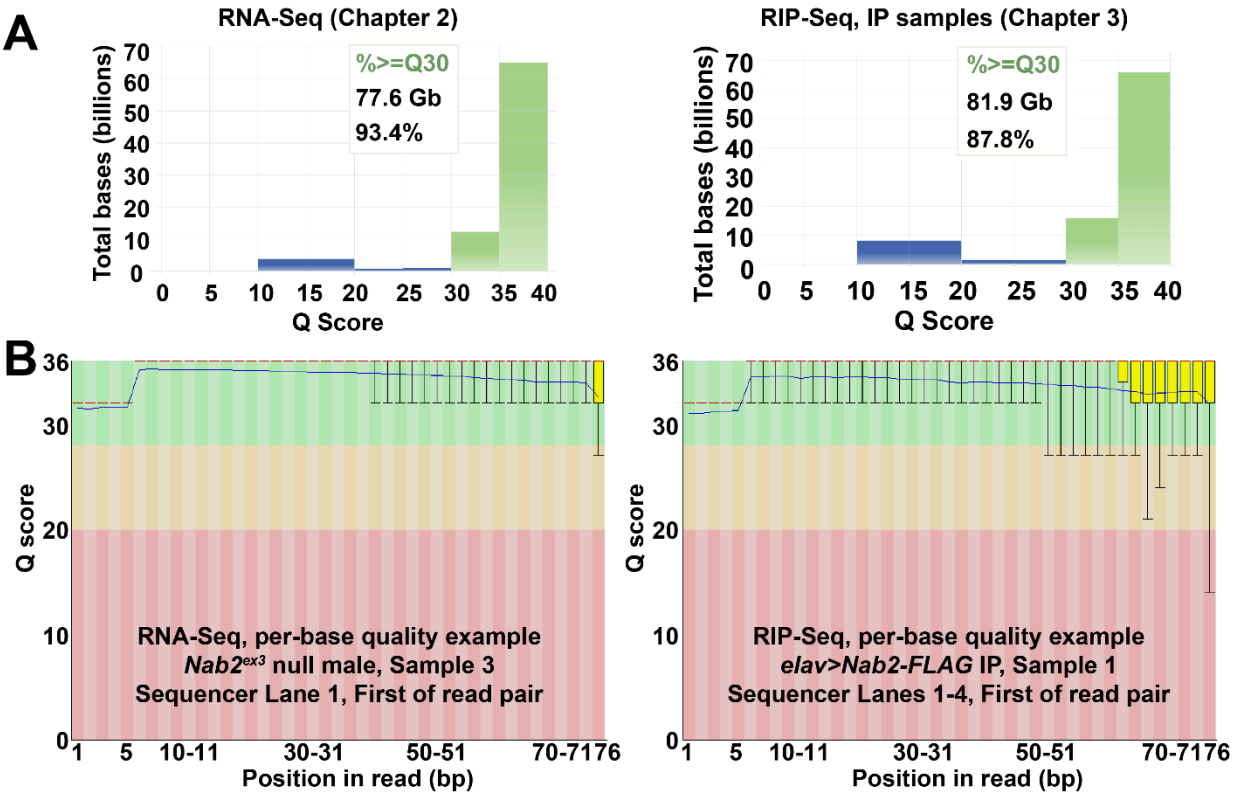

C

Sample	Experiment	Total number of reads	Uniquely mapped reads	Reads mapped to multiple loci
Nab2^{pex41} control, female, Sample 1	RNA-Seq	44,318,117	71.92%	22.77%
elav>Nab2-FLAG IP, Sample 1	RIP-Seq	52,049,759	4.74%	84.42%
elav>Nab2-FLAG Input, Sample 1	RIP-Seq	50,149,079	2.55%	84.67%

Figure 4-5. Comparative analyses of read quality and mapping details are consistent with an unsuccessful rRNA depletion in RIP- but not RNA-Seq. (A) Output from the Illumina BaseSpace web platform. This output demonstrates the vast majority of sequenced bases in both our RNA-Seq (detailed in Chapter 2) and our RIP-Seq IP samples (detailed in Chapter 3) are of a high quality—that is, each possesses an extremely high likelihood of accuracy. Over 85% of bases, at least 77 billion in either case, posses a quality (Q) score greater than or equal to 30, a common threshold for reliability in base calls in high-throughput sequencing that reflects an individual base call accuracy of 99.9% (i.e. only a 1 in 1,000 chance of inaccuracy) (Illumina 2011). (B) Output

from FastQC (Andrews and Babraham Bioinformatics) on two representative samples—*Nab2*^{ex3} null male sample 3 (RNA-Seq) and *elav>Nab2-FLAG* IP Sample 1 (RIP-Seq). These data display the base-by-base Q scores across aggregated reads for each sample. In both cases, read quality and Q score variability gradually decrease over the aggregated read length as expected. But in each case mean Q scores remain similar and well-within the Q 30 threshold (green shading). (C) Descriptive statistics on read mapping output by STAR (Dobin *et al.* 2013) as accessed through the Galaxy project on the public server at usegalaxy.org (Afgan *et al.* 2018). Descriptive statistics are shown for the representative samples *Nab2*^{pex41} control female Sample 1 (RNA-Seq), *elav>Nab2-FLAG* IP Sample 1 (RIP-Seq), and *elav>Nab2-FLAG* Input Sample 1 (RIP-Seq). For each sample over 40 million reads were sequenced. For the RNA-Seq sample over 70% of reads were uniquely mapped to one genomic locus, while approximately 23% mapped to multiple loci. In contrast, for each RIP-Seq sample less than 5% of reads were uniquely mapped to one genomic locus and over 80% mapped to multiple loci. Additional analyses (e.g. BLAST of the most frequent read sequences as identified by FastQC, IGV read visualization; data not shown) confirm the implications of these read mapping statistics. Namely, these analyses taken together show rRNA depletion was unsuccessful as part of cDNA library preparation in our RIP-Seq samples, unlike in our RNA-Seq. This unexpected issue limited RIP-Seq read depth and curtailed the number of RBP-associated transcripts we were able to call. Fortunately, this issue did not prevent identification of any RBP-associated transcripts—we still identified over 100 Nab2-associated and over 100 Atx2-associated transcripts through these RIP-Seq experiments (see Chapter 3).

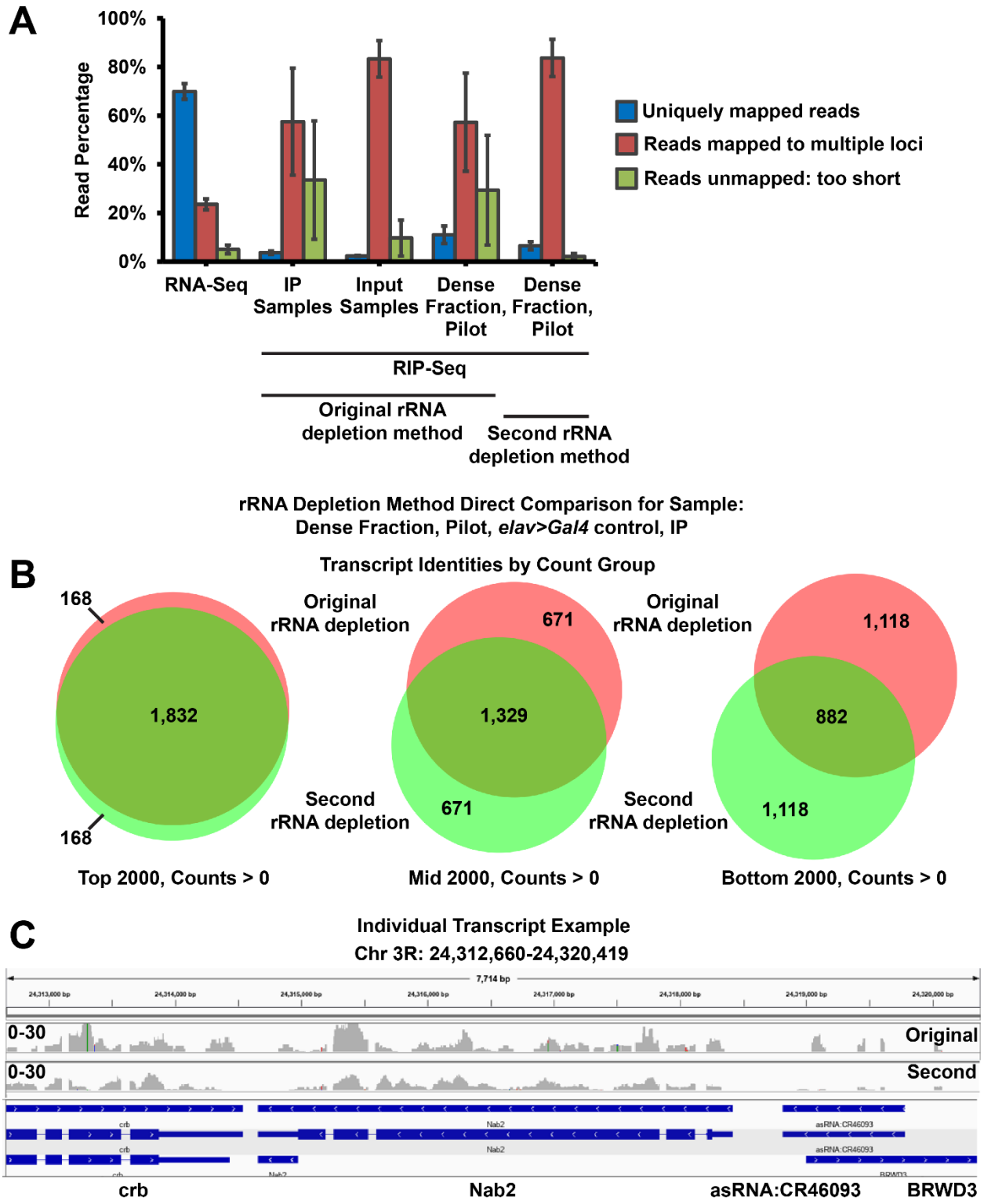

Figure 4-6. A second rRNA depletion attempt proved similarly unsuccessful as the first, recommending analyses proceed for the original RIP-Seq samples. (A) Descriptive read

mapping statistics output by STAR (Dobin *et al.* 2013) as accessed through the Galaxy project on the public server at usegalaxy.org (Afgan *et al.* 2018). Descriptive statistics are averaged across all samples within each listed group. The Dense Fraction, Pilot samples are 6 samples in total—3 IP-Input sample pairs derived from one each of *elav>Gal4* alone controls, *elav>Nab2-FLAG*, and *elav>Atx2-3xFLAG*. These Dense Fraction samples were isolated as part of lysate filtration and centrifugation steps for RIP-Seq samples proper (see Chapter 3, *Materials and Methods*, subsection *Immunoprecipitation* for these steps). Here, these samples are used to test a second rRNA depletion method, the Low Input v2 RiboMinus Eukaryote kit (ThermoFisher Cat. No. A15027). This second depletion method proves unable to increase the percentage of uniquely mapped reads or decrease the percentage of multi-mappers as compared to the original depletion method. In fact, if the second depletion method exerts any detectably different effects, it proved more unsuccessful by these metrics. (B) Identities of transcripts rank-ordered by total counts overlap well between results of each sequencing run following each rRNA depletion method for a representative Dense Fraction, Pilot sample—*elav>Gal4* alone control IP. This overlap is particularly pronounced for the top 2,000 transcripts by total read count, but is notable even for the bottom 2,000 transcripts with counts greater than 0. These data demonstrate our sequencing protocols and bioinformatic analysis pipelines are reproducible and imply the second rRNA depletion method was truly as unsuccessful as the original method. (C) A snapshot from IGV of the *Nab2* locus and neighboring genes for the same representative sample as in B). Consistent with the overall read and transcript analyses in A) and B), the individual transcript analysis shown here demonstrates similarly low read depth for each rRNA depletion method. Reads appropriately map throughout gene lengths and only to exon-coding regions in each case. In fact, the second rRNA depletion method appears to have resulted in a lower read depth than the original method, likely

owing to the second experimental handling of sensitive, unstable RNA samples required to perform this second depletion. These data, taken together, show the second rRNA depletion method would not produce higher read depth than the first, original method. In response, RIP-Seq analysis proceeded with the original sequencing results for the IP and Input sample sets of interest shown in A).

A

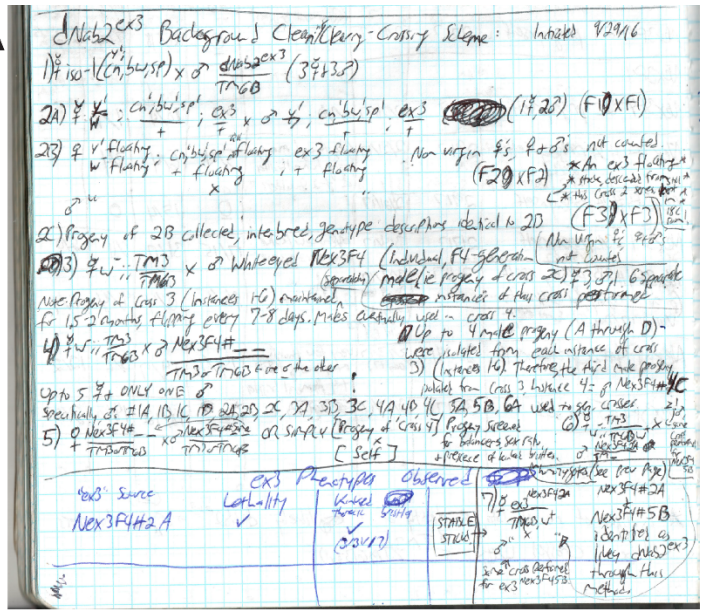

B

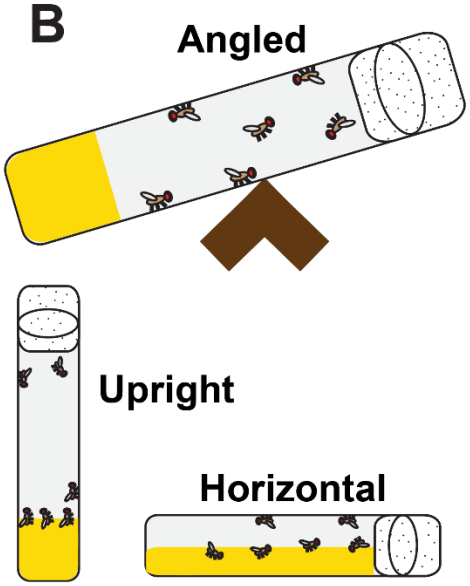

C

Genotype (Stock)	% Adult Viability (Relative to expected by Mendelian inheritance)	Sources
Nab2^{ex3} (historical)	~3%	(Pak et al. 2011; Kelly et al. 2014)
Nab2^{ex3} (*Nex3F42A*)	14%	(Rounds et al., 2021; current document, n=2,046)

D

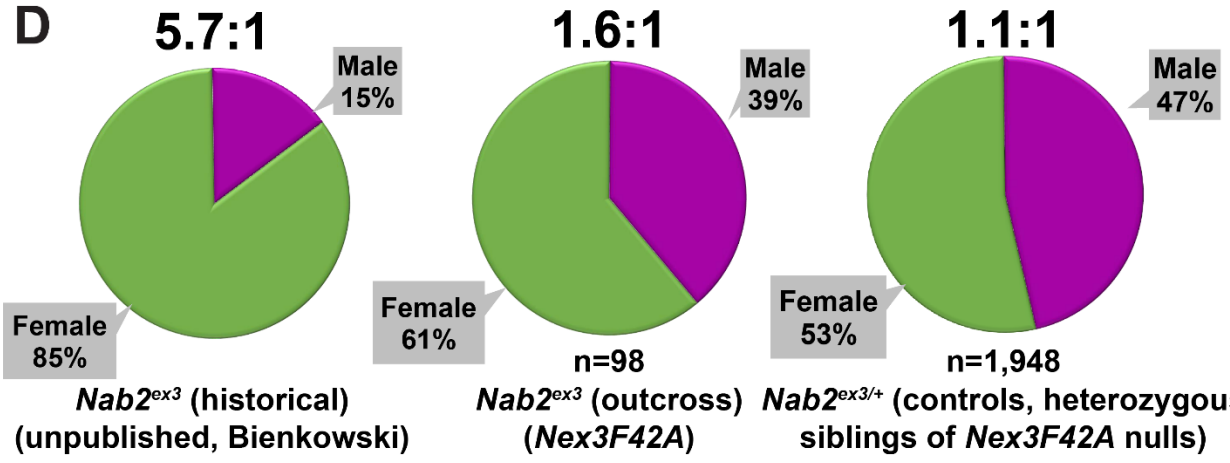

E

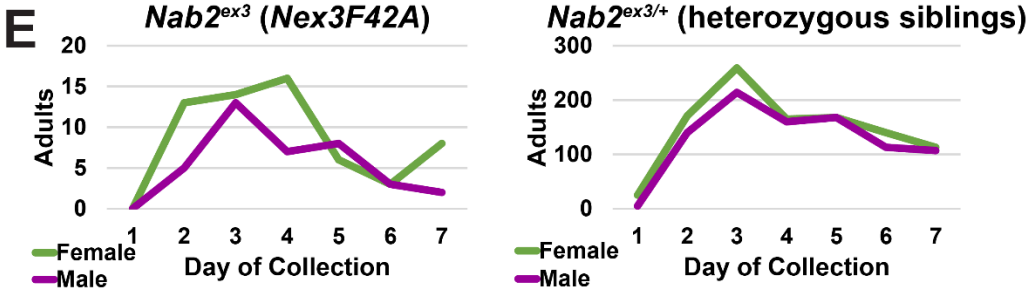

Figure 4-7. Outcross and subsequent recovery of the historical *Nab2^{ex3}* allele, combined with simple methodological innovations, modestly improve viability and substantially rescue the female:male sex skew of *Nab2^{ex3}* null adults. (A) The outcrossing and allele recovery scheme for the historical *Nab2^{ex3}* allele. 10 individual *Nex3F4#_ _* lines produced by this scheme were screened for *Nab2^{ex3}* null phenotypes. Two lines, *Nex3F42A* and *Nex3F45B*, demonstrated the greatly reduced adult viability in non-balanced homozygotes characteristic of *Nab2^{ex3}* balanced stocks. Thus, these lines were selected as highly likely to be carrying the *Nab2^{ex3}* allele and used to generate new stable, balanced outcrossed *Nab2^{ex3}* stocks. If the former line is raised using (B) the ~30° *Angled* vial method instead of to the *Upright* or *Horizontal* methods, (C) the outcrossed *Nab2^{ex3}* allele (specifically *Nab2^{Nex3F42A}*) exhibits moderately increased adult viability (14%) compared to the historical *Nab2^{ex3}* allele (~3%). (D) The outcrossed *Nab2^{ex3}* allele (specifically *Nab2^{Nex3F42A}*) also produces a less female-skewed female:male sex ratio in viable *Nab2^{ex3}* null adults as compared to the historical *Nab2^{ex3}* stock. (E) Raw numbers of female and male adults collected on each day of a seven-day collection period from vials all established on the same day. Daily sex ratios are much more variable for *Nab2^{Nex3F42A}* null adults than for heterozygous *Nab2$^{Nex3F42A/+}$* sibling controls, though this may be informed by differences in sample sizes (n). Depending on any differences used in collection frequency by different experimenters with the outcrossed and historical stocks, this variability may provide a partial or full alternative explanation for the differences in sex skewing observed between the outcrossed and historical *Nab2^{ex3}* alleles.

CHAPTER 5: DISCUSSION AND CONCLUSION

This chapter has been written by J. Christopher Rounds specifically for inclusion in this dissertation.

DISCUSSION

Chapter-by-chapter discussion of research performed and questions answered herein

In this dissertation, we present extensive, detailed evidence to address fundamental gaps in knowledge concerning metazoan Nab2/ZC3H14. With our research on *Drosophila* Nab2, we provide evidence answering some questions of metazoan Nab2/ZC3H14 **specificity**, **directness**, and **associated RNA identity**, with a particular focus on the first and third questions. First, the RNA-Seq experiment detailed in Chapter 2 provides high-resolution detail into changes in steady-state RNA abundance and structure in the absence of Nab2 in $Nab2^{ex3}$ homozygous null neuronally-enriched head tissues (Figures 2-1, 2-2, 2-3, 2-S1, 2-S2, 2-S3, 2-S4; Tables 2-1, 2-S1, 2-S2, and 2-S3). This experiment also provides crucial support arguing that *Drosophila* Nab2 molecularly exerts effects on a specific subset of the transcriptome, rather than the vast majority of it. Importantly, this assertion of specificity stands in contrast to the function of *S. cerevisiae* Nab2, which is thought to regulate the transcriptome pervasively (Moore 2005; Tuck and Tollervey 2013; Chen and Shyu 2014; Baejen *et al.* 2014; Schmid *et al.* 2015; Fasken *et al.* 2019; Stewart 2019; Alpert *et al.* 2020). To wit, many RNAs change in steady-state abundance by a statistically significant amount in $Nab2^{ex3}$ homozygous null heads compared to controls, but only a relatively specific set of 453 and 305 transcripts significantly change in abundance by two-fold or more in $Nab2^{ex3}$ females and males, respectively, (Figure 2-1C) and much of these sets overlap (Figure 2-1B,D; Table 2-S1). These sets represent 3.7% and 2.2% of all the detectable and statistically testable transcripts identified in female and male samples, respectively, demonstrating that loss of Nab2 exerts specific effects and alters the steady-state abundance of only a specific subset of the transcriptome. Even more informatively, we find in the absence of Nab2 in $Nab2^{ex3}$ homozygous nulls a small, very specific subset of transcripts show splicing differences based on exon usage differences compared to controls. In females and males, respectively, 151 and 114

transcripts meet this criterion (Tables 2-1, 2-S3). Taken together, results of this RNA-Seq experiment support and provide indirect evidence for **specificity** of Nab2 function.

In Chapter 3 we test the hypothesis of Nab2 **specificity** more directly, presenting the first high-throughput identification of Nab2-/ZC3H14-associated transcripts in any metazoan. We identify 141 transcripts associated statistically significantly with neuronally-expressed, epitope-tagged Nab2 (Figures 3-4, 3-5, 3-S3, Table 3-S2). These 141 Nab2-associated transcripts represent a focused, specific transcript subset, approximately 2.4% of the 5,760 detectable and statistically testable set of RIP-Seq transcripts. We detail the neuronal and neurodevelopmental function of some of the proteins encoded by Nab2-associated transcripts, revealing these functions are linked to phenotypes of Nab2 depletion such as defects in axonal morphology, bulk poly(A) tail length, and memory (Pak *et al.* 2011; Kelly *et al.* 2014, 2016; Bienkowski *et al.* 2017). These protein functions (and related Nab2-associated transcripts) include axonal development/guidance and synapse formation (*Arpc2* and *side-II*; Hudson and Cooley 2002; Yang *et al.* 2012; Tan *et al.* 2015), neuronal culling in development (*fwe*; Merino *et al.* 2013), poly(A)-tail formation (*Cpsf160*; Mandel *et al.* 2008), and suppression of olfactory memory formation in the mushroom bodies (*SLC22A*; Gai *et al.* 2016). This finding supports the argument that Nab2 exerts influence on biology at least in part through regulating the transcripts we identify. Importantly, we demonstrate that neuronal Nab2-associated transcripts are overrepresented for A-rich motifs in the sequences outside the poly(A) tail—that is, in genetically-encoded regulatory and protein-coding sequences (Figure 3-6). These A-rich motifs therefore represent potential sequences mediating Nab2-RNA association (e.g. as Nab2 binding motifs) and providing a mechanism by which the polyadenosine RBP Nab2 could associate with only a subset of all polyadenylated transcripts despite its theoretical potential to bind all polyadenylated transcripts via their poly(A) tails.

This finding carries a key corollary—while the A-rich motifs we describe are overrepresented in neuronal Nab2-associated RNAs, they are not at all exclusive to them. That is, these A-rich motifs are observed less frequently but still commonly in non-Nab2 associated transcripts (Figure 3-6). This finding indicates Nab2 behaves consistently with other RBPs—these proteins do not generally occupy all of their available binding motifs throughout the transcriptome (Li *et al.* 2010; Taliaferro *et al.* 2016). But, the non-exclusivity of the A-rich motifs we describe here for Nab2-associated transcripts argues an important point when coupled with our identification of Nab2 specificity in associating with only a subset of all polyadenylated transcripts. Specifically, these findings emphasizes that sequence affinity alone is insufficient to explain Nab2-RNA association and other mechanisms must also contribute to this process. Such mechanisms include RNA secondary structure, competition with other RBPs such as the nuclear polyadenosine RBP PABPN1 (reviewed in Müller-McNicoll and Neugebauer 2013), RNA localization, epitranscriptome modifications like m6A (Chapter 2), and the influence of other RBP partners; our results argue the effect of each of these mechanisms on Nab2-RNA association should be explored in future research to build on our motif analysis. In total, the Nab2 RIP-Seq and related analyses we present in Chapter 3 demonstrate the **specificity** of *Drosophila* Nab2 and reveal **associated RNA identities** for this RBP in neurons, addressing these long-standing gaps in knowledge on this RBP and contributing to understanding of metazoan Nab2/ZC3H14 in general.

In Chapter 3 we also present and detail novel genetic interactions between *Nab2* and *Atx2*, the gene encoding the neuronal translational regulator Atx2 (reviewed in Ostrowski *et al.* 2017; Lee *et al.* 2018). We establish Nab2 and Atx2 as functionally linked in guiding axonal morphology (Figure 3-2) and influencing adult viability (Figures 3-1, 3-S1). We submit the first high-throughput identification of Atx2-associated RNAs in *Drosophila* neurons, revealing the Nab2-

and Atx2-associated transcript sets overlap; we identify 28 transcripts shared between these two RBPs (Figures 3-4, 3-5, 3-S3, Tables 3-1, 3-S2). Some of these 28 transcripts encode proteins linked to, among other functions, axonal morphology and development (*sm* and *stai*; Layalle *et al.* 2005; Lachkar *et al.* 2010; Zwarts *et al.* 2015), memory formation and retrieval (*drk*, *shi*, *Gαo*, and *me31B*; Dubnau *et al.* 2001; Ferris *et al.* 2006; Moressis *et al.* 2009; Sudhakaran *et al.* 2014), and eye cell development and survival (*drk* and *HmgZ*; Kanuka *et al.* 2005; Almudi *et al.* 2010; Schoenherr *et al.* 2012) (Figure 3-4, Table 3-S3). Of these, some shared transcripts have been linked specifically to mushroom body morphology (*stai*; Lachkar *et al.* 2010; Zwarts *et al.* 2015) or function (*drk*; Moressis *et al.* 2009) or are known to be expressed in mushroom body neurons (*me31B*; Hillebrand *et al.* 2010). Thus, the identities of these transcripts raise the promising possibility that the Nab2-Atx2 functional links we identify are explained by their shared regulation of these shared transcripts. Importantly, we also show Nab2 and Atx2 primarily localize to separate subcellular compartments—the nucleus and cytoplasm, respectively—in adult mushroom body neurons and weakly physically associate in neurons by co-immunoprecipitation (Figures 3-3, 3-S2). Taken together with our shared transcript data, these results propose a sequential handoff model for Nab2-Atx2 regulation of shared associated transcripts.

We detail this sequential handoff model in Figure 3-7, but in brief we propose nuclear Nab2 protects transcript stability, regulates poly(A) tail length, and facilitates nuclear export of its associated transcripts. This proposal is based on some data from *Drosophila* (Pak *et al.* 2011; Kelly *et al.* 2014, 2016; Bienkowski *et al.* 2017; Chapter 2, RNA-Seq; Chapter 3, RIP-Seq) and on homology to the more-thoroughly-functionally-characterized *S. cerevisiae* Nab2 (key sources of Nab2 function include Green *et al.* 2002; Hector *et al.* 2002; Kelly *et al.* 2010; Schmid *et al.* 2015; Aibara *et al.* 2017; Fasken *et al.* 2019; Stewart 2019; Alpert *et al.* 2020). In our model Nab2

shuttles out of the nucleus with its target transcripts—as it is proposed to do in *S. cerevisiae* (Aitchison *et al.* 1996; Lee and Aitchison 1999; Duncan *et al.* 2000)—before releasing them during nuclear/cytoplasmic mRNP remodeling (reviewed in Müller-McNicoll and Neugebauer 2013; Chen and Shyu 2014) and re-entering the nucleus. Atx2 may become associated with shared Nab2- and Atx2-associated transcripts at this cytoplasmic stage of mRNP remodeling near the nucleus, explaining the weak, potentially indirect physical association we observe between Nab2 and Atx2 (Figure 3-3). Atx2 proceeds to suppress the translation of its associated transcripts, likely in an activity-dependent manner in RNP granules in association with RNAi machinery (McCann *et al.* 2011; Sudhakaran *et al.* 2014; Bakthavachalu *et al.* 2018). Loss of substantial decrease in levels of either protein disrupts these processes and induces the phenotypic defects we observe, while loss or decreases in levels of both RBPs partially balances these effects, resulting in the suppression observed in double *Nab2-Atx2* mutants (e.g. Figures 3-1, 3-2, 3-S1). This Nab2-Atx2 sequential handoff model presents a second, novel mode of possible functional interaction between *Drosophila* Nab2 and another RBP, as Nab2-Fmr1 physical and functional interactions, which may occur in the same RNP complex, are the only *Drosophila* Nab2-RBP interactions to have been previously explored in detail (Bienkowski *et al.* 2017). In fact, we originally expected to find Nab2 may interact with Atx2 to regulate translation, as has been suggested for Nab2 and Fmr1 (Bienkowski *et al.* 2017); instead, we find evidence for this sequential handoff model and propose that Nab2 regulates nuclear processing events such as stability, poly(A) tail length, and RNA export on associated RNAs, the translation of which is later regulated by Atx2.

Our findings in Chapter 3, that Nab2 and Atx2 share associated RNAs and coregulate neuronal morphology, represent valuable insights alone, while the sequential handoff model of Nab2-Atx2 functional interaction emphasizes the importance of understanding the **directness** of

the function of RBPs on their associated RNAs. By providing a set of **associated RNA identities** of neuronal Nab2 along with strong evidence of Nab2 **specificity**, our data enable such experiments to establish the direct molecular function of neuronal Nab2 on its associated transcripts. Defining this function is fundamental to understanding metazoan Nab2/ZC3H14 and its roles in human intellectual disability and neurodevelopment.

Finally, in Chapter 4 we present data expanding on the themes of Chapters 1-3, while providing additional methodological insights and details. We reveal the *Atx2* loss-of-function allele $Atx2^{06490}$ (Satterfield *et al.* 2002) generally behaves as $Atx2^{DG08112}$ and $Atx2^{X1}$ with respect to modulating Nab2 phenotypes—this allele dominantly suppresses the effects of $Nab2^{ex3}$ null homozygosity on adult viability and mushroom body α lobe morphology (Figures 4-1, 4-2). However, intriguingly, unlike the *Atx2* loss-of-function alleles detailed in Chapter 3, heterozygosity for $Atx2^{06490}$ does not suppress phenotypes of Nab2 overexpression in fated eye cells (i.e. in *GMR>Nab2* flies). The reasons for this discrepancy are unclear, particularly as $Atx2^{06490}$ and $Atx2^{DG08112}$ are similar alleles caused by P-element insertions in the 5' UTR of *Atx2* (Satterfield *et al.* 2002; Huet *et al.* 2002; Bellen *et al.* 2004). Perhaps these inserted P-elements exert subtly different effects *in cis*, such that the regulation or expression of Atx2 is more substantially disrupted by heterozygosity for $Atx2^{DG08112}$ as compared to heterozygosity for $Atx2^{06490}$. Regardless, reasons underlying the differences in the effects of these *Atx2* alleles on overexpression of Nab2 in fated eye cells may be worthy of further investigation. Critically, while the distinctions between the effects of these *Atx2* loss-of-function alleles on Nab2 overexpression are scientifically intriguing and hold promise for better understanding functional links between Nab2 and Atx2, that heterozygosity for an additional *Atx2* loss-of-function allele suppresses

phenotypes of Nab2 loss in axonal morphology and adult viability lends further credence to our model of counterbalanced Nab2 and Atx2 regulation of shared associated transcripts.

In Chapter 4 we next ask questions of *Nab2-Atx2* interaction reciprocal to investigations in Figures 3-1, 3-2, 3-S1, 4-1, and 4-2. That is, in these previous figures we test whether alleles of *Atx2* present or modify canonical phenotypes of Nab2 loss such as defects in mushroom body axonal morphology. By contrast, in Figures 4-3 and 4-4 we explore whether depletion of Nab2 presents or modifies canonical circadian rhythm and neuronal morphology phenotypes of Atx2 depletion (Lim and Allada 2013; Zhang *et al.* 2013). We find that *timeless*-Gal4-driven RNAi-induced knockdown of Nab2 in circadian clock neurons indeed suppresses some, but not all, circadian behavior defects caused by Atx2 knockdown in these cells (Figure 4-3). Approximately 95% of *timeless-Gal4*-driven Atx2 knockdown flies lose rhythmicity in their daily "free-running" or light-cue-independent circadian activity; *timeless-Gal4*-driven Nab2 knockdown suppresses this effect in the context of Atx2 knockdown and does not decrease the percentage of rhythmic flies when driven alone. These data indicate circadian neuron activity is robust to some decrease in Nab2 abundance but that depletion of Atx2 may sensitize these neurons to such a decrease. Importantly, these data also illustrate the potential for nuance in Nab2-Atx2 interactions in potentially regulating circadian behavior—knockdown of either RBP alone does not alter period length, but knockdown of both produces a synergistic increase. In contrast, *timeless-Gal4*-driven Nab2 knockdown does not suppress or enhance the non-statistically-significant trend towards a decrease in circadian rhythm power induced by *timeless-Gal4*-driven Atx2 knockdown. To complement these behavioral analyses, we explore effects of Nab2 loss on axonal morphology of Pigment-dispersing factor (Pdf) circadian neurons. These neurons exhibit axonal morphological defects when Atx2 is depleted in all circadian clock neurons by *timeless*-Gal4-driven RNAi,

complementing the circadian behavioral defects observed in the same conditions (Lim and Allada 2013). In contrast, we find that Nab2 loss alone in *Nab2*^{ex3} homozygous nulls does not appear to alter axonal morphology of Pdf circadian neurons, though higher-resolution imaging of axon termini and optimization of α-Pdf immunostaining should be performed before drawing definitive conclusions on this point (Figure 4-4). Future research should explore the potential for Nab2 depletion to suppress the morphological defects in Pdf neurons induced by Atx2 depletion—this remains an open question, but such a finding would align with the suppression of some circadian behavior defects observed in Figure 4-3. In summary, that knockdown of Nab2 suppresses some circadian behavior phenotypes of Atx2 knockdown provides further evidence to support our model of counterbalanced Nab2 and Atx2 regulation of shared associated transcripts. Indeed, these results reveal Nab2 and Atx2 may coregulate circadian rhythms and behavior by similar mechanisms to those we propose for their coregulation of axonal morphology and adult viability. However, that combined knockdown of both Nab2 and Atx2 appears to synergistically increase period length, rather than suppress an effect of either knockdown alone, does not neatly align with our model and more closely fits a model of cooperative, not counterbalanced, Nab2 and Atx2 regulation of shared associated transcripts. Taken together then, these circadian data suggest the functional relationship of these RBPs in regulating circadian behavior may instead be more nuanced than we propose for axonal morphology and adult viability. Future research should explore these possibilities.

In Chapter 4 we also provide much greater detail on the rRNA depletion setbacks that limited read depth in our RIP-Seq results (Figures 4-5, 4-6). We provide these details first to explain our conviction that we performed crucial work in identifying many neuronal Nab2-associated RNAs in this research presented here, applying for the first time the breadth and benefits of a high-throughput approach to this fundamental question, but that more neuronal Nab2-

associated transcripts remain to be discovered in future research. Higher sensitivity methods such as CLIP-Seq (cross-linking immunoprecipitation coupled with high-throughput sequencing; see Licatalosi *et al.* 2008; and Yeo *et al.* 2009) and related methods in the lineage of RBP-RNA UV-crosslinking techniques could be used to map Nab2 binding sites directly, even at single-base resolution (e.g. by individual-nucleotide resolution CLIP or iCLIP, see König *et al.* 2010). These CLIP methods are likely the most productive avenues to pursue to further and definitively expand the repertoire of known neuronal Nab2-associated transcripts in future research. To that end, we also include these rRNA depletion data and related analyses to emphasize the value of and need for identifying a reliable but still externally-performed rRNA depletion method for the *Drosophila* Nab2 research project to use in future experiments. The issue of ineffective rRNA depletion will otherwise prove prohibitive to future sequencing experiments necessary for the further study of Nab2. We coordinated with the same sequencing core—the Georgia Genomics and Bioinformatics Core (GGBC) at the University of Georgia—for the sequencing experiments described in Chapters 2 and 3, but reagent availability and other changes between the rRNA depletions used for each seem to have dramatically, unsustainably reduced rRNA depletion effectiveness. This loss of a reliable, effective rRNA depletion method must be resolved prior to future sequencing experiments undertaken as part of the *Drosophila* Nab2 research project.

Finally, in Chapter 4 we describe both the outcrossing scheme and vial maintenance techniques employed to generate the $Nab2^{Nex3F42A}$ outcross stock and to substantially increase $Nab2^{ex3}$ homozygous null adult viability from historical values of approximately 3% (Pak *et al.* 2011; Kelly *et al.* 2014) to the 14% value reported in Chapters 3 and 4 (Figures 3-1, 3-S1, 4-7). We reveal that this outcross combined with our collection techniques resulted in substantial reductions in the female skew of $Nab2^{ex3}$ null adult viability, reducing the female:male ratio of

viable adults from historical values of 5.7:1 (Bienkowski, unpublished) to 1.6:1 (Figure 4-7). Notably, our careful staging of cross age and detailed accounting for potential daily variability in *Nab2*^{ex3} female:male viable adult ratios may partially explain the ratio difference we observe for the *Nab2*^{Nex3F42A} outcrossed null allele compared to historical *Nab2*^{ex3} null allele (Figure 4-7). However, the most parsimonious explanation is that, like with adult viability rates overall, outcrossing *Nab2*^{ex3} to generate the *Nab2*^{Nex3F42A} outcross stock resulted in reduced severity of some *Nab2*^{ex3} null phenotypes. This reduction in phenotype severity strongly argues outcrossing separated the *Nab2*^{ex3} allele from unknown genetic or epigenetic background modifier(s) that enhance at least some *Nab2*^{ex3} null phenotypes, modifier(s) that the historical *Nab2*^{ex3} null stock acquired over many generations.

Curiously, evolutionary pressures on any stock carrying a null mutation like *Nab2*^{ex3} would be expected to select for genetic or epigenetic background modifier(s) that suppress, not enhance, *Nab2*^{ex3} null phenotypes. That is, the *a priori* expectation for a stock carrying the *Nab2*^{ex3} null allele would be that *Nab2*^{ex3} homozygous null phenotype severity would decrease rather than increase over multiple generations, if any significant phenotypic changes occurred over research-project-scale generational time at all. Crucially, that stocks carrying the *Nab2*^{ex3} null allele appear to accumulate enhancing, rather than suppressing, background modifier(s) over generational time has proven reproducible across different contexts, experimentalists, and independent populations of stocks carrying the *Nab2*^{ex3} null allele. The outcrossing scheme to generate the *Nab2*^{Nex3F42A} stock detailed in Chapter 4 was executed in response to declining *Nab2*^{ex3} homozygous null adult viability in *Nab2*^{ex3} stocks maintained by different experimentalists at Emory in Georgia and The College of Wooster in Ohio working with independent populations derived from the same original *Nab2*^{ex3} progenitor stock. At the time of this writing, even the *Nab2*^{Nex3F42A} stock has begun

exhibiting the now-familiar decline in *Nab2*^{ex3} homozygous null adult viability over generational time, necessitating another outcrossing and recovery process, currently underway. This reproducibility is surprising and strongly argues the observed declines in *Nab2*^{ex3} homozygous null adult viability over generational time reflect actual, reproducible biological defects. Rather than a chance curiosity of limited biological meaning, this decline in viability over generational time may be best understood as a phenotype of stocks of exclusively *Nab2*^{ex3} hetero- and homozygous animals. That is, this phenotype is likely directly or indirectly downstream of Nab2 dysfunction and reflects an unknown, potentially novel biological role for Nab2. These observations and this possibility indicate there would be great research value in understanding this accumulation of enhancing background modifier(s) in the *Nab2*^{ex3} stock and identifying the responsible genetic and epigenetic alterations. Such modifiers are likely closely related to Nab2 function. Importantly, successfully identifying these modifiers represents an experimentally difficult and time-consuming challenge that therefore may not be feasible to prioritize. However, the possibility of truly novel, informative insight into Nab2 function and into a confounding, unusual genetic phenomenon represented by this unexplained viability decline phenotype strongly recommends resources should be allocated to at least systematically track the viability of *Nab2*^{ex3} homozygous null adults over generational time. Such tracking would lead to better understanding and quantification of this *Nab2*^{ex3} homozygous null adult viability decline and would build an even more firm case for studying and explaining it.

The nuclear polyadenosine RBP PABPN1 raises a promising evolutionary hypothesis—with testable implications—to explain greater functional specificity for metazoan Nab2/ZC3H14 compared to *S. cerevisiae* Nab2

The potential, raised above in discussing Chapter 3, for competition between Nab2 and fellow nuclear polyadenosine RBP PABPN1 specifically for binding polyadenosine holds great promise in possibly explaining the increased specificity of metazoan Nab2/ZC3H14 compared to *S. cerevisiae* Nab2. PABPN1 at least in mammals employs a different mechanism than Nab2 in *S. cerevisiae* to achieve similar ends (for examples of this proposal, see Moore 2005; Eckmann *et al.* 2011; Stewart 2019), acting to relatively globally control poly(A) tail length and regulate nuclear export (Apponi *et al.* 2010; reviewed in Lemay *et al.* 2010; and Müller-McNicoll and Neugebauer 2013). With respect to poly(A) tail length control, *S. cerevisiae* Nab2 may primarily function to limit tail length upon homodimerization on sufficiently long tails, while Fip1 and Cft1, members of the cleavage and polyadenylation specificity factor (CPSF) protein complex, support poly(A) polymerase processivity (Hector *et al.* 2002; Kelly *et al.* 2010; Aibara *et al.* 2017; Fasken *et al.* 2019; Stewart 2019). In contrast, PABPN1 appears to serve both functions, supporting poly(A) polymerase processivity until a tail length of ~250 nucleotides, after which point the growing PABPN1 homo-oligomer physically, sterically disrupts poly(A) processivity and largely halts polyadenylation (Wahle 1995; Keller *et al.* 2000; Kühn *et al.* 2009; Eckmann *et al.* 2011). PABPN1 is such a key nuclear regulator of poly(A) tail length and nuclear export in mammals and likely metazoans generally as, unlike Nab2/ZC3H14 (Bienkowski *et al.* 2017; Rha *et al.* 2017; Al-Nabhani *et al.* 2018), PABPN1 is essential for cellular and/or organismal viability in *Drosophila* (Benoit *et al.* 2005), mice (Vest *et al.* 2017), and humans (Hart *et al.* 2015). However, PABPN1 is absent in *S. cerevisiae* and is evolutionarily distinct from Nab2 (Mangus *et al.* 2003). These data

on PABPN1 suggest the tantalizing possibility that metazoan Nab2/ZC3H14 has been able to evolve greater specificity for only certain transcripts and contexts in the presence of PABPN1, as this presence could make the pervasive regulatory role of Nab2 in poly(A) tail length control, nuclear poly(A) export, and transcript stability redundant and unnecessary for viability.

This hypothesis of PABPN1 relieving selective pressure on Nab2 function, allowing Nab2 to evolve specificity over time, is particularly well-supported by the functional similarities of and differential viability requirements for PABPN1 and Nab2/ZC3H14 in metazoans and *S. cerevisiae* detailed above. This hypothesis is also well-supported by the observed ability of polyadenosine RNA-binding proteins (PABPs) to partially compensate for one another under certain experimental conditions. Specifically, the cytoplasmic *S. cerevisiae* PABP Pab1, if targeted to the nucleus by the addition of a nuclear localization (NL) signal, is able to partially compensate for the deleterious effects of Nab2 depletion on poly(A) RNA export from the nucleus—but not to compensate for the deleterious effects of this depletion on poly(A) tail length (Hector *et al.* 2002). Similarly, RNAi-driven depletion of PAPBN1 in human HeLa and HEK293 cells induces nuclear translocation of the cytoplasmic PABP PABP4 along with increases in abundance of the cytoplasmic PABP PABP5; when altered as such, PABP4 and PABP5 appear competent to compensate for the effects of PABPN1 loss on poly(A) tail length and nuclear export of mRNA, as these processes appeared unchanged despite an increase in apoptosis markers following PABPN1 depletion (Bhattacharjee and Bag 2012). The hypothesis that the presence of PABPN1 allowed the evolution of Nab2 specificity, and the implied corollary that PABPN1 may outcompete Nab2 for binding nascent poly(A) tails and/or polyadenosine RNA on many but not necessarily all transcripts *in vivo*, holds great potential for enhancing understanding of function both RBPs in

general and metazoan Nab2/ZC3H14 in particular; this hypothesis should be explored further in future research.

CONCLUSION

In summary, the research we present in this dissertation represents a series of valuable contributions to Nab2/ZC3H14 research, advancing our understanding of this gene family linked to intellectual disability and neuronal development. We address gaps in knowledge that formerly impeded Nab2/ZC3H14 research. We present strong evidence that metazoan Nab2/ZC3H14 exhibits **specificity** in its function and associations with the transcriptome, a specificity consequentially different form the pervasive regulation of its homolog *S. cerevisiae* Nab2. Our results argue Nab2 and Atx2 share associated transcripts in neurons and coregulate neuronal morphology, interacting in a sequential handoff from nucleus to cytoplasm. This finding re-emphasizing the need to continually test for and reveal **directness** and indirectness in Nab2 function on its associated transcripts and in its associations with other RBPs to better understand Nab2. Finally, we reveal **associated RNA identities** for Nab2 along with Atx2, presenting for the first time high-throughput identifications of associated RNAs for each RBP in *Drosophila* neurons, and for Nab2 in any metazoan. The identities of these transcripts, revealed by this research, will be essential in and a major boon for future Nab2/ZC3H14 research, enabling definitive and precise understanding of the molecular function of Nab2 on its target transcripts.

Our results provide a foundation for exploring the next questions and topics in metazoan Nab2/ZC3H14 research. These questions and topics include the following. The first topic: defining whether the activities of *S. cerevisiae* Nab2 in regulating transcript stability, controlling poly(A) tail length, and facilitating nuclear export are conserved for *Drosophila* Nab2 on its more select

associated transcript set. Importantly, the *a priori* expectation, given homology between these proteins, would be for these functions to be well-conserved. Findings in support or to the contrary of this expectation are both completely possible—either would be highly informative and would require further study and explanation. Without addressing this question, critical gaps will remain in understanding metazoan Nab2/ZC3H14 and which results from *S. cerevisiae*, *Drosophila*, and mice are applicable to human ZC3H14 and its links to intellectual disability and neurodevelopment. The second topic: determining the precise binding site of Nab2 and establishing a more complete repertoire of Nab2-associated transcripts, in neurons or otherwise. The third topic: testing whether the epitranscriptomic role for Nab2 in suppressing m6A deposition supported by Chapter 2 represents a direct function of Nab2 or a downstream effect of its regulation of its target RNAs. The fourth topic: identifying which Nab2-target RNA regulatory relationships contribute most substantially to the role of Nab2/ZC3H14 in neurons and neurodevelopment.

The research presented in this dissertation significantly expands our understanding of *Drosophila* Nab2 and thus its mammalian ZC3H14 ortholog, revealing Nab2 **specificity**, the functional relationship between Nab2 and Atx2, and many neuronal Nab2-**associated RNA identities**. Our research provides a foundation to pursue the next questions and topics in Nab2/ZC3H14 research detailed above through our results, our methodological contributions and detail, and our analysis. Ultimately, this research provides better clarity and enables future research on metazoan Nab2/ZC3H14, bringing us closer to fully understanding the human polyadenosine RBP ZC3H14 and how this ubiquitously-expressed RBP links to intellectual disability and contributes to human neurodevelopment.

REFERENCES

Aibara S., J. M. B. Gordon, A. S. Riesterer, S. H. McLaughlin, and M. Stewart, 2017 Structural basis for the dimerization of Nab2 generated by RNA binding provides insight into its contribution to both poly(A) tail length determination and transcript compaction in Saccharomyces cerevisiae. Nucleic Acids Res. 45: 1529–1538. https://doi.org/10.1093/nar/gkw1224

Aitchison J. D., G. Blobel, and M. P. Rout, 1996 Kap104p: A karyopherin involved in the nuclear transport of messenger RNA binding proteins. Science (80-.). 274: 624–627. https://doi.org/10.1126/science.274.5287.624

Al-Nabhani M., S. Al-Rashdi, F. Al-Murshedi, A. Al-Kindi, K. Al-Thihli, *et al.*, 2018 Reanalysis of exome sequencing data of intellectual disability samples: Yields and benefits. Clin. Genet. https://doi.org/10.1111/cge.13438

Almudi I., M. Corominas, and F. Serras, 2010 Competition between SOCS36E and Drk modulates sevenless receptor tyrosine kinase activity. J. Cell Sci. 123: 3857–3862. https://doi.org/10.1242/jcs.071134

Alpert T., K. Straube, F. Carrillo Oesterreich, and K. M. Neugebauer, 2020 Widespread Transcriptional Readthrough Caused by Nab2 Depletion Leads to Chimeric Transcripts with Retained Introns. Cell Rep. 33: 108324. https://doi.org/10.1016/j.celrep.2020.108324

Apponi L. H., S. W. Leung, K. R. Williams, S. R. Valentini, A. H. Corbett, *et al.*, 2010 Loss of nuclear poly(A)-binding protein 1 causes defects in myogenesis and mRNA biogenesis. Hum. Mol. Genet. 19: 1058–1065. https://doi.org/10.1093/hmg/ddp569

Baejen C., P. Torkler, S. Gressel, K. Essig, J. Söding, *et al.*, 2014 Transcriptome Maps of mRNP Biogenesis Factors Define Pre-mRNA Recognition. Mol. Cell 55: 745–757. https://doi.org/10.1016/j.molcel.2014.08.005

Bakthavachalu B., J. Huelsmeier, I. P. Sudhakaran, J. Hillebrand, A. Singh, *et al.*, 2018 RNP-Granule Assembly via Ataxin-2 Disordered Domains Is Required for Long-Term Memory and Neurodegeneration Article RNP-Granule Assembly via Ataxin-2 Disordered Domains Is Required for Long-Term Memory and Neurodegeneration. Neuron 98: 754-766.e4. https://doi.org/10.1016/j.neuron.2018.04.032

Bellen H. J., R. W. Levis, G. Liao, Y. He, J. W. Carlson, *et al.*, 2004 The BDGP gene disruption project: Single transposon insertions associated with 40% of Drosophila genes. Genetics 167: 761–781. https://doi.org/10.1534/genetics.104.026427

Benoit B., G. Mitou, A. Chartier, C. Temme, S. Zaessinger, *et al.*, 2005 An essential cytoplasmic function for the nuclear poly(A) binding protein, PABP2, in poly(A) tail length control and early development in Drosophila. Dev. Cell 9: 511–522. https://doi.org/10.1016/j.devcel.2005.09.002

Bhattacharjee R. B., and J. Bag, 2012 Depletion of Nuclear Poly(A) Binding Protein PABPN1 Produces a Compensatory Response by Cytoplasmic PABP4 and PABP5 in Cultured Human Cells. PLoS One 7. https://doi.org/10.1371/journal.pone.0053036

Bienkowski R. S., A. Banerjee, J. C. Rounds, J. Rha, O. F. Omotade, *et al.*, 2017 The Conserved, Disease-Associated RNA Binding Protein dNab2 Interacts with the Fragile X Protein Ortholog in Drosophila Neurons. Cell Rep. 20: 1372–1384. https://doi.org/10.1016/j.celrep.2017.07.038

Chen C. Y. A., and A. Bin Shyu, 2014 Emerging mechanisms of mRNP remodeling regulation. Wiley Interdiscip. Rev. RNA 5: 713–722. https://doi.org/10.1002/wrna.1241

Dubnau J., L. Grady, T. Kitamoto, and T. Tully, 2001 Disruption of neurotransmission in Drosophila mushroom body blocks retrieval but not acquisition of memory. Nature 411: 476–480. https://doi.org/10.1038/35078077

Duncan K., J. G. Umen, and C. Guthrie, 2000 A putative ubiquitin ligase required for efficient mRNA export differentially affects hnRNP transport. Curr. Biol. 10: 687–696. https://doi.org/10.1016/S0960-9822(00)00527-3

Eckmann C. R., C. Rammelt, and E. Wahle, 2011 Control of poly(A) tail length. Wiley Interdiscip. Rev. RNA 2: 348–361. https://doi.org/10.1002/wrna.56

Fasken M. B., A. H. Corbett, and M. Stewart, 2019 Structure-function relationships in the Nab2 polyadenosine-RNA binding Zn finger protein family. Protein Sci. 28: 513–523. https://doi.org/10.1002/pro.3565

Ferris J., H. Ge, L. Liu, and G. Roman, 2006 G(o) signaling is required for Drosophila associative learning. Nat. Neurosci. 9: 1036–1040. https://doi.org/10.1038/nn1738

Gai Y., Z. Liu, I. Cervantes-Sandoval, and R. L. Davis, 2016 Drosophila SLC22A Transporter Is a Memory Suppressor Gene that Influences Cholinergic Neurotransmission to the Mushroom Bodies. Neuron 90: 581–595. https://doi.org/10.1016/j.neuron.2016.03.017

Green D. M., K. A. Marfatia, E. B. Crafton, X. Zhang, X. Cheng, *et al.*, 2002 Nab2p is required for poly(A) RNA export in Saccharomyces cerevisiae and is regulated by arginine methylation via Hmt1p. J. Biol. Chem. 277: 7752–7760. https://doi.org/10.1074/jbc.M110053200

Hart T., M. Chandrashekhar, M. Aregger, Z. Steinhart, K. R. Brown, *et al.*, 2015 High-Resolution CRISPR Screens Reveal Fitness Genes and Genotype-Specific Cancer Liabilities. Cell 163: 1515–1526. https://doi.org/10.1016/j.cell.2015.11.015

Hector R. E., K. R. Nykamp, S. Dheur, J. T. Anderson, P. J. Non, *et al.*, 2002 Dual requirement for yeast hnRNP Nab2p in mRNA poly(A) tail length control and nuclear export. EMBO J. 21: 1800–10. https://doi.org/10.1093/emboj/21.7.1800

Hillebrand J., K. Pan, A. Kokaram, S. Barbee, R. Parker, *et al.*, 2010 The Me31B DEAD-Box Helicase Localizes to Postsynaptic Foci and Regulates Expression of a CaMKII Reporter mRNA in Dendrites of Drosophila Olfactory Projection Neurons. Front. Neural Circuits 4: 121. https://doi.org/10.3389/fncir.2010.00121

Hudson A. M., and L. Cooley, 2002 A subset of dynamic actin rearrangements in Drosophila requires the Arp2/3 complex. J. Cell Biol. 156: 677–687. https://doi.org/10.1083/jcb.200109065

Huet F., J. T. Lu, K. V. Myrick, L. R. Baugh, M. A. Crosby, *et al.*, 2002 A deletion-generator compound element allows deletion saturation analysis for genomewide phenotypic annotation. Proc. Natl. Acad. Sci. U. S. A. 99: 9948–9953. https://doi.org/10.1073/pnas.142310099

Kanuka H., T. Hiratou, T. Igaki, H. Kanda, E. Kuranaga, *et al.*, 2005 Gain-of-function screen identifies a role of the Sec61α translocon in Drosophila postmitotic neurotoxicity. Biochim. Biophys. Acta - Gen. Subj. 1726: 225–237. https://doi.org/10.1016/j.bbagen.2005.06.020

Keller R. W., U. Kühn, M. Aragón, L. Bornikova, E. Wahle, *et al.*, 2000 The nuclear poly(A) binding protein, PABP2, forms an oligomeric particle covering the length of the poly(A) tail. J. Mol. Biol. 297: 569–583. https://doi.org/10.1006/jmbi.2000.3572

Kelly S. M., S. W. Leung, L. H. Apponi, A. M. Bramley, E. J. Tran, *et al.*, 2010 Recognition of polyadenosine RNA by the zinc finger domain of nuclear poly(A) RNA-binding protein 2 (Nab2) is required for correct mRNA 3'-end formation. J. Biol. Chem. 285: 26022–32. https://doi.org/10.1074/jbc.M110.141127

Kelly S. M., S. W. Leung, C. Pak, A. Banerjee, K. H. Moberg, *et al.*, 2014 A conserved role for the zinc finger polyadenosine RNA binding protein, ZC3H14, in control of poly(A) tail length. RNA 20: 681–8. https://doi.org/10.1261/rna.043984.113

Kelly S. M., R. Bienkowski, A. Banerjee, D. J. Melicharek, Z. A. Brewer, *et al.*, 2016 The Drosophila ortholog of the Zc3h14 RNA binding protein acts within neurons to pattern axon projection in the developing brain. Dev. Neurobiol. 76: 93–106. https://doi.org/10.1002/dneu.22301

König J., K. Zarnack, G. Rot, T. Curk, M. Kayikci, *et al.*, 2010 iCLIP reveals the function of hnRNP particles in splicing at individual nucleotide resolution. Nat. Struct. Mol. Biol. 17: 909–915. https://doi.org/10.1038/nsmb.1838

Kühn U., M. Gündel, A. Knoth, Y. Kerwitz, S. Rüdel, *et al.*, 2009 Poly(A) tail length is controlled by the nuclear Poly(A)-binding protein regulating the interaction between Poly(A) polymerase and the cleavage and polyadenylation specificity factor. J. Biol. Chem. 284: 22803–22814. https://doi.org/10.1074/jbc.M109.018226

Lachkar S., M. Lebois, M. O. Steinmetz, A. Guichet, N. Lal, *et al.*, 2010 Drosophila stathmins bind tubulin heterodimers with high and variable stoichiometries. J. Biol. Chem. 285: 11667–11680. https://doi.org/10.1074/jbc.M109.096727

Layalle S., E. Coessens, A. Ghysen, and C. Dambly-Chaudière, 2005 Smooth, a hnRNP encoding gene, controls axonal navigation in Drosophila. Genes to Cells 10: 119–125. https://doi.org/10.1111/j.1365-2443.2005.00822.x

Lee D. C. Y., and J. D. Aitchison, 1999 Kap104p-mediated nuclear import. Nuclear localization signals in mRNA- binding proteins and the role of Ran and RNA. J. Biol. Chem. 274: 29031–29037. https://doi.org/10.1074/jbc.274.41.29031

Lee J., M. Kim, T. Q. Itoh, and C. Lim, 2018 Ataxin-2: A versatile posttranscriptional regulator and its implication in neural function. Wiley Interdiscip. Rev. RNA 9: e1488. https://doi.org/10.1002/wrna.1488

Lemay J. F., C. Lemieux, O. St-André, and F. Bachand, 2010 Crossing the borders: Poly(A)-binding proteins working on both sides of the fence. RNA Biol. 7: 1–6. https://doi.org/10.4161/rna.7.3.11649

Li X., G. Quon, H. D. Lipshitz, and Q. Morris, 2010 Predicting in vivo binding sites of RNA-binding proteins using mRNA secondary structure. RNA 16: 1096–1107. https://doi.org/10.1261/rna.2017210

Licatalosi D. D., A. Mele, J. J. Fak, J. Ule, M. Kayikci, *et al.*, 2008 HITS-CLIP yields genome-wide insights into brain alternative RNA processing. Nature 456: 464–469. https://doi.org/10.1038/nature07488

Lim C., and R. Allada, 2013 ATAXIN-2 Activates PERIOD Translation to Sustain Circadian Rhythms in Drosophila. Science (80-.). 340. https://doi.org/10.1126/science.1234785

Mandel C. R., Y. Bai, and L. Tong, 2008 Protein factors in pre-mRNA 3′-end processing. Cell. Mol. Life Sci. 65: 1099–1122.

Mangus D. A., M. C. Evans, and A. Jacobson, 2003 Poly(A)-binding proteins: Multifunctional scaffolds for the post-transcriptional control of gene expression. Genome Biol. 4: 1–14. https://doi.org/10.1186/gb-2003-4-7-223

McCann C., E. E. Holohan, S. Das, A. Dervan, A. Larkin, *et al.*, 2011 The Ataxin-2 protein is required for microRNA function and synapse-specific long-term olfactory habituation. Proc. Natl. Acad. Sci. U. S. A. 108: E655-62. https://doi.org/10.1073/pnas.1107198108

Merino M. M., C. Rhiner, M. Portela, and E. Moreno, 2013 “Fitness fingerprints” mediate physiological culling of unwanted neurons in drosophila. Curr. Biol. 23: 1300–1309. https://doi.org/10.1016/j.cub.2013.05.053

Moore M. J., 2005 From birth to death: The complex lives of eukaryotic mRNAs. Science (80-.). 309: 1514–1518. https://doi.org/10.1126/science.1111443

Moressis A., A. R. Friedrich, E. Pavlopoulos, R. L. Davis, and E. M. C. Skoulakis, 2009 A dual role for the adaptor protein DRK in Drosophila olfactory learning and memory. J. Neurosci. 29: 2611–2625. https://doi.org/10.1523/JNEUROSCI.3670-08.2009

Müller-McNicoll M., and K. M. Neugebauer, 2013 How cells get the message: Dynamic assembly and function of mRNA-protein complexes. Nat. Rev. Genet. 14: 275–287. https://doi.org/10.1038/nrg3434

Ostrowski L. A., A. C. Hall, and K. Mekhail, 2017 Ataxin-2: From RNA control to human health and disease. Genes (Basel). 8: 2–21.

Pak C., M. Garshasbi, K. Kahrizi, C. Gross, L. H. Apponi, *et al.*, 2011 Mutation of the conserved polyadenosine RNA binding protein, ZC3H14/dNab2, impairs neural function in Drosophila and humans. Proc. Natl. Acad. Sci. U. S. A. 108: 12390–5. https://doi.org/10.1073/pnas.1107103108

Rha J., S. K. Jones, J. Fidler, A. Banerjee, S. W. Leung, *et al.*, 2017 The RNA-binding protein, ZC3H14, is required for proper poly(A) tail length control, expression of synaptic proteins, and brain function in mice. Hum. Mol. Genet. 26: 3663–3681.

https://doi.org/10.1093/hmg/ddx248

Satterfield T. F., S. M. Jackson, and L. J. Pallanck, 2002 A Drosophila Homolog of the Polyglutamine Disease Gene SCA2 Is a Dosage-Sensitive Regulator of Actin Filament Formation. Genetics 162: 1687–1702.

Schmid M., P. Olszewski, V. Pelechano, I. Gupta, L. M. Steinmetz, *et al.*, 2015 The Nuclear PolyA-Binding Protein Nab2p Is Essential for mRNA Production. Cell Rep. 12: 128–139. https://doi.org/10.1016/j.celrep.2015.06.008

Schoenherr J. A., J. M. Drennan, J. S. Martinez, M. R. Chikka, M. C. Hall, *et al.*, 2012 Drosophila Activated Cdc42 Kinase Has an Anti-Apoptotic Function, (H. Steller, Ed.). PLoS Genet. 8: e1002725. https://doi.org/10.1371/journal.pgen.1002725

Stewart M., 2019 Polyadenylation and nuclear export of mRNAs. J. Biol. Chem. 294: 2977–2987. https://doi.org/10.1074/jbc.REV118.005594

Sudhakaran I. P., J. Hillebrand, A. Dervan, S. Das, E. E. Holohan, *et al.*, 2014 FMRP and Ataxin-2 function together in long-term olfactory habituation and neuronal translational control. Proc Natl Acad Sci U S A 111: E99–E108. https://doi.org/10.1073/pnas.1309543111

Taliaferro J. M., N. J. Lambert, P. H. Sudmant, D. Dominguez, J. J. Merkin, *et al.*, 2016 RNA Sequence Context Effects Measured In Vitro Predict In Vivo Protein Binding and Regulation. Mol. Cell 64: 294–306. https://doi.org/10.1016/j.molcel.2016.08.035

Tan L., K. X. Zhang, M. Y. Pecot, S. Nagarkar-Jaiswal, P. T. Lee, *et al.*, 2015 Ig Superfamily Ligand and Receptor Pairs Expressed in Synaptic Partners in Drosophila. Cell 163: 1756–1769. https://doi.org/10.1016/j.cell.2015.11.021

Tuck A. C., and D. Tollervey, 2013 A transcriptome-wide atlas of RNP composition reveals diverse classes of mRNAs and lncRNAs. Cell 154: 996–1009. https://doi.org/10.1016/j.cell.2013.07.047

Vest K. E., B. L. Phillips, A. Banerjee, L. H. Apponi, E. B. Dammer, *et al.*, 2017 Novel mouse models of oculopharyngeal muscular dystrophy (OPMD) reveal early onset mitochondrial defects and suggest loss of PABPN1 may contribute to pathology. Hum. Mol. Genet. 26: 3235–3252. https://doi.org/10.1093/hmg/ddx206

Wahle E., 1995 Poly(A) Tail Length Control Is Caused by Termination of Processive Synthesis. J. Biol. Chem. 270: 2800–2808.

Yang Q., X. F. Zhang, T. D. Pollard, and P. Forscher, 2012 Arp2/3 complex-dependent actin networks constrain myosin II function in driving retrograde actin flow. J. Cell Biol. 197: 939–956. https://doi.org/10.1083/jcb.201111052

Yeo G. W., N. G. Coufal, T. Y. Liang, G. E. Peng, X. D. Fu, *et al.*, 2009 An RNA code for the FOX2 splicing regulator revealed by mapping RNA-protein interactions in stem cells. Nat. Struct. Mol. Biol. 16: 130–137. https://doi.org/10.1038/nsmb.1545

Zhang Y., J. Ling, C. Yuan, R. Dubruille, and P. Emery, 2013 A Role for Drosophila ATX2 in Activation of PER Translation and Circadian Behavior. Science (80-.). 340.

Zwarts L., L. Vanden Broeck, E. Cappuyns, J. F. Ayroles, M. M. Magwire, *et al.*, 2015 The genetic basis of natural variation in mushroom body size in Drosophila melanogaster. Nat. Commun. 6: 1–11. https://doi.org/10.1038/ncomms10115